NASA SP-355

COMET KOHOUTEK

A WORKSHOP HELD AT
ARSHALL SPACE FLIGHT CENTER
JUNE 13-14, 1974

NATIONAL AERONAUTICS AND SPACE ADMINISTRATION

NASA SP-355

COMET KOHOUTEK

A Workshop held at
Marshall Space Flight Center
Huntsville, Alabama
June 13–14, 1974

Edited by
Gilmer Allen Gary
Space Sciences Laboratory
Marshall Space Flight Center

Scientific and Technical Information Office 1975
NATIONAL AERONAUTICS AND SPACE ADMINISTRATION
Washington, D.C.

For sale by the Superintendent of Documents, U.S. Government Printing Office
Washington, D.C. 20402-Price $3.35
Stock Number 033–000–00598
Cat. No. NAS 1.21:355
Library of Congress Catalog Card Number 74–600125

FOREWORD

By their unexpected apparition, their unusual appearance, and their peculiar motion over the heavens, comets impressed the imagination of mankind in many ways. While superstition once exaggerated the importance of comets among the heavenly bodies, modern exact astronomical sciences went to the other extreme. It was realized that the amount of matter in a comet is extremely small. As the source of meteor streams and meteors in general, they are presently viewed as a third-rate cosmic population lacking any influence on the goings-on of this world. Nevertheless, comets have been used by the astronomers and astrophysicists as a kind of laboratory probe to check the effects of gravitation on the masses of the planets which perturb their motion, and on the interaction of solar radiations with gases and plasmas of extreme tenuity not attainable in the laboratory. They are studied as a scientific curiosity, their physical and chemical structure evolving into a great cloud of dust and gas, and the huge comet tails often growing for a short moment into the largest objects in the solar system. Perhaps their study may lead to unexpected discoveries despite the insignificance of these bodies.

Although treated as an inferior category in the study of the universe, comets may represent, next to the Earth and the Sun, the most important class of objects in the history of the solar systems. They are the survivors and replicas of an ancient population of small bodies and planetesimals from which the present planets originated. By a curious interplay of the laws of gravitation, remnants of the original population of planetesimals have remained in cold storage in the outer portions of the solar system or were ejected into interstellar space. They offer a unique opportunity to study the properties of materials used in making the planets and Sun itself at the dawn of the solar system. Their present insignificant total mass is a remnant of their mass when the planets were forming.

The appearance of a new apparition—a bright, long-period comet—is a rare phenomenon, perhaps occurring once per decade. The great pace of technological and scientific developments allows comprehensive studies of the nature of the evolution of the coma and tail as the comet approaches the Sun and then recedes from it. The extended observing capability in the ultraviolet from Earth-orbiting observatories, the new infrared observatories on airborne

platforms, radio telescopes, and the ability to send a space probe through the comet's coma and tail should lead to many discoveries about the physical nature of comets and the evolution of the solar system.

Comet Kohoutek (1973f) is a true long-period comet, the period prior to planetary perturbations, was nearly four million years, or perhaps, Comet Kohoutek is a primordial body from another solar system. This comet of relatively large mass approached very close to the Sun, perihelion distance of 0.14 AU, opened the way to a comprehensive ultraviolet and photographic and visual observations of Comet Kohoutek's transformation through perihelion.

The uniquely early discovery of a bright, long-period comet with perihelion occurring during the third manned mission to Skylab opened the way to the most comprehensive study of the evolution and transformation of a comet. In 1970 the major discovery of the amount and size of the cloud of hydrogen gas (and OH) in the comas of Comet Tago-Sato-Kosaka, Comet Bennett, and Comet Encke from the ultraviolet detectors in the Orbiting Astronomical Observatory of the Orbiting Geophysical Observatory had a substantial effect on our knowledge of the structure of the cometary nucleii. For Comet Kohoutek a substantial program—Operation Kohoutek—was organized to coordinate, interrelate, and manage the observations encompassing the ground-based optical and radio astronomy observations, and the observations from aircraft, sounding rockets, an Orbiting Solar Observatory, the Orbiting Astronomical Observatory, the Mariner-Venus-Mercury, and Skylab. The results of these investigations have turned out to be substantial and significant as demonstrated in these proceedings.

The study of Comet Kohoutek has been the most comprehensive and detailed for any comet up to now. A great number of scientists have contributed new approaches, techniques, and many hours of work to produce results in this comprehensive cometary investigation. These results will, I am sure, be applied in future research involving extended astronomical observations from radio, infrared, and large space observatories. Missions to comets are expected soon—a flyby of Comet Encke during its 1980 apparition, followed by a rendezvous with Comet Encke in 1984 and a flyby of Comet Halley in 1986.

MAURICE DUBIN
Chief, Cometary Physics
Physics and Astronomy Programs
National Aeronautics and Space Administration

PREFACE

The early results from these various observations were brought together at the Comet Kohoutek Workshop held on June 13–14, 1974, at the Marshall Space Flight Center (MSFC). At this scientific symposium, 42 papers were presented for discussion and dissemination of data actually obtained from Comet Kohoutek with NASA facilities and NASA-coordinated observations from Skylab, aircraft, rockets, and ground-based systems. The wide interest in cometary structure and composition was reflected by the attendance of over 100 scientists.

The organizing committee for the workshop was composed of A. H. Delsemme, M. Dubin, H. Floyd, S. P. Maran, B. Marsden, C. R. O'Dell (Chairman), and W. C. Snoddy. Bertram Donn was an invited participant at the first organizing meeting. The Marshall Space Flight Center was host for the participants, and Dr. W. R. Lucas, the Center Director, opened the workshop with the welcome address. The chairmen were, in order of the sessions, M. J. S. Belton, A. H. Delsemme, R. A. R. Parker, E. Stuhlinger, and C. R. O'Dell.

The organization of the report follows that of the workshop. There were four sessions: tail form, structure, and evolution; H_2O-related observations; molecules and atoms in the coma and tail; and photometry and radiometry. A fifth session was a summary and discussion period.

Appreciation is expressed to the MSFC Skylab Office for support of the workshop, and to Martin Marietta Aerospace, the MSFC Space Sciences Laboratory, and the individual authors and participants in the workshop.

Where the material was to be published elsewhere, a summary of the author's paper is given.

GILMER ALLEN GARY
Space Sciences Laboratory
Marshall Space Flight Center
National Aeronautics and Space Administration

Page intentionally left blank

Page intentionally left blank

CONTENTS

Page

FOREWORD ---------- III
Maurice Dubin

PREFACE ---------- V
Gilmer A. Gary

SESSION I:
TAIL FORM, STRUCTURE, AND EVOLUTION

Skylab Visual Observation of Comet Kohoutek ---------- 3
Edward G. Gibson

Large-Scale Observations of the Ion Tail From the Joint Observatory for Cometary Research ---------- 15
John C. Brandt

Photography of Comet Kohoutek by the Skylab White Light Coronagraph --- 19
Robert M. MacQueen, J. T. Gosling, E. Hildner, R. H. Munro, A. I. Poland, C. L. Ross, H. U. Keller, and H. U. Schmidt

The Anti-Tail of Comet Kohoutek ---------- 21
Zdenek Sekanina

Interpretation of the Anti-Tail of Comet Kohoutek as a Particle Flow Phenomenon ---------- 27
G. A. Gary and C. R. O'Dell

Hale Observatories' Photographs of Comet Kohoutek ---------- 31
Charles T. Kowal

SESSION II:
H_2O-RELATED OBSERVATIONS

Mariner 10 Observations of Comet Kohoutek ---------- 35
A. L. Broadfoot, M. J. S. Belton, M. B. McElroy, and S. Kumar

S201 Far-Ultraviolet Photographs of Comet Kohoutek From Skylab 4 (Preliminary Report) ---------- 37
Thornton L. Page

Page

Observations of Comet Kohoutek (1973f) With a Ground-Based Fabry-Perot Spectrometer ---- 77
David H. Huppler, Fred L. Roesler, Frank Scherb, and John T. Trauger

Observations of Comet Kohoutek (1973f) in the Resonance Light ($A^2\Sigma^+$-$\chi^2\pi$) of the Radical OH ---- 81
Jacques E. Blamont and M. Festou

Ultraviolet Hydroxyl Observations of Comet Kohoutek on January 24, 1974 ---- 83
Gale A. Harvey

Ground-Based Near-Ultraviolet Observations of Comet Kohoutek ---- 87
Arthur L. Lane, Alan N. Stockton, and Frederick H. Mies

Comet Kohoutek Observations from Copernicus ---- 95
J. F. Drake and E. B. Jenkins

OH Observation of Comet Kohoutek (1973f) at 18-cm Wavelength ---- 97
F. Biraud, G. Bourgois, J. Crovisier, R. Fillit, E. Gérard, and I. Kazes

Ultraviolet Fluorescent Pumping of OH-18-cm Radiation in Comets ---- 101
Frederick H. Mies

H_2O^+ in the Tail Spectrum of Comet Kohoutek (1973f) ---- 103
P. A. Wehinger and S. Wyckoff

Rocket Ultraviolet Images and Spectrum of Comet Kohoutek ---- 107
C. B. Opal, G. R. Carruthers, D. K. Prinz, and R. R. Meier

Rocket Ultraviolet Spectrophotometry of Comet Kohoutek (1973f) ---- 109
Paul D. Feldman, P. Z. Takacs, W. G. Fastie, and B. Donn

Observations of the Hydrogen Ly-α (1216Å) Emission Line of Comet Kohoutek (1973f) by the Skylab/ATM S082B Spectrograph ---- 113
Horst Uwe Keller, J. D. Bohlin, and R. Tousey

SESSION III: MOLECULES AND ATOMS IN THE COMA AND TAIL

Detection of Methyl Cyanide in Comet Kohoutek ---- 119
B. L. Ulich and E. K. Conklin

Detection of HCN Radio Emission From Comet Kohoutek (1973f) ---- 123
L. E. Snyder, W. F. Huebner, and D. Buhl

Observations of Comet Kohoutek With Skylab Experiment S019 ---- 129
Karl G. Henize, A. L. Lane, J. D. Wray, G. F. Benedict, and S. B. Parsons

λ9-cm CH Emission in Comet Kohoutek (1973f) ---- 135
J. H. Black, E. J. Chaisson, J. A. Ball, H. Penfield, and A. E. Lilley

The $^{12}C/^{13}C$ Ratio in Comet Kohoutek (1973f) ---- 137
A. C. Danks, D. L. Lambert, and C. Arpigny

On the Structure of the Nucleus of Comet Kohoutek (1973f) ---- 145
W. F. Huebner

Page

High-Resolution Spectrophotometry of Selected Features in the 1.1-Micron Spectrum of Comet Kohoutek (1973f) (Summary) ---------- 153
David D. Meisel and Richard A. Berg

An Upper Limit for Methane Production From Comet Kohoutek by High-Resolution Tilting-Filter Photometry at 3.3 μ ---------- 155
A. E. Roche, C. B. Cosmovici, S. Drapatz, K. W. Michel, and W. C. Wells

A Search for Extreme Ultraviolet Radiation From Comet Kohoutek ---------- 159
Guenter R. Riegler and Gordon P. Garmire

Ultraviolet (2558 Å) Photography of Comet Kohoutek Using S-183 on Skylab 161
Georges Courtes, Michel Laget, Andre Vuillemin, and Harry L. Atkins

SESSION IV:
PHOTOMETRY AND RADIOMETRY

Observations of Comet Kohoutek at Wavelengths From 0.55 μ to 18 μ ------ 167
Edward P. Ney

Infrared Observations of Comet Kohoutek ---------- 175
G. H. Rieke, Frank J. Low, T. A. Lee, and W. Wisniewski

Photographic Photometry From Skylab ---------- 183
P. D. Craven, R. V. Hembree, and Charles A. Lundquist

The Detection of Continuum Microwave Emission From Comet Kohoutek (1973f) ---------- 185
Stephen P. Maran, Robert W. Hobbs, John C. Brandt, William J. Webster, Jr., and K. S. Krishna Swamy

Upper Limit on the Radar Cross Section of Comet Kohoutek ---------- 189
Eric J. Chaisson, R. P. Ingalls, A. E. E. Rogers, and I. I. Shapiro

An Analysis of the Visual Magnitude of Comet Kohoutek ---------- 193
William A. Deutschman

Physical Interpretation of the Brightness Variation of Comet Kohoutek ------ 195
A. H. Delsemme

On Predicting the Brightness of Comets ---------- 205
E. J. Öpik

Dynamical and Colorimetric Study of the Dust Tail of Comet Kohoutek ----- 209
Bruno J. Jambor

SESSION V:
SUMMARY TALKS AND DISCUSSION

Molecular Processes in the Cometary Coma and Tail ---------- 219
A. H. Delsemme

Implications for Models and Origin of the Nucleus ---------- 227
Fred L. Whipple

Spectroscopy of the Coma and Tail ---------- 233
George Herbig

	Page
Physics of the Tail *John C. Brandt*	237
Discussions of Session V	241
APPENDIX 1. List of Participants	247
APPENDIX 2. Author Index	251
APPENDIX 3. Photograph Identification	253
APPENDIX 4. Comprehensive Ephemeris of Comet Kohoutek (1973f)	255

SESSION I:

SKYLAB VISUAL OBSERVATION OF COMET KOHOUTEK

EDWARD G. GIBSON
Johnson Space Center

Visual observations of Comet Kohoutek were made during the flight of Skylab 3. Sketches based on these observations were made on the 9 days following perihelion. During this time period, the comet could be observed from Skylab unobstructed by space station structure, but it could not be properly observed from the ground. These sketches, which were put on downlink TV, were not in the pre-mission plans and were drawn when the crew could find free time. Ten-power binoculars were used to aid in most of the observations. The sketches were made in black and white by the author and then reviewed by the other two crewmembers, Commander Gerald P. Carr and Pilot William R. Pogue, to ensure that the sketches were consistent with their observations. Following the flight the author made color sketches corresponding to each of the in-flight sketches. Both the original black and white and the color sketches are presented in figures 1 through 11.

Figure 1 shows how the comet appeared approximately 10 days before perihelion. After this time it was occulted by space station structure until perihelion. On December 29, 1973, one day after perihelion, the comet was first seen while the author was outside during extravehicular activity (EVA) looking through a sun visor. The comet was extremely bright and its most unusual feature was a sunward spike (figure 2). This spike was faint in relation to the coma and tail immediately behind the coma. A very faint diffuse feature could be seen in the acute angle between the spike and tail.

The format of figure 2 is used in all of the remaining figures except the last. The nomenclature in the upper right-hand corner shows how the comet was observed; either during EVA, out of the No. 3 window of Skylab's structural transition section (STS_3), or out of the No. 1 window of the command module (CM_1). The length of the comet is given in degrees (4–5°) and, because of the public use of the TV downlink, it was also given in a compre-

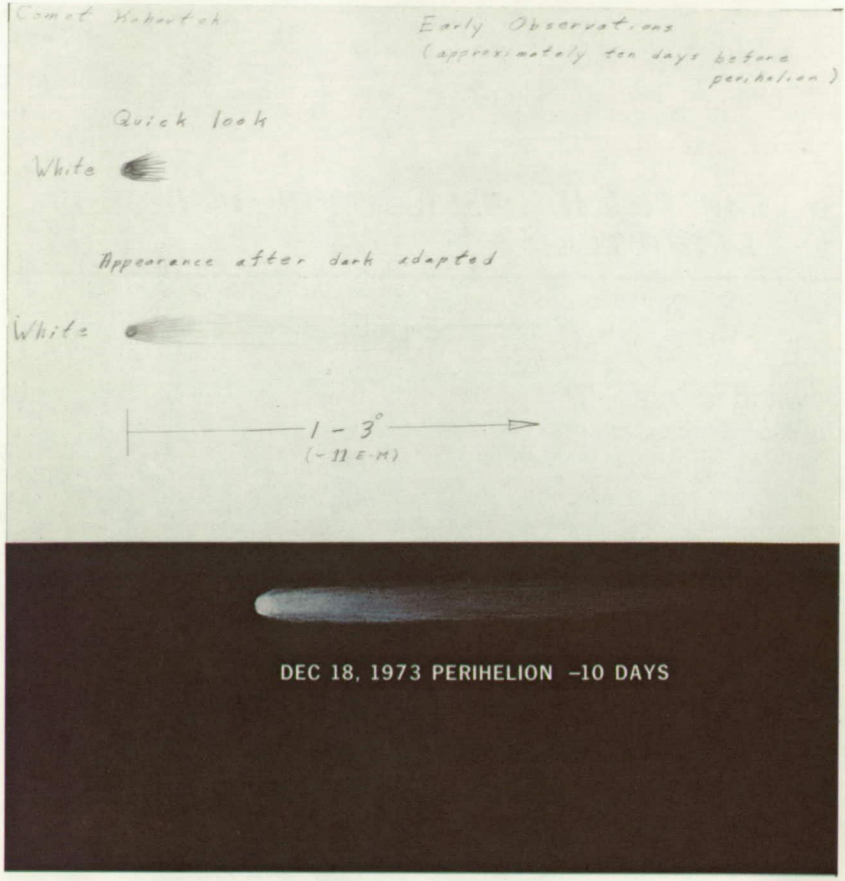

FIGURE 1.—*December 18, 1973: Perihelion minus 10 days.*

hendible physical length, 25 E–M or 25 Earth-Moon distances. The top sketch presents a somewhat subjective picture of the comet in which the darker color implies a higher observed brightness. The middle sketch is an attempt to show what the isophotes would look like, if we had been able to measure them. The bottom sketch, which was made postflight, is an attempt to illustrate the observed color, texture, intensity, and form. White is used to imply a higher intensity even though the color itself may be uniform. Figure 11 is a compilation of all of the color sketches.

Figures 2 through 11 show that the appearance of the comet changed appreciably in form, color, texture, and length after perihelion. The sunward spike, so evident on one day after perihelion ($p + 1$) faded away until on $p + 5$ it was no longer visible to the eye. The color, which was essentially white before perihelion, was yellow on $p + 1$. Because the spike was relatively faint, its color was very difficult to perceive. On $p + 2$ the comet had a

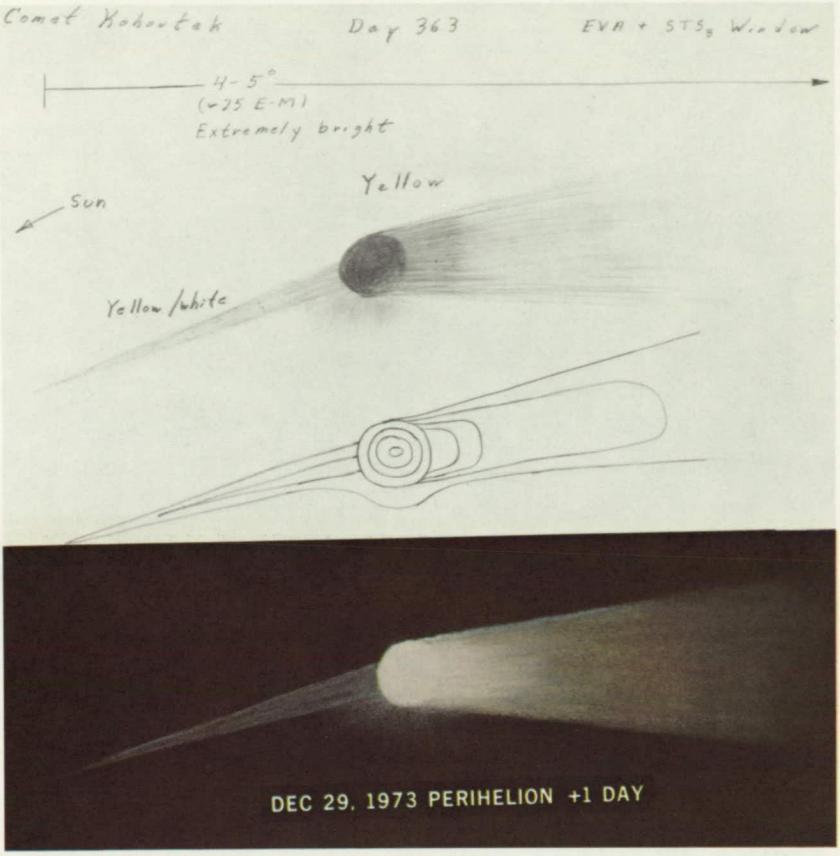

FIGURE 2.—*December 29, 1973: Perihelion plus 1 day.*

very definite orange cast but returned to yellow on $p + 3$. By $p + 5$ the comet appeared white which gave way to a white with a violet cast and a mottled appearance in the tail by $p + 8$. The mottling which is drawn is an attempt to indicate its nature but not its exact geometry.

The apparent length of the comet's tail also underwent some interesting changes. It increased from approximately 2–3° on $p + 1$ to 5–6° on $p + 3$ most likely because the axis of the tail became more normal to the line of sight and its apparent distance from the disk of the Sun increased so that the eye became better adapted as it attempted to focus only on the comet. Since we were moving around the Earth at approximately 4 degrees per minute, the time between sunset and cometset was short during this time period. By $p + 5$ the apparent length of the comet had decreased to 4–5°, primarily because of the increase in its actual radial distance from the Sun. From $p + 5$ to $p + 7$ the apparent length of the tail increased to 6–7°. This probably resulted

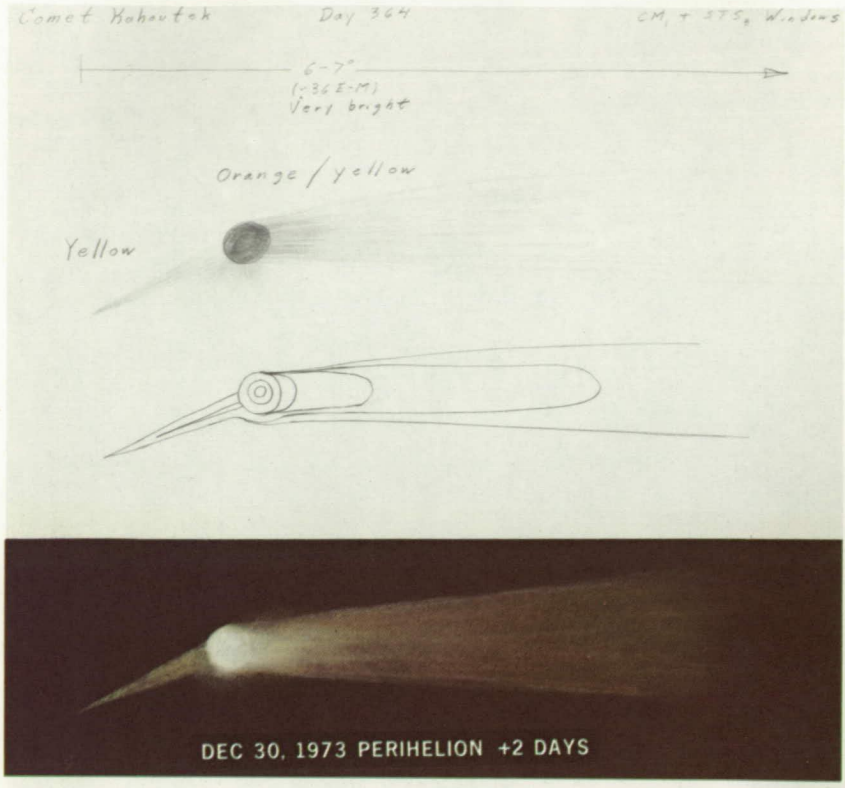

FIGURE 3.—*December 30, 1973: Perihelion plus 2 days.*

from the ability of the eye to properly dark adapt and perceive the very faint features of the tail when the air glow was no longer in front of or immediately adjacent to the comet. After $p + 7$, however, the apparent length and the brightness of the comet decreased as it continued to move away from the Sun.

Two separate tails of the comet, dust and gas, were looked for but not observed. Only the transition from a uniform white/yellow texture to a mottled white/violet texture was observed. At the time of the observations it was assumed that this corresponded to a transition from observation of the dust to observation of the gas in the tail.

DISCUSSION

LANE: In your isophote drawings of the coma, you seem to show relatively concentric circles without compression on the sunside. Do you have any feeling or recollection of any nonconcentric isotopes? Or was the brightness

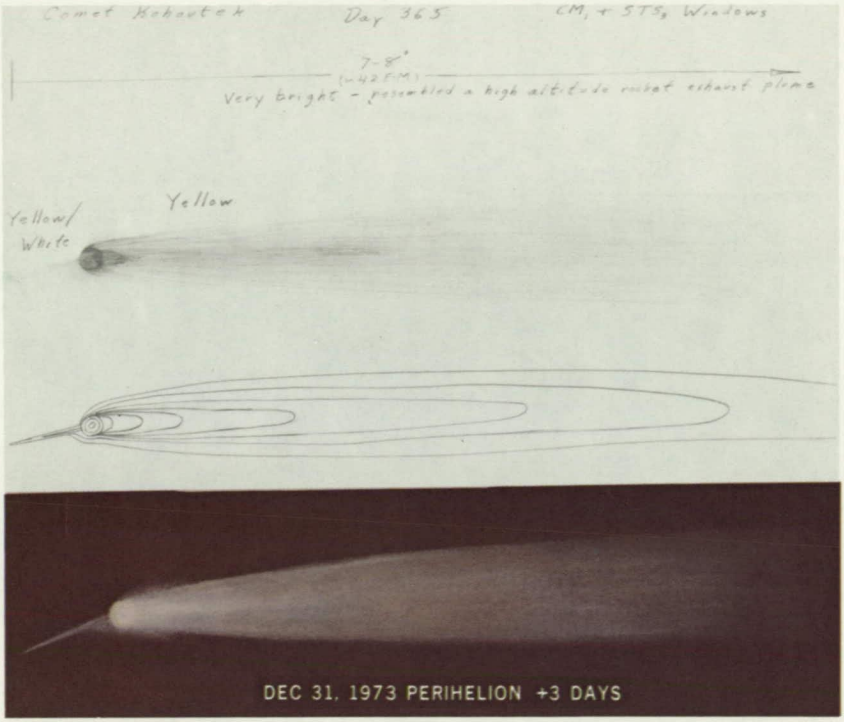

FIGURE 4.—*December 31, 1973: Perihelion plus 3 days.*

so great that you could not tell if there was any variation or compression on the sunside?

GIBSON: We could see that the center of the coma was much brighter than the outside, but could not see that level of detail which was below our perception.

DRYER: In looking at the sketches, am I correct that you definitely would see some waviness in the tail?

GIBSON: Yes. We used binoculars to observe the comet once it got 3 or 4 days past perihelion. We used them before but it was essentially afterward that we noticed that appearance. Waviness is not the best word, but a mottled appearance where some areas were lighter and darker than others.

DRYER: It is very reminiscent of Karman vortices within the tail.

GIBSON: I wouldn't attribute Karman vortices to it. It may have been, but we did not see that level of detail. We did not try to duplicate every blotch or every high point and low point, but strictly to pick up characteristics of it.

KELLER: How long would you estimate the spike was on December 29?

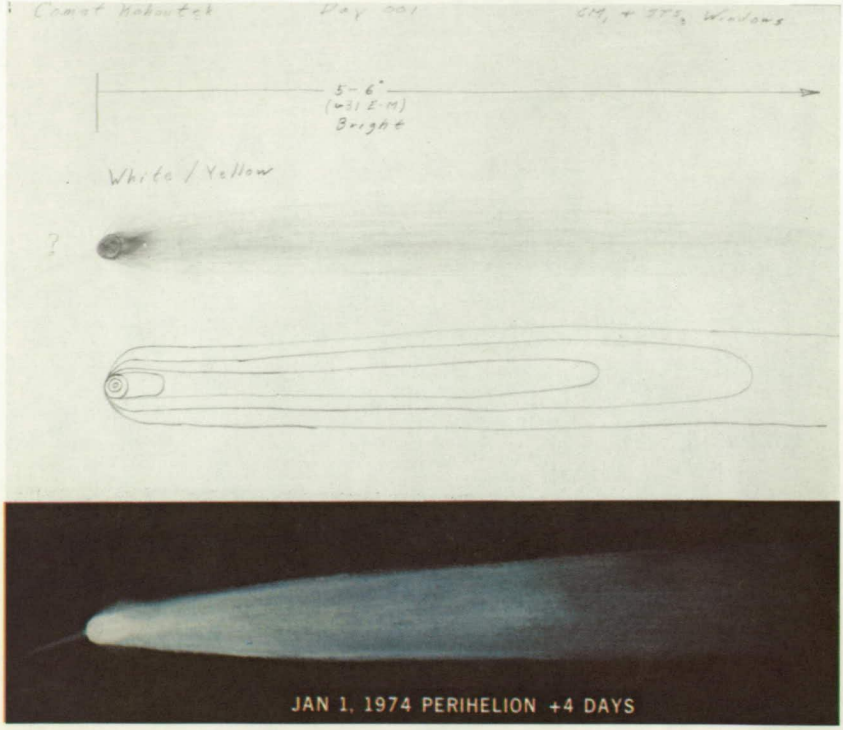

FIGURE 5.—*January 1 1974: Perihelion plus 4 days.*

GIBSON: I would estimate maybe 2° or so.

SEKANINA: I just wonder whether the comet was above the airglow during the time when you observed the anti-tail. And what would you say about the rise of the anti-tail? Was there a rapid change in brightness?

GIBSON: It was a very strong function of how far it was from the Sun, in that when you look at it where it is against or very close to the airglow, you have a tough time distinguishing it. Once it gets above that layer and you are able to get dark adapted, then you are able to see it against the black of the sky and we could get a better look at it.

SEKANINA: Could you compare it with the ground-base conditions?

GIBSON: I would think you are better off up there once you are away from the airglow.

NEY: Question about the tail compared to the anti-tail. First, the feeling that you had about the relevant colors; second, the anti-tail was easily visible. At what point in the anti-tail did you feel the surface brightness was the same as it was in the tail? How much farther did you have to look out in the tail to get a comparative brightness with the anti-tail?

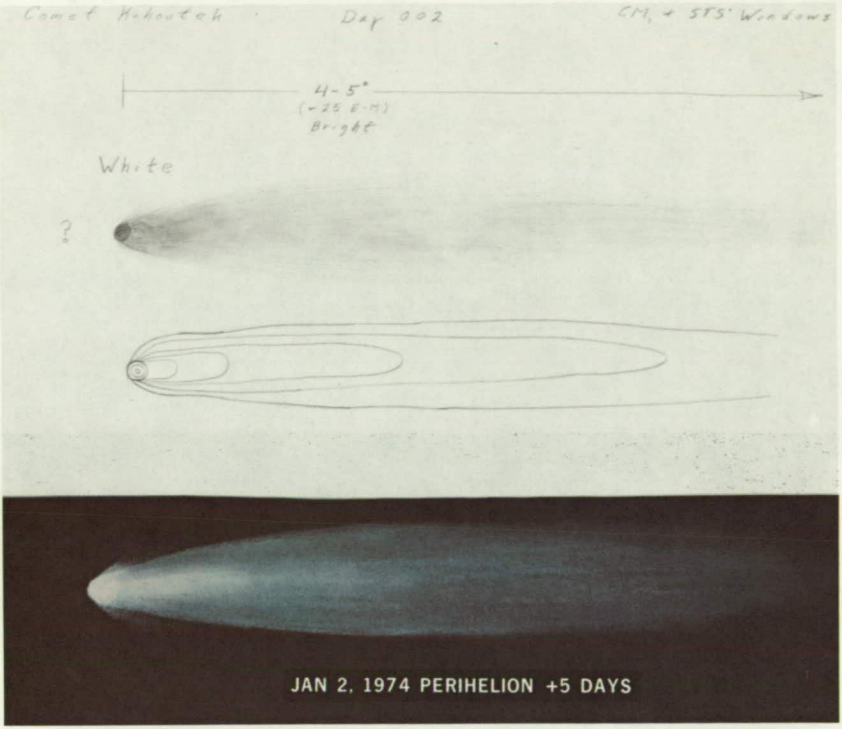

FIGURE 6.—*January 2, 1974: Perihelion plus 5 days.*

GIBSON: You are pushing us and it's good that you do but, first of all, the color: when we looked at it and said it was yellow or orange, it was a general overall appearance, and when we looked at it one day after perihelion the comet was all yellow. We could get a general yellow color across the whole comet and looked at the anti-tail and could say its color is not inconsistent with the whole comet, but it's not white. It's pretty much the same color as the other. There may have been some differences.

WHIPPLE: Your picture said yellow/white in the anti-tail and yellow in the tail.

GIBSON: It referred to the front part in the coma. The coma itself was more intense and therefore perhaps appeared to us as slightly more white than the darker part of the tail further back. I don't think that was meant to be attributed to the anti-tail itself, which was very faint. I don't think we had very good perception of even the intensity function or distances.

SEKANINA: I just would like to ask you, can one basically say that you had more difficulty with distinguishing the color of the anti-tail because it was faint and therefore colorless?

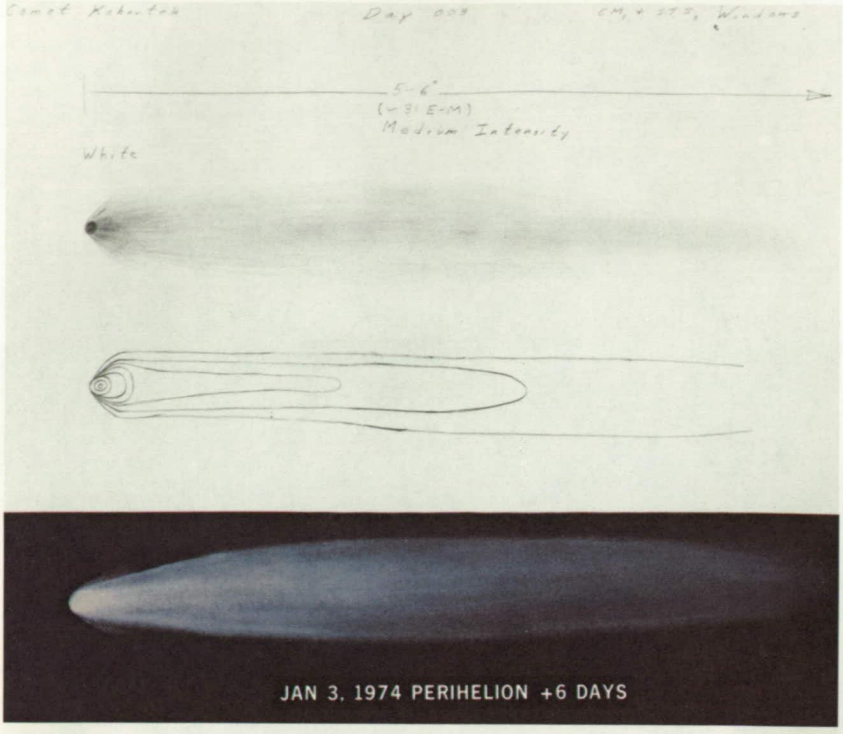
Comet Kohoutek
Day 003
CM, + STS, Windows
5-6°
(~3 E-M)
Medium Intensity
White
JAN 3, 1974 PERIHELION +6 DAYS

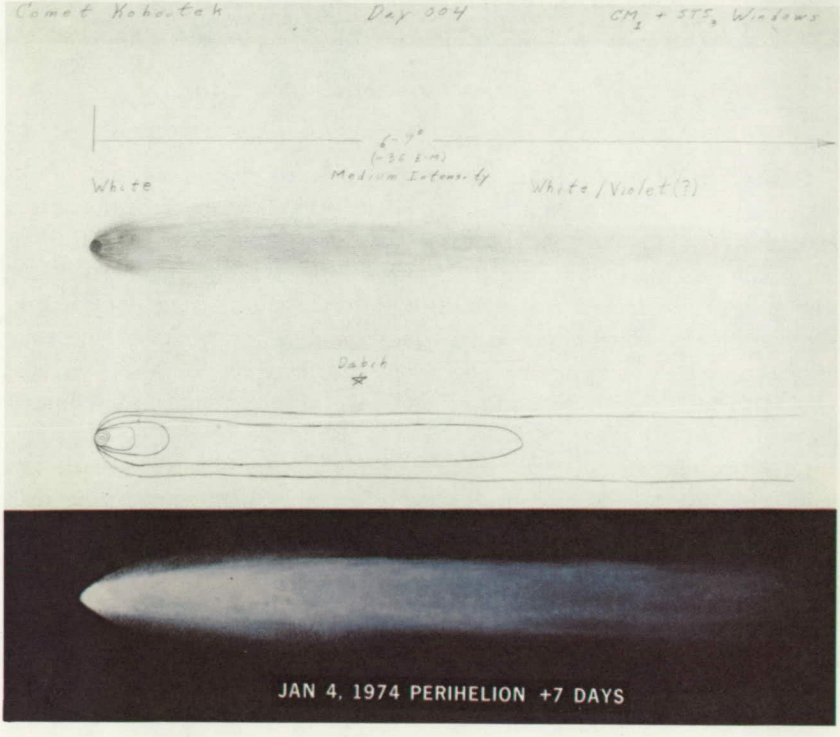
Comet Kohoutek
Day 004
CM, + STS, Windows
6-7°
(~3 E-M)
Medium Intensity
White
White / Violet (?)
Dubhe
JAN 4, 1974 PERIHELION +7 DAYS

← FIGURE 7.—*January 3, 1974: perihelion plus 6 days.*

↙ FIGURE 8.—*January 4, 1974: Perihelion plus 7 days.*

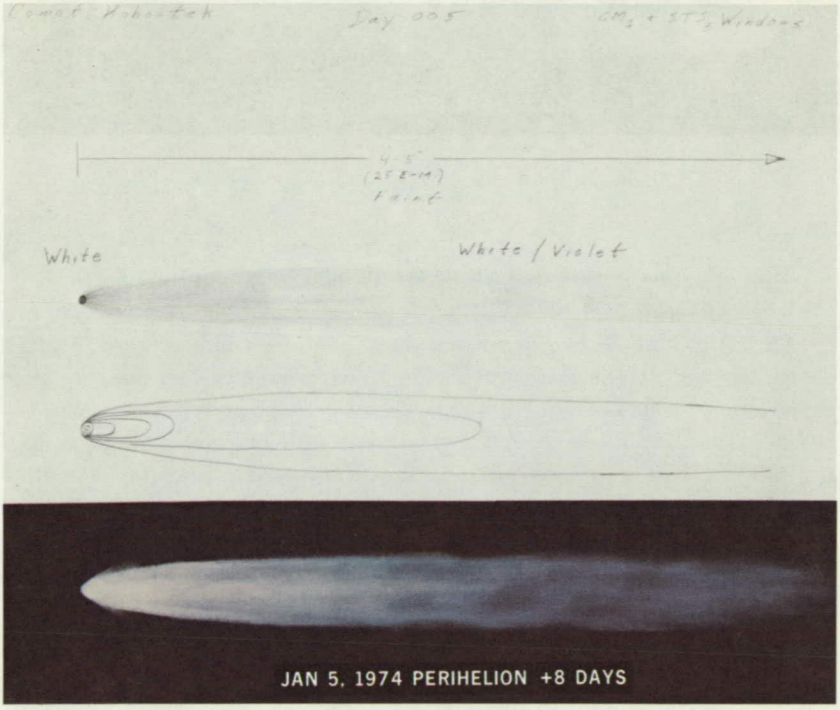

FIGURE 9.—*January 5, 1974: Perihelion plus 8 days.*

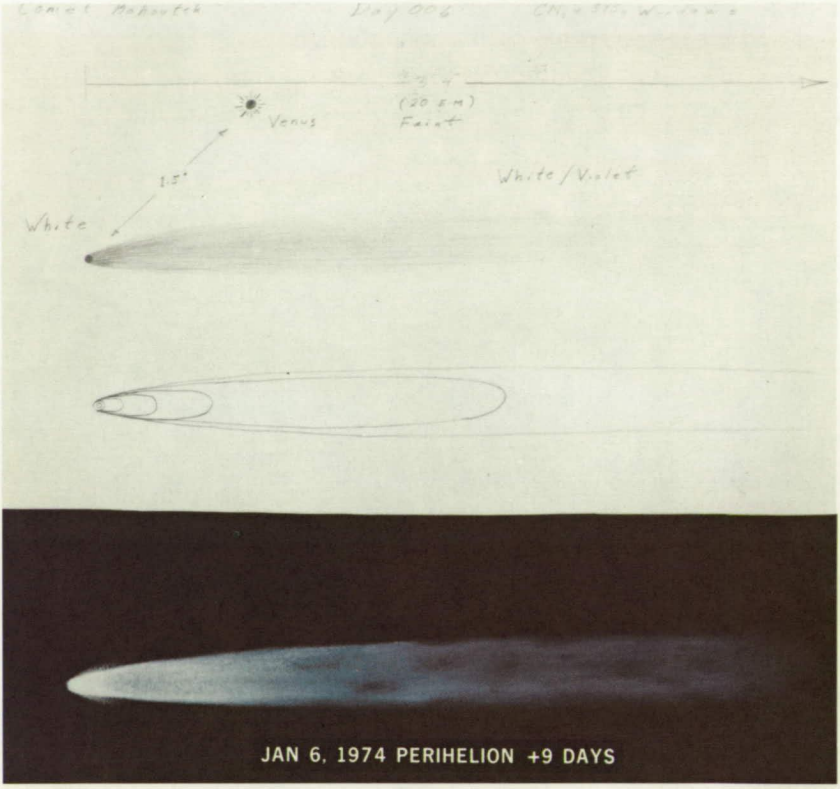

FIGURE 10.—*January 6, 1974: Perihelion plus 9 days.*

GIBSON: That is correct. I would be the first to say, because it was faint —we had a difficult time doing that.

JAMBOR: I would like to ask you three questions which concern the days of one day and two days after perihelion. You mentioned that one day after perihelion you were observing during EVA. Where did you observe it when it was two days after perihelion? If I gave you a scale of pale, medium, bright, and brilliant, how would you describe the colors one day and two days after perihelion? Looking at the sketches we have that are 10 days after perihelion, the tail was kind of narrow and whitish, whereas, one and two days after perihelion you drew it very broad, which suggests that it could be due to dust particles.

GIBSON: I will take your last question first. It did appear to us that it was rather broad in a relative sense. You must realize that the comet was 4 to 5 degrees as compared with the other days when it was always twice that in length so that you got to look at the true geometry of it. It did appear in a

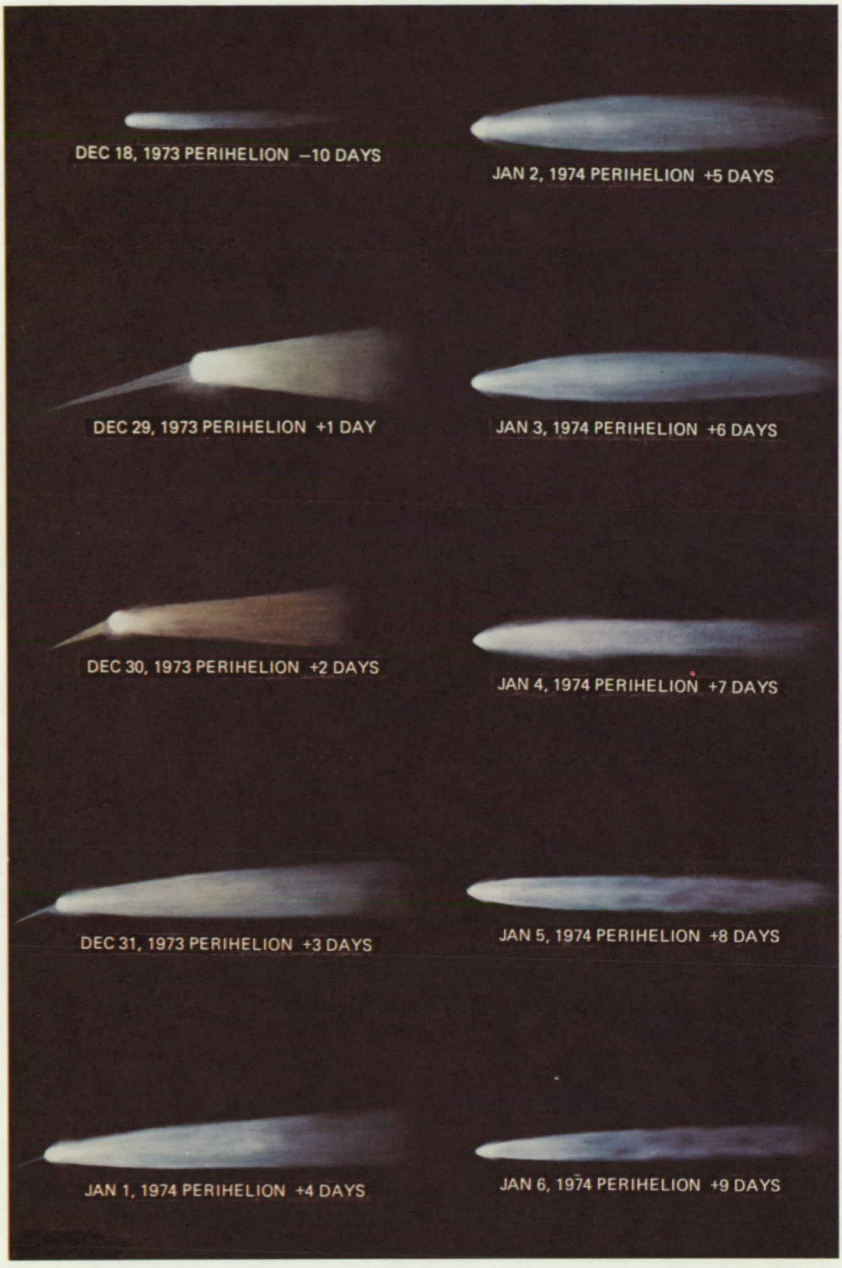

FIGURE 11.—*Ten sketches of Comet Kohoutek, showing observed changes in the comet's appearance between December 18, 1973 (perihelion minus 10 days), and January 6, 1974 (perihelion plus 9 days).*

relative sense that the tail was broader one day after perihelion. Now as far as colors and intensities, I am going to skirt your question by saying, what we saw I put down in the drawings and the color sketches, and have tried to put in the intensities. Maybe I am missing the point of your question. Is there something which is not there on those colored drawings which you feel is some additional information which I can give you?

JAMBOR: Really, what I am trying to say is, did you see the colors as something definite or very bright, or did you see a general hue?

GIBSON: A general hue, although you could look at the coma and see that it was brighter and appeared whiter because of it.

JAMBOR: Two days after perihelion you mentioned different colors. Were you able to differentiate between orange and yellow then?

GIBSON: We questioned ourselves on it and the answer is "Yes." We did see it on the first day of EVA but when we came back inside we noticed we could then see it out from behind Transition Structure Window No. 3.

LARGE-SCALE OBSERVATIONS OF THE ION TAIL FROM THE JOINT OBSERVATORY FOR COMETARY RESEARCH

JOHN C. BRANDT
Laboratory for Solar Physics and Astrophysics
Goddard Space Flight Center

Clear skies in central New Mexico during mid-January enabled us to obtain a good series of comet photographs from a new, fully dedicated comet observatory. The Joint Observatory for Cometary Research (JOCR) is located near Socorro, New Mexico, at an altitude of 10 615 feet and is operated by the Laboratory for Solar Physics and Astrophysics, Goddard Space Flight Center and the New Mexico Institute of Mining and Technology. The principal instrument is an $f/2$ Schmidt camera which records an 8-degree by 10-degree field on 4- by 5-inch plates or film. The observatory also has a 16-inch Boller and Chivens telescope used for photometry.

The comet was extensively observed during the period January 9 through January 27, 1974. The comet was an object visible with the naked eye from the Joint Observatory for Cometary Research during this entire period, and was an impressive object on a few days around January 14. Color photographs of the comet were obtained and show the (blue) ion tail quite clearly, but no dust tail. This confirms the general impression that the normal type 2 (dust) tail was much weaker, for example, than in Comet Bennett. On January 14, 1974, Universal Time (UT), offset photographs of Comet Kohoutek traced the type 1 (ion) tail to a distance of 0.333 AU from the nucleus.

Several structures were observed in the ion tail of Comet Kohoutek at distances approximately 0.1 AU from the head, and two of these will be discussed here. Details concerning these events are discussed by Hyder, Brandt, and Roosen (*Icarus,* The Comet Kohoutek Issue, (1974) 23,601). On January 11, 1974 (UT), we observe a large tail structure resembling a swan-like cloud. The "Swan" was 7° or 15 million km from the head and had a characteristic size of 5 million km. (See figure 1.) The entire structure is traveling down the tail at a velocity of approximately 250 km/s. We have searched the available literature for solar and solar wind events that could have been respon-

FIGURE 1.—*JOCR photograph of Comet Kohoutek taken on January 11, 1974 (UT), showing the "Swan" cloud in the lower, right-hand corner.*

sible for the "Swan." Although the spacecraft information is far from complete, our preliminary conclusion is that there is no obvious solar event responsible. On the other hand, the "Swan" may be an advanced state of the kink instability discussed below.

On January 13, 1974 (UT), we observed a wavy structure in the tail of Comet Kohoutek, which resembles a helix. We have interpreted this helix as the form resulting from the kink instability caused by currents flowing along the tail axis. We have used simplifying assumptions to derive the phase speed of this wave and it turns out to be the Alfvén speed. We can measure the phase speed both from studying our own observations and by comparing our observations with photographs taken with the Palomar Schmidt (figure 2). The speed is 235 km/s. If the CO^+ densities are assumed to be at the low end of the range normally quoted in the literature, i.e., approximately $10/cm^3$, the magnetic field in the tail can be determined and is 100 γ ($=10^{-3}G$). This result represents a cometary magnetic field enhanced by a factor 4 or 5 over the solar wind values.

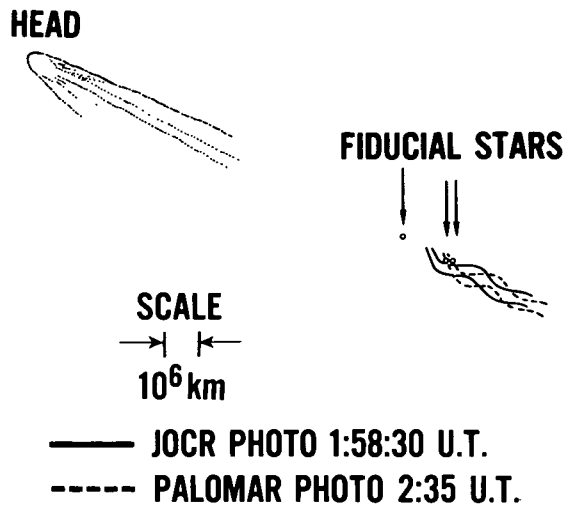

FIGURE 2.—*Schematic diagram showing the change in position of the helical structure photographed on January 13, 1974 (UT).*

DISCUSSION

BELTON: How long did your coverage extend for the comet?

BRANDT: February 19 was our last. After that we could still take long exposures and get a little dot. But images showing some structure and anti-tail do persist on into February. That is when our effective coverage stopped.

LANE: What was the general length of the exposures?

BRANDT: Essentially between 1 and 40 minutes, depending on the day and whether it was an offset. Obviously, as it went farther away from the Sun, we used an increased exposure time.

DUBIN: The "Swan" structure looks like it is not a helix, or not part of the helix.

BRANDT: But the speeds are the same.

DUBIN: Even though there is a much more morphological thing to it?

BRANDT: Yes. Now the numbers do come out differently. One came out 250 km/s and one at 235, but within the accuracy that we can measure (which is 10 percent or so). I don't think it is an accident that both of those features are almost the identical distance from the head, i.e., about a tenth of an AU. This is one of the reasons I suspect that the "Swan" structure is not a detached piece of the comet but is a good finite plasma amplitude wave running down the tail.

DONN: That the intricate structure should be reproduced implies to me that it was a material cloud; therefore, a very complex structure.

BRANDT: I am saying I don't think it is the case. We only have observations on that day that extend over a 20- to 30-minute period. I don't know what it looked like 2 hours before and 2 hours after. If you look at the growth rate for waves of that amplitude and those kinds of conditions—our observations are exactly consistent with that. It is moving not at the Alfvén speed or the solar wind velocity but at an intermediate number.

WEHINGER: I gather the films are all blue sensitive? Did you expose in the red or yellow region?

BRANDT: Photos were made through the red region.

WEHINGER: You see the plasma tail features in the red region?

BRANDT: They are faint but we do see them. We have also taken photographs with filters in combination with the IIa–O which isolates it better into the ultraviolet. So it gives us much better contrast with respect to the sky. We have taken some IIIa–J's some IIa–E's, and some IIa–F's to be sure that we had some crude spectral coverage. The most efficient way to go about it is to use IIa–O.

BELTON: Is it true that there were no features in the dust tail?

BRANDT: No features that we have any observations on, except the anti-tail.

PHOTOGRAPHY OF COMET KOHOUTEK BY THE SKYLAB WHITE LIGHT CORONAGRAPH

R. M. MACQUEEN
J. T. GOSLING
E. HILDNER
R. H. MUNRO
A. I. POLAND
C. L. ROSS
High Altitude Observatory, National Center for Atmospheric Research [1]

H. U. KELLER
Laboratory for Atmospheric and Space Physics, University of Colorado

H. U. SCHMIDT
Max Planck Institut für Astronomie and Astrophysik

Approximately 1600 photographs of Comet Kohoutek were obtained near the time of perihelion passage. The passband of the instrument was 3500–7000 Å, and linear polaroid filters were sometimes used. The (photographic) photometry of coronagraph photographs is accurate to ±10 percent.

[1] NCAR is sponsored by the National Science Foundation.

Page intentionally left blank

Page intentionally left blank

THE ANTI-TAIL OF COMET KOHOUTEK

Z. SEKANINA
Smithsonian Astrophysical Observatory

The theory of dust comets, formulated by Finson and Probstein (1968) for the case of small emission velocities, has been applied to the anti-tail of Comet Kohoutek. The results, reported here indicate that the anti-tail can be described as a flat formation, confined essentially to the comet's orbit plane and composed of relatively heavy particles (mostly in the size range of 0.1 to 1 mm), whose motions are controlled only by solar gravity and solar radiation pressure. The derived model fits the semiquantitative descriptions of the anti-tail by various observers, including the Skylab 3 astronauts, and allows us to arrive at the following tentative conclusions regarding the properties of the solid particles.

The main body of the anti-tail was made up entirely of the material shed by the comet before perihelion. The onset of appreciable dust production has been established from the position of the sharp edge of the anti-tail on its sunward side. The sharp edge showed up at positional angle $253.0° \pm 0.3°$ on a photograph of the comet, taken at the Pic-du-Midi Observatory on January 17.8, 1974 (UT). (See Sekanina, 1974.) From this we derive that the emission of dust started 210 to 250 days before perihelion at heliocentric distances 3.7 to 4.2 AU, and that the heaviest particles ejected at that time were at least 0.6 to 0.7 mm in diameter (at an assumed density of 1 g/cm^3). Water vapor could not provide the momentum necessary to drag such large grains away from the nuclear surface at the quoted heliocentric distances, except perhaps near the subsolar point. On the other hand, carbon dioxide (and all other substances of a comparable or higher degree of volatility, including hydrogen cyanide and methyl cyanide) should do the work all over the nuclear surface.

The production rate of dust appears to have varied in proportion to about the inverse fourth power of heliocentric distance far from the Sun, less steeply nearer the Sun, and then to have leveled off at 0.2 AU from the Sun. The derived rate is about an order of magnitude higher than the emission rates of micron-sized particles established from studies of the regular type II tails of Comets Arend-Roland and Bennett. Absolute calibration of anti-tail photographs will be necessary to check this result.

The population index s of the differential particle mass distribution $m^{-s}\,dm$ comes out to be near 1.4. The theoretical photometric profiles of the anti-tail, calculated with this value of the population index and with the aforementioned production-rate law, are plotted in figure 1. The value of the population index, which is substantially lower than a commonly accepted value derived from various radio-meteor studies ($s \geq 2$), means a strong relative excess of heavy particles, in which practically all the mass of the anti-tail was concentrated, and can be interpreted as an indication of a severe evaporation effect. If the "intrinsic" population index of the debris from Comet Kohoutek was about 2, the observed value of s may suggest that the particles have lost a significant fraction of their original mass through evaporation near the Sun. The evaporation effect would, of course, also influence the particle dynamics; this aspect of the problem remains to be studied.

Since the evaporation loss of radius depends exponentially on the latent heat of vaporization of the particle material, the above reasoning, if correct, can give a fairly reliable estimate of the effective heat of vaporization from the observed range of particle sizes and the orbital dynamics. The inferred figure lies in the range of 40 to 45 kcal/mole, if the absorptivity of the particles for solar radiation equals their emissivity for reradiation, but may be greater, if the emissivity is lower than the absorptivity. If the latent heat were higher than required, the evaporation effect would be practically negligible and the population index consistent with other determinations. If the latent heat were lower than required, the particles (from the size range under consideration) would have been completely evaporated near perihelion.

Unfortunately, at present we do not know the "intrinsic" population index of the heavy particles that compose the anomalous comet tails. However, a preliminary study of the anti-tail of Comet Arend-Roland (Sekanina, unpublished), where the evaporation effect should be considerably less important, does indeed suggest that s somewhat exceeded 2.

The inferred value of the latent heat of vaporization of 40 kcal/mole or more is much higher than that for sodium. Consequently, sodium, which apparently accounted for the spectacular display of the anti-tail during the early days, must obviously come from more complex substances of a higher effective vaporization heat. Sodium atoms released from such substances can be shown to have emitted, in the D doublet, an energy that may have exceeded by several orders of magnitude the intensity of solar light scattered by the particles shortly after perihelion. Later, as the rate of evaporation of particles subsided with the comet's continuing recession from the Sun, the sodium's contribution to the anti-tail's brightness dropped considerably, and particle scattering clearly prevailed in the anti-tail's light after January 1.

This report is a condensed version of a more comprehensive study of the anti-tail of Comet Kohoutek, which has been published in the journal *Icarus* ((1974) 23, 502).

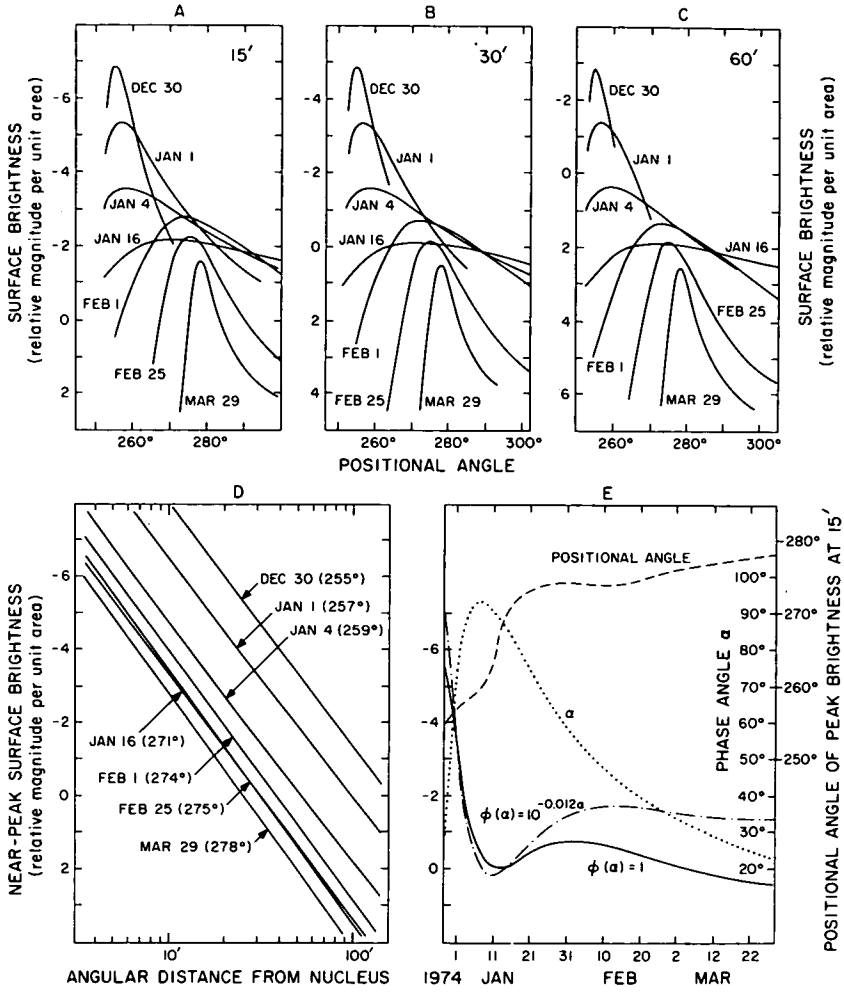

FIGURE 1.—*Calculated photometric profiles of the anti-tail. A,B,C: Surface brightness (assuming a constant phase effect φ (a)) versus positional angle at 15, 30, and 60 arc-min from the nucleus on different days (1973/1974). D: Near-peak surface brightness (assuming a constant phase effect) versus angular distance from the nucleus in the indicated positional angle and on different days (following, approximately, an inverse 2.7 power law, practically independent of time). E: Peak surface brightness for a constant phase law and an asteroidal phase law (normalized in mid-January), positional angle of the peak brightness at 15 arc-min from the nucleus, and phase angle versus time. In all plots, only particle scattering of solar light is considered.*

ACKNOWLEDGMENT

This work was supported by grant NGR 09–015–159 from the National Aeronautics and Space Administration.

REFERENCES

FINSON, M. L.; and PROBSTEIN, R. F.: 1968, Ap. J. 154, 327.
SEKANINA, Z.: 1974, Sky Tel. 47, 374.

DISCUSSION

LANE: What is the effect if you chose your density of 3 g/cc instead of the 1 g/cc?

SEKANINA: The product of density and particle size is a constant, therefore if you increase density by 3 you would have to decrease the particle size by 3.

LANE: But that changes your evaporation phenomenon, does it not?

SEKANINA: That it does, but actually what is involved here is the heat of the evaporation of the particles. The evaporation rate depends strongly on the evaporation heat. We still come up with a fairly reasonable estimate for the heat of evaporation of the particles and that comes up to about 40 to 45 kcal/mole.

WHIPPLE: A comment on assuming density 3: I think it is completely out of the order of magnitude of practicality. In the Geminied meteor showers from an old comet the resolved densities are still low, well below unity. I want to discourage any serious calculation based upon a density much above water.

KELLER: Observations by the crew pointed out that dust and the tail length of the comet increased very rapidly after perihelion up to 7 to 8 degrees and if you make some calculations you need $1-\mu$ values larger than one, up to ten. Therefore, you need very small particles or you have to include evaporation effects. The decrease afterwards may be due to the effect of evaporation cleaning up the particles.

SEKANINA: We basically come up with the evaporation rate of something like 0.1 mm per revolution—which means that all particles smaller than that evaporate completely. This also explains the situation that there was practically no dust coming from the comet after perihelion. Because the dust evaporated almost immediately after it was released, we could not see it. In a regular dust tail we see particles 10 or 20 days old, but in this case the Sun evaporated micron-size particles in about one day or a tenth of a day.

KELLER: How does this argument compare with Ikeya-Seki, which shows the definite dust tail after perihelion passage?

SEKANINA: One possibility, of course, is that this is a new comet. Ikeya-Seki is definitely not a new comet. In Ikeya-Seki the iron particles, if you work with 80 or 90 kcal/mole, such particles are untouched. You get evaporation rates of 10^{-18} cm per revolution.

BELTON: Did you mean to say that the Ikeya-Seki was not a new comet?

SEKANINA: Definitely not. Ikeya-Seki was not a new comet in the Oort-Schmidt sense. It is a very old comet. It did not come from the Oort cloud since its period was 1000 years or something like that. It is a very old comet in the cosmological term.

MENDIS: In all these calculations for the particle size, you assign a value for $1-\mu$ and do not allow variation in that.

SEKANINA: That is correct. This is something that remains to be done.

MENDIS: For water-ice material, this picture is completely misleading.

SEKANINA: It would be misleading if the characteristic of the particles were basically icy. We are pretty sure since we see the particles after perihelion that the material must be in the range of about 40 to 45 kcal/mole.

MENDIS: You see particle sizes of almost a centimeter?

SEKANINA: I would say millimeter size and if we assume lower densities we can go up to centimeters.

MENDIS: It's inconceivable how you can get particles of this size by normal reactions.

SEKANINA: It's inconceivable if you assume H_2O. It's not inconceivable if you assume more volatile substances in the comet. I came up with the conclusion from a study of distant comets that some of the tails are formed at 15 AU. And you can still assume that submillimeter particles are coming off at 15 AU if you have methane or carbon dioxide.

Page intentionally left blank

Page intentionally left blank

INTERPRETATION OF THE ANTI-TAIL OF COMET KOHOUTEK AS A PARTICLE FLOW PHENOMENON

G. A. GARY
C. R. O'DELL
Marshall Space Flight Center

The theory of Finson and Probstein (1968) was amended to include the gravitational field of the comet nucleus for very large particles. The addition of the gravitation term to the derivation of the terminal velocity V of the particle from the coma gives the following result:

$$V^2=\frac{9V_g^2}{\beta}-\frac{2GM_c}{R_n}$$

where V_g is the thermal velocity of the expanding gas, G is the gravitational constant, M_c is the total mass of the nucleus, R_n is the radius of the comet nucleus, and β is the dimensionless parameter.

An important result of considering gravity is that at any time there will be a maximum size for particles lost. Our theory was tested by comparison of orientation, brightness, and form of the anti-tail of Comet Kohoutek. It can be shown that the shape and orientation are satisfactory. The apparent length of the spike can be a measure of the particle size (d) and the density (p_d), and a value of $p_d d = 0.004$ g/cm^2 fits the Skylab crew observation. The width of the tail at the coma is established by the increased gas velocity and rate of mass lost at small heliocentric distances.

The dominant size ($p_d d = 0.004$) contributing to the observed spike directly establishes the presence of large particles in this comet. The size is about 100 times larger than that of particles dominating the type II tail.

This would be the first direct evidence for cometary loss of those particles large enough to account for the observed meteor showers. It has been widely known that those particles coming off the comet with significant velocities will be rapidly dispersed; however, this model, like Whipple's original discussion, means that there will always be some particles coming off with nearly zero relative velocity.

An immediate question that arises is "What is the nature of these particles?" We know that the largest volume of particulate material ejected by the comets is about $p_a d/Q_{rp} \simeq 5 \times 10^{-5}$ g/cm^{-2} (O'Dell, 1974); therefore, of much smaller size. Two major possibilities exist: the large particles are larger forms of the same basic structures as the small particles, or the large particles are composites of the small particles. If the former is true, then the presence on the comet surface of large solid particles has an important evolutionary impact. This would mean that at any inner solar system passage selectively more of the fine particles would be removed, leaving relatively more of the coarse particles on the surface. This would mean progressive change to a very coarse surface texture, which would be highly insulating and could account for the changes of photometric nuclear diameter, intrinsic luminosity and change to a gas-dominated spectrum that is observed in old comets (O'Dell, 1973). The alternate interpretation—that the large particles are composites of small particles—may be confirmed by studies of meteor streams. Jacchia (1963) has determined that meteors associated with identifiable comets have a much greater fragility than those of apparently asteroidal origin. This would be entirely consistent with the larger cometary particles, presumably the ones forming the visual meteors in these showers, being low-strength composites of the basic particles which are much smaller.

NOTE: The complete paper has been published in the journal *Icarus* ((1974) 23, 519).

REFERENCES

FINSON, M. L.; and PROBSTEIN, R. F.: 1968, Astrophys. J. 154, 327.
JACCHIA, L. G.: 1963, The Solar System, Volume 4 (B. M. Middlehurst and G. P. KUIPER, eds.). The University of Chicago Press, Chicago.
O'DELL, C. R.: 1973, Icarus 19, 137.
———: 1974, Icarus 21, 96.

DISCUSSION

BRANDT: Are the last three speakers basically saying the same thing? I have seen divergent approaches to this problem, and some similarity of results, and different emphasis. Are the last three speakers basically interpreting it the same way?

GARY: I think all of us are saying that the spike is a result of particles of about a 10th of a millimeter or in that range. And it can be derived from the Finson-Probstein ejection model and with the correct orbital mechanics. There are unique differences between the different models presented. We have included the gravitation term.

SEKANINA: Absolutely. I would like to say that as far as some minor differences between the three presentations are concerned, this can possibly be

explained in terms of the fact that none of us has had at his disposal the perfect comet treatment. And therefore, everybody simply tries to substitute for this something that he felt would be the next best method. And according to that, I believe that there could be some minor differences which should be clear when one can sit down and formulate a photometric profile. But we are still waiting for measurements from observations before we can claim anything specific.

WHIPPLE: Point of clarification: did you use just $p_d d = 4 \times 10^{-3}$?

GARY: No, but that was the best fit.

Page intentionally left blank

Page intentionally left blank

HALE OBSERVATORIES' PHOTOGRAPHS OF COMET KOHOUTEK

CHARLES T. KOWAL
Hale Observatories
California Institute of Technology
Carnegie Institution of Washington

In the summer of 1973, before Comet Kohoutek emerged from the vicinity of the Sun, users of the Schmidt telescopes at Palomar Mountain were asked to obtain photographs of the comet whenever possible. Many photographs were taken with both the 48-inch and the 18-inch Schmidt cameras. Generally, the plates were taken on blue-sensitive emulsions, or with panchromatic emulsions and a yellow filter. Table I lists the 48-inch plates which were obtained. Prints of those plates marked with an asterisk are available from the California Institute of Technology Bookstore, Pasadena, California 91109.

Table I.—*Schmidt Camera Photographs of Comet Kohoutek*

Plate Number	Date 1973	UT	Plate and Filter	Exposure (minutes)
PS-9463	Oct 25	12:21	103a-O —	5
PS-9480	Oct 27	12:17	IIIa-J+Wr. 2c	15
PS-9500	Oct 30	12:37	103a-O+GG13	5
*PS-9513	Oct 31	12:18	103a-O+GG13	7
PS-9619	Nov 24	12:15	103a-O+GG13	10
PS-9620	Nov 24	12:42	103a-O+GG13	6
*PS-9621	Nov 24	12:58	103a-D+Wr. 12	12
*PS-9655	Dec 1	12:48	103a-O+GG13	10
	1974			
*PS-9702	Jan 13	02:35	103a-O —	3
PS-9703	Jan 13	02:45	103a-D+yellow plexiglass	10
PS-9704	Jan 13	03:05	103a-O —	4
*PS-9708	Jan 15	02:32	103a-O —	3
*PS-9709	Jan 15	02:49	103a-D+yellow plexiglass	8

Table I.—*Schmidt Camera Photographs of Comet Kohoutek*—Concluded

Plate Number	Date 1974	UT	Plate and Filter	Exposure (minutes)
PS-9710	Jan 15	03:07	103a-O —	6
*PS-9714	Jan 16	02:43	103a-O —	3
*PS-9715	Jan 16	02:58	103a-O —	3
PS-9727	Jan 22	02:42	103a-O —	3
PS-9728	Jan 22	02:58	103a-D+yellow plexiglass	6
PS-9740	Jan 25	02:48	103a-D+yellow plexiglass	10
PS-9741	Jan 25	03:10	103a-O —	5
PS-9751	Jan 26	03:21	103a-O —	3
PS-9752	Jan 26	03:30	103a-D+yellow plexiglass	6

SESSION II:

MARINER 10 OBSERVATION OF COMET KOHOUTEK

A. L. BROADFOOT
M. J. S. BELTON
Kitt Peak National Observatory

M. B. McELROY
Harvard University

S. KUMAR
University of Virginia

(No paper submitted for publication)

Page intentionally left blank

Page intentionally left blank

S201 FAR-ULTRAVIOLET PHOTOGRAPHS OF COMET KOHOUTEK FROM SKYLAB 4 (SL4) (Preliminary Report)

THORNTON PAGE
Naval Research Laboratory and Johnson Space Center

The S201/SL4 Far-Ultraviolet Camera experiment obtained 126 frames exposed on Comet Kohoutek between November 26, 1973, and February 2, 1974, of which 30 have been measured for analysis of the comet's hydrogen halo on nine separate dates from 31.7 days pre-perihelion to 13.0 days post-perihelion. Over 350 frames were exposed on other targets, and 35 of them have been measured to check the unexpected changes in camera sensitivity during 5 hours of operation in the 61-day interval. The results given below show the development and decline of the hydrogen halo photographed in Lyman-α light (1216 Å), but they are still subject to some uncertainty because of the change in camera sensitivity and some erratic film fogging that affected about 25 percent of the flight film.

The S201 Electronographic Camera

The electronographic Schmidt camera (Carruthers and Page, 1972, and Carruthers, 1973) has been used on several rocket flights above the atmosphere and outside the geocorona during the Apollo-16 Mission, when it was equipped with an objective grating and mounted on a leveled tripod for both imagery and spectrography. The Apollo-16 backup model was modified at the Naval Research Laboratory (NRL) for observations of Comet Kohoutek from Skylab 4, through the antisolar Scientific Air Lock (SAL), by use of the Articulated Mirror System (AMS) or Extravehicular Activity (EVA). The electronographic camera is an $f/1$ Schmidt of 75-mm focal length with a 12.7-cm Al + MgF_2-coated primary mirror and 75-mm corrector plates, one of LiF transparent to 1050 Å, the other of CaF_2 with cutoff at 1250 Å. The KBr photocathode at the focal surface produces photoelectrons from light quanta of $\lambda < 1600$ Å, and these are focused by axial electrostatic and magnetic fields on a special-order Kodak film with 6-micron-thick NTB–3 (nuclear track) emul-

sion. The electrostatic field is provided by −25 kV from a high-voltage power supply applied to the photocathode, and the magnetic field (about 400 G) by a cylinder of Alnico bar magnets around the camera. The KBr photocathode is "blind" to visible and near-UV light. Its sensitivity in the far UV can be degraded by humidity above about 25 percent relative humidity (RH).

Figure 1 shows the S201/SL4 camera configuration. The camera, high-voltage power supply, film transport, and electronic sequencer were mounted in a vacuum-tight canister with removable covers front and rear. With the front cover removed, the adapter flange was sealed with double O-rings to the AMS on the antisolar SAL, or the camera could be pointed manually on EVA, clamped to the Apollo Telescope Mount (ATM) truss. On EVA, the full 20° field of view was utilized, and the camera was shaded from direct sunlight by one of the ATM solar panels.

The AMS provided a 6.°8 unvignetted beam from a direction between 60° and 90° from the −Z axis (antisolar), vignetted 50 percent at about 5.°8 off axis, and including a "rim view" 5.°8 to 10° off the −Z axis. This was asymmetrical, as shown in figure 2. Thus, each S201 frame shows an area 12.°9 × 6.°8 around the selected target, plus a ring around that out to 9°

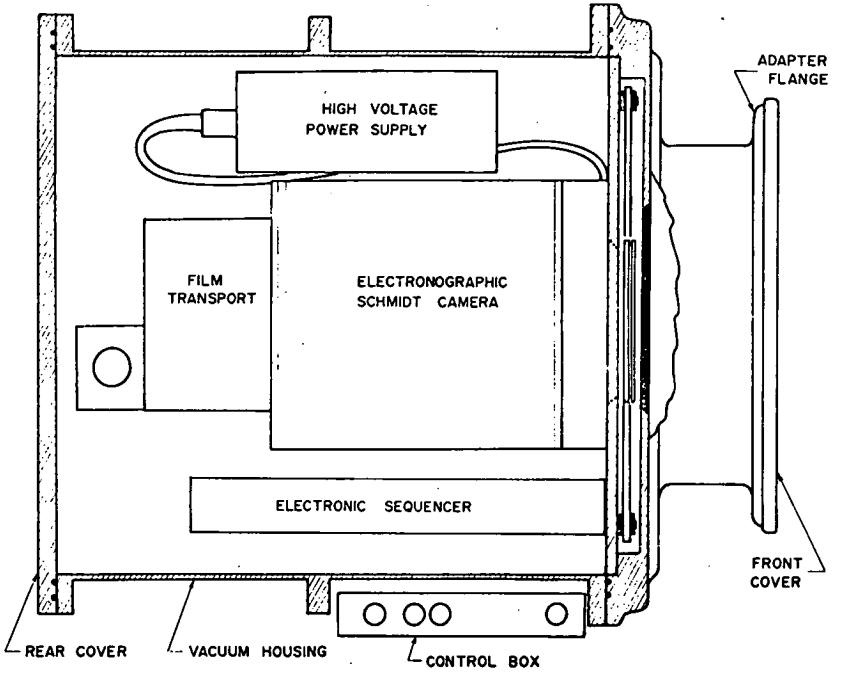

FIGURE 1.—*Cutaway diagram of S201/SL4 canister.*

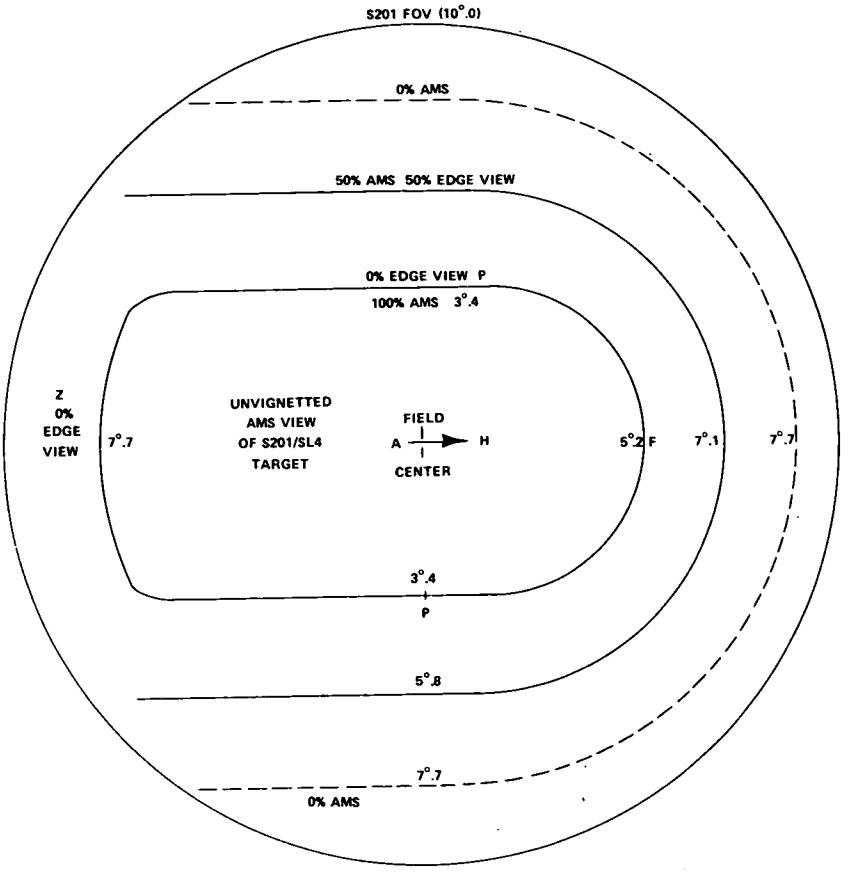

FIGURE 2.—*Diagram of the S201/SL4 field of view through AMS–SAL. The central region, from 7.°7 left of field center to 5.°2 right, and 3.°4 up and down, marks the unvignetted target field of view in the AMS mirror. Between this and the dashed line, the AMS target field is progressively vignetted, and the "rim view" of a different star field near the -Z axis increases. Outside the dashed curve, the camera views the latter field only.*

from the AMS pointing direction including stars and background from both AMS direction and $-Z$ axis, plus a third ring 9° to 10° from the center showing stars and background from the $-Z$ axis only. This situation, accepted with the S201/SL4 modification, complicates the identification of stars on the far-UV photos.

Preflight calibration was performed by Dr. Carruthers at NRL with the camera in a vacuum chamber pointed at a He–O_2 light source monitored by calibrated pulse-counting photomultipliers. The camera recorded four expo-

sures through the LiF corrector (1, 2.5, 6, and 15 sec) and four through CaF_2 (3, 10, 30, and 107 sec), yielding a calibration curve relating film density above background, ΔD, with exposure, E (the product of target brightness, B, by exposure time, Δt). Figure 3 shows that this characteristic curve is closely linear, with a minor "toe" at the zero-density end, and a slope $d\Delta D/dE = 0.033$. It has been extended to ΔD over 3.5 by measures of densities on two or more frames in later sequences showing targets or background of unknown B. Each pair of $\Delta D's$ with known ratio of $E's$ gives a slope, and these are shown in figure 3. (Star densities are integrated to give a density-volume for each star image, shown by open circles in figure 3.)

The Flight Films

Lengths of 35-mm NTB–3 film, each approximately 10.7 m long, were loaded in three film transports (FT's) for the SL4 Mission. From launch to December 16, 1973, FT #001 was in place on the S201 camera in the canister, and FT's #002 and #003 were stowed in the Skylab film vault. After S201

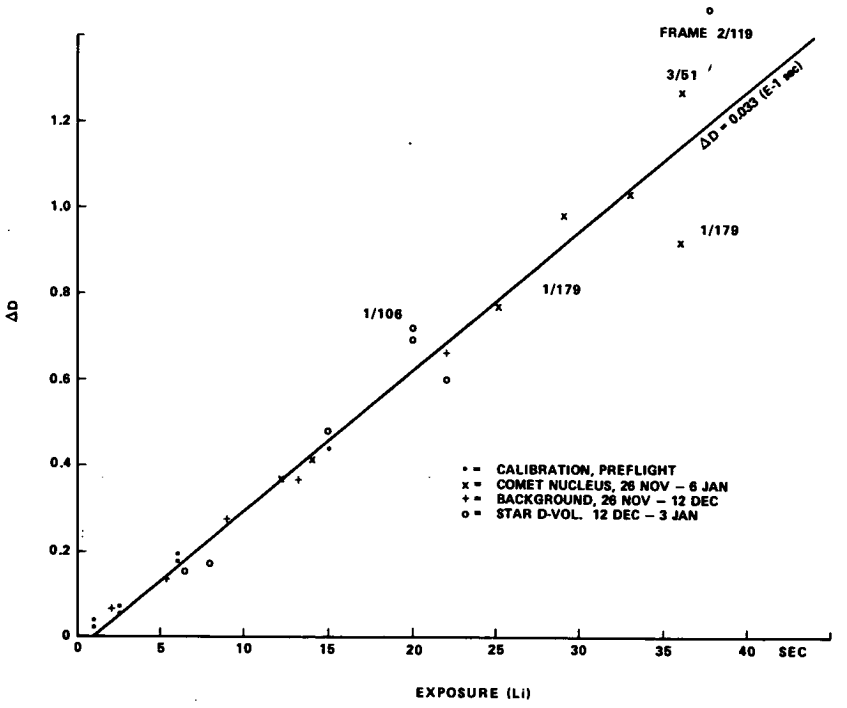

FIGURE 3.—*Plot of density above background, ΔD, versus Exposure, E, through LiF corrector.*

operation on December 16, the rear cover of the canister was removed briefly, FT #001 was replaced by #002, and the humid cabin air was promptly exhausted after the cover was replaced (to minimize photocathode degradation). After each camera operation, the canister was repressurized with dry nitrogen. On December 28, FT #002 was replaced by #003, and on February 2, 1974 FT #003 was removed for return to Johnson Space Center (JSC). On February 14, all three FT's were delivered to the Photographic Technology Division at JSC, and the film was given uniform development (9 min D–19 at 85°F) together with test films from the same NTB–3 batch that had remained at JSC during the SL4 Mission.

Examination of the processed films revealed three major defects: (1) Irregular edge fog, in some places extending right across the film, thought to be caused by condensate water during splashdown—hence termed "water fog" in table I. (2) Discharge fog, limited to the 32-mm (20°) field of view on each frame, due to residual gas in the canister allowing glow discharge or sparks across the 25-kV potential gap. Even at fairly hard vacuum (10^{-5} torr), a central "ion point" appears, as on figure 4, to the left of the comet image, due to negative ions of residual gas. (3) A large graininess, and irregular areas of reduced density, particularly on film #003, possibly due to sudden temperature changes. The latter are termed "watermarks" in table I.

Exposed frames were identified and numbered, from Frame No. 1/0 through 1/183 on Film #001, 2/1 through 2/150 on #002, and 3/0 through

Table I.—*S201/SL4 Frames Exposed, November 26, 1973, to February 2, 1974*

Date	Film/ Frames	NASA Nos.	Target	SpecScans	Features
Oct 25	1/0 – 9	6127–6136	Calibration	40 x,y, 9 raster	1 sequence; 0.02 to 4.0D
Nov 26.98	1/12 – 21	6139–6148	S M C	24 x,y, 4 r	1 seq; stars, SMC, water fog
	1/24 – 32	6151–6161	A426	6 x,y, 2 r	1 seq; many stars
	1/34 – 44	6164–6174	*Comet K*	24 x,y, 5 r	1 seq; comet, stars
	1/46 – 55	6176–6185	Virgo Cl.	4 x,y, 2 r	1 seq; stars
	1/57 – 66	6188–6196	Tau Stars	6 x,y, 2 r	1 seq; many stars
Dec 5.92	1/68 – 79	6198–6209	Coma Cl.	4 x,y, 2 r	1 seq; no stars
	1/82 – 90	6214–6224	*Comet K*	18 x,y, 4 r	1 seq; comet, stars
Dec 12.07	1/92 –102	6226–6236	Virgo Cl.	8 x,y, 2 r	1 seq; stars
	1/104–114	6238–6248	*Comet K*	44 x,y, 7 r	1 seq; comet, few stars
Dec 12.25	1/120–129	6252–6262	Eri Gp.	4 x,y, 2 r	1 seq; stars
	1/131–140	6264–6274	NGC134	6 x,y, 2 r	1 seq; stars
	1/141–151	6276–6286	A2199	6 x,y, 2 r	1 seq; many stars
	1/152–161	6288–6300	Crab Neb.	6 x,y, 2 r	1 seq; many stars
Dec 16.74	1/166–174	6304–6313	Moon	16 x,y, 4 r	1 seq; moon, few stars, water fog
	1/176–183	6315–6321	*Comet K*	16 x,y, 2 r	1 seq; comet, stars, fog, film end

Table I.—*S201/SL4 Frames Exposed, November 26, 1973, to February 2, 1974*—Concluded

Date	Film/ Frames	NASA Nos.	Target	SpecScans	Features
Dec 22.94	2/1 – 10	6322–6331	N. Aurora	8 x,y, 4 r	1 seq; band, watermarks
	2/12 – 23	6333–6343	Fornax Cl.	8 x,y, 2 r	1 seq; few stars
	2/24 – 44	6346–6367	NGC6643	8 x,y, 2 r	2 seq; few stars
	2/46 – 55	6369–6378	Gum Neb.	8 x,y, 3 r	1 seq; many stars
	2/57 – 66	6380–6389	Gum E	4 x,y, 2 r	1 seq; stars
Dec 23.65	2/68 – 77	6392–6401	Crab Neb.	4 x,y, 2 r	1 seq; stars, cathode specks
	2/79 – 88	6403–6413	NGC1068	6 x,y, 2 r	1 seq; 2 stars, cathode specks
	2/91 –101	6416–6426	A1060	2 x,y	1 seq; few stars
	2/104–113	6429–6439	NGC5128	2 x,y	1 seq; stars
	2/116–124	6442–6450	*Comet K*	18 x,y, 3 r	1 seq; comet, 0 Oph
Dec 25.9	2/128–150	6453–6475	*Comet K*	24 x,y, 9 r	2 seq on EVA; comet stars, film end
Jan 2.94	3/1 – 7	6477–6487	*Comet K*	12 x,y, 3 r	1 seq; comet, stars, watermarks
	3/12 – 22	6489–6499	A2634	2 x,y	1 seq; few stars, watermarks
	3/24 – 33	6502–6511	Pleiades	10 x,y, 3 r	1 seq; stars, discharge fog
	3/35 – 45	6514–6524	NGC6300	2 x,y	1 seq; few stars
Jan 6.57	3/47 – 57	6527–6537	*Comet K*	12 x,y, 3 r	1 seq; comet, watermarks
Jan 10.72	3/59 – 68	6543–6553	N. Airglow	1 r	1 seq; watermarks
	3/70 – 80	6555–6566	*Comet K*	6 x,y, 2 r	1 seq; comet, watermarks
Jan 13.05	3/82 – 91	6570–6580	S. Airglow	1 r	1 seq; 1 star, watermarks
	3/93 –103	6581–6591	*Comet K*		1 seq; watermarks, discharge fog
Jan 15.06	3/105–107	6595–6597	*Comet K*		¼ seq; background only
Jan 26.01	3/109–111	6600–6602	*Comet K*	1 r	¼ seq; background only
	3/113–123	6605–6615	Fornax Cl.	2 x,y, 2 r	1 seq; stars, watermarks
	3/125–135	6619–6629	A1228	2 x,y, 1 r	1 seq; stars
	3/137–163	— —	Missile		2½ seq for NRL missile launch experiment
Feb 2.00	3/165–168	6632–6635	*Comet K*	8 x,y, 1 r	¼ seq; streaks, watermarks
	3/170–178	6637–6646	Moon	26 x,y, 2 r	1 seq; moon, watermarks, fog
	3/181–188	6651–6658	M101		1 seq; water fog

FIGURE 4.—*Frame 1/108, a 15-s exposure through LiF showing Comet Kohoutek just above the horizon at 01:45:55 GMT on December 12, 1973. The small patch left of the comet image is caused by ions of residual gas in the S201 camera. The large semicircle is geocorona Lyman-α background, partly vignetted by the SL4 Articulated Mirror System.*

3/188 on #003. Later examination eliminated some gaps in this numbering scheme, and NASA numbers were assigned as follows: SL4–182–6126 through 6321 on Film #001, SL4–183–6322 through 6475 on #002, and SL4–184–6476 through 6658 on #003, as shown in table I.

About 25 percent of the exposed frames are badly affected by one or more of the three defects noted above. However, some 50 frames show Comet Kohoutek on nine different occasions with fairly good resolution (4 arc-min), six of them through LiF corrector shown in figure 5, and one through CaF_2 in figure 6. The vignetting effects shown in figure 2, and discharge points on some frames, complicate star identification except near the field center, but reliably identified images of 11 stars on Frames 1/176 and 1/180, 5 stars on 2/55, and 7 (the Pleiades) on 3/33, were measured with accuracy of 2 or 3 microns to give the camera scale of 26.6μ per arc-min.

These, and the density measurements, were made with the SpecScan microdensitometer at the Photographic Technology Division, JSC. The flight films were scanned emulsion up, pressed between two glass plates on the microdensitometer platen together with a standard diffuse-density (D) step-wedge

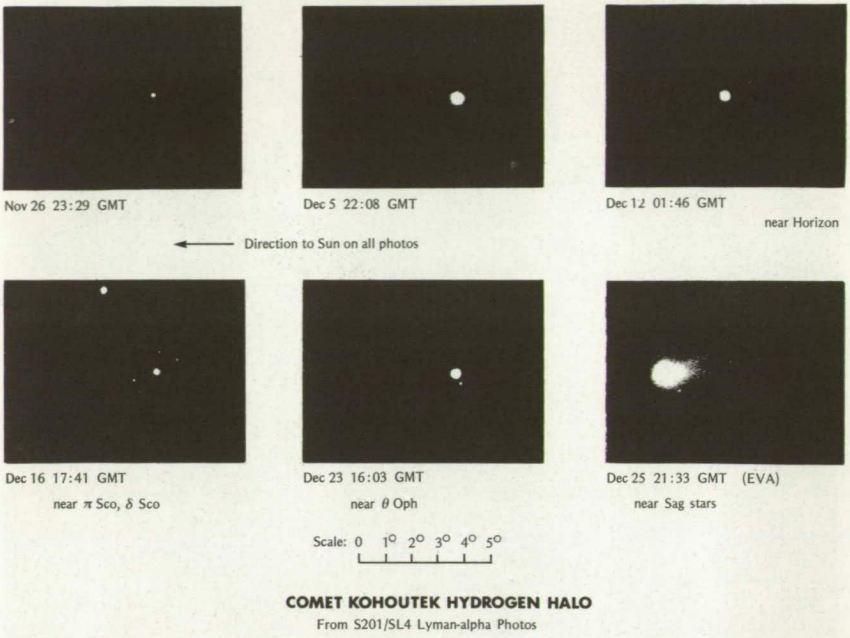

FIGURE 5.—*Comet Kohoutek hydrogen halo. Frames 1/38, 1/84, 1/108, 1/180, and 2/119, taken through the AMS at 15s exposure, and frame 2/128 taken on EVA at 1-s, all LiF corrector, 1050–1600 Å bandpass, showing Lyman-α emission.*

(0.10 D and 2.25 D) film and a frame-numbered copy negative to ensure proper identification. As shown in table I, tracings were made along x, parallel to the film edge, and along y, across the film, at various scales. Tracings were centered on comet or star images by adjusting x and y for maximum D. Full-field traces were centered on the film in y, and between the field edges when the 32-mm (20°) circle could be detected. Raster scans of 512 × 512 or 1024 × 1024 measurements were recorded on magnetic tape and converted to density contour plots, as in figures 7 and 8.

These density measurements revealed the changes in camera sensitivity, $S(x,y,t)$, a function of position on the frame (x,y measured in mm from the frame center) and time (t, measured in days after the first S201/SL4 use on November 26.98). The most obvious evidence is shown in figure 9, a full x-trace of Frame 2/128 taken on EVA, where the decreased sensitivity ($S <$ 1.00) shows near the center of what should be a uniform background. The geocorona Lyman-α background provides the most convenient source for measuring sensitivity changes, since every frame was exposed to it in varying degrees. Figure 10 shows the x-section of this background as recorded on six frames taken on November 26.98 ($t = 0$), when the sensitivity $S(x,y,0) =$ 1.00, by assumption. Similar traces on 34 other frames yield the decreasing

FIGURE 6.—*Comet Kohoutek and blue stars in Sagittarius, Lyman-α excluded. From frame 2/137, 95-s exposed through CaF_2 corrector, 1250–1600 Å bandpass. The long, pointed tail extends 2 × 10^6 km antisolar from the comet nucleus. The dark edge is part of the film holder defining the edge of the 20° circular field.*

values of $S(x,y,t)$ partly shown in figures 11 and 12. The edge values ($x > 10$, $y > 10$) are poorly determined because measured ΔD's there are small ($\leq 0.05\ D$); they seem to show an increase in S after $t = 27.4$ days. Note that the major decrease in sensitivity took place in the first 20 days of S201/SL4 operation, after only 13 sequences of photographs in 86 minutes of operation. Humid air cannot have caused this decrease because it would degrade the full photocathode, while the measured values of S are roughly one-half as large at the center as at the edges. Figure 13 shows the measured values of $S(x,0,29)$ on EVA without the AMS mirror, and 2 days earlier, using the AMS. Apparently, the central value, $S(0,0,27)$, was degraded by a factor of about 5 due to degraded Lyman-α reflectance of the AMS mirror during the first 27.4 days of S201/SL4 operation. Karl Henize (1974) has estimated a factor of 2 at longer wavelengths (about 1800 Å). This conclusion is based on one assumption: that the background on EVA, December 25.9, is uniform, so that the upper curve in figure 13 represents only the S201/SL4 camera sensitivity, $S_c(x,0,29.9)$. The lower curve in figure 13 shows $S(x,0,27.4) = R_M S_c(x,0,27.4)$, where R_M is the fractional decrease in AMS mirror reflect-

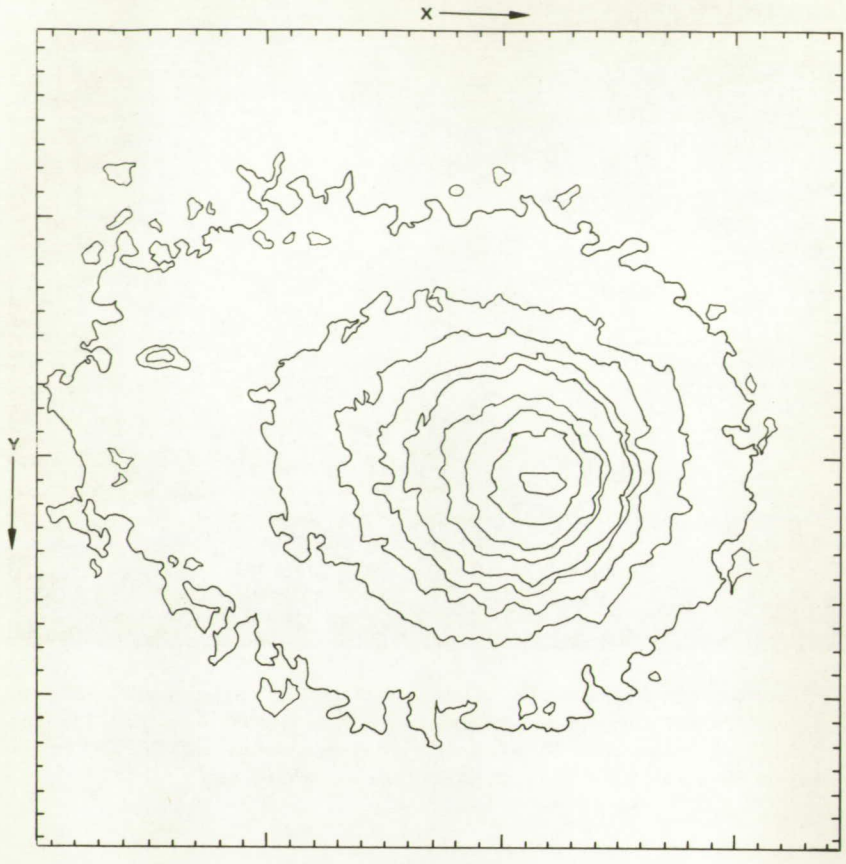

FIGURE 7.—*Isodensity contours from frame 2/128 showing Comet Kohoutek's Lyman-halo in 1-s exposure at 21:32:45 GMT on December 25, 1973. The halo center is more than 4.00 D. The outer contour intervals are 0.20 D. Directions to the Sun is toward the lower right. The square is 64 arc-min on a side (1.7 mm on the original film).*

→

FIGURE 9.—*Microdensitometer tracing across frame 2/129 showing Lyman-α background. The background density is fairly uniform at about 0.86 D in the outer 9-mm ring of the 32-mm field, but decreases to 0.62 D near the center, implying a 28 percent loss of camera sensitivity there.*

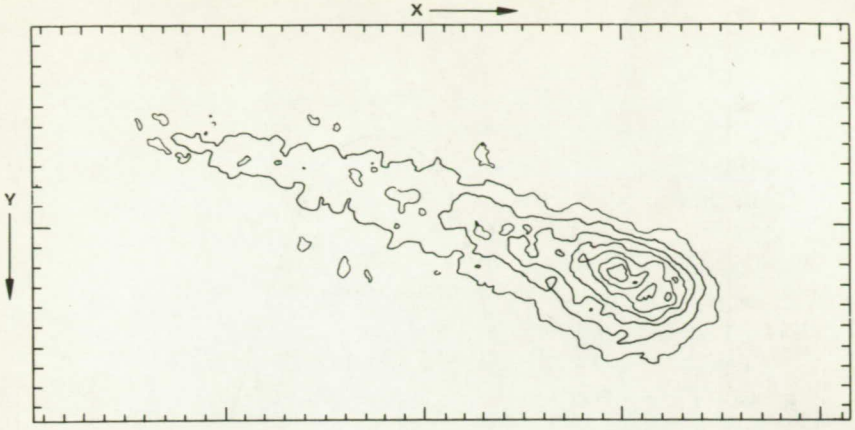

FIGURE 8.—*Isodensity contours from frame 2/146 showing Comet Kohoutek on a 30-s exposure through CaF_2 corrector, 1250–1600 Å bandpass, at 21:38:38 GMT on December 25, 1973. The tail extends off the plot, antisolar, to the upper left. The base side is 75.5 arc-min (2.0 mm on the original film).*

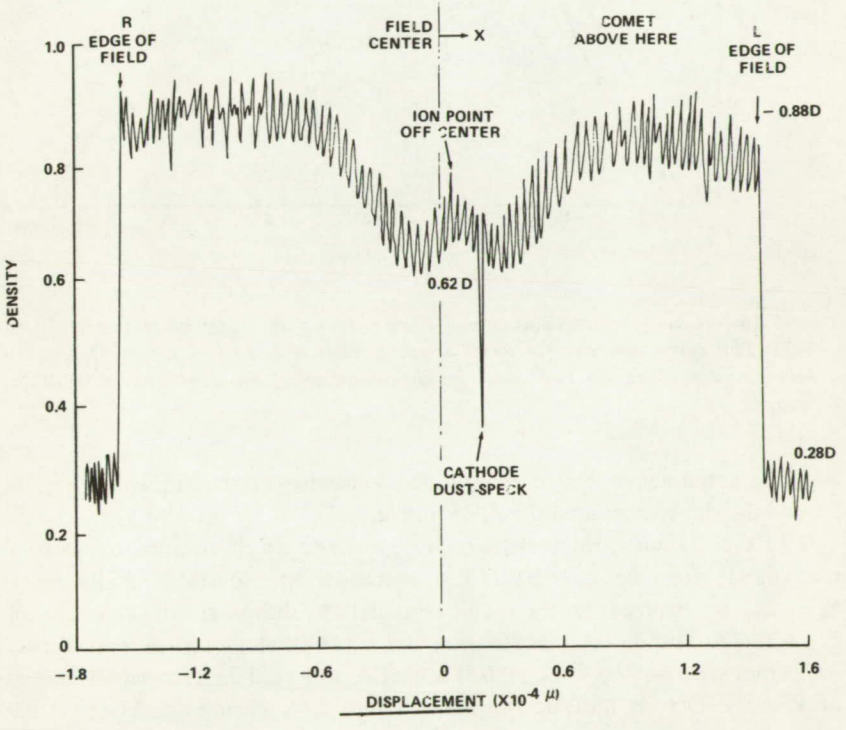

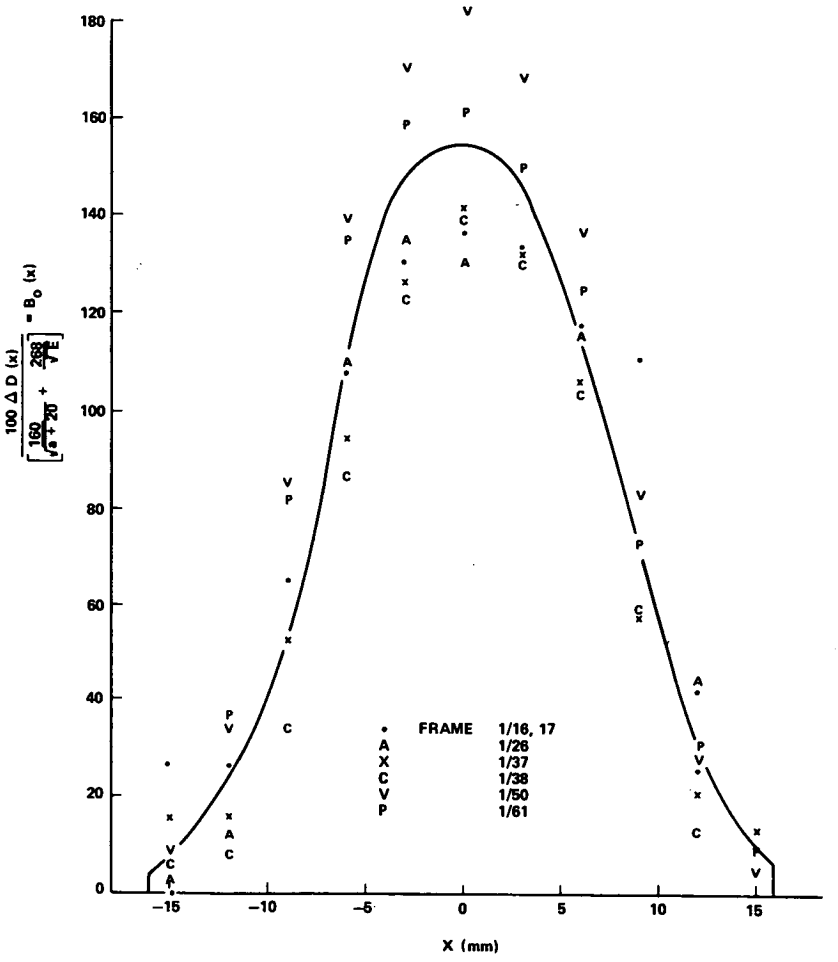

FIGURE 10.—*Mean geocorona background density from AMS views on November 26.98, 1973. This curve, corrected for target direction relative to the Sun, is used to calibrate background measures on later dates for determination of the S201 camera sensitivity change.*

ance. As noted above, this is complicated somewhat by the vignetting (figure 2) and the rim view around the AMS mirror.

Whatever its cause, the sensitivity $S(x,y,t)$ has been determined for each of nine dates after the first S201/SL4 operation on November 26.98 when $S(x,y,0)$ is assumed to be 1.00. Figure 14 shows rough contours of $S(x,y,38.7)$. The Moon, the Pleiades, and three other groups of stars appear on frames separated by 47.3, 30.0, 16.0, 11.4, and 34.0 days, at various values of x and y. Density measures on these frames show changes in $S(x,y,t)$ that

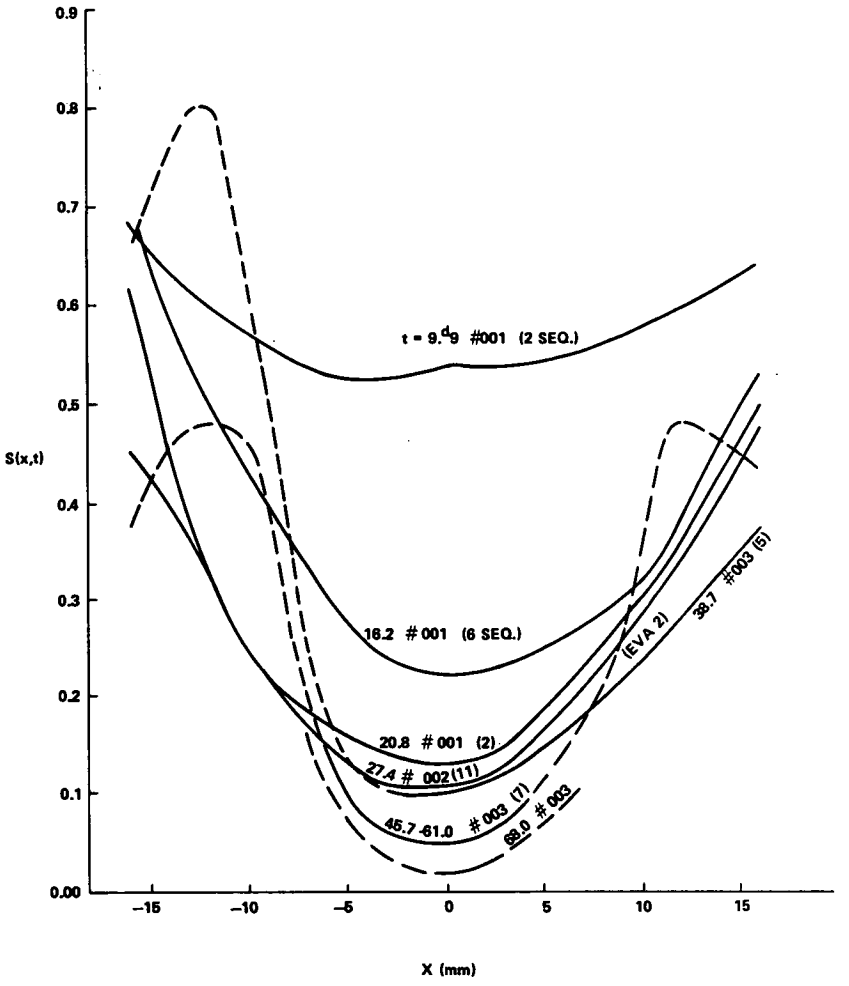

FIGURE 11.—*Plots of camera sensitivity versus X-distance from the field center on eight different dates.*

tend to confirm the values in figures 11 to 13. These are used to correct measurements of Comet Kohoutek's Lyman-α halo.

Comet Kohoutek Lyman-Alpha Halo Size and Brightness

Figures 15 and 16 show microdensitometer x- and y-traces centered on the comet image on Frame 1/108, December 12.07. Except for uncertainty in the background density, D_B, the linear relation $\Delta D = 0.033\ E$ (figure 3) allows

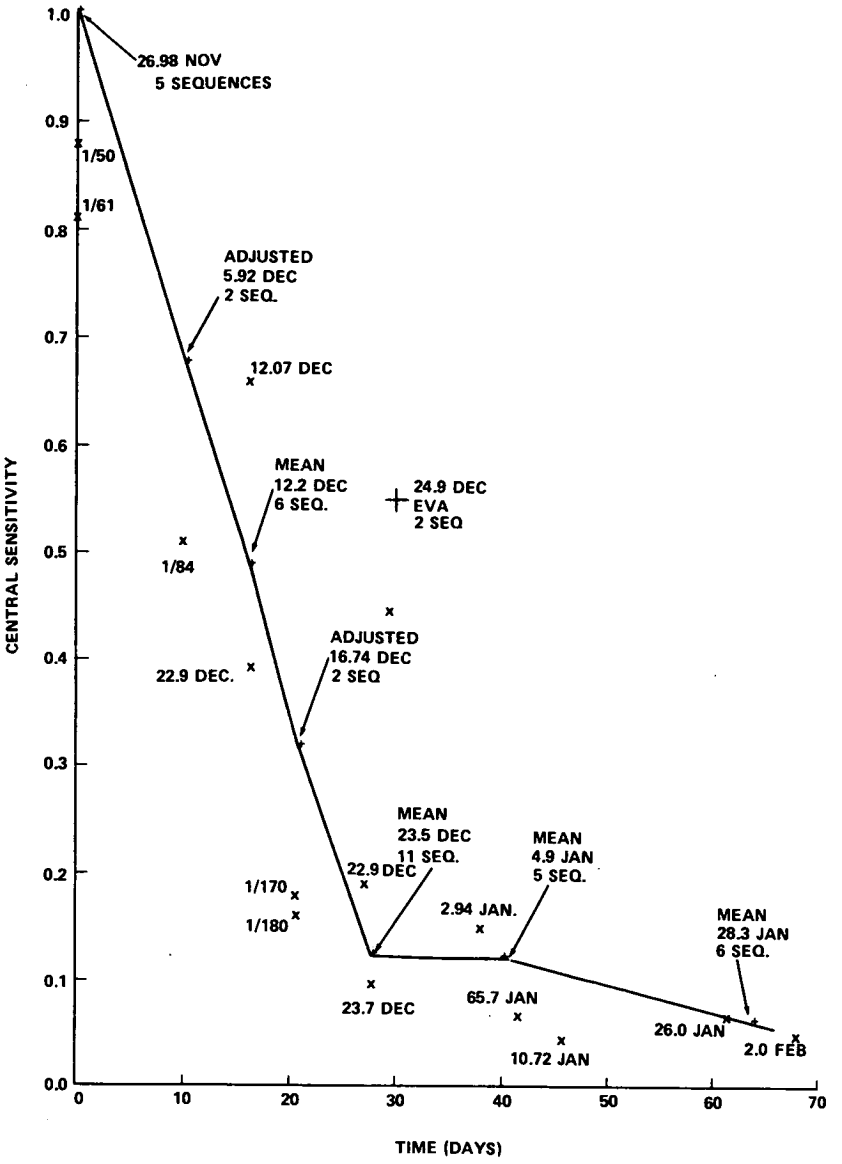

FIGURE 12.—*Smoothed plot of central sensitivity, S(0,0,t) versus time. "×" = measured values; "+" = means and adjusted values. (Based on Meier's model of the geocorona Lyman alpha intensity.)*

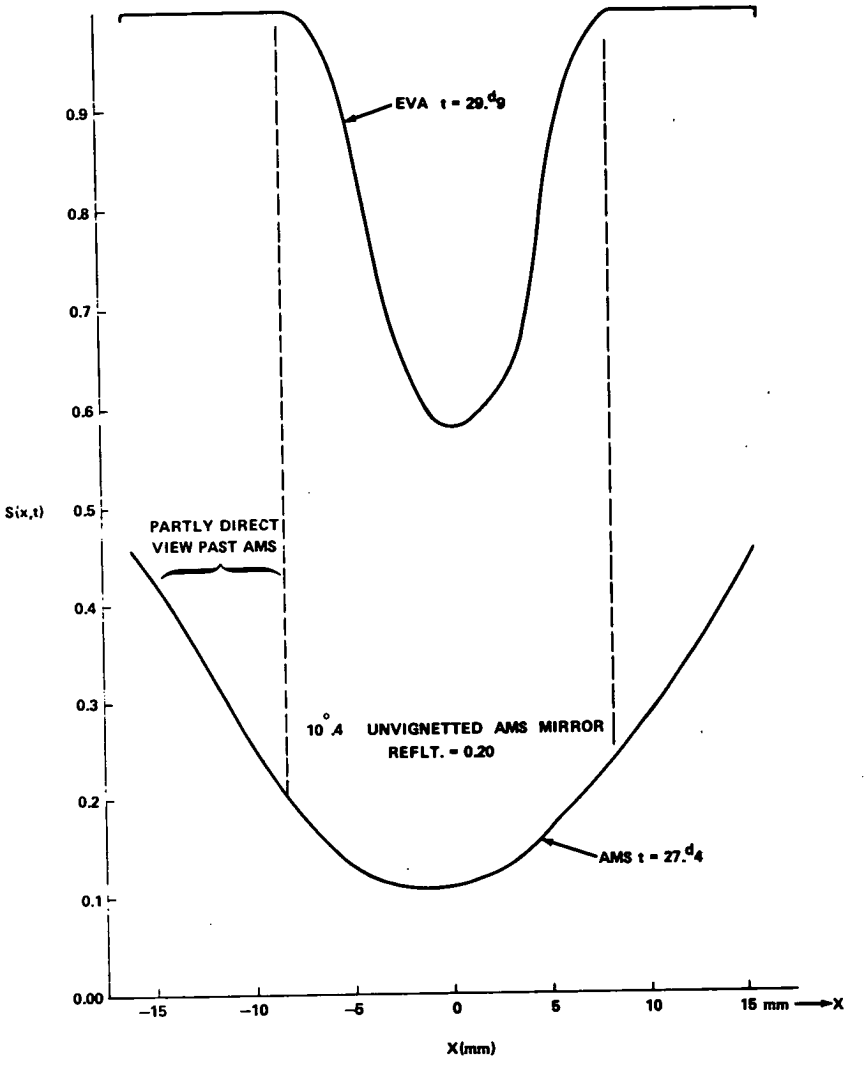

FIGURE 13.—*Plots of camera sensitivity versus X-distance from field center on December 23 and 25, 1973. The upper curve, from frames 2/128–146 taken on EVA, shows S201 camera sensitivity after 29 days. The lower curve, from frames 2/17–119 exposed through the AMS, shows the combination of camera sensitivity and AMS mirror reflectance 2 days earlier.*

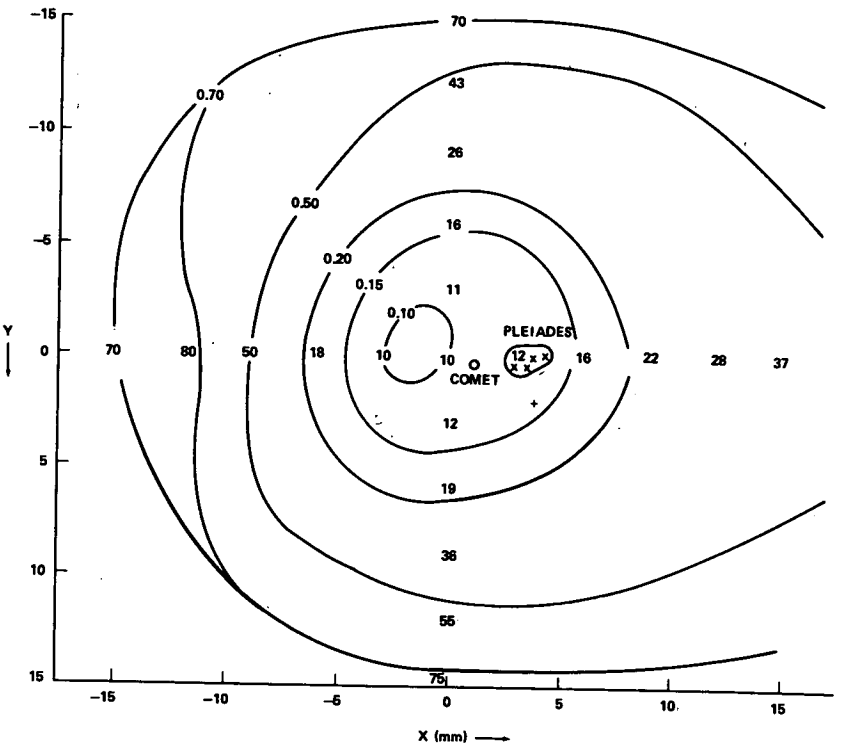

FIGURE 14.—*Contours of S(x,y,38.7) for January 3, 1974. The camera sensitivity differs from one part of the field to another. So far, the values are only roughly determined.*

a fairly accurate measurement of the comet's Lyman-α (hydrogen) halo to an "edge" of constant brightness corresponding to a density above background, $\Delta D_o = 0.1\ E\ S(x,y,t)$. This edge brightness level is estimated to be about 20 kilo-Rayleighs in Lyman-α, and will be more accurately determined later on. Table II lists the measurements of halo widths, Δx and Δy in microns, on 21 frames exposed on nine different dates. The comet's central (nuclear) density above background, ΔD_n, is listed first for each frame; then other density levels above and below ΔD_o are given. (The density ratio 2.5 reflects the S201/SL4 exposure sequence of 1, 2.5, 6, and 15 seconds through the LiF corrector, assumed to record primarily Lyman-α brightness.)

Of course, these comet halo diameters are somewhat increased by the camera's limited resolution, including instability of the spacecraft and, in the case of x-traces, advance of the film into and out of position, starting and stopping the exposure. (This accounts for values of Δx larger than Δy.) Figure 17 shows one of the traces of star images used to determine the resolution on each frame. The dimensions s_x and s_y are full widths of the star image at half

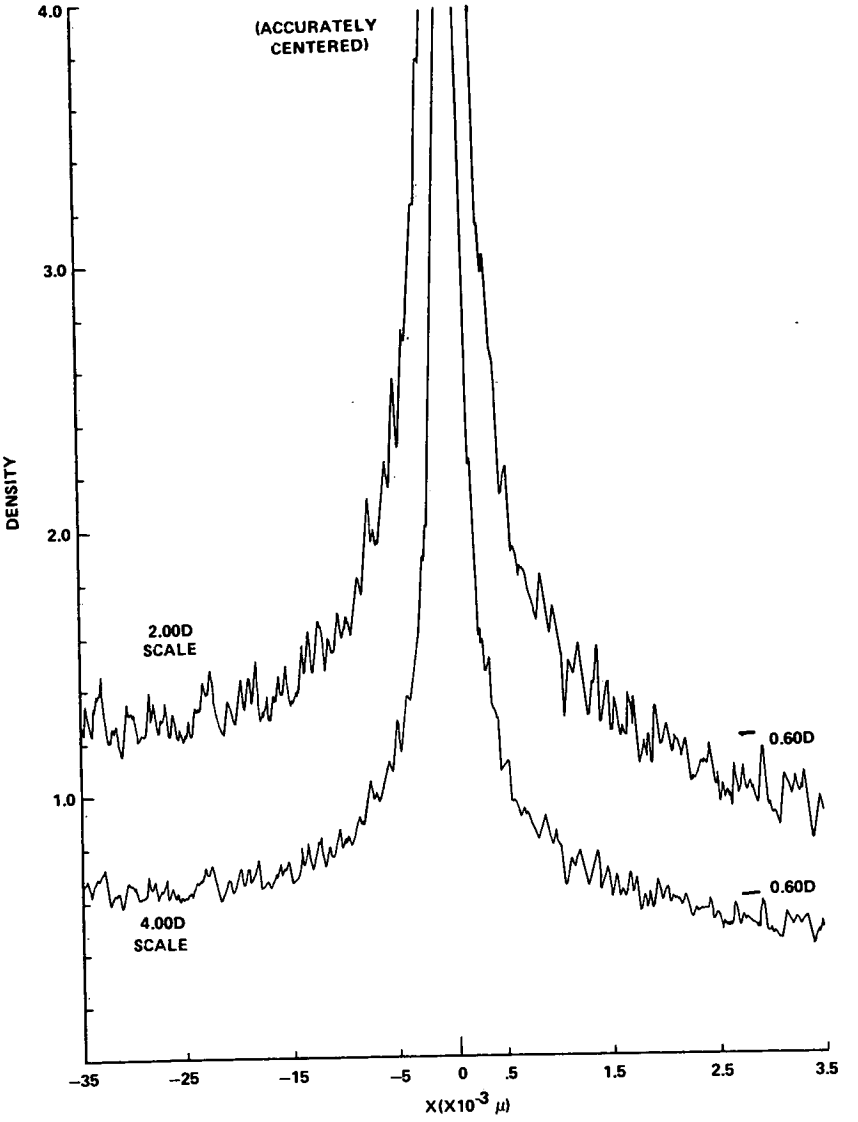

FIGURE 15.—*Microdensitometer X-trace across Comet Kohoutek's Lyman-α halo on frame 1/108. The upper curve is the same scan plotted at double scale.*

maximum ($\frac{1}{2}\Delta D_{max}$), and the halo diameters are $\delta x = \Delta x - s_x$, $\delta y = \Delta y - s_y$ in microns. These are converted to linear diameters by use of the scale factor (26.5μ/arc-min, or 6.°28 × 10^{-4}/micron) and the Earth-comet distance, R_{EC}, in Astronomical Units. Thus the halo diameters perpendicular to

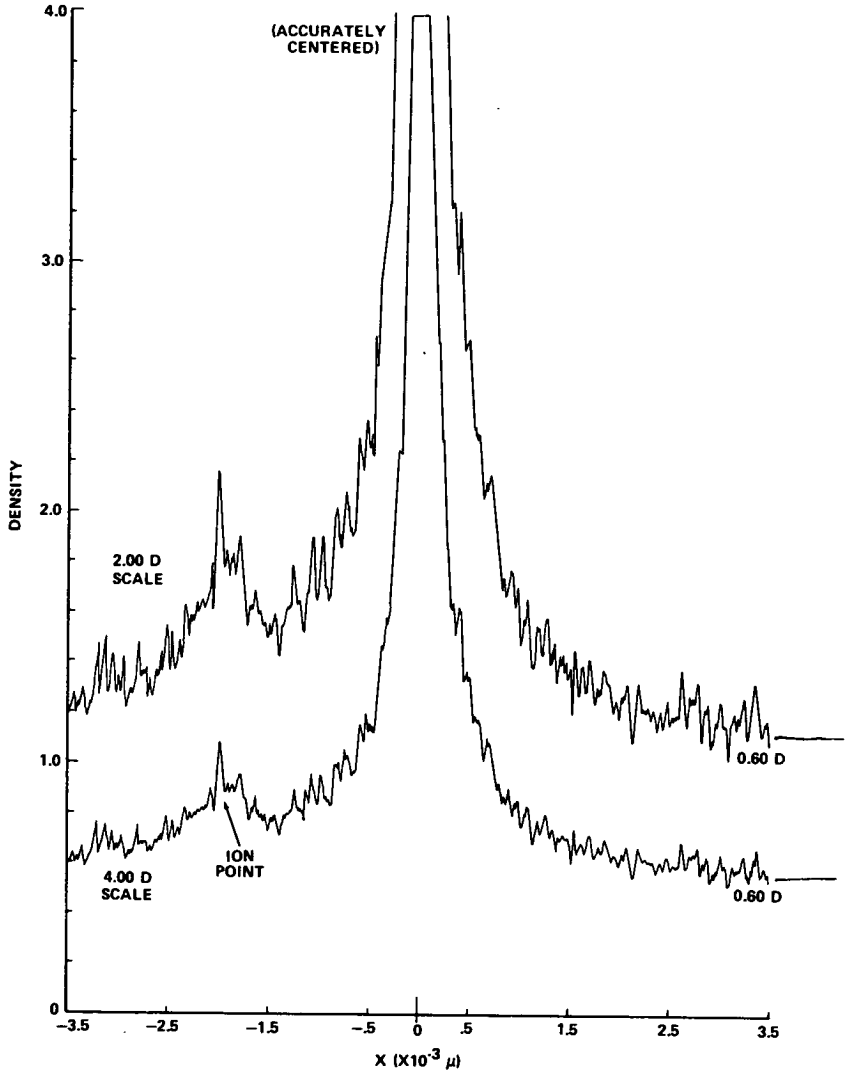

FIGURE 16.—*Microdensitometer Y-trace across Comet Kohoutek's Lyman-α halo on frame 1/108. The horizontal scale is in microns from the maximum-D center of the halo.*

the line of sight are

$d = 6.°28 \times 10^{-4} \delta R_{EC} / 57.°2 = 1.10 \times 10^{-5} \delta R_{EC}$ in AU, and the halo radius

$r = 1.496 \times 10^{8}\, d/2 = 0.832 \times 10^{3} \delta R_{EC}$ in km.

The measured values are listed in Table II (without rounding—the third place is not significant) and are plotted on figures 18–21. The $\Delta D/\Delta D_o$

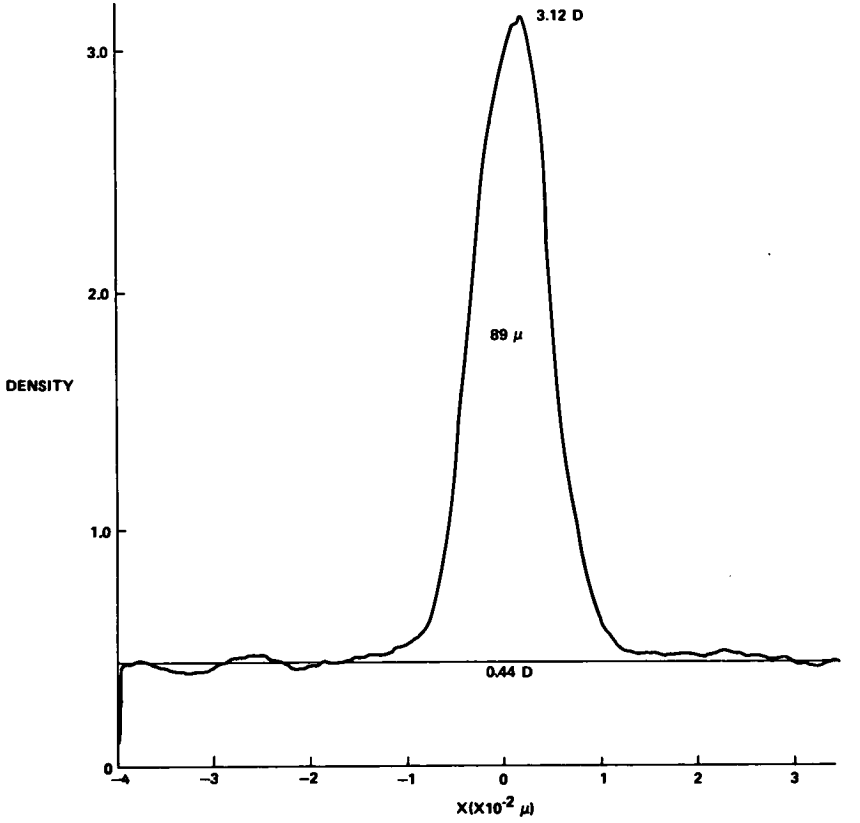

FIGURE 17.—*Microdensitometer X-trace of a star image on frame 1/108. Star traces like this are used to correct for image resolution. The width at half maximum is* s_x = *89 microns. A similar trace along y shows* s_y = *135 microns on frame 1/108.*

scale is logarithmic: "x" denotes r_x, "+" denotes r_y. In general, separate frames taken at the same time agree within a few percent, although nuclear densities ΔD_n are often above 4.0 D, the highest density measurable on the microdensitometer. Table III shows the mean values of ΔD_n, D_x, d_y, r_x, and r_y, and includes the Sun-comet distance, R_{SC}, aspect angle, β, and Earth-comet radial velocity, V_{EC}.

Figure 22 shows the variation of halo diameter, d, with R_{SC} and time. As expected, the hydrogen halo increased with decreasing R_{SC} before perihelion, but it has an unexpected pre-perihelion maximum on December 12, and another maximum presumably at perihelion, with a minimum between. It is also clear from tables II and III that the ratio of peak nuclear brightness (as measured by $\Delta D_n/\Delta D_o$) to diameter is much larger near perihelion. Such an

Table II.—*Measurements of the Lyman-α Halo*

Frame, Date (GMT)	Δt (s)	S	ΔD	$\Delta D/\Delta D_o$	Δx (μ)	Δy (μ)	δx (μ)	δy (μ)	R_{EC} (AU)	$1.10\delta R_{EC}$ d_x (10^{-5} AU)	$1.10\delta R_{EC}$ d_y (10^{-5} AU)	$0.823\delta R_{EC}$ r_x (10^3 km)	$0.823\delta R_{EC}$ r_y (10^3 km)	log $\Delta D/\Delta D_o$
1/37	6	1.00	1.01	1.68	0	0	0	0	1.45	0	0	0	0	0.235
Nov 27.0			0.95	1.58	40	40	0	0		0	0	0	0	0.200
P − 31.7 da			*0.60*	1.00	170	160	72	45		115	72	86	54	0.000
			0.38	0.63	280	270	182	155		290	247	217	185	−.200
$s_x = 98\ \mu$			0.24	0.40	380	400	282	285		450	455	336	340	−.398
$s_y = 115\ \mu$			0.15	0.25	590	660	492	545		785	870	587	650	−.602
			0.095	0.16	870	930	772	815		1230	1300	920	970	−.796
			0.06	0.10	1200	1250	1102	1135		1760	1810	1310	1350	−1.000
			0.038	0.063	1730	1540	1632	1425		2600	2270	1950	1700	−1.200
1/38	15	1.00	2.98	1.99	0	0	0	0	1.45	0	0	0	0	0.298
Nov 27.0			2.37	1.58	90	80	0	0		0	0	0	0	0.200
P − 31.7 da			*1.50*	1.00	180	200	67	47		107	75	80	56	0.000
			0.95	0.63	330	330	217	177		346	282	259	211	−.200
$s_x = 113\ \mu$			0.60	0.40	490	490	377	337		600	535	450	400	−.398
$s_y = 153\ \mu$			0.38	0.25	780	800	667	647		1060	1030	795	770	−.602
			0.24	0.16	1150	1170	1037	1017		1650	1620	1235	1210	−.796
			0.15	0.10	1870	1600	1757	1447		2800	2300	2090	1725	−1.000
			0.095	0.063	2550	1980	2437	1827		3880	2900	2900	2180	−1.200
			0.06	0.04	3200	2250	3087	2097		4900	3340	3680	2500	−1.400
1/83	6	0.68	2.12	5.17	0	0	0	0	1.28	0	0	0	0	0.714
Dec 5.92			1.61	3.93	80	70	10	0		14	0	11	0	0.595
P − 22.8 da			1.02	2.48	180	190	110	120		155	169	116	126	0.396
			0.65	1.58	350	350	280	280		394	394	295	295	0.200

$s_x = 70\,\mu$			*0.41*	1.00	490	490	420	420		590	590	440	440	0.000
$s_y = 70\,\mu$			0.26	0.63	740	720	670	650		940	915	705	685	−.200
			0.165	0.40	1070	1000	1000	930		1400	1300	1050	980	−.398
			0.105	0.25	1580	1450	1510	1380		2120	1940	1590	1450	−.602
			0.065	0.16	2350	2000	2280	1930		3200	2710	2400	2030	−.796
1/84	15	0.68	>3.25	>3.17	180	−00	108	128	1.28	152	180	114	135	>0.500
Dec 5.92			2.54	2.49	250	300	178	228		250	321	187	240	0.388
P − 22.8 da			1.61	1.58	400	430	328	358		472	505	345	377	0.200
			1.02	1.00	600	630	528	558		745	785	555	590	0.000
$s_x = 72\,\mu$			0.65	0.64	880	850	808	778		1140	1100	850	820	−.196
$s_y = 72\,\mu$			0.41	0.40	1170	1310	1098	1238		1550	1740	1160	1300	−.398
			0.26	0.26	1730	1850	1658	1778		2340	2500	1750	1870	−.593
			0.165	0.16	2260	2250	2188	2178		3080	3060	2300	2300	−.791
			0.105	0.10	2800	2660	2728	2588		3840	3650	2600	2460	−.988
			0.065	0.06	3250	3180	3178	3108		4480	4370	3340	3270	−1.196
1/106	2.5	0.49	0.77	6.30	0	0	0	0	1.19	0	0	0	0	0.800
Dec 12.07			0.48	3.94	170	160	110	92		144	121	108	90	0.596
P − 16.6 da			0.30	2.46	300	260	240	192		314	252	235	186	0.391
			0.19	1.58	480	440	420	372		550	487	411	364	0.200
			0.12	1.00	690	650	630	582		825	762	615	570	0.000
$s_x = 60\,\mu$			0.08	0.65	940	900	880	832		1050	1090	860	815	−.187
$s_y = 68\,\mu$			0.05	0.41	1400	1300	1340	1232		1760	1610	1310	1200	−.387
			0.03	0.25	1800	1770	1740	1702		2280	2230	1700	1670	−.606
1/107	6	0.49	2.19	7.44	0	0	0	0	1.19	0	0	0	0	0.872
Dec 12.07			1.83	6.21	70	70	0	0		0	0	0	0	0.794
P − 16.6 da			1.16	3.94	180	180	110	85		144	111	108	83	0.596
			0.74	2.51	350	380	280	285		367	374	274	279	0.400
$s_x = 70\,\mu$			0.465	1.58	480	530	410	435		535	570	400	425	0.200
$s_y = 95\,\mu$			*0.295*	1.00	730	770	660	675		865	885	645	660	0.000

Table II.—*Measurements of the Lyman-α Halo*—Continued

Frame, Date (GMT)	Δt (s)	S	ΔD	$\Delta D/\Delta D_o$	Δx (μ)	Δy (μ)	δx (μ)	δy (μ)	R_{EC} (AU)	$1.10\delta R_{EC}$ d_x (10^{-5} AU)	$1.10\delta R_{EC}$ d_y (10^{-5} AU)	$0.823\delta R_{EC}$ r_x (10^3 km)	$0.823\delta R_{EC}$ r_y (10^3 km)	log $\Delta D/\Delta D_o$
			0.185	0.63	1020	1050	950	955		1250	1250	930	935	−.200
			0.115	0.39	1470	1470	1400	1375		1830	1800	1370	1350	−.408
			0.075	0.25	1900	1980	1830	1885		2400	2470	1790	1850	−.594
			0.045	0.15	2500	2700	2430	2605		3180	3410	2380	2550	−.816
1/108	15	0.49	>3.40	>4.62	180	170	80	35	1.19	105	46	78	34	>0.665
Dec 12.07			2.89	3.93	210	220	120	85		157	111	118	83	0.595
P − 16.6 da			1.83	2.48	350	390	260	255		340	334	265	250	0.396
			1.16	1.58	520	560	430	425		561	555	420	415	0.200
$s_x = 90\,\mu$			*0.735*	1.00	820	890	730	755		955	987	715	740	0.000
$s_y = 135\,\mu$			0.465	0.63	1170	1270	1080	1135		1410	1485	1060	1110	−.199
			0.295	0.40	1600	1750	1510	1615		1970	2110	1480	1580	−.396
			0.185	0.25	2220	2300	2130	2165		2780	2830	2080	2120	−.600
			0.115	0.156	2830	2800	2740	2665		3580	3480	2680	2700	−.805
			0.07	0.095	3400	3200	3310	3065		4330	4000	3240	3000	−1.022
			0.045	0.061	3830	3500	3740	3365		4880	4400	3660	3300	−1.213
1/179	6	0.32	0.87	4.58	0	0	0	0	1.15	0	0	0	0	0.661
Dec 16.74			0.76	4.00	40	40	0	0		0	0	0	0	0.602
P − 12.0 da			0.48	2.53	150	150	92	91		116	115	87	86	0.404
			0.30	1.58	280	280	222	221		281	280	210	209	0.200
$s_x = 58\,\mu$			*0.19*	1.00	500	450	442	391		560	495	418	370	0.000
$s_y = 59\,\mu$			0.12	0.63	720	690	662	631		839	800	625	600	−.200
			0.075	0.395	960	970	902	911		1140	1155	855	860	−.404
			0.05	0.263	1250	1260	1192	1201		1510	1520	1130	1135	−.580

1/180	15	0.32	>3.59	>7.48	80	30	0	0	1.15	0	0	0	0	>0.874
Dec 16.74			3.00	6.25	100	90	20	0		25	0	19	0	0.796
P — 12.0 da			1.90	3.96	200	190	120	95		152	120	113	90	0.598
			1.20	2.50	290	330	210	235		266	298	198	222	0.398
$s_x = 80\,\mu$			0.76	1.58	450	440	370	345		468	437	350	326	0.200
$s_y = 95\,\mu$			*0.48*	1.00	600	580	520	485		659	615	490	460	0.000
			0.30	0.625	780	740	700	645		885	817	660	610	−.203
			0.19	0.40	1010	1000	920	900		1165	1140	870	850	−.402
			0.12	0.25	1410	1320	1300	1200		1650	1520	1230	1130	−.602
			0.075	0.157	2000	1600	1900	1500		2400	1900	1800	1420	−.804
			0.05	0.104	2500	1800	2400	1700		3040	2150	2270	1610	−.982
			0.03	0.063	2950	2100	2900	2000		3670	2540	2740	1900	−1.204
2/117	2.5	0.12	0.37	12.3	0	0	0	0	1.14	0	0	0	0	1.091
Dec 23.65			0.29	9.67	60	80	7	28		9	35	7	26	0.986
P — 5.0 da			0.185	6.16	150	180	97	128		122	160	91	120	0.790
			0.12	4.00	300	380	247	268		310	336	232	252	0.602
$s_x = 53\,\mu$			0.075	2.50	500	570	447	518		580	650	420	485	0.398
$s_y = 52\,\mu$			0.05	1.67	730	780	677	728		850	910	635	685	0.224
			0.03	1.00	1200	1000	1147	948		1440	1190	1075	890	0.000
2/118	6	0.12	0.98	14.0	0	0	0	0	1.14	0	0	0	0	1.147
Dec 23.65			0.71	10.15	80	90	28	22		35	28	26	21	1.007
P — 5.0 da			0.45	6.43	170	180	118	112		148	140	111	105	0.808
			0.285	4.07	270	280	218	212		274	266	204	198	0.610
$s_x = 52\,\mu$			0.18	2.57	480	470	428	402		535	505	402	378	0.410
$s_y = 68\,\mu$			0.115	1.64	670	570	618	502		775	630	580	470	0.215
			0.07	1.00	980	870	928	802		1160	1000	870	750	0.000
			0.045	0.64	1330	1180	1278	1112		1600	1390	1200	1040	−.192
			0.03	0.43	1600	1350	1548	1282		1940	1610	1450	1200	−.367

Table II.—*Measurements of the Lyman-α Halo*—Continued

Frame, Date (GMT)	Δt (s)	S	ΔD	$\Delta D/\Delta D_o$	Δx (μ)	Δy (μ)	δx (μ)	δy (μ)	R_{EC} (AU)	$1.10\delta R_{EC}$ d_x (10^{-5} AU)	$1.10\delta R_{EC}$ d_y (10^{-5} AU)	$0.823\delta R_{EC}$ r_x (10^3 km)	$0.823\delta R_{EC}$ r_y (10^3 km)	log $\Delta D/\Delta D_o$
2/119	15	0.12	2.31	12.8	0	0	0	0	1.14	0	0	0	0	1.109
Dec 23.65			1.77	9.84	60	100	0	7		0	9	0	7	0.993
P − 5.0 da			1.12	6.23	160	180	90	87		113	109	85	82	0.795
			0.71	3.94	260	280	190	187		238	234	178	175	0.596
$s_x = 70\,\mu$			0.45	2.50	430	450	360	357		451	448	337	335	0.398
$s_y = 93\,\mu$			0.285	1.58	700	640	630	537		790	673	590	505	0.200
			0.18	1.00	1030	900	930	800		1165	1000	875	750	0.000
			0.115	0.64	1430	1200	1330	1100		1670	1380	1250	1030	−.194
			0.07	0.39	2050	1750	1930	1600		2420	2000	1810	1500	−.409
			0.045	0.25	2450	2400	2330	2200		2920	2760	2180	2060	−.602
			0.03	0.167	2700	2700	2630	2500		3300	3140	2470	2340	−.777
2/128	1	1.00	>3.50	>35.0	100	60	10	0	1.14	13	0	9	0	>1.544
Dec 25.9			2.46	24.6	190	200	100	122		126	153	94	114	1.392
P − 2.8 da			1.56	15.6	300	320	210	242		264	304	197	227	1.194
			0.99	9.9	470	420	380	342		477	430	356	320	0.996
$s_x = 90\,\mu$			0.625	6.25	580	530	490	452		615	555	460	423	0.796
$s_y = 78\,\mu$			0.395	3.95	760	630	670	552		840	695	630	517	0.597
			0.25	2.5	930	750	840	672		1055	845	785	630	0.398
			0.16	1.6	1160	920	1070	842		1340	1060	1000	790	0.204
			0.10	1.00	1500	1120	1410	1042		1770	1310	1320	980	0.000
			0.065	0.65	1750	1300	1660	1222		2080	1535	1560	1150	−.188
			0.04	0.4	2150	1550	2060	1472		2580	1850	1930	1380	−.398
2/129	2.5	1.00	>3.12	>12.5	470	400	355	297	1.14	445	373	332	278	>1.098

Dec 25.9			2.46	9.85	520	470	405	367		510	460	380	344	0.993
P — 2.8 da			1.56	6.25	750	630	635	527		800	662	595	495	0.796
			0.99	3.96	950	800	835	697		1050	875	785	655	0.598
$s_x = 115\,\mu$			0.625	2.50	1170	970	1055	867		1325	1090	990	815	0.398
$s_y = 103\,\mu$			0.395	1.58	1400	1170	1285	1067		1610	1340	1200	1000	0.200
			0.25	1.00	1770	1420	1655	1317		2080	1650	1550	1235	0.000
			0.16	0.64	2180	1700	2065	1597		2600	2000	1940	1500	−.194
			0.10	0.40	2650	2000	2535	1897		3180	2380	2380	1780	−.398
2/139	1	1.00	>3.52	>35.2	100	70	15	0	1.14	19	0	14	0	>1.547
Dec 25.9			2.46	24.6	210	200	125	117		157	147	117	110	1.391
P — 2.8 da			1.56	15.6	300	280	215	197		270	247	202	185	1.194
			0.99	9.9	430	420	345	337		433	423	323	316	0.996
$s_x = 85\,\mu$			0.625	6.25	550	520	465	437		585	550	435	410	0.796
$s_y = 83\,\mu$			0.395	3.95	740	600	655	517		823	650	615	485	0.596
			0.25	2.5	930	770	845	687		1060	865	795	645	0.398
			0.16	1.6	1180	900	1095	817		1380	1030	1030	765	0.204
			0.10	1.00	1600	1080	1515	997		1900	1250	1420	935	0.000
			0.065	0.65	2150	1250	2065	1167		2590	1470	1930	1090	−.187
2/140	2.5	1.00	>2.86	>11.4	850	670	680	500	1.14	853	627	636	470	>1.058
Dec 25.9			2.46	9.85	900	720	730	550		915	690	685	515	0.994
P — 2.8 da			1.56	6.25	1150	900	980	730		1230	915	930	685	0.796
			0.99	3.96	1350	1120	1180	950		1480	1190	1110	890	0.598
$s_x = 170\,\mu$			0.625	2.50	1630	1280	1460	1110		1830	1390	1370	1040	0.398
$s_y = 170\,\mu$			0.395	1.58	2030	1500	1860	1330		2330	1670	1740	1250	0.200
			0.25	1.00	2500	1750	2330	1580		2920	1980	2180	1480	0.000
			0.16	0.64	3030	2150	2860	1980		3590	2480	2680	1860	−.194
			0.10	0.40	3450	2500	3280	2330		4110	2920	3080	2180	−.400

Table II.—*Measurements of the Lyman-α Halo*—Concluded

Frame, Date (GMT)	Δt (s)	S	ΔD	$\Delta D/\Delta D_o$	Δx (μ)	Δy (μ)	δx (μ)	δy (μ)	R_{EC} (AU)	$1.10\delta R_{EC}$ (10^{-5} AU) d_x	$1.10\delta R_{EC}$ (10^{-5} AU) d_y	$0.823\delta R_{EC}$ (10^{3} km) r_x	$0.823\delta R_{EC}$ (10^{3} km) r_y	log $\Delta D/\Delta D_o$
3/4	6	0.12	0.57	8.15	0		0		0.97	0		0		0.911
Jan 2.94			0.53	7.57	80	0	23			25		18		0.880
P + 5.3 da			0.45	6.43	190	280	133	235		142	251	106	187	0.808
			0.285	4.07	390	480	333	435		355	465	266	347	0.610
$s_x = 57\,\mu$			0.18	2.57	670	650	613	605		655	645	488	482	0.410
$s_y = 45\,\mu$			0.115	1.64	840	840	783	795		835	850	624	634	0.216
			0.07	1.00	1030	1100	973	1055		1040	1125	775	840	0.000
			0.045	0.64	1250	1270	1193	1225		1273	1310	950	975	−.192
			0.03	0.43	1500	1440	1443	1395		1540	1490	1150	1110	−.368
3/5	15	0.12	>3.52	19.5					0.97					>1.292
Jan 2.94			2.80	15.6										1.192
P + 5.3 da			1.77	9.93		450		397			423		316	0.997
			1.12	6.22	580	560	510	507		545	540	406	404	0.794
$s_x = 70\,\mu$			0.71	3.94	690	710	620	657		660	700	495	525	0.596
$s_y = 53\,\mu$			0.45	2.50	800	800	730	747		780	795	582	595	0.398
			0.285	1.58	950	940	880	887		940	950	702	707	0.200
			0.18	1.00	1150	1130	1080	1077		1155	1150	860	860	0.000
			0.115	0.64	1420	1300	1350	1247		1440	1330	1075	995	−.194
			0.065	0.36	1720	1570	1650	1517		1760	1620	1315	1210	−.442
3/50	6	0.12	0.41	5.85	0	0	0	0	0.89	0	0	0	0	0.767
Jan 6.57			0.37	5.28	75	120	25	70		24	69	18	51	0.723
P + 8.9 da			0.285	4.07	140	205	90	155		88	152	66	113	0.610
			0.18	2.57	440	400	390	350		382	342	286	256	0.410

$s_x = 50\,\mu$			0.115	1.64	690	630	640	580		626	567	470	425	0.216
$s_y = 50\,\mu$			*0.07*	1.00	900	870	850	820		832	802	623	600	0.000
			0.045	0.64	1110	1170	1060	1120		1037	1096	775	820	−.192
			0.03	0.43	1250	1400	1200	1350		1175	1320	880	990	−.368
3/51	15	0.12	1.28	7.11	0	0	0	0	0.89	0	0	0	0	0.852
Jan 6.57			1.12	6.22	80	80	20	20		20	20	15	15	0.794
P + 8.9 da			0.71	3.94	250	250	190	190		186	186	139	139	0.596
			0.45	2.50	470	400	410	340		400	333	300	249	0.398
$s_x = 60\,\mu$			0.285	1.58	710	670	650	610		635	597	475	447	0.200
$s_y = 60\,\mu$			*0.18*	1.00	980	920	920	860		900	840	675	630	0.000
			0.115	0.64	1400	1350	1340	1290		1310	1260	980	945	−.194
			0.07	0.39	1850	1800	1790	1740		1750	1700	1280	1245	−.409
			0.045	0.25	2300	2080	2240	2020		2190	1980	1600	1450	−.602
3/74	15	0.11	0.66	4.00		0		0	0.83		0		0	0.602
Jan 10.72			0.55	3.33		80		30			27		18	0.523
P + 13.0 da			0.46	2.79	0		0					0		0.446
			0.41	2.49	90	190	40	140		37	128	27	96	0.396
$s_x = 50\,\mu$			0.26	1.58	360	330	310	280		283	256	212	191	0.200
$s_y = 50\,\mu$			*0.165*	1.00	580	550	530	500		485	455	362	341	0.000
			0.105	0.64	830	900	780	850		712	775	532	580	−.195
			0.065	0.395	1100	1160	1050	1110		960	1010	715	757	−.403
			0.04	0.24	1550	1450	1500	1400		1370	1280	1020	955	−.615

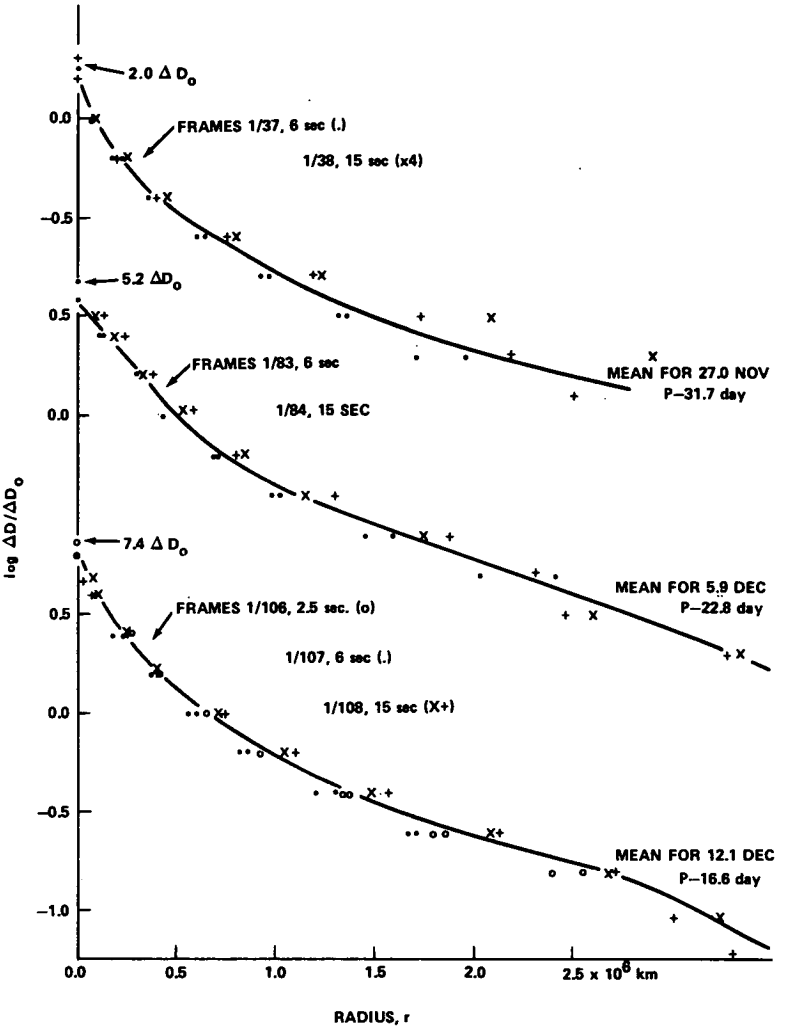

FIGURE 18.—*Brightness versus radius in the Comet's Lyman-α halo on November 27, and December 6 and 12, 1973. Measures of the density relative to the "standard" Do are plotted for two or three frames on each date. ΔDo = 0.1 S Δt corresponds to edge brightness Bo ≈ 20 kilo-Rayleighs. Different symbols (x, +) are used for the x- and y-radii measured on the longest exposure on each date.*

increase in "concentration" of the hydrogen halo might be expected from the increase in hydrogen production from the comet nucleus near perihelion.

The mean curves of log D/D_o versus radius in figure 21 are fairly well fitted by the empirical relation log $\Delta(r)$ = log Δ_n − $(r/r_o)^n$ log Δ_n, where $\Delta(r) = \Delta D/\Delta D_o$ = density normalized to 1.00 for 20 kilo-Rayleigh bright-

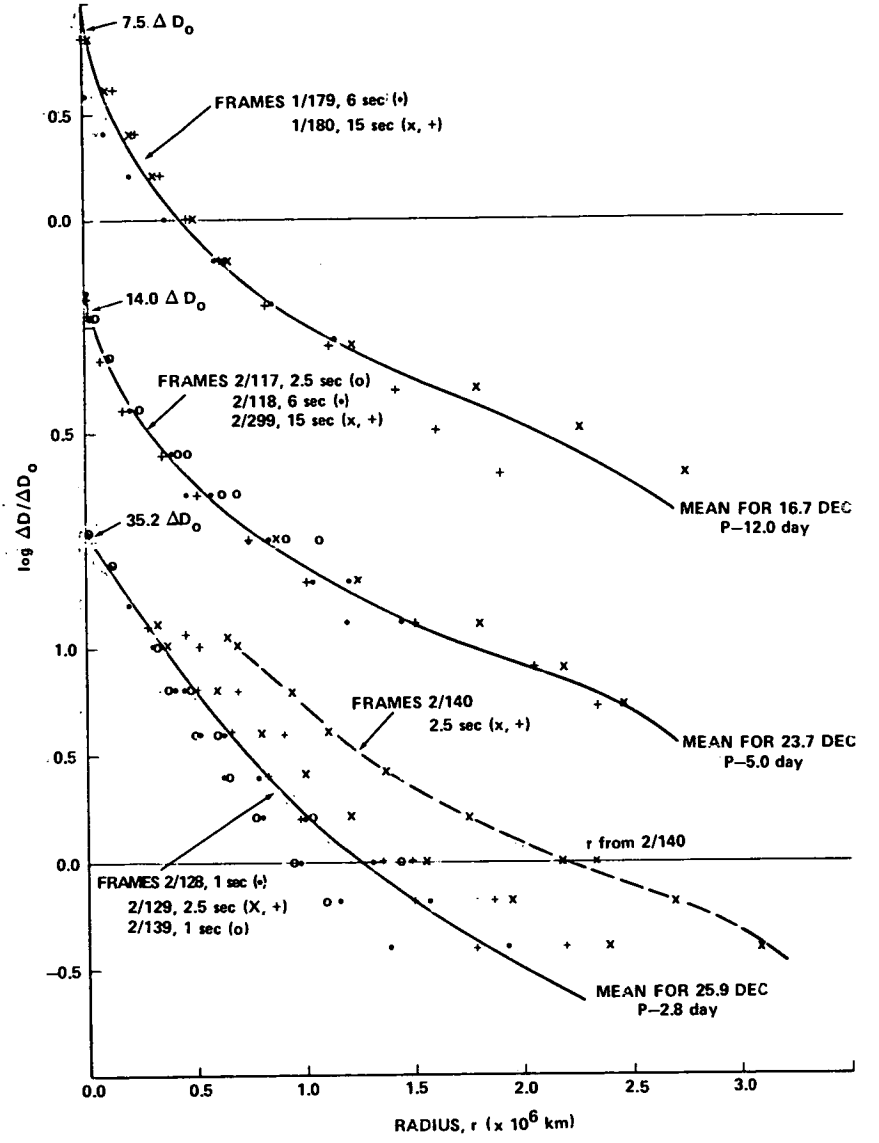

FIGURE 19.—*Brightness versus radius in the Lyman-α halo on December 16, 23, and 25, 1973. Frame 2/140, 2.5-s exposure, shows an oversize halo for undetermined reason.*

ness, $\Delta_n = \Delta D_h/\Delta D_o$ = the peak central density, $r_o = (r_x + r_y)/2$ at $\Delta D = \Delta D_o$ from table III, and $n = 1/2$ before December 24, $n = 2/3$ after December 24. (This change in the index n represents the steeper gradi-

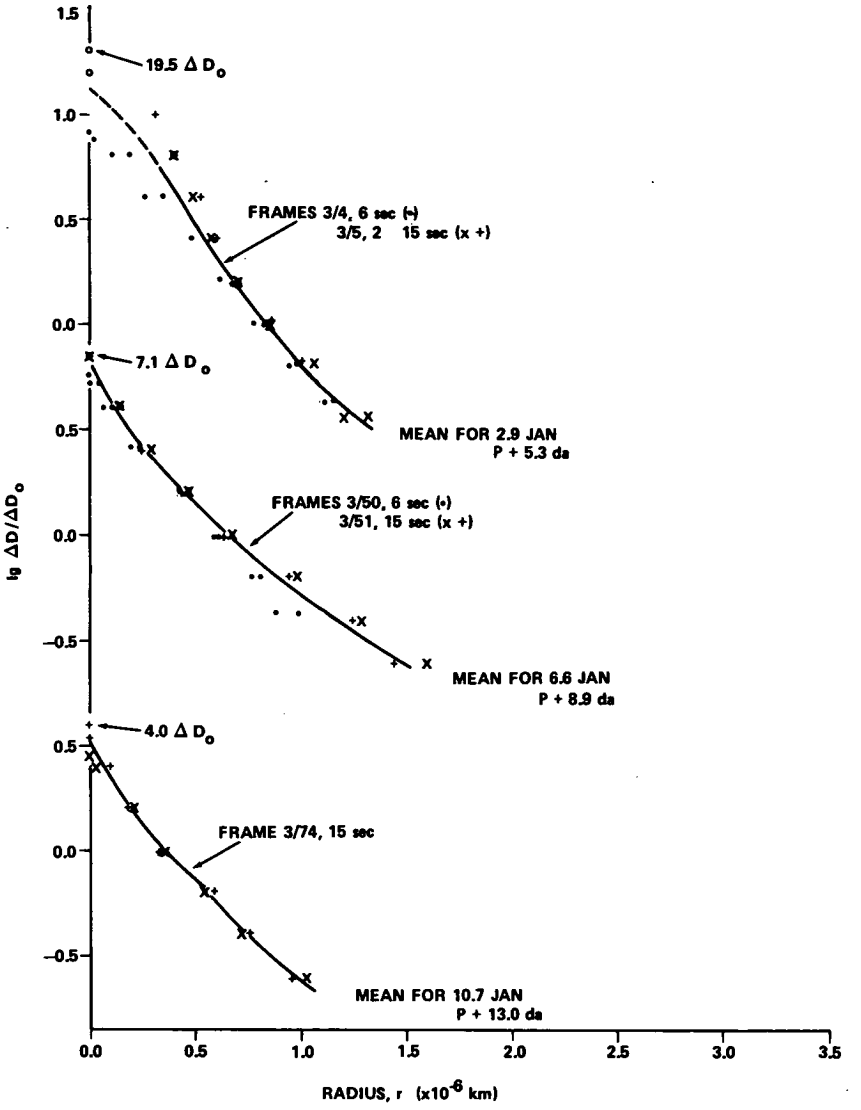

FIGURE 20.—*Brightness versus radius in the Lyman-α halo on January 3, 6, and 10, 1974.*

ent of brightness with radius, or greater "concentration" of the halo after December 24.) Using this empirical relation, the integrated density volume, $2\pi \int_o^\infty \Delta(r)\ dr$ is $\Delta(\text{total}) = 32.8\ r_o^2\ \Delta_n/1g\ \Delta_n$ before December 24, and $8.2\ r_o^2\ \Delta_n/1g\ \Delta_n$ after December 24. These estimates of the total Lyman-α brightness of the comet halo are also plotted in figure 22.

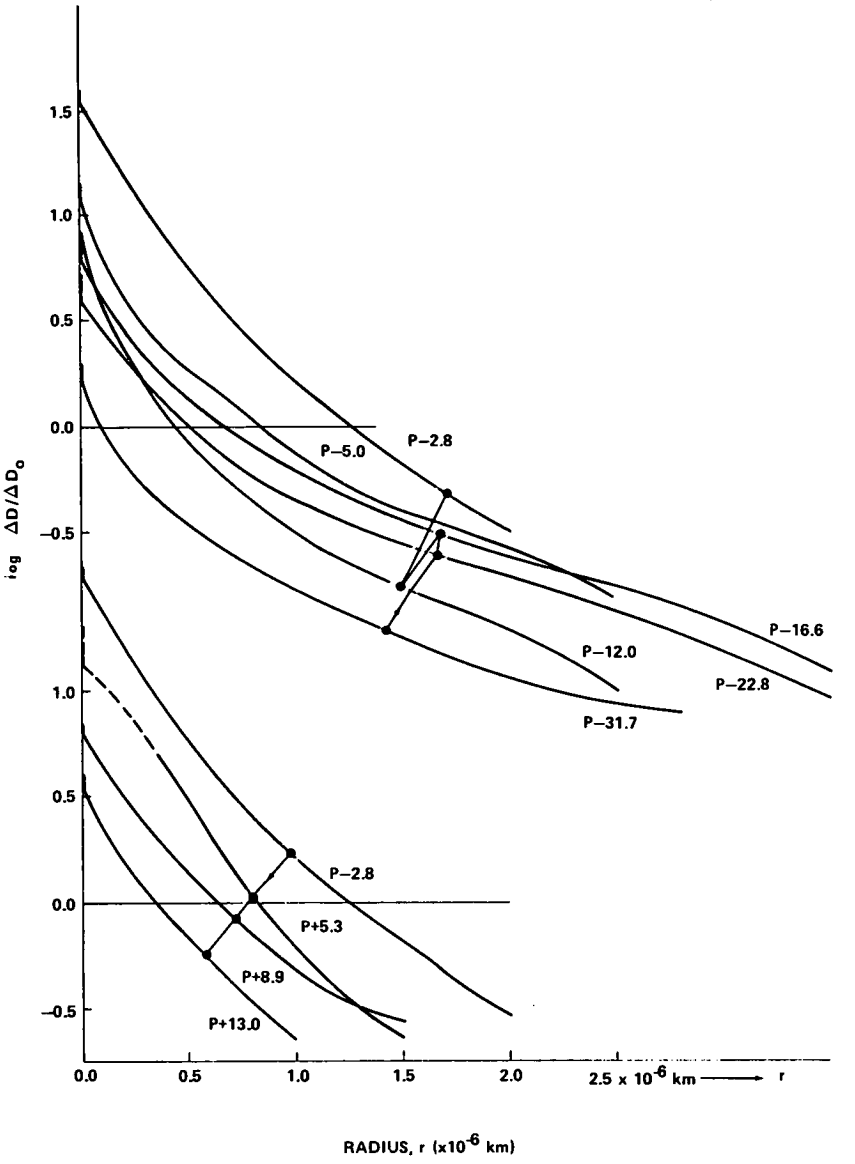

FIGURE 21.—*Mean curves of brightness versus radius in the halo on nine different dates. The upper set show the pre-perihelion Lyman-α halo development from P − 31.7 days through P − 2.8 days. The lower set show the post-perihelion decline from P − 2.8 through P + 13.0 days.*

Table III.—*Time Variations in the Lyman-α Halo*

Date (GMT day)	Frame	ES/10 (D)	$\Delta D_n/\Delta D_o$	d_x (10^{-5} AU)	d_y (10^{-5} AU)	r_x (10^3 km)	r_y (10^3 km)	Peak/$(r_x + r_y)$ (10^{-6} km^{-1})	R_{SC} (AU)	β	V_{EC} (km/s)	V_{SC} (km/s)
	1/37	0.60	1.68	115	72	85	54					
Nov 26.98	1/38	1.50	1.99	107	75	80	56					
P − 31.7	Mean		1.84	111	74	83	55	(13.3)	0.974	42°	−37.8	−39.4
	1/83	0.41	5.17	590	590	440	440					
Dec 5.92	1/84	1.02	>3.17	745	785	555	590	5.10	0.760	50°	−29.4	−43.6
P − 22.8	Mean		5.17	667	688	498	515					
	1/106	0.12	6.30	825	762	615	570					
Dec 12.07	1/107	0.295	7.44	865	885	645	660					
P − 16.6	1/108	0.735	>4.62	955	987	715	740					
	Mean		6.87	882	878	658	657	5.22	0.599	56°	−19.9	−47.5
	1/179	0.19	4.58	560	495	418	370					
Dec 16.74	1/180	0.48	7.48	659	615	490	460					
P − 12.0	Mean		6.03	610	555	454	415	6.95	0.466	58°	−10.5	−51.4
	2/117	0.03	12.33	1440	1190	1075	890					
Dec 23.65	2/118	0.072	14.00	1160	1000	870	750					
P − 5.0	2/119	0.18	12.80	1165	1000	875	750					
	Mean		13.00	1255	1063	940	797	7.50	0.249	47°	+2.6	−55.2
	2/128	0.10	>35.00	1770	1310	1320	980					
	2/129	0.25	≫12.50	2080	1650	1550	1235					
Dec 25.9	2/139	0.10	>35.20	1900	1250	1420	935					
P − 2.8	2/140	0.25	≫11.40	2920	1980	2180	1480					

	Mean		⩾40.00	2168	1548	1618	1158	⩾14.4	0.182	29°	+2.3	−45.8
	3/4	0.072	8.15	1040	1125	775	840					
Jan 2.94	3/5	0.18	⩾19.50	1156	1150	860	860					
P + 5.3	Mean		19.50	1098	1138	818	850	11.7	0.271	85°	−45.7	+55.7
	3/50	0.072	5.85	832	802	622	600					
Jan 6.57	3/51	0.18	7.11	900	840	675	630					
P + 8.9	Mean		6.48	866	821	649	615	5.13	0.389	92°	−31.3	+53.8
Jan 8.1	Aerobee								0.434	92°	−25.8	+52.4
P + 10.4	(20 kR)											
Jan 10.72	3/74	0.165	4.00	485	455	362	341	5.7	0.512	91°	−16.1	+50.0
P + 13.0												

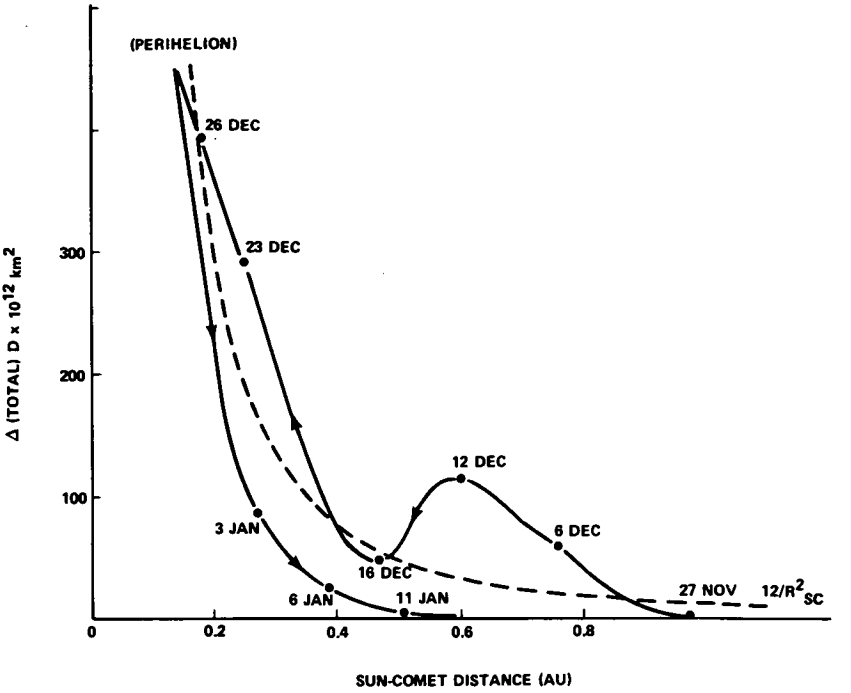
(PERIHELION)
26 DEC
23 DEC
12 DEC
3 JAN
6 DEC
16 DEC
6 JAN
11 JAN
27 NOV
12/R²SC
Δ (TOTAL) D x 10¹² km²
300
200
100
0
0.2
0.4
0.6
0.8
SUN-COMET DISTANCE (AU)

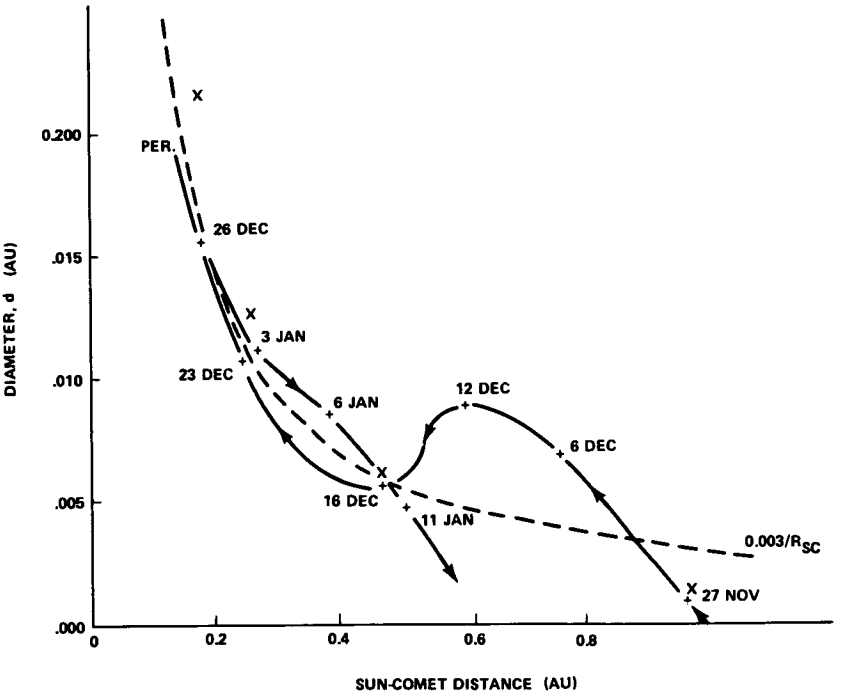
PER.
26 DEC
3 JAN
23 DEC
6 JAN
12 DEC
6 DEC
16 DEC
11 JAN
0.003/RSC
27 NOV
DIAMETER, d (AU)
0.200
.015
.010
.005
.000
0
0.2
0.4
0.6
0.8
SUN-COMET DISTANCE (AU)

Hydrogen Production Rate in the Comet Nucleus

Opal et al. (1974) have analyzed photos of Comet Kohoutek taken by a similar camera on an Aerobee rocket launched on January 8, 1974. Their results, shown in figure 22 and table III, give somewhat higher peak density, ΔD_n, than the S201/SL4 data. Their analysis shows that the hydrogen atoms released from the comet nucleus diffuse outward at about 8 km/s. In a steady state, with Q atoms per second-steradian leaving the nucleus at 8 km/s, they show that halo brightness at r km from the nucleus will be

$$B(r) = 3.93 \times 10^{-20}\, g_o Q / R_{SC}^2 \quad r \text{ kilo-Rayleighs} \qquad (1)$$

where $g_o \approx 0.000212$ solar Lyman-α photons scattered per second-atom in the line of sight at $R_{SC} = 1$ AU. Their measurement of $B(r) = 25$ kR at $r = 6.2 \times 10^5$ km yields $Q = 3.6 \times 10^{28}$ atoms per second-steradian.

If ΔD_o corresponds to $B_o = 20$ kR, the brightness corresponding to other densities, ΔD in tables II and III, is

$$B(r) = 20\, \Delta D / \Delta D_o \qquad \text{in kilo-Rayleighs.} \qquad (2)$$

Combining this with equation (1) yields

$$Q = 2.40 \times 10^{23}\, R_{SC}^2\, r\, \Delta D / \Delta D_o \qquad \text{per second-steradian.} \qquad (3)$$

Applied to the measurements in table II, equation (3) yields ranges of values shown in table IV. Because the model is imperfect (no allowance for changing Doppler shift or possible changes in solar activity), four distinct values of Q are listed, as well as the mean for each date: Q_n based on the smallest reliable value of r, Q_e based on the largest value of r, and Q_o based on the standard density ΔD_o. Following Opal et al. (1974), the slope of $B(r)$ versus $1/r$ was also determined in order to combine all the measurements in table II. Two plots of $\Delta D / \Delta D_o$ versus $10^6/r$ are shown in figure 23. From equation (3), Q is related to the slope, Σ, by

$$Q_s = 2.40 \times 10^{29}\, R_{SC}^2\, \Sigma \qquad \text{per second-steradian.} \qquad (4)$$

As table IV shows, Q_s is generally larger than the other values; Q_n and Q_e are smaller except on December 25.9, 2.8 days before perihelion. Figure 24 also shows that Q is approximately proportional to R_{SC} in the interval covered by these observations, except for the low value on November 26.98, 31.7 days pre-perihelion.

FIGURE 22.—*Diameter and brightness of the Lyman-α halo versus Sun-comet distance. The dashed curves show a rough fit to d = 0.003/Rsc (in AU) and Δ (total) = 12/R²sc (in D × 10¹²km²), except for the preperihelion maximum on December 12.*

Table IV.—*H-Production in Comet Kohoutek*

Frame	$r_n/10^6$ (km)	$Q_n/10^{28}$	$r_e/10^6$ (km)	$Q_e/10^{28}$	$r_o/10^6$ (km)	$Q_o/10^{28}$	$Q_s/10^{28}$	Range in $Q/10^{28}$	Mean $Q/10^{28}$, Error	t (days)	R_{SC} (AU)
1/37	0.070	1.6	1.70	2.4	0.054	1.2	2.9	1.2–3.3	2.3	P − 31.7	0.974
1/38	0.068	1.6	2.50	2.3	0.056	1.3	3.7	1.3–4.5	± .7		
1/83	0.121	4.2	2.03	4.5	0.440	6.1	6.4	4.5– 6.9	6.2	P − 22.8	0.760
1/84	0.125	5.5	3.27	2.7	0.590	8.2	9.0	2.7–10.7	±1.7		
1/106	0.099	3.4	1.67	3.6	0.570	4.9	4.5	3.4– 4.9			
1/107	0.095	3.2	2.55	3.3	0.660	5.7	6.0	3.2– 6.4	4.6	P − 16.6	0.599
1/108	0.056	2.2	3.3	1.7	0.740	6.4	5.5	1.7– 6.4	±1.2		
1/179	0.086	1.1	1.14	1.6	0.370	1.9	1.8	1.1– 1.9	1.9	P − 12.0	0.466
1/180	0.102	2.1	1.90	0.6	0.460	2.4	3.2	0.6– 3.2	± .6		
2/117	0.105	1.0	0.89	1.3	0.890	1.3	1.0	1.0– 1.4			
2/118	0.024	0.4	1.20	0.8	0.750	1.1	1.0	0.4– 1.4	1.0	P − 5.0	0.249
2/119	0.084	0.8	2.34	0.6	0.750	1.1	0.9	0.6– 1.1	± .2		
2/128	0.104	2.0	1.38	0.4	0.980	0.8	3.3	0.4– 3.3			
2/129	0.280	2.8	1.78	0.6	1.235	1.0	3.3	0.6– 3.3			
2/139	0.114	2.2	1.09	0.6	0.935	0.7	2.7	0.6– 2.7	1.7	P − 2.8	0.182
2/140	0.470	4.2	2.18	0.7	1.480	1.2	4.7	0.7– 4.7	±1.2		
3/4	0.146	1.7	1.11	0.8	0.840	1.5	3.2	0.8– 3.2	2.4	P + 5.3	0.271
3/5	0.405	4.4	1.21	0.8	0.860	1.5	6.7	0.8– 6.7	±1.7		
3/50	0.035	0.7	0.99	1.5	0.600	2.2	1.9	0.7– 2.3	1.9	P + 8.9	0.389
3/51	0.015	0.3	1.45	1.3	0.630	2.3	2.1	0.3– 2.5	± .3		
Aerobee			0.62	3.6						P + 10.4	0.434
3/74	0.062	1.0	0.95	1.4	0.341	2.1	1.7	1.0– 2.1	1.8 ± .2	P + 13.0	0.512

Atomic Oxygen Emission

It was expected that the S201/SL4 far-UV photographs would provide data on oxygen as well as hydrogen production in Comet Kohoutek, but preliminary measures do not confirm this. Spectrograms taken by Opal et al. (1974) on January 8.1, 1974, show C I λ1657 Å and O I λ1304 Å emission in roughly 3:1 brightness ratio. With KBr photocathode cutoff at 1600 Å, the S201/SL4 camera could not detect the carbon emission, and it does not show oxygen (even on exposures as long as 500 seconds) except on December 25.9, as shown in figures 6 and 8. A remarkable tail appears on six different frames with exposures of 10, 30, and 107 seconds through CaF_2, 1250–1600 Å bandpass. It is about 500 000 km wide near the nucleus, and its

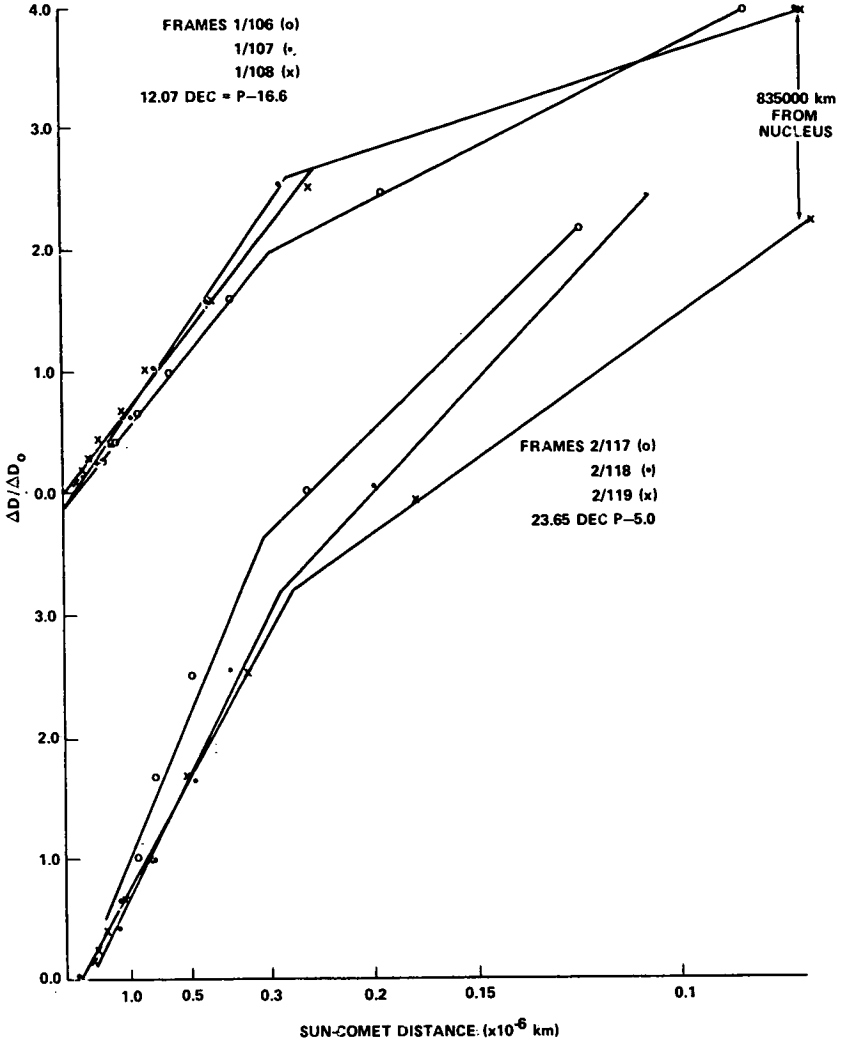

FIGURE 23.—*Halo brightness versus 1/radius. The slopes of these curves are proportional to hydrogen production rate. Note the fair agreement between three frames on each date, and the lower slopes for* $r < 300\,000$ *km, possibly the result of Lyman-α self-absorption near the halo center.*

projected length (at $\beta = 29°$) is at least 2×10^6 km, narrowing to a point at the antisolar end. This length and shape make it unlikely that these far-UV photographs recorded oxygen in the ion tail of Comet Kohoutek, particularly since the earlier (December 23.65) and later (January 2.94) CaF_2

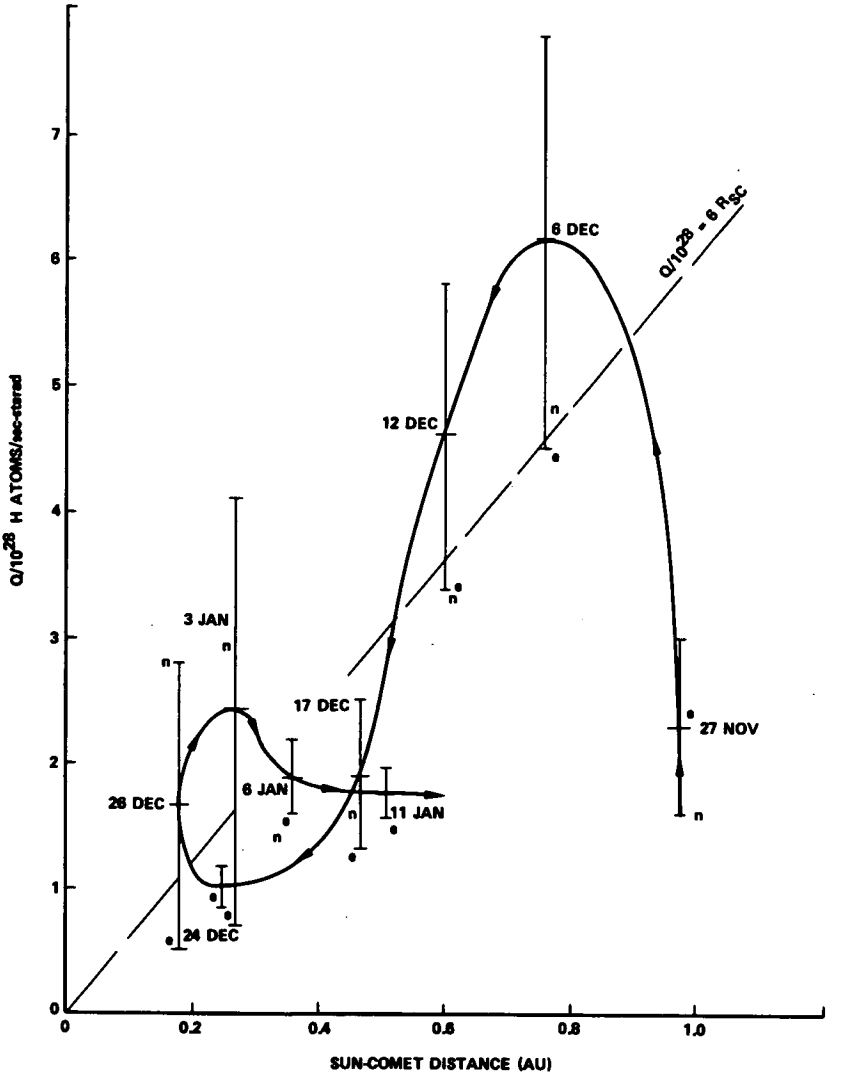

FIGURE 24.—*Hydrogen production rate, Q, versus Sun-comet distance, R_{SC}. The error bars show the range in estimates listed in table 4. Nuclear (Q_n) and edge (Q_e) estimates are denoted by "n" and "e." The dashed line shows a rough fit to $Q/10^{28} = 6\ R_{SC}$, except for the low November 27 estimate.*

photographs do not show it. It may be sunlight scattered from the comet's dust tail or 1370 Å band emission from C + O combination (^3P levels).

A great deal more analysis is necessary to get all pertinent data on Comet Kohoutek from the S201/SL4 far-UV photographs.

REFERENCES

CARRUTHERS, G. R.; and PAGE, T.: 1972, Science 177, 788.
CARRUTHERS, G. R.: 1973, Appl. Opt. 12, 2501.
HENIZE, K. G.: 1974, private communication.
OPAL, C. B.; CARRUTHERS, G. R.; PRINZ, D. K.; and MEIER, R.: 1974 Science (in press).

OBSERVATIONS OF COMET KOHOUTEK (1973f) WITH A GROUND-BASED FABRY-PEROT SPECTROMETER

D. H. HUPPLER
F. L. ROESLER
F. SCHERB
J. T. TRAUGER
Department of Physics
University of Wisconsin

A Fabry-Perot spectrometer with an aperture of 150 mm was installed at the Kitt Peak McMath Solar Telescope to observe various emission lines from the gas cloud surrounding Comet Kohoutek between December 1, 1973, and February 2, 1974. Over this time period the intensity of the Hα 6563 Å line tended to vary as the minus 3.3 $\pm$ 0.4 power of the Sun-comet distance (fig. 1). The Hα line profiles (fig. 2) can be fitted well assuming the hydrogen atoms were expanding radially with a Maxwellian speed distribution, with mean speed 7.8 $\pm$ 0.5 km s^{-1} (T = 2900 K), but are inconsistent with a single-speed distribution. The absolute Hα intensities thus yield a hydrogen atom production rate, which on December 7, 1973, was 10^{30} atoms s^{-1}. Observations of Hα on the head and within about 200 000 km of the head in the tailward direction show blending with an H_2O^+ line (Wehinger et al., 1974) Doppler-shifted in the tailward direction by a variable amount, typically 20 to 40 km s^{-1}. Presumably these ions were accelerated tailward by interaction with the solar wind. (Production rates for H_2O^+ can be determined pending determination of the relevant cross sections.)

From the intensity of the [OI] 6300 Å line, one finds a production rate of ^{1}D oxygen atoms of 2 $\times$ 10^{28} atoms s^{-1} on December 8, 1973. The instrumental resolution of 40 000 was insufficient to determine the [OI] line profile (fig. 3), but an effective temperature greater than 2000 K is precluded. Measurements at the Dα wavelength before and after perihelion put an upper limit of 0.01 on the D/H ratio. Observations incompletely analyzed at this time are expected to yield upper limits for the intensities of the Hα 4861 Å, [OI] 5577 Å, and HeI 5015 Å lines.

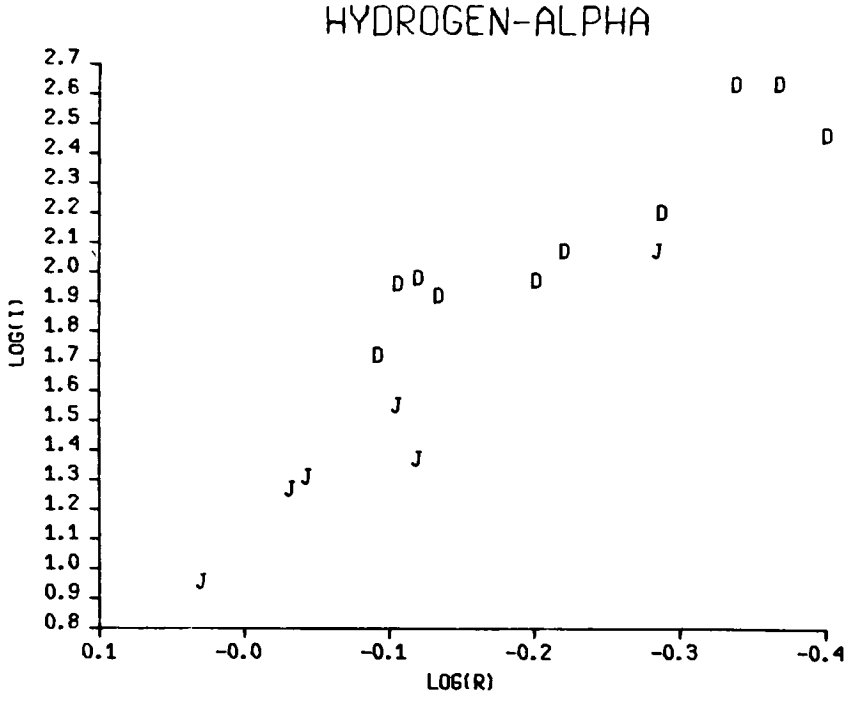

HYDROGEN-ALPHA (N=3→N=2)

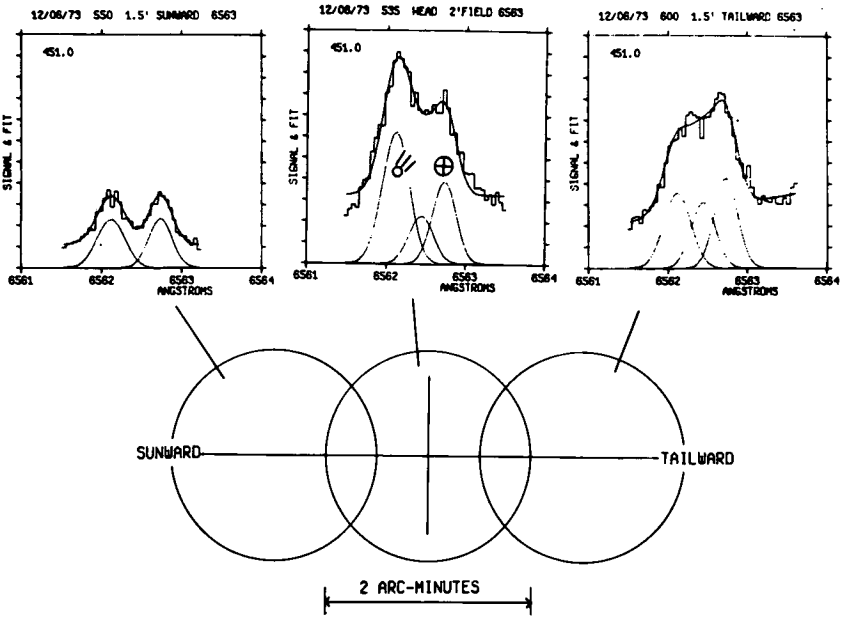

FIGURE 1.—*Hydrogen-Alpha emission in a circular 2-arc-minute field centered on the comet head. The log of the intensity in Rayleighs is plotted versus the log of the Sun-comet distance in AU. The D's are pre-perihelion and the J's are post-perihelion. A least-squares fit to a straight line gives* $I \propto r^{-3.8}$.

FIGURE 2.—*Hydrogen-Alpha scans with circular 2-arc-minute field of view. The left scan is 1-1/2 arc-minutes sunward, the center scan is centered on the head, and the right scan is 1-1/2 arc-minutes tailward. The comet Hα emission is blue-shifted from the geocorona Hα by the comet-Earth relative velocity on December 6, 1973. The* H_2O^+ *line is seen in the head and tailward scan red-shifted relative to the comet Hα.*

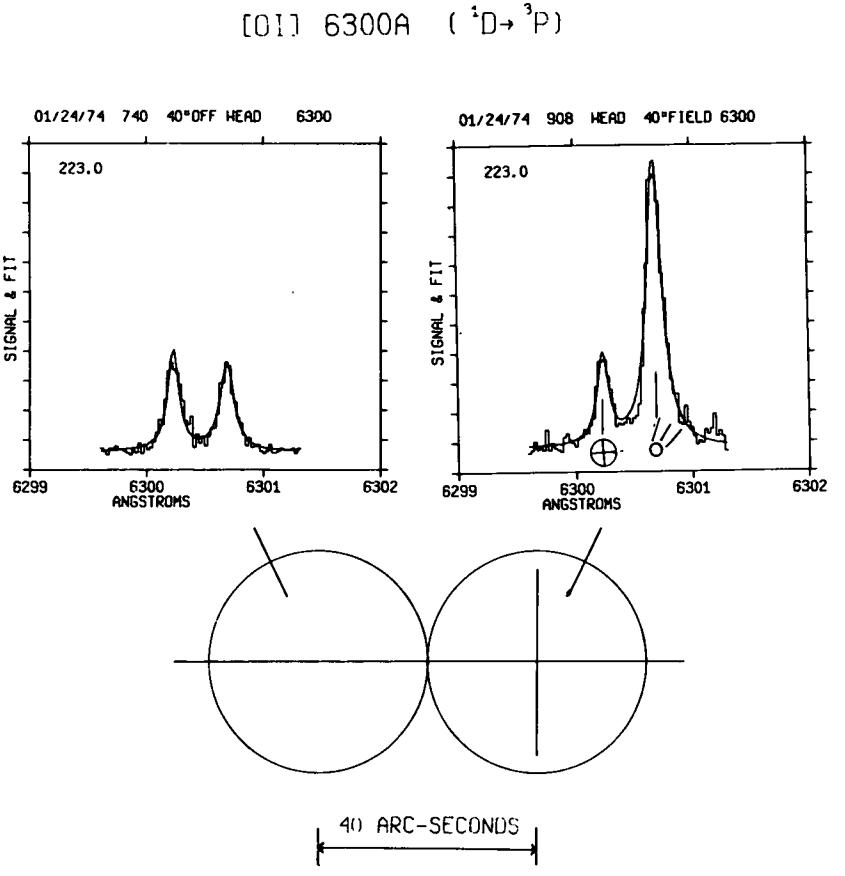

FIGURE 3.—*Forbidden Oxygen 6300 Å scans with circular 40 arc-second field of view. The left scan is 40 arc-seconds off the head and the right scan is centered on the head. The comet line is red-shifted from the airglow line by the comet-Earth relative velocity on January 24, 1974.*

REFERENCES

WEHINGER, P. A.; WYCKOFF, S.; HERBIG, G. H.; HERZBERG, G.; and LEW, H.: 1974, Ap. J. 190, L43.

DISCUSSION

OPAL: We looked at corrected production rates from the Skylab results, and it looks as if the production rates for hydrogen before perihelion were some four or five times higher than after perihelion.

HUPPLER: That is nice.

HERBIG: If someone claimed this effect was entirely H_2O^+, not hydrogen at all, how would you defend against that?

HUPPLER: If it is H_2O^+ totally then (if it had no Doppler shift relative to the comet) you would see it where we see it, sunward; but, there should be a Hydrogen Alpha ($H\alpha$) emission that is equivalent to what we see, because of the Lyman Alpha observations, and we are not really sure that we can identify this H_2O^+. It occurs at the right place and has the right width and height for Hydrogen Alpha emission. The oxygen also occurs at the right place.

WEHINGER: There are a few other H_2O^+ lines that are not very far from $H\alpha$. Could you compress your scan on variable spacing?

HUPPLER: The problem is that with our instrument we came up with a 10 Å interference filter. We wish we had known about the H_2O^+ before we went after $H\alpha$. We would have looked at a line that was clear to find out what the velocity shift is and exactly how it varies, to map it around the comet. I would not like to place too much emphasis on our width.

The Lyman Alpha velocity is 8 km per second. We don't observe the higher velocity components because they are in the wings of our profile. There could be easily a lower velocity component and a higher velocity component. The lower velocity components would have been ionized already before they got out where the Lyman Alpha people were looking.

OBSERVATION OF THE COMET KOHOUTEK (1973f) IN THE RESONANCE LIGHT ($A^2\Sigma^+$–$X^2\Pi$) OF THE RADICAL OH

J. E. BLAMONT
M. FESTOU
Service d'Aéronomie
Centre National de la Recherche Scientifique d'Études Spatiales

Two monochromatic pictures of Comet Kohoutek (1973f) were taken on January 15, 1974, at 03.00 UT (Sun-comet distance = 0.62 AU; Earth-comet distance = 0.82 AU) in the resonance light ($A^2\ \Sigma^+ - X^2\Pi$) of the radical OH. The equipment was a photographic telescope ($f/2$), 300 mm in diameter, placed behind a heliostat. The measurements were made onboard the NASA 990 Convair airplane operated by Ames Research Center. The heliostat was stabilized by two gyros correcting in azimuth and elevation in sidereal time. The first flights revealed an important drift in one direction. Effects due to instrumental drift and motion of the comet on the position of the image have been manually corrected. However, there remains a broadening of the comet image in the direction parallel to the drift. The pointing accuracy is $\pm$ 10 arc-seconds in the direction perpendicular to the drift.

An interference filter, with a peak transmission at 3090 Å of 30 percent and a bandpass of 70 Å was placed in the focal plane. From a complete study of the transmission of the filter and of the features shown on the spectra of Comet Kohoutek, it is concluded that no contamination of the data by emission other than that of the (0-0) band occurred.

The film was calibrated before and after each flight. Absolute calibration of the film has been carried out. Total transmission is a function of the atmospheric transmission causing the features deduced from our data to be in error as much as a factor of 2.

Isophotes of the (0-0) band are presented and analyzed in a direction perpendicular to the drift (*Icarus*, 1974). Such a picture provides two types of information:

(1) The value of the intensity recorded at the peak is 6 kilo-Rayleighs (kR) at the airplane level, which corresponds to a value of $\simeq$ 300 kR emitted by the comet. The OH cloud is optically thin and integration over the iso-

photes provides the total number of OH radicals in the comet: $n \simeq (2 \pm 1) \times 10^{34}$ radicals.

(2) The comparison of a profile with an Haser model distribution of the OH radicals leads to a lifetime of the OH radical of

$$\tau_{OH} = (4.8 \pm 1) \times 10^4 \text{ s}$$

This is the first measurement of the lifetime of the OH radical in a comet. The value appears very close to the lifetime of H_2O.

The photodissociation of H_2O and OH produce the H-atoms previously observed in comets. The short lifetime of OH combined with the high total production rate of gas in comets ($> 3 \times 10^{30}$ mol.s^{-1} sr^{-1}) can explain the observed velocity of 8 km s^{-1} for the H-atoms: H_2O is photodissociated inside a sphere of radius 30 000 to 40 000 km and produces H-atoms thermalized by neutral compounds. Between 4×10^4 km and 10^5 km, OH is the parent molecule of the H-atoms; collisions are negligible and the H-atoms retain the major portion of the excedent energy E resulting from the dissociation of OH. These H-atoms reach the outer part of the hydrogen envelope with the observed velocity of 8 km s^{-1}. The value of E is $\simeq 2 \times 10^4$ cm^{-1}, in good agreement with values deduced from the OH energy diagram level.

NOTE: The complete paper has been submitted to the journal *Icarus*.

REFERENCE

BLAMONT, J. E.; and FESTOU, M.: 1974, Icarus, 23, 538.

DISCUSSION

LANE: The interference filter you used included both the 0–0 and the 1–1 OH band?

BLAMONT: 0–0 only.

LANE: There is a very sharp time dependence on individual line intensities in OH in the 0–0 band and the total surface brightness is time-dependent. One needs to check total line intensity.

WEHINGER: In the model you show that H_2O dissociates into hydrogen at 40 000 km. We have obtained that H_2O^+ lines are still strong in the comet tail at that distance and may extend twice that far.

KELLER: Do you know the cross section you used for your calculation?

BLAMONT: It was 10^{-15} cm^2.

KELLER: Comet Bennett showed a similar result in OH.

ULTRAVIOLET HYDROXYL OBSERVATIONS OF COMET KOHOUTEK ON JANUARY 24, 1974

GALE A. HARVEY
Langley Research Center

Observations of hydroxyl (OH) emission in the electronic band system ($^2\Sigma$-$^2\Pi$) near λ3100 from Comet Kohoutek were made during the evening of January 24, 1974. The severe atmospheric attenuation in the ultraviolet OH spectral region and the low-elevation angles resulting from observing the comet while it was inside the Earth's orbit led to use of the NASA Convair 990 Flying Laboratory as an observing platform. The observations were made from an altitude of 41 000 ft; i.e., above the bulk of the Earth's atmosphere. Low-resolution spectra of the comet in the wavelength interval λ3000 to λ4600 were obtained during an evening flight just off the coast of the state of Washington. These observations are described in more detail elsewhere (Harvey, 1974).

The comet was of visual magnitude 5.5 as determined by Bobrovnikoff's method with 7 × 50 binoculars. The spectra were recorded with an $f/1.3$ Maksutov slitless spectrograph of 150-mm aperture. The dispersion element was a double fused-silica prism of 54° combined apex angle. The spectra were recorded on single-coated medical X-ray film and processed for high contrast. An inertial image-stabilization mirror system was used to reduce trailing of the comet image due to aircraft roll.

The spectra consist of three features: strong OH-NH radiation unresolved, a weak λ3880 CN band, and a still weaker continuum between the OH-NH and the CN bands. These slitless spectra have been compared with the slit spectra taken during a similar period by A. L. Lane, et al. (Comet Kohoutek Workshop Proceedings) which are of much higher spectra resolution and show well-resolved (0-0) and (1-1) OH band sequences, a strong NH band system at λ3360, and a continuum increasing with wavelength over the region $\lambda\lambda$3000–3500.

It was determined, by correcting the high-resolution data of Lane to an altitude of 41 000 ft by using the atmospheric attenuation model of Elterman,

that about two-thirds of the unresolved OH-NH radiation was contributed by OH. The energy radiated in the unresolved OH-NH bands of the slitless spectra was two and one-half times that in the CN band. The diameter of the OH-NH coma as measured on the spectrum plate was three minutes of arc. The NH coma as determined by Lane is of the same general diameter as the OH coma. The dominant characteristic of the slitless spectra is that most of the energy in the region λλ3000–4600 is in the OH-NH bands.

The energy radiated by Comet Kohoutek in the OH-NH bands and received outside the Earth's atmosphere was determined by using χ Pisces (A2, 4.94 mag) as the reference star. (See fig. 1.) The irradiance from OH-NH outside the Earth's atmosphere was thus determined as 4×10^{-9} erg/cm²-s, or 2.7×10^{-9} erg/cm²-s from OH alone. The total energy W_{OH} radiated by Comet Kohoutek in OH was 5.9×10^{18} ergs/s. The uncertainty of this energy determination is a factor of about 2 and is due primarily to the severe atmospheric attenuation and low irradiance of reference stars in this region of the spectrum. This January 24, 1974, OH measurement is in agreement with a January 15, 1974, OH filter-photometry measurement scaled according to R^{-2} Δ^{-2}, of 4×10^{18} ergs/s by Blamont and Festou (1974) and Festou (1974).

REFERENCES

BLAMONT, J.; and FESTOU, M.: 1974, Note aux Comptes Rendus de L'Academie des Sciences, Session of January 28, 1974.

HARVEY, G. A.: 1974, Pub. A.S.P. 86, No. 512, 552.

FESTOU, M.: 1974 (personal communication).

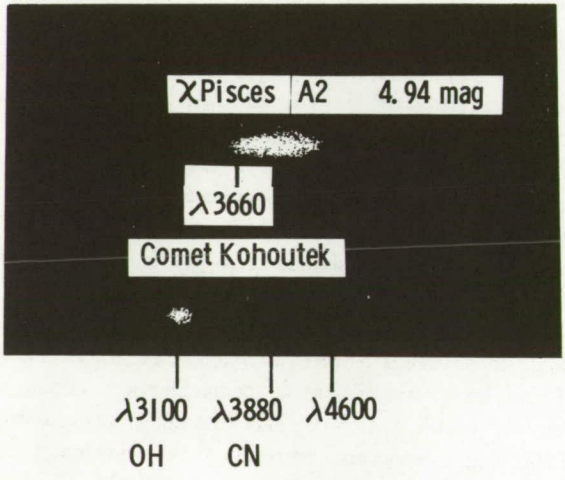

FIGURE 1.—*Ultraviolet spectra of Comet Kohoutek on January 24, 1974.*

DISCUSSION

MARAN: What is the spatial resolution in the direction perpendicular to the dispersion?

HARVEY: About 1 minute of arc.

VOICE: What exposure time did you use?

HARVEY: That was a 1-minute exposure time.

NEW: How do your production rates compare with what we just heard?

HARVEY: I did not do any work at all in production rates. I believe it would be similar to Blamont's when scaled for distances.

Page intentionally left blank

Page intentionally left blank

*GROUND-BASED NEAR-ULTRAVIOLET OBSERVATIONS OF COMET KOHOUTEK**

ARTHUR L. LANE
Jet Propulsion Laboratory
California Institute of Technology

ALAN N. STOCKTON
Institute for Astronomy
University of Hawaii

FREDERICK H. MIES
National Bureau of Standards

The discovery of Comet Kohoutek (1973f) more than 9 months before its perihelion passage, and the preliminary trajectory analysis which seemed to imply an auspicious brightening, both suggested that a number of classically "difficult" ultraviolet observations might be possible. The study of the evolution and spatial extent of hydroxyl radicals (OH) was one such effort in this category because the OH emission band system of the first excited state lies in the near-ultraviolet (near-UV) in the region of the growing atmospheric opacity caused by ozone. A feasibility estimate, based on several of the brighter recent comets (Comets Bennett and Arend-Roland) showed that these studies of excited state OH emissions were possible, and under carefully controlled conditions, could even be quantitative. To partially ameliorate the atmospheric extinction problem it was necessary to obtain observing time at a high-altitude site. The University of Hawaii Mauna Kea Observatory, at an altitude of 4200 meters, was equipped to perform the OH measurements and was able to accommodate the observing request.

* This paper presents the results of one phase of research carried out at the Jet Propulsion Laboratory, California Institute of Technology, under Contract No. NAS7-100, sponsored by the National Aeronautics and Space Administration; and jointly supported, in part, by the National Bureau of Standards and the Institute for Astronomy, University of Hawaii.

Spectroscopic measurements were recorded with a Cassegrain image tube spectrograph at the 2.24-m telescope. For most of the near-UV spectra the central wavelength of the instrument was set to 3200 Å, with a total possible range of 2900 to 3600 Å, and a linear dispersion of 27 Å mm^{-1}. All the spectra were recorded with the 1.5 arc-sec by 2 arc-min slit aligned parallel to the Sun-tail direction and with the nucleus centered in the slit. Exposures were between 1-minute's and 30-minutes' duration on Kodak IIa-O plates. The comet was observed at 0.93 ± .02 AU, both pre- and post-perihelion for the most detailed studies, and was also examined once on March 2, 1974, when it was at a post-perihelion distance of 1.6 AU.

Figure 1 is a print of two pre-perihelion spectra of the wavelength range 2900 to 3600 Å. The upper spectrum is a 9-minute exposure; the lower one, a 2-minute exposure. In addition to the labeled OH and NH spectral features, numerous ion lines and other unknown emissions are present. Figure 2 portrays the post-perihelion behavior of the comet in the near-UV. The upper spectrum was recorded January 25, 1974 (30-minute exposure), and the lower spectrum on March 2, 1974 (30-minute exposure). The heavy dark lines between the spectra connect regions of identical spectral wavelength. Comparison of figures 1 and 2 shows the temporal changes in the behavior of the comet. The spectral intensity distributions in the OH and NH bands change with time, and a dramatic loss of NH and ion line intensity is observed at a heliocentric distance of 1.6 AU in the March 2, 1974, spectrum. Figure 3 is a microdensitometer tracing of the January 25, 1974, spectrum. The OH A-X

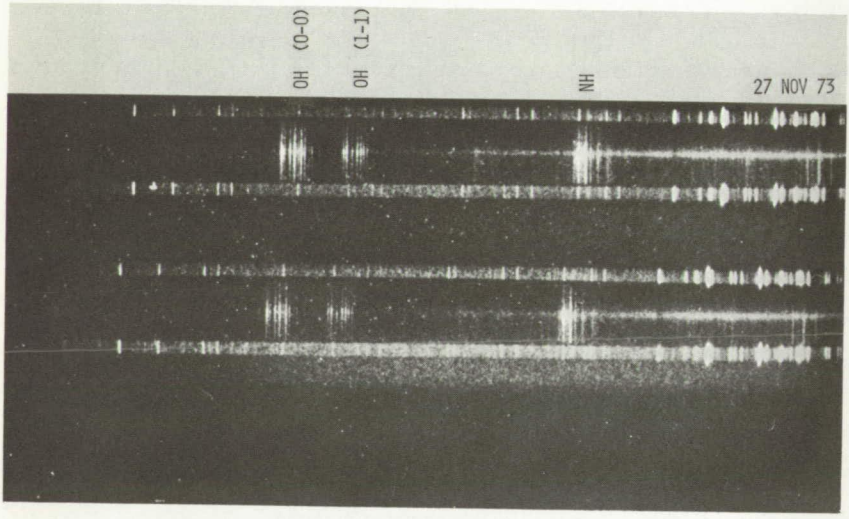

FIGURE 1.—*Pre-perihelion near-UV spectra of Comet Kohoutek. The upper spectrum is a 9-minute exposure, bottom spectrum a 2-minute exposure. No spectral information is seen short of the 3072 Å feature in the OH A-X (O-O) band.*

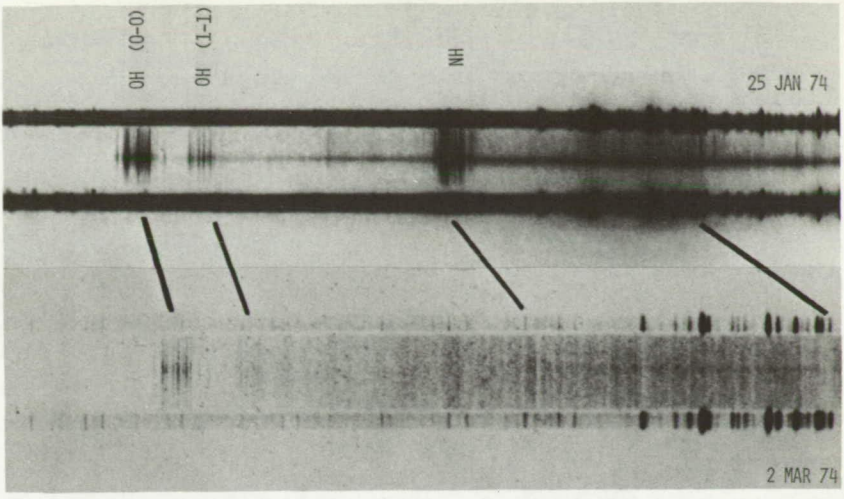

FIGURE 2.—*Post-perihelion near-UV spectra of Comet Kohoutek. The emissions of the NH A-X band and the ion lines near 3550 to 3600 Å which were strong at a heliocentric distance of 0.9 AU have disappeared in emission by 1.6 AU.*

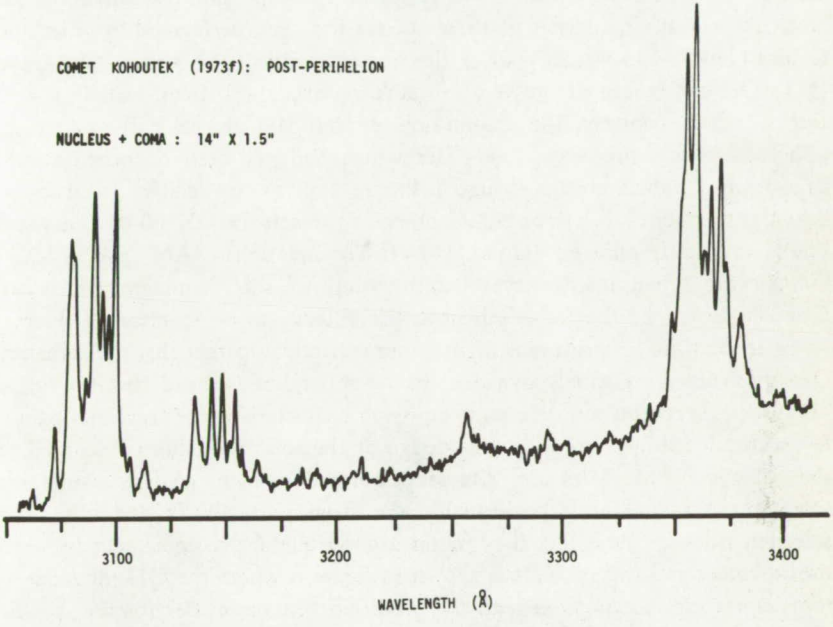

FIGURE 3.—*Microdensitometer tracing of the January 25, 1974, Comet Kohoutek spectrum. OH emission at 3072 to 3118 Å and 3130 to 3170 Å. NH emission is between 3345 and 3390 Å. Unidentified features near 3250 Å are found both pre- and post-perihelion.*

(0-0) and (1-1) bands are respectively 3072 to 3118 Å and 3130 to 3170 Å. The NH A-X band is between 3345 and 3390 Å. An unidentified feature appears at 3257 Å and is present in the pre- and post-perihelion spectra. The features near 3300 Å require further microdensitometry to determine their veracity. The relative intensities of the OH A-X (0-0) and (1-1) bands are about 4:1 as measured, but the atmospheric ozone attenuates the (0-0) band much more strongly. Rocket measurements above the atmosphere (Feldman, Fastie, et al., 1974) indicate a ratio of about 15:1, which is in general agreement with the correction factors determined from the 1966 U.S. Standard Atmosphere Supplement.

Preliminary inspection of the pre- and post-perihelion spectra revealed a dramatic change in the intensity characteristics of the OH emission bands. Careful microdensitometer tracings centered on the nucleus region are shown in figure 4. These tracings are at approximately 1.5 Å resolution and the temporal variability of the individual emission lines within each band is evident. The predominant difference in the comet is its heliocentric velocity (not distance) which was about -40 km s^{-1} at the pre-perihelion measurement time and about $+41$ km s^{-1} at the post-perihelion date. If the assumption that the observed emission is resonant fluorescent scattering is correct, one must examine the solar spectrum in this 3100 Å region for a possible explanation. The molecular transition analysis of these spectra has been performed by Mies and Krauss (1974) and virtually all of the line intensities for both the (0-0)and (1-1) OH bands result from very low rotation excitation states, namely $J = 0$ and 1, which confirms the assumption of resonant fluorescence scattering. (Photochemically produced "hot" OH which had not been quenched would have many J values greater than 6.) Figure 5 gives the relative intensity of the solar spectrum (disk) for a 2 Å interval in which the OH (0-0) 3081.6 Å line is resonantly pumped (Donn, 1974). The notations "JAN" and "NOV" indicate the actual intensity-wavelength points of solar emission which are Doppler-shifted by the comet's heliocentric velocity to be in resonant fluorescence at the time of measurement. It is immediately apparent that the cometary OH spectrum is extremely dynamic, in a temporal sense, and that no single "snapshot" spectrum can determine emission characteristics or brightnesses unless a detailed, high-resolution knowledge of the solar spectrum is included in the analysis. When Mies and Krauss performed such an analysis using this solar spectrum and also the available transition probabilities and molecular selection rules for emission, they found a good qualitative agreement between measurement and theory. This is shown in figure 6 where the OH microdensitometer tracing is compared with the predicted line intensities for the specific time of measurement. The fact that some intensities do not match well indicates either that the solar spectrum is still not adequately known in intensity and resolution (a difference of 0.03 Å can make a difference factor of from 2 to 5 in the intensity of an OH emission line), that the molecular transition

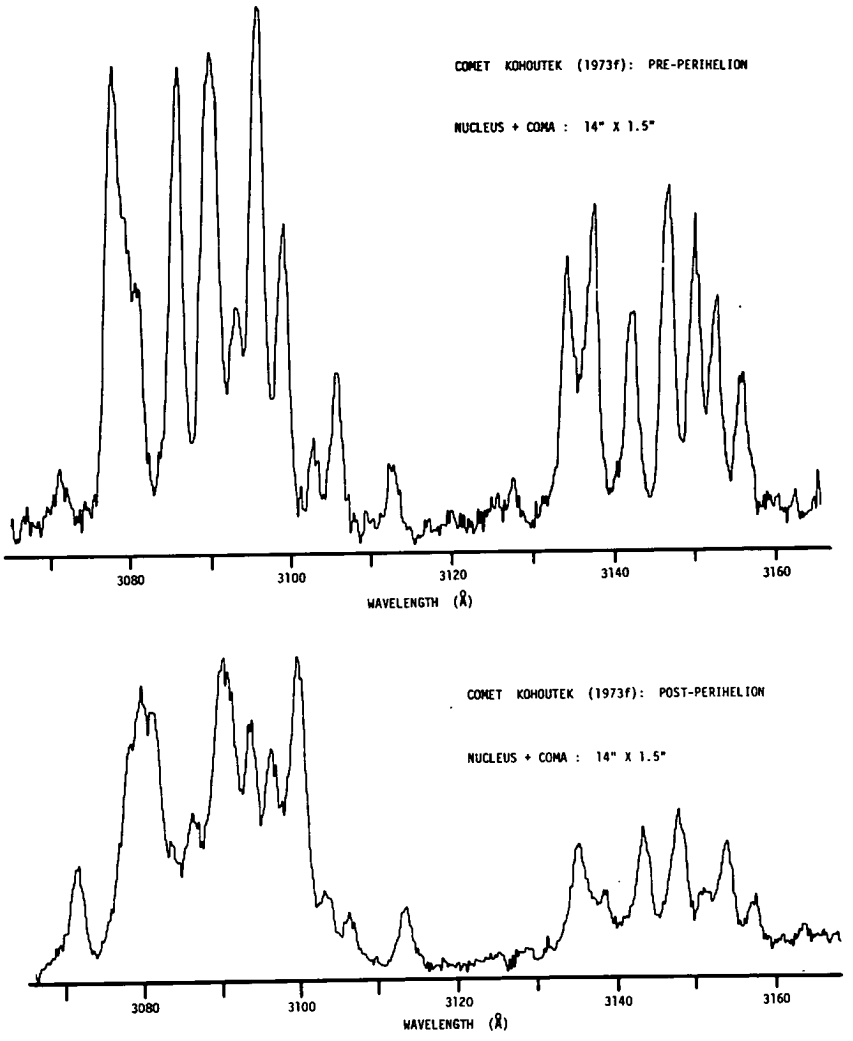

FIGURE 4.—*Higher resolution tracing of the pre- and post-perihelion OH emissions. The same region around the nucleus is examined in each spectral tracing.*

probabilities are not correct, or possibly that the collisional environment is perturbing the rotational population distribution. Careful analysis of all the available spectra may indicate what should be considered as suspect.

In summary, we have demonstrated that moderately high-resolution near-UV spectroscopy of comets is feasible and important in ascertaining their characteristics and compositions. It is also very apparent that spectra recorded "out-of-context" do not necessarily portray the correct behavior of a molecular emission band.

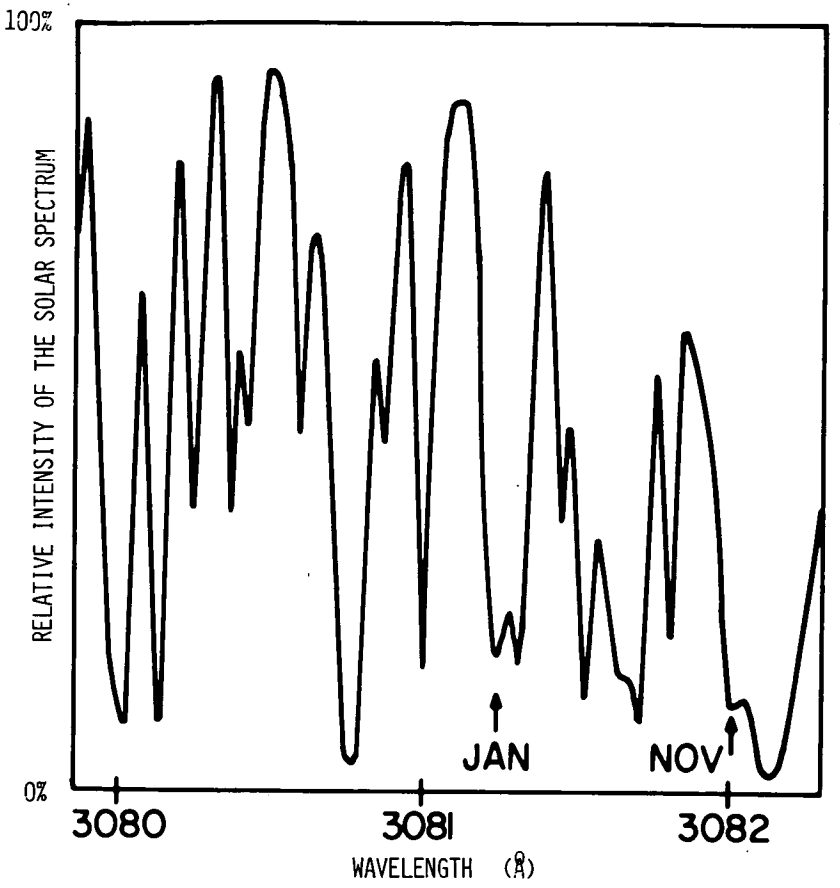

FIGURE 5.—*Relative intensity of the disk solar spectrum between 3080 and 3082 Å. "JAN" and "NOV" refer to the position of the rest wavelength emanating from the Sun which is in resonance with the Doppler-shifted 3081.6 Å OH line at the time of the cometary observations.*

ACKNOWLEDGMENTS

Arthur L. Lane is indebted to the University of Hawaii, Mauna Kea Observatory, for the granted 2.24-m telescope time, and to W. E. Brunk, NASA Headquarters, Planetary Programs Office, for graciously permitting him time to pursue this interesting problem.

REFERENCES

DONN, B.: 1974 (private communication). The solar spectrum was recently acquired by the Kitt Peak National Observatory.

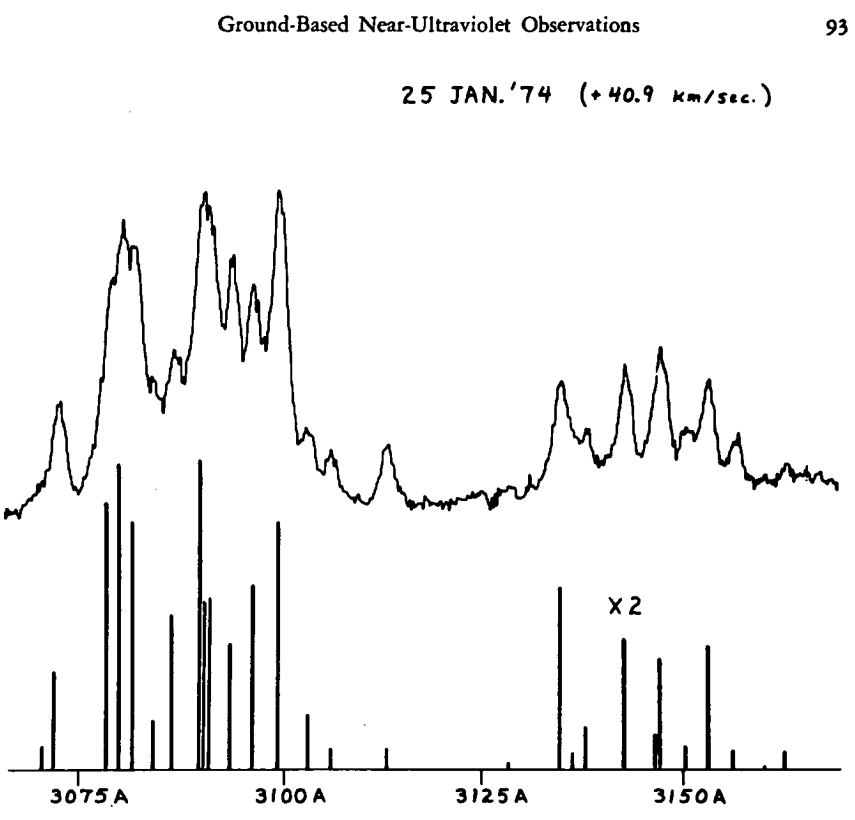

FIGURE 6.—*Comparison of observed OH A-X emission and the line intensities predicted by Mies and Krauss for the conditions of Doppler shift at the time of measurement. Note that some of the agreements are excellent, especially on the principal lines.*

FELDMAN, P. D.; TAKACS, P. Z.; FASTIE, W. G.; and DONN, B.: 1974, Science, August 1974.
MIES, F.; and KRAUSS, M.: 1974, Ap. J. (Letters), 191, L145.

DISCUSSION

FELDMAN: Do you account for the difference of OH and NH intensities between January and March simply by different elevation angles of the observations made?

LANE: The NH will not be as straightforward as we thought and it may have a pumping phenomenon very similar to OH. We will be able to extrapolate above the atmosphere by calibration on the plate.

WHIPPLE: You were guiding in the optical region?

LANE: Yes. Visually.

WHIPPLE: How did the nucleus look? Was it pretty sharp?

LANE: On March 1 it was a blur. We had a difficult time. In the November period (pre-perihelion) the nucleus was more condensed and very sharp. In the January period it was more difficult.

WHIPPLE: This is not atmospheric?

LANE: No. In Haleakala, if the weather is good, then the seeing is incredible. With this instrument you get down to 2940 Å in 5 minutes, looking at the dark side, not the bright side, of Venus near the horizon.

BRANDT: I called and asked E. Roemer what the false nucleus looked like in January and she said that its size was several arc-seconds. From that, it would be completely compatible.

WHIPPLE: Back in November it was what?

LANE: It was stellar, almost.

COMET KOHOUTEK OBSERVATIONS FROM COPERNICUS

J. F. DRAKE
E. B. JENKINS
Princeton University

(Preliminary data presented and no paper submitted.)

OH OBSERVATION OF COMET KOHOUTEK (1973f) AT 18 CM WAVELENGTH

F. BIRAUD
G. BOURGOIS
J. CROVISIER
R. FILLIT
E. GÉRARD
I. KAZÈS
Observatoire de Meudon

Comet Kohoutek (1973f) was monitored in the 1667- and 1665-MHz OH lines with the Nancay radio telescope from November 29, 1973, through February 15, 1974. A signal in absorption was observed during the first half of December (peak line antenna temperature of $-$ 0.09 $\pm$ 0.01 K at 1667 MHz and $-$ 0.07 $\pm$ 0.01 K at 1665 MHz, with a line width of 4 $\pm$ 1 km s^{-1}). Then the signal faded. It reappeared in emission around January 20 (peak line antenna temperature of + 0.09 $\pm$ 0.02 K at 1667 MHz and + 0.05 $\pm$ 0.02 K at 1665 MHz with a line width of 4 $\pm$ 1 km s^{-1}). (See fig. 1.) For both detections, the velocity of the lines coincides within $\pm$ 0.5 km s^{-1} with the velocity derived from the ephemeris. Measurements made in the first half of December gave an upper limit of 20 percent of circular polarization; the satellite lines at 1720 and 1612 MHz were not detected at a level of 0.02 K.

These results may be explained by an ultraviolet (UV) pumping of the OH molecule: when the Fraunhofer spectrum is taken into account, the inversion of the OH ground state Λ-doublet is strongly dependent on the comet radial heliocentric velocity (Swings effect) and can exceed $\pm$ 50 percent. There is a good agreement between our observations and the variations with time of the inversion calculated from this model for the orbit of Comet Kohoutek. The number of OH molecules seen by the Nançay radio telescope beam (3.5 $\times$ 19 arc-min) is then estimated to be 6 $\times$ 10^{33} in December and 3 $\times$ 10^{33} in January. Blamont and Festou have observed in January, in the λ3090 Å emission band of OH, a small OH cloud (100 000 km) (C. R. Acad. Sc. Paris 278, B479). However, comparision of our results with those

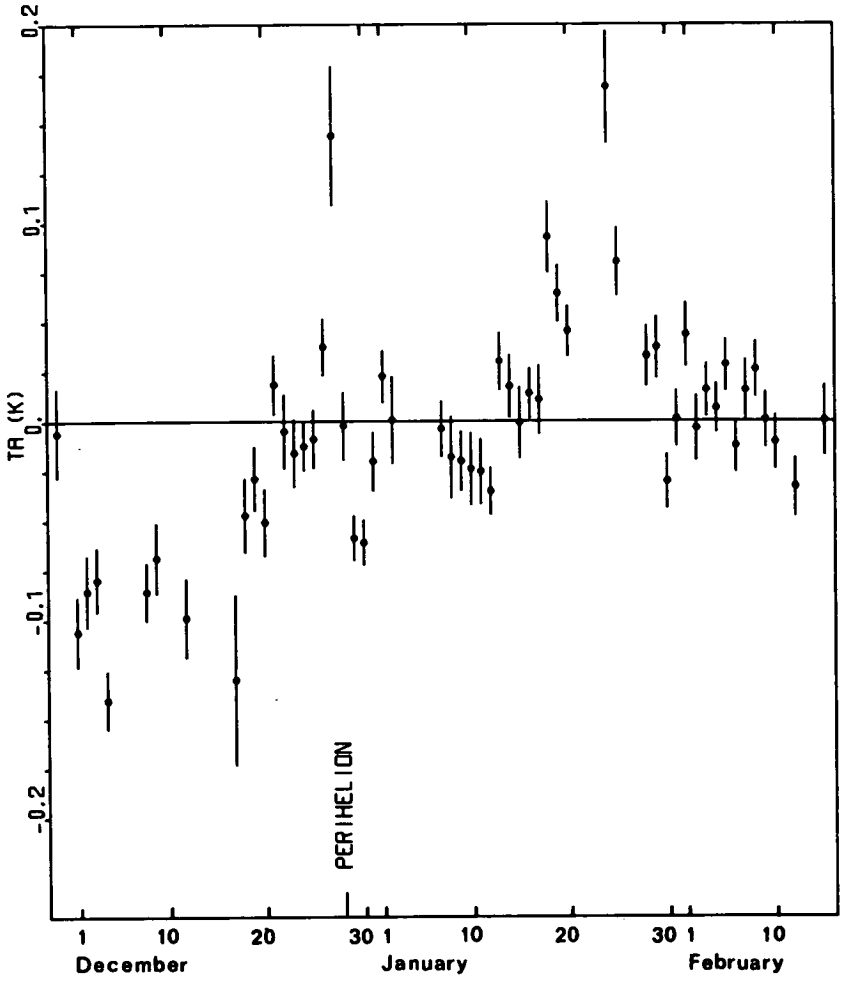

FIGURE 1.—*Daily peak antenna temperatures, normalized to 1667 MHz assuming a L.T.E. ratio of the main line intensities; the error bars represent the r.m.s. fluctuation.*

of Turner (IAU Circular No. 2610) favors an OH halo of large angular extent, possibly greater than 18 arc-min (10^6 km).

NOTE: The complete paper was submitted to *Astronomy & Astrophysics.*

DISCUSSION

KELLER: I wonder how sensitive the population is against collision. How many collisions do you need to destroy these populations?

CROVISIER: This was questioned by Turner and he found that there

were collisions. The collision rate was quite low in comparison with the UV radiation rate for a distance of about 1 AU.

KELLER: Is this necessary to maintain an inverse population?

CROVISIER: Yes, it is.

LANE: In fact, you can invert that, given the UV data.

LANE: CH is a similar structure and a group tried to see it; they did not detect it.

CROVISIER: Yes. Maybe there is pumping of CH.

WHIPPLE: The direct measurement of the collision rate here is extremely important because we don't know how many particles there are. This looks like the first opportunity to get an accurate measurement. This is a great contribution.

DELSEMME: The width of the beam is not thin enough to detect the major region where collisions are. Could you comment on the width of the beam that is being used?

CROVISIER: Yes. The beam width was 3.5 arc-minutes in RA.

DELSEMME: It would be great to be able to detect collisions if we were able to use a beam that is thin enough to detect the inner region where these collisions are possible.

DONN: In this respect the ideal thing would be some OH spectroscopy, which is not a very easy thing to provide. But this is similar to what we optically tried to do.

CROVISIER: Yes, but the point is that the signal is very faint.

ULTRAVIOLET FLUORESCENT PUMPING OF OH–18–CM RADIATION IN COMETS

FREDERICK H. MIES
National Bureau of Standards

In the absence of collisions, optical pumping of cometary OH by solar UV radiation determines the relative population of OH molecules in the Λ-doubled levels of the $^2\Pi_{3/2}$ *ground state. The distribution is extremely sensitive to the heliocentric radial velocity of the comet, and at appropriate velocities the level populations will be either inverted or anti-inverted. Thus the OH–18–cm spectrum of a comet, measured with respect to the 10K galactic background at 1665 and 1667 MHz, may be observed either in emission or in absorption at different periods during the trajectory. Optical pumping also will produce an alignment of the magnetic sublevels along the axis of the incident solar radiation, and variable degrees of linear polarization are expected.*

NOTE: The complete paper was submitted to the *Astrophysical Journal* (Letters) 191, L 145 (1974).

H_2O^+ IN THE TAIL SPECTRUM OF COMET KOHOUTEK (1973f)

P. A. WEHINGER
S. WYCKOFF
Wise Observatory
Tel-Aviv University

Spectrograms of Comet Kohoutek were obtained at the Wise Observatory between November 29, 1973, and February 16, 1974, with the one-meter reflector located at Mitzpeh Ramon on the Negev Desert. An ITT F4089 magnetically focused image tube with an S-25 photocathode was used with a Cassegrain spectrograph. The spectra cover the region from 5000 to 9000 Å with a reciprocal dispersion of 150 Å mm^{-1}. The spectral resolution is about 5 Å while the spatial resolution is on the order of 2000 km. The spectra were recorded on Kodak 103a-D plates with typical exposures of 15 to 45 minutes. The comet's heliocentric distance ranged from 0.4 to 0.9 AU. All the spectrograms were unwidened with the slit oriented in the direction of the tail and the coma located on the center of the slit. The observed extent from the nucleus into the tail was 50 000 km. The spectra of the coma were purposely overexposed in order to detect the faint tail features.

The identification of H_2O^+ in the tail of Comet Kohoutek, reported elsewhere (Wehinger, Wyckoff, Herbig, Herzberg, and Lew, 1974), is based on these observations plus higher dispersion spectrograms (33 Å mm^{-1}) taken by Herbig in November 1973 and January 1974. Unidentified features were first noted in Comet Kohoutek by Benvenuti and Wurm (1974). Shortly thereafter, Herzberg and Lew (1974) proposed the tentative identification of H_2O^+ on the basis of two features due to the 8–0 vibronic band and two other features due to the 6–0 band, at 6200 and 7000 Å, respectively, seen in Benvenuti and Wurm's spectrum.

Nearly 50 previously unidentified lines are seen in the Wise Observatory spectrograms of Comet Kohoutek, all of which are in excellent agreement with the laboratory data on H_2O^+ obtained by Lew (1974). The spectrum of H_2O^+ was discovered by Lew and Heiber (1973) and is being analyzed by Lew. Herzberg (1973) had predicted that H_2O^+ would be found in comet tail spectra.

The observed emission features due to the H_2O^+ are vibronic bands with transitions from the upper vibronic state to the ground state, in a progression of bands from the 5–0 band at 7500 Å to the 10–0 band at 5400 Å. The H_2O^+ vibronic band structure alternates between π and Σ, Δ bands and is similar to NH_3 which is seen in the coma of this comet and previous comets. The synthetic spectrum of rotational electronic transitions, computed for the 8–0 and the 7–0 bands, is in good agreement with the observed line intensities within each band. The vibronic states are populated by resonance fluorescence simulating a gas at very low temperature (50 to 100 K). The predicted spin splitting is seen in Herbig's spectrograms for rotational lines with the largest splitting (i.e., of the order of 3–4 Å).

The presence of H_2O^+ is expected since OH and H are observed; the OH in the $A^2\Sigma^+ - X^2\Pi_i$ band ($\lambda\lambda$ 2800 to 3160 Å) and H in Lyman-α (due to Swings and Haser, 1961; Jenkins and Wingert, 1972; and Bless and Code, 1972).

In summary, the identification of H_2O^+ is confirmed from the wavelength measures, the band structure, the line intensities, and the spin splitting. All of these quantities are in excellent agreement with the laboratory data on H_2O^+ The positive identification of H_2O^+ in the tail spectrum of Comet Kohoutek confirms the presence of water in comets as postulated by Whipple (1950, 1951) in his icy conglomerate model of cometary nuclei, and also supports Delsemme's (1973) indirect arguments concerning the presence of water ice in comets.

ACKNOWLEDGMENTS

This research is supported by the Smithsonian Research Foundation, Grant SFC–O–3005. We also gratefully acknowledge the assistance of Marshall Space Flight Center, NASA, for partial support to attend this conference.

REFERENCES

BENVENUTI, P.; and WURM, K.: 1974, Astr. and Ap. 31, 121.
BLESS, R. C.; and CODE, A. D.: 1972, Ann. Rev. Astr. and Ap., 10, 197.
DELSEMME, A. H.: 1973, Space Sci. Rev. 15, 89.
HERZBERG, G.: 1973, IAU Trans., 15A, 174.
HERZBERG, L.; and LEW, H.: 1974, Astr. and Ap., 31, 123.
JENKINS, E. B.; and WINGERT, D. W.: 1972, Ap. J., 174, 697.
LEW, H.: 1974, to be published.
LEW, H.; and HEIBER, I.: 1973, J. Chem. Phys., 58, 1246.
SWINGS, P.; and HASER, L.: 1961, Atlas of Representative Cometary Spectra. Liège: Liège Institut d'Astrophysique.
WEHINGER, P. A.; WYCKOFF, S.; HERBIG, G.; HERZBERG, G.; and LEW, H.: 1974, Ap. J. Letters 190, L43.
WHIPPLE, F. L.: 1950, Ap. J. 111, 375.
———.: 1951, ibid. 113, 464.

DISCUSSION

LANE: Please speculate on the formation of the H_2O^+ by ionization or electron bombardment.

WEHINGER: I have some figures on this. There are several processes involved—charge transfer, 0.2 to 1 KEV solar wind protons and the electron collision ionization with solar wind electrons in the 20- to 100-electron volt range. Charge transfer is 10 ionizations per 10^7 water molecules per second. Electron collision is 2×10^7 particles per second.

LANE: Do you mean photoelectrons from other species?

WEHINGER: When you have a radiation short of about 1300 Å, the Lyman-Alpha from the Sun, it is energetic enough to dissociate the water. There are two effects—photoionization and photodissociation.

LANE: What is the process of the ionization?

WEHINGER: The charge transfer from solar wind protons is one; the solar wind electrons causing collision ionization is another; and then, the solar UV short of 980 Å is a third. All three of these contribute to the production of the H_2O ions.

PAGE: What is the significance of 1300 Å?

WEHINGER: That is where photons are energetic enough to dissociate water.

DELSEMME: You will find that 99 percent of the rest of the water is still dissociated, less than 1 percent is ionized. It is understandable that you are really using a lot of water.

KELLER: How do you figure out 1 percent?

DELSEMME: That figure is still highly unknown.

WEHINGER: These are just typical values.

MENDIS: My guess is that the photoionization is much more important.

BRANDT: The temperature of electrons is four times the temperature of the protons. Is that the correct range?

WEHINGER: I had an electron temperature equivalent to 20 to 100 eV.

DELSEMME: The problem is, what is the distribution inside the shock wave?

VOICE: Will you be able to separate the relative intensities of the various lines?

WEHINGER: The spectra that I have from Wise Observatory are at 150 Å/mm and you can't begin to separate H Alpha to get relative intensities and fluxes of the lines.

DUBIN: What is the history of the ions versus distance?

WEHINGER: We have data from about 0.4 to 0.7 AU. We don't have details yet on the variation in the line strengths with distance.

ROCKET ULTRAVIOLET IMAGES AND SPECTRUM OF COMET KOHOUTEK

C. B. OPAL
G. R. CARRUTHERS
D. K. PRINZ
R. R. MEIER
E. O. Hulburt Center for Space Research
Naval Research Laboratory

Emissions of atomic oxygen (1304 Å), atomic carbon (1657 Å), and atomic hydrogen (1216 Å) from Comet Kohoutek were observed with electronographic cameras carried on a sounding rocket on Janury 8.1, 1974 (at this time the comet was at $R = 0.43$ AU).

The cameras incorporated 75-mm focal length $f/1$ Schmidt optical systems with fields of view of 20° and resolutions of 2 arc-min. The cameras were calibrated in flight by comparison with airglow brightnesses measured simultaneously with accurately calibrated photometers.

A camera with 1250–1900 Å passband (CsI photocathode and CaF_2 corrector plate) produced a circular image of the comet about 10 arc-min across (4×10^5 km). A similar camera pointed at a grating to form an objective spectrograph revealed that the emissions in this band were mainly the 1657 Å line of C and the 1304 Å lines of 0 in ratio of peak brightness of 3:1. Taking the diameter of the direct image to give the size of the carbon line emitting region, we derived a total luminosity in this line of 1.2×10^{29} photons/s (somewhat less than half that observed by Feldman et al., at $R = 0.34$ AU).

A third camera sensitive to the 1100–1500 Å band (KBr photocathode and LiF corrector plate) recorded the extensive atomic hydrogen halo in the light of resonantly scattered solar Lyman-α (1216 Å) radiation. The peak brightness was about 100 kR. Emission was detected out to distances of about 2×10^7 km, at which point the comet emissions faded into the 7-kR terrestrial Lyman-α airglow. The brightness distribution out to a distance of 10^6 km followed that expected from a simple model, in which it is assumed that the hydrogen initially flows radially outward at a velocity $v = 8$ km/s, with shells of different radii displaced down-Sun according to the cumulative effect

of the acceleration produced by solar Lyman-α radiation pressure. At greater distances it was necessary to use a numerical individual-particle fountain model to take into account the actual parabolic orbits of the atoms. A good fit with this model was obtained for a thermal velocity distribution with $v = 8$ km/s and a long lifetime against loss through charge exchange with the solar wind. Both models gave a production rate of 3.6×10^{28} atoms/second-steradian.

NOTE: The complete paper was submitted by the Journal *Icarus* ((1974) 23, 526).

DISCUSSION

KELLER: You did not mention one very important figure and that is the solar-flux curve. The velocity is proportional to the square of solar flux and also the production rate.

OPAL: I think it is the 3/2 power of the solar flux.

LANE: In the region near the nucleus at ejection, is it possible you are starting to get photon screening by molecules that have larger cross sections?

OPAL: I would think that they would absorb the solar Lyman-Alpha also, and we would see some shadowing behind the comet—which we do see in a way, but not very strongly.

BRANDT: There are changes in the solar wind properties but all of them correlate very poorly or not at all with solar spot number. You cannot use the sunspot number for any known property of the solar wind.

OPAL: Not even the total flux over the sunspot cycle?

BRANDT: Total flux is almost a constant (within 50 percent). This is a source of difficulty.

OPAL: I looked into that matter and saw some data which show there is great variation in velocity and flux at times.

ROCKET ULTRAVIOLET SPECTROPHOTOMETRY OF COMET KOHOUTEK (1973f)

P. D. FELDMAN
P. Z. TAKACS
W. G. FASTIE
Physics Department
The Johns Hopkins University

B. DONN
Astrochemistry Branch
Goddard Space Flight Center

Spectrophotometric observations of Comet Kohoutek (1973f) between 1200 and 3200 Å were made from an Aerobee rocket launched from White Sands Missile Range at 0145 UT on January 5, 1974. A brief description of the instrumentation and results has been given by Feldman et al. (1974) and table I from that reference is reproduced below. In addition to HI Lyman-α (λ1216 Å) and the OH bands at $\lambda\lambda$3090 and 3142 Å, both of which are very intense, the only features detected were the resonance transitions of atomic oxygen (λ1304 Å) and carbon ($\lambda\lambda$1561 and 1657 Å). These features were also detected by Opal et al. (1974) in a rocket experiment launched 3 days later.

Several possible cometary features were not observed. Among these are the CO Fourth Positive Bands (1400–1600 Å), the CO_2^+ doublet at 2890 Å, and the H_2 Lyman bands (1300–1650 Å). However, the fluorescent scattering efficiency for these bands is quite small (see table I) so that the absence of the bands does not significantly contribute to our knowledge of the composition of the comet. There is also no evidence of scattered solar radiation near 3100 Å, so that an upper limit to the cometary albedo of 0.05 can be set at 3100 Å, based on the 5500-Å albedo of 0.20 given by Ney (1974). This sharp decrease in albedo in the ultraviolet is consistent with the general increase in emissivity of cometary dust in the infrared as noted by O'Dell (1971).

The quantity of interest is the total production rate, Q, in s^{-1} of each of the observed species. Assuming the only excitation processes to be those in-

Table I.—*Spectrophotometric Observations of Comet Kohoutek*

	λ(A)	F (photons $s^{-1}cm^{-2}$)	L (photons s^{-1})	g (photons $s^{-1}mol^{-1}$)[a]	τ(s)[a]	Q (s^{-1})
OI	1304	120 ± 40	2.8×10^{29}	5.0×10^{-7}[b]	4.0×10^{6}	1.4×10^{29}
CI	1657	140 ± 50	3.3×10^{29}	1.1×10^{-5}[b]	2.5×10^{6}	1.2×10^{29}
OH	3090	3100 ± 100	7.4×10^{30}	1.2×10^{-3}[b]	7.9×10^{4}	0.8×10^{29}
CO	1510	≤15	$\leq 4 \times 10^{28}$	8.2×10^{-8}	6.9×10^{5}	$\leq 7 \times 10^{29}$
CO_2	2890	≤18	$\leq 4 \times 10^{28}$	9.1×10^{-8}	3.9×10^{5}	$\leq 1.1 \times 10^{30}$
H_2	1608	≤15	$\leq 4 \times 10^{28}$	1.1×10^{-7}	8.5×10^{6}	$\leq 3 \times 10^{28}$
H	1216	...	...	2.1×10^{-3}	...	5.4×10^{29}

[a] At 1 AU.
[b] Allowing for Doppler shift of 55 km s^{-1}.

duced by solar radiation, Q is related to the observed flux F by

$$Q = \frac{4\pi\Delta^2 F}{g\tau}$$

where Δ = Earth-comet distance,
g = emission rate factor for resonance scatttering or fluorescence,
and τ = mean lifetime of the species, determined from photoionization and photodissociation loss rates.

Note that the product $g\tau$ is independent of the heliocentric comet distance.

Both g and τ are generally uncertain to about a factor of 2. In addition, the large heliocentric Doppler shift at the time of observation, 0.25 Å, exceeds the width of the solar OI lines and thereby removes resonance scattering as a strong source of λ1304 emission. Fluorescence of oxygen in OI ($^3P - {}^3D$) transition at 1025.77 Å excited by the nearly degenerate solar Lyman-β line at 1025.72 Å is found to be an important source of the observed λ1304 emission. The situation for the CI multiplet at λ1657 Å is not as severe since there are accidental coincidences between the shifted and unshifted lines.

The values of g and τ used in deriving the production rates are given in the table, along with the Q values for each species. The most striking result is the high value of Q for atomic carbon, which implies that the parent molecule containing carbon is evaporated at the same rate as H_2O. On the basis of the upper limits on all possible hydrocarbon species, the observed carbon could not have derived from those parent molecules. Thus, the most likely candidates for the carbon parent molecule are CO or CO_2, neither of which can be excluded on the basis of the upper limits given in the table.

ACKNOWLEDGMENT

This work was supported by NASA Grant NGR 21–001–001.

REFERENCES

FELDMAN, P. D.; TAKACS, P. Z.; FASTIE, W. G.; and DONN, B.: 1974, Science, vol. 185, 705.

NEY, E. P.: 1974, Ap. J. (Letters) 189, L141.

O'DELL, C. R.: 1971, Ap. J. 166, 675.

OPAL, C. B.; CARRUTHERS, G. R.; PRINZ, D. K.; and MEIER, R. R.: 1974, Science, vol. 185, 702.

DISCUSSION

BLAMONT: If your explanation of the emission of oxygen is correct, you should have some emission of 8446. Have you looked for it?

FELDMAN: I did not look for it but I asked Steve Maran about it. He said that as part of Operation Kohoutek, he has not seen any observations out that far.

OBSERVATIONS OF THE HYDROGEN LYMAN-α (1216 Å) EMISSION LINE OF COMET KOHOUTEK (1973f) BY THE SKYLAB ATM S082B SPECTROGRAPH

H. U. KELLER*
Laboratory for Atmospheric and Space Physics
University of Colorado

J. D. BOHLIN
R. TOUSEY
Naval Research Laboratory

The S082B spectrograph designed and operated by the Naval Research Laboratory was part of the Skylab Apollo Telescope Mount (ATM). The ATM consisted of a cluster of solar observational instruments. The resolution of the S082B spectrograph was superb, but its sensitivity was less. In order to view the comet, the whole Skylab spaceship had to be moved and stabilized to point away from the Sun. The stability and pointing errors are known only theoretically and are of the order of several minutes of arc, e.g., comparable to the target size—the coma of Comet Kohoutek.

The entrance slit of the S082B instrument corresponded to a field of view (FOV) of 2 × 60 arc-seconds. The spectrograph operated in two wavelength regions: from 1000 to 1970 Å and from 1940 to 3940 Å. The nominal resolution changed from 0.08 Å to 0.16 Å with increasing wavelength. About 100 frames of high-speed film Kodak 101 were used for cometary observations. No results were obtained in the long wavelength channel, where the OH emission lies and would have been of great interest.

During the observing period from December 19, 1973, to January 6, 1974 the spectrograph recorded five images of the cometary Lyman-α emission (1216 Å). The three best exposures of December 29, 00:14 UT (13 min exposure time); December 30, 15:09 UT (9 min); and December 31, 23:27 UT (30 min) have been analyzed. The radial velocity component of the

* On leave from Max-Planck-Institut for Physics and Astrophysics, Munich, Germany.

comet with respect to the Earth was greater than 40 km s^{-1} and, therefore, the geocorona did not interfere with the cometary emission.

The results are still preliminary since not all effects determining the line images have been studied as yet. The peak plate densities of the lines are 0.1 to 0.2 above background (fig. 1). The calculated instrumental profile is appreciably smaller ($FWHM$ = 0.055 Å) than the recorded line images, typically $FWHM$ = 0.14 Å ($FWHM$ full width at half maximum). Unfortunately the photographic images are too noisy to be deconvoluted to yield the actual cometary line profiles. However, the line widths can be determined with sufficient accuracy. Gaussian profiles with varying half widths were assumed for the cometary line and convoluted with the theoretical instrumental profile, and the resulting half widths were compared with those observed. Table I displays the results of the observational and the calculated widths of the cometary line profiles. The scatter of the H and D curve determines the estimated errors.

The average of all three profiles is $FWHM = 0.140(^{+0.034}_{-0.017})$ Å for the observed images and $FWHM = 0.130(^{+0.032}_{-0.015})$ Å for the cometary line. This line width corresponds to a Doppler velocity of $v_D = 19.3$ km s^{-1} or an outflow velocity $v_H = 2/\sqrt{\pi}\ v_D = 21.7(^{+6}_{-3})$ km s^{-1}. This interpretation

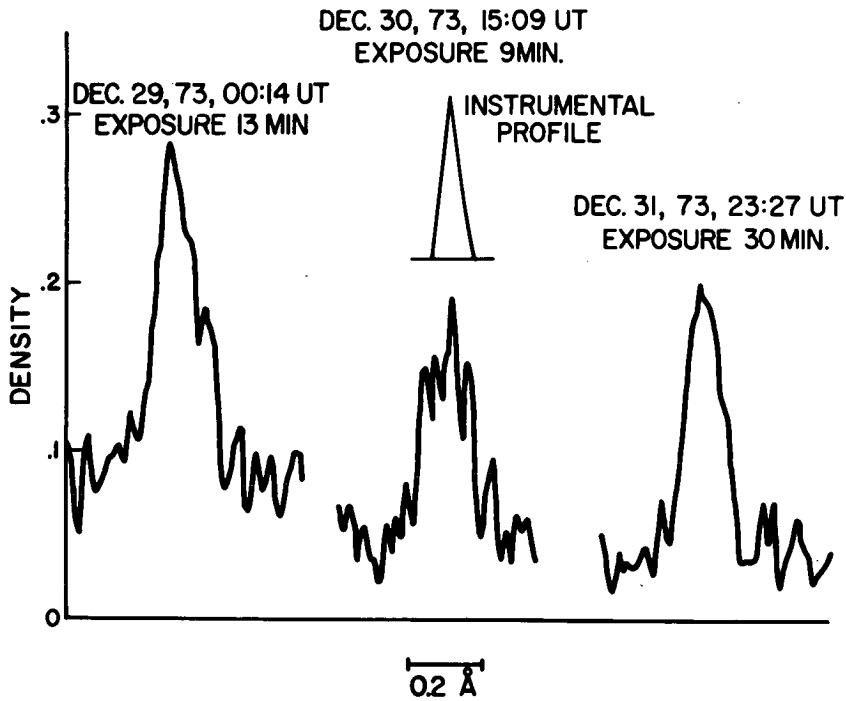

FIGURE 1.—*Cometary line and instrumental profiles.*

Table I.—*Cometary Line Profiles*

Date	*FWHM*[Å] on plate	*FWHM*[Å] of cometary line	Limits and Value
Dec 29	0.177	0.168	upper limit
	0.135	0.125	determined value
	0.120	0.108	lower limit
Dec 30	0.161	0.153	upper limit
	0.146	0.135	determined value
	0.140	0.131	lower limit
Dec 31	0.166	0.158	upper limit
	0.140	0.131	determined value
	0.120	0.108	lower limit

implies that the cometary emission is optically thin, which is certainly not true for the FOV of the instrument centered on the nucleus. The actual pointing will be verified by using the white light coronagraph exposures taken for this purpose during the spectrograph observations. Since only a small number of all short wavelength exposures (with even longer exposure times) were successful, it is almost certain that the instrument was pointed at the brightest part of the hydrogen atmosphere, i.e., the nuclear optically thick region.

Multiple scattering calculations by Keller (1973a) show that in the region around the nucleus determined by the FOV, the optical thickness is certainly larger than 10 and might well reach values of 100 and even more. For simplicity, a plane parallel layer with constant source function was assumed to study the optical thickness effects. For an average optical thickness of 50, the broadening factor would be 2.1 and the outflow velocity would decrease to $10(^{+3}_{-1})$ km s^{-1}. This value is reasonably close to the values of 8 km s^{-1} for the outflow velocities established by using observations of the optically thin parts of the hydrogen atmospheres of Comets Bennett and Kohoutek (Keller, 1973b; Opal et al., 1974).

In summary, the cometary Lyman-α emission line of Comet Kohoutek was resolved by the Skylab ATM S082B spectrograph observations for the first time. This line is probably strongly broadened by optical thickness effects. The preliminary line width yields an outflow velocity in agreement with observed outflow velocities of the hydrogen atmospheres of Comets Bennett and Kohoutek.

REFERENCES

KELLER, H. U.: 1973a, Astron. Astrophys. 23, 269.
KELLER, H. U.: 1973b, Astron. Astrophys. 27, 51.
OPAL, C. B.; CARRUTHERS, G. R.; MEIER, R. R.; and PRINZ, D. K.: 1974, Science, 185, 702.

SESSION III:

DETECTION OF METHYL CYANIDE IN COMET KOHOUTEK

B. L. ULICH
National Radio Astronomy Observatory

E. K. CONKLIN
National Astronomy and Ionospheric Center

In this paper we report the first detection of radio emission from a comet. We observed Comet Kohoutek from December 1, to December 5, 1973, using the National Radio Astronomy Observatory (NRAO) 36-foot radio telescope on Kitt Peak. The receiver was a double sideband mixer radiometer operating at a wavelength of 2.7 mm. The spectrometer consisted of a 50-channel filter bank with a resolution of 100 kHz and 256-channel filter bank with a resolution of 250 kHz.

The data obtained on December 1 and December 5, 1973, are shown in figure 1. Two lines are visible in emission with half widths of about 0.3 km/s. We are confident they are of cometary origin for the following reasons:

First, during our observations the comet moved about 7° in the sky with respect to background sources. These lines were observed several times during a 5-day period, but were always seen only at the predicted position of the nucleus. No lines were detected at points 1 minute of arc away in the tail.

Second, the change in observed line frequency during this period matched the Doppler shift calculated from the changing geocentric velocity of the comet.

Third, the narrow line widths are consistent with thermal broadening at temperatures typical of comets at this heliocentric distance.

We have identified the two emission lines with the $J = 6 \rightarrow 5$, $K = 0$, and $K = 3$ vibrationally excited transitions of methyl cyanide, CH_3CN. When the observed frequencies are corrected for the calculated Doppler shift of the comet, the rest frequencies agree with the known values for methyl cyanide. In addition, the frequency separation and relative intensities of the two lines are in excellent agreement with both theoretical calculations and laboratory measurements.

The ground state of methyl cyanide has been observed previously in the

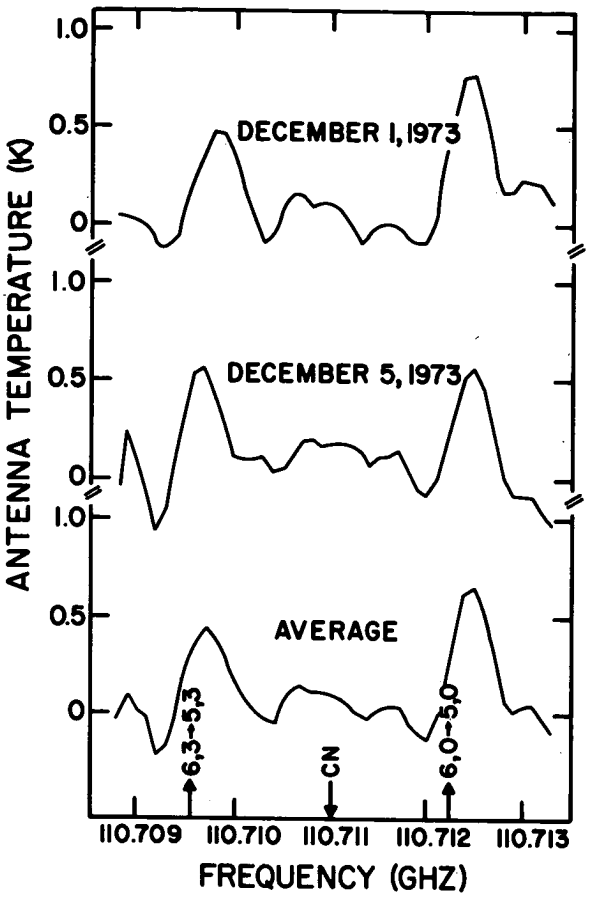

FIGURE 1.—*Radio emission from Comet Kohoutek, December 1 and 5, 1973.*

galactic center, and its presence in comets was postulated by Huebner and others.

The fluid dynamic model of the photochemical coma of a comet assumes that the molecular density decreases as $1/r^2$ away from the nucleus out to a critical radius at which photodissocation occurs. If we adopt a value of 10^5 km for this critical radius and a gas temperature of 150 K, the column density of CH_3CN averaged over the 1 arc-minute antenna beam is about 6×10^{14} molecules/cm^2. This corresponds to a production rate (at a heliocentric distance of 0.8 AU) of about 10^{29} CH_3CN molecules/second, which is an order of magnitude larger than that of HCN.

We were unsuccessful in detecting either the CN radical or the $J = 1 \rightarrow 0$ transition of CO at the nearby wavelength of 2.6 mm. Upper limits on the

column densities are about 3×10^{13} molecules/cm^2 for CN and 6×10^{15} molecules/cm^2 for CO. The corresponding upper limits on the production rates are 5×10^{27} molecules/second for CN and 10^{30} molecules/second for CO.

In conclusion, our detection of a complex molecule such as methyl cyanide in considerable abundance in the nucleus of Comet Kohoutek is the first direct confirmation of the parent molecule hypothesis.

DISCUSSION

LANE: With two transitions, are you able to make an estimate of the temperature as opposed to having to assume the 150° for your calculation?

ULICH: No. You can derive a value for the temperature based on the width of line. But we are limited by resolution of the filters which would give us unreliable data.

CARRUTHERS: If you have 10^{29} CH_3CN, would you expect all those to be dissociated and produce CH and CN at some point in the breakup, and that 10^{29} would then be the upper limit of CH and CN?

ULICH: Yes. I thought about that and all I can say is that these are the numbers I come up with, based on a straightforward interpretation of the data, and I don't understand it.

DONN: I think you have to be careful of straightforward interpretation of data. You can assume 150° temperature to get the number of molecules. You really need a detailed analysis of what is going on.

ULICH: I agree, the production rate is highly dependent on the type of assumptions you make and on the dissociation radius you use. It can change easily by an order of magnitude but I think, on a relative scale compared with HCN observations, the numbers are pretty good.

BELTON: Have you tried to compare the CN number with that derived from optical observation? Is there a chance that the transition will be pumped by ultraviolet?

ULICH: It would be an interesting thing to do, to compare it with the optical data, but I have not done that.

LANE: I do have two plates of both NH and the CN simultaneously that should allow me some overlap to tie OH and NH together. One should get OH, NH, and CN together.

DETECTION OF HCN RADIO EMISSION FROM COMET KOHOUTEK (1973f)

L. E. SNYDER
Joint Institute for Laboratory Astrophysics
University of Colorado and National Bureau of Standards

W. F. HUEBNER
*Los Alamos Scientific Laboratory**

D. BUHL
National Radio Astronomy Observatory†

Radio emission of HCN has been detected from Comet Kohoutek before and after perihelion passage. Multiple Doppler shifts in the observed spectrum indicate jets with velocities ranging up to several km s^{-1}. The HCN column density of the "quiescent" triplet, averaged over the antenna beam, is 1.5 × 10^{13} cm^{-2}. With some reasonable assumptions, this corresponds to an HCN gas production rate of (3−12) × 10^{27} molecules s^{-1}.

We report the radio detection of hydrogen cyanide in Comet Kohoutek (1973f) and the first quantitative observations of the velocities of jets in the inner coma while the comet was at small heliocentric distances. Observations of the ground state $J = 1 - 0$ transition of $H^{12}C^{14}N$ were made on December 15 and 16, 1973, before perihelion, and on January 3 and 6, 1974, after perihelion passage. A 3-mm line receiver mounted on the National Radio Astronomy Observatory (NRAO) 36-ft (11-m) radio telescope at Kitt Peak was

* Work performed, in part, under the auspices of the U. S. Atomic Energy Commission.
† The NRAO Green Bank, West Virginia, is operated by Associated Universities, Inc., under contract with the National Science Foundation.

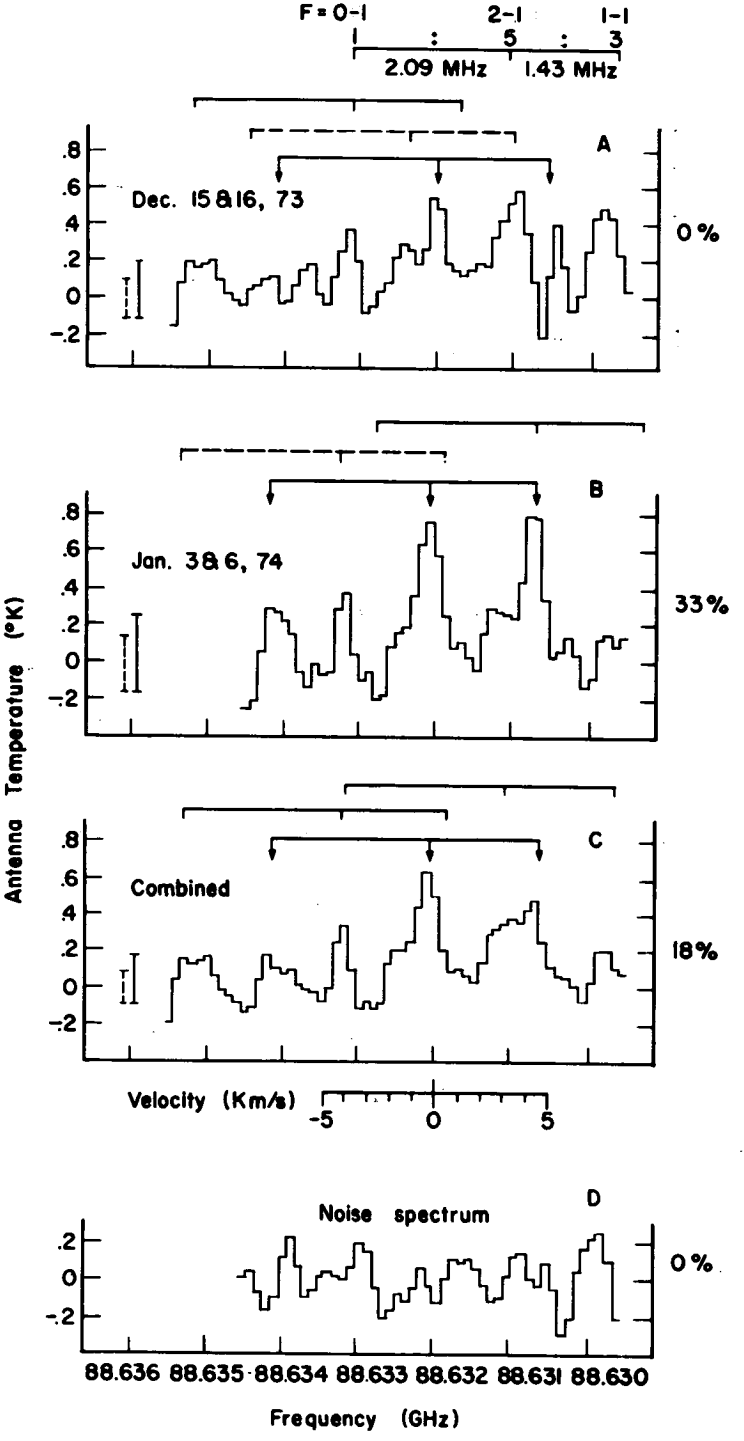
F = 0-1 2-1 1-1
1 : 5 : 3
2.09 MHz 1.43 MHz
A
Dec. 15 & 16, 73
0 %
B
Jan. 3 & 6, 74
33 %
C
Combined
18 %
Antenna Temperature (°K)
.8
.6
.4
.2
0
-.2
Velocity (Km/s)
-5
0
5
D
Noise spectrum
0 %
88.636 88.635 88.634 88.633 88.632 88.631 88.630
Frequency (GHz)

used for the observations. The system was calibrated with a chopper wheel and was checked by observing the HCN emission from the galactic sources W 51 and Sgr A (NH_3 A). Because of solar heating of the telescope, most of the observations had to be made through the fabric dome. Since our observations are discussed in detail by Huebner, Snyder, and Buhl (1974), we will briefly summarize here the results of our data analysis.

Figure 1(A–C) shows the observed HCN emission spectra obtained with 100-kHz filter resolution. The $J = 1 - 0$ transition is split into three quadrupole hyperfine components: $F = 0 - 1$ at 88.63394 GHz, $F = 2 - 1$ at 88.63185 GHz, and $F = 1 - 1$ at 88.63042 GHz (De Lucia and Gordy, 1969) with theoretical intensity ratios 1:5:3 as indicated over the top bar of the figure. The data have been smoothed by adjacent filter averaging and, for all data taken through the closed dome, the temperature scale has been increased by 1.6 to account for the dome attenuation of $\sim$ 40 percent. Figure 1(D) is a noise spectrum taken while tracking $\sim$ 7.5 minutes of arc off the comet nucleus and observing through the closed dome. The dotted vertical bars in figure 1(A–C) show the peak-to-peak noise levels found from scaling figure 1(D) by the appropriate ratios of system temperature and integration time. The larger, solid vertical bars are the dotted bars multiplied by 1.6 to show how use of the dome scaling factor artificially increases the displayed noise levels. Since the closed dome attenuates the HCN spectral line data by about 40 percent (but the noise level determined from figure 1(D) properly accounts for the closed dome), an open dome estimate for the HCN data in figure 1(A–C) may be made by reading the spectral line intensities from the antenna temperature ordinates and the noise levels from the corresponding dotted vertical bars. Figure 1(A) presents the preperihelion observations. Several of the strongest Doppler-shifted triplets, marked by bars above the spectrum, indicate the presence of jets and the magnitude of their velocity components in the line of sight (1 MHz corresponds to 3.4 km s^{-1} as indicated by the scale below figure 1(C)). The true signal-to-noise ratio of the strongest features in figure 1(A) is about 3. Figure 1(B) shows the post-perihelion observations. The jets produce Doppler-shifted components which exhibit different intensities and shifts with respect to the comet's radial velocity. The

FIGURE 1.—*Emission spectrum of the HCN $J = 1 - 0$ transition observed in Comet Kohoutek (A) before perihelion, (B) after perihelion, and (C) combined average spectrum. Each horizontal bar connects hyperfine triplet components of the same Doppler-shifted jet. Bars with arrows indicate the "quiescent" emission triplet. Dashed bars connect hyperfine triplets not significantly above the noise level. A noise spectrum (D) was obtained by tracking ~7.5′ of arc (~5.6 beam widths) off the comet nucleus while observing through the closed dome. As explained in the text, (D) was used to determine the true noise levels of (A), (B), and (C), which are indicated by the vertical dotted bars. The percentages of time for which observations were carried out with the dome open are given to the right of each spectrum.*

"quiescent" triplet (marked by a horizontal bar with arrows) is always present at the expected position in the spectrum in the pre- as well as post-perihelion observations. There is no evidence of abatement in the post-perihelion spectrum. Figure 1(C) presents the combined observational data. Some of the weaker triplets are suppressed by the averaging of all the data, and only the strongest remaining triplets are identified by horizontal bars. The $F = 2 - 1$ component of the "quiescent" triplet in figure 1(C) has a true signal-to-noise ratio of about 4.

Each HCN hyperfine component ($F = 2, 1, 0$) has an optical depth τ_F given by

$$\bar{\tau}_F = \left(\frac{hB\,N}{kT}\right)\left(\frac{8\pi^3\nu}{3ch\,\Delta\nu}\right)(2F+1)\begin{Bmatrix} 1 & F & 1 \\ 1 & 0 & 1 \end{Bmatrix}^2 |\mu_{0\to1}|^2\left[1 - \exp\left(-\frac{h\nu}{kT}\right)\right] \quad (1)$$

where N is the column density of the total number of HCN molecules (assuming Boltzmann statistics); $|\mu_{0\to1}|$ the matrix element for the unsplit $J = 1 - 0$ transition; $\Delta\nu$ the line width at half-height; ν the transition frequency; B the HCN rotational constant; and the term in braces is the usual $6 - j$ symbol. If the comet coma is optically thin with a negligibly small optically thick central region, and ignoring any weak 3-mm continuum emission from the comet, then the antenna temperature, T_A^*, of the $F = 2 - 1$ HCN hyperfine component is related to the optical depth by

$$T_A^* = \beta\,\frac{h\nu}{k}\,\frac{[1 - \exp(-\bar{\tau}_{2-1})]}{[\exp(h\nu/kT) - 1]} \approx \beta\,\frac{2.127N}{T}\,\frac{8\pi^3\nu^2}{3ck\,\Delta\nu}\,\frac{5}{9}\,|\mu_{0\to1}|^2\,e^{-h\nu/kT} \quad (2)$$

where T is the excitation temperature and β the beam dilution factor. In the absence of enhancement of emission, e.g., through solar radiation, the excitation temperature will be the kinetic temperature of the radiating gas. Since the molecules can only radiate in the inner coma before they are destroyed by solar UV, it can be assumed that the gas is in thermal equilibrium with the surface from which it evaporates, i.e., $T \approx 150$ K. Average values for the $F = 2 - 1$ component of the HCN "quiescent" triplet are $T_A^* \approx 0.8$ K and $\Delta\nu \approx 200$ kHz, although smoothing gives the lines in figure 1 a broader appearance. Thus, for the "quiescent" triplet, equation (2) gives a total column density $N = \beta^{-1}$ (1.5×10^{13} cm^{-2}); substitution into equation (1) yields 0.0054 for the mean optical depth $\langle\bar{\tau}_{2\text{-}1}\rangle \equiv \beta\,\bar{\tau}_{2\text{-}1}$ which includes the effects of beam dilution. The lifetime of HCN under the influence of solar radiation is not known, but typically the range of molecules in the coma, at 1 AU heliocentric distance, is 10^4 to 10^5 km. We shall use these values for the cutoff range, r_o, in the model described by Huebner and Snyder (1970) for the average, uniformly smeared out, column density in the antenna beam.

$$\langle N\rangle = \frac{4Q'}{\pi v\Delta^2\theta_B{}^2}\left[s\cos^{-1}\frac{s}{r_o} - (r_0{}^2 - s^2)^{1/2} - r_o\right] \quad (3)$$

In this equation $s = \min [r_o, \Delta \cdot \theta_B/2]$, $\langle N \rangle \equiv \beta N = 1.5 \times 10^{18}$ cm^{-2}, Q' is the total production rate of HCN molecules, $v \approx 0.3$ km s^{-1} is the average (thermal) expansion velocity of the gas, Δ is the geocentric distance of the comet, and $\theta_B \approx 80$ of seconds of arc is the half-power beam width of the antenna. To a good approximation, the production rate, Q', is the same during the observing periods before and after perihelion. Thus for the "quiescent" triplet at $\Delta \approx 1$ AU, Q' ranges from 12×10^{27} s^{-1} for $r_o = 10^4$ km to 3×10^{27} s^{-1} for $r_o = 10^5$ km. Taking into account the Doppler-shifted components, the overall HCN production rate is about two to three times higher. Further analysis of other molecular observations is in progress.

ACKNOWLEDGMENTS

We thank the NRAO personnel for their support during the observations. We were assisted in telescope operations by D. Cardarella, D. Myers, C. Sparks, and P. Rhodes. It is a pleasure to acknowledge the help we received from Drs. T. Clark, Rh. Lüst, and B. G. Marsden on the ephemerides; and to express our thanks to Dr. B. L. Ulich for helpful discussions on calibration, and to M. L. Stein for invaluable help in the reduction of the data on the MANIAC II computer. L. E. Snyder received partial financial support during this work from NSF Grant GP-34200 to the University of Virginia.

REFERENCES

De Lucia, F.; and Gordy, W.: 1969, Phys. Rev. 187, 58.
Huebner, W. F.; and Snyder, L. E.: 1970, Astron. J. 75, 759.
Huebner, W. F.; Snyder, L. E.; and Buhl, D.: 1974, Icarus, 23, 580.

DISCUSSION

MILLER: What were the other two comets you tried this out on?

SNYDER: Tago-Sato-Kosaka and Bennett. I did not try it out on HCN.

MILLER: Did you use the same equipment?

SNYDER: We did not use the same telescope and did not look at the same molecule. We went for a strong molecular emission and correct beam width. But we had to look through the dome due to solar heating of the antenna.

CHAISSON: Were you able to map at all with such a small beam?

SNYDER: We tried some maps but we were unable to do it successfully. In fact, we don't see any difference between taking small offsets. If we had an open dome and cool receiver, then we might try some maps.

OBSERVATIONS OF COMET KOHOUTEK WITH SKYLAB EXPERIMENT S019

K. G. HENIZE
Johnson Space Center

A. L. LANE
Jet Propulsion Laboratory

J. D. WRAY
G. F. BENEDICT
S. B. PARSONS
University of Texas

Useful images of Comet Kohoutek taken with the SO19 objective-prism spectrograph were obtained on nine dates ranging from November 25, 1973 to January 11, 1974. The plate data are listed in table I.

Photographs on five separate dates are illustrated in figure 1. Although the image of the nucleus is generally elongated toward the left as a result of spectral dispersion, this elongation does not extend to shorter wavelengths than 3000 Å. The well-dispersed spectra of several stars extending from 5000 Å at the right to 1300 Å at the left in the December 16 exposure illustrate the usual extent of stellar spectra produced with this instrument. It is clear that none of the emissions which may occur between 1300 and 3000 Å has an intensity approaching that of emissions in the 3000 to 5000 Å region.

The images of the nucleus on December 13 and December 16 show a binuclear structure which suggests that two distinct emission bands are being observed. Isophotes of the December 13 image (fig. 2) confirm its binuclear structure. The 0.3-mm separation of the two images corresponds to within 0.03 mm of the expected separation of the OH λ3090 and the CN λ3883 bands. Since these are the two strongest emissions in the spectrum of Comet Kohoutek between 3000 and 4500 Å, we conclude that these two bands account for its binuclear structure. It is interesting to note that the elongation of the nucleus and the binuclear structure is more evident in December than in January. This suggests that the strength of the OH band was greater in December than in early January. We expect to isophote all the images in order to confirm this suspicion in a more quantitive way.

Table I.—*SO19 Observations of Comet Kohoutek*

Date	Start Time (UT)	Exposure (seconds)	Tail Length
Nov 25	2236	900	1.5°
Dec 7	2351	300	1°
Dec 13	1501:30	120	1.5°
Dec 14	1556	180	? edge
	1559	30	? edge
Dec 16	2220	270	1.5°
Dec 17	0300	270	1.5°
Jan 7	2349	400	2.5°
Jan 8	1215	500	2°
	1224	70	2°
Jan 11	0148	720	4°

It is also interesting to attempt to map the extent of the OH image. Using density data obtained with the SO19 PDS Microdensitometer at the University of Texas, we have drawn a line of symmetry through the comet tail and extended this through the nucleus. Then the long wavelength half of the image has been subtracted from the short wavelength half. A distinct diffuse image remains which may be attributed to OH emission at λ3090. (See fig. 3.) We expect to apply this technique to the analysis of all our comet images.

On December 17 we attempted to obtain an absorption spectrum of the comet as it occulted the bright B1 V star, π Scorpii. A spectrum of π Scorpii was obtained 20 minutes after closest approach. When compared with a spectrum obtained 4 hours before closest approach, no obvious changes are visible to the naked eye. A detailed photometric analysis of the two spectra has not yet been made.

DISCUSSION

PAGE: On your contour chart it looked as if there were also two different regions of the tail. Is that possible?

HENIZE: I would not say it is impossible, but I must admit I have not placed any significance in what I saw in the tail.

BRANDT: What emissions do you identify in the tail? Your observations may yield tail orientations against solar wind orientation in the region close to the Sun and would be unique. Such observations may be very valuable.

HENIZE: That is an interesting question. Unfortunately, we don't see much tail structure. We have that data if you want it. The question is what sort of radiation is it? As I say, if we had some nice sharp points or rays in that tail we might make a good interpretation. We are looking more or less at a continuum. I have heard that there is very little dust in this comet. I see no

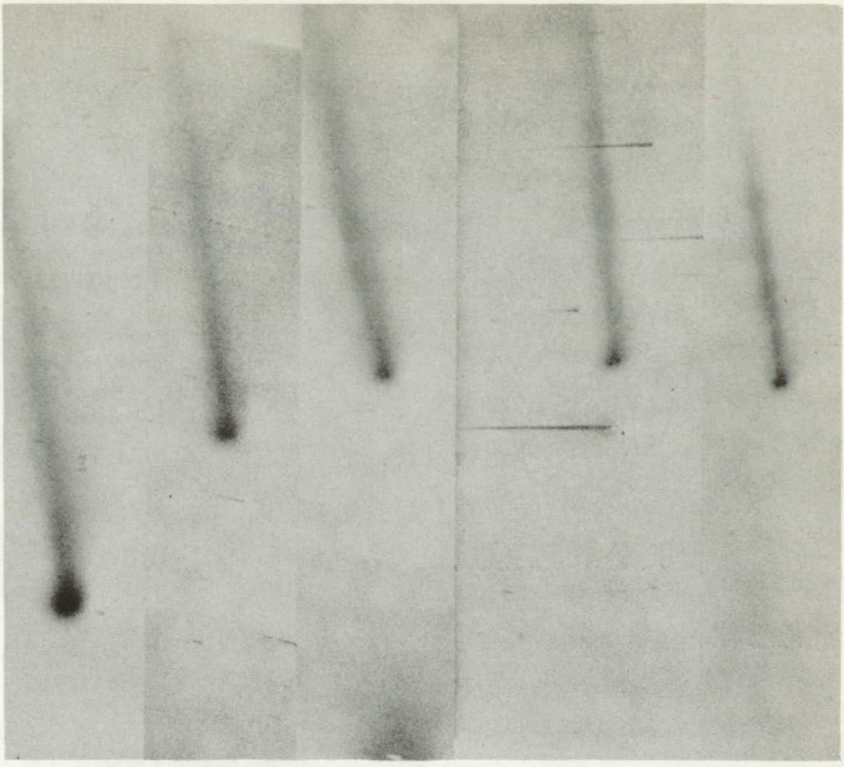

FIGURE 1.—*Objective-prism images of Comet Kohoutek obtained by Skylab experiment S019. From right to left, the dates and exposure times are December 13 (120 s), December 16 (270 s), January 7 (400 s), January 8 (500 s), and January 11 (720 s). Several stellar spectra appear on the exposure taken on December 16. The star directly below the comet, π Scorpii, was occulted by the comet 4 hours later. The double image of the nucleus on the first three dates is probably due to the separation of the OH λ 3090 image from the image of the CN band at λ 3883.*

evidence of structure in the tail corresponding to structure in the nucleus. I think of the tail as a continuum.

BRANDT: For what it's worth, you can probably get some information from this orientation.

MILLER: I would not be surprised if some of that tail extension was 3880. We have a single objective prism connected with the Schmidt. The CN at 3880 and C_2 at 4737 go way out in the tail to a million km and are very unique.

VOICE: I have observations that extend through December. I find that the CN energy is very strong and extends a couple of degrees into the tail.

WHIPPLE: The way the sodium went off in the tail and the fact that particles in this comet were vaporizing imply that you are getting a source of the

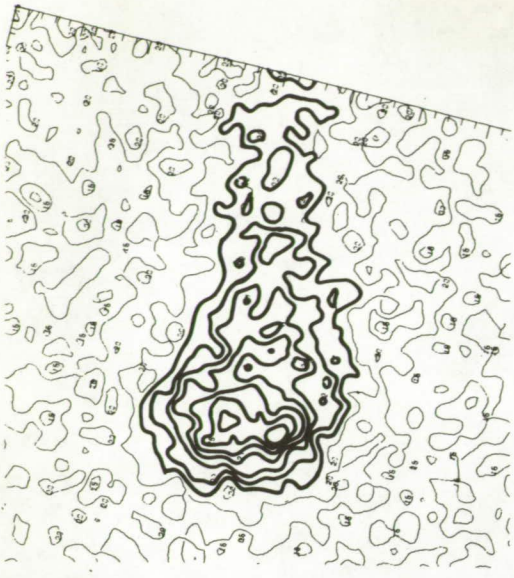

FIGURE 2.—*Isophote map of of comet image on December 13. The data are displayed in density units with the contour interval being 0.1 density units. The numbers indicate the number of 0.05-density intervals above the clear film reading.*

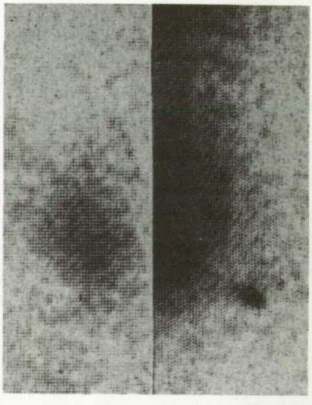

FIGURE 3.—*Symmetrical subtractions of the image of January 11. The right side shows the original right half of the image which was subtracted from the left half. The left side shows what remains of the left half after the subtraction.*

dust way back into the tail. It begins to seem that these particles may last a little longer than in most comets. Sodium is on the back side, not on the Sun side at all, which indicates that the particles are being carried back and disintegrated in the tail structure rather than the nucleus.

HENIZE: We may have something significant here. The comet turns black at about 3000 and chops off. What one needs to do is compare the comet spectral distribution with the solar distribution, and I have not done that.

KELLER: There is the same thing on the OAO–2 spectra of Bennett where you don't see below 3000 Å.

HENIZE: Where we really had the burned-out image was on January 11, when we get a good sharp cutoff at 3000 Å.

VOICE: Commenting on the sodium again—between December 13 and 20, there seems to be an increase in narrow-band cometary emission of the sodium line. It became extremely brilliant just as the comet was lost. The sodium emission was way out into the tail.

HERBIG: Is it really surprising that the ultraviolet is so faint? On your spectrogram we saw B stars which ran out into the ultraviolet, and A stars which died rather quickly, and F stars which had nothing.

HENIZE: I could compare the comet spectra to a G-type star. The late F stars and the G stars go out at least to 2800 and then there are iron bands that really start chopping that spectrum off. I must admit, the question is—does it chop at 3000 or does it chop at 2600? And if it chops at 3000, I am surprised.

Λ9-cm CH EMISSION IN COMET KOHOUTEK (1973f)

J. H. BLACK
E. J. CHAISSON
J. A. BALL
H. PENFIELD
A. E. LILLEY
Center for Astrophysics
Harvard College Observatory
Smithsonian Astrophysical Observatory

The principal hyperfine transition ($F = 1 \rightarrow 1$) Λ9 cm of the $^2\Pi_{1/2}$, $J = 1/2$ Λ-doublet state of CH, has been detected in emission from Comet Kohoutek. The spectral feature was monitored for several days after perihelion, until the signal strength diminished below the radiometric sensitivity. The average column density of ground state matter $N(CH) \simeq 4 \times 10^{14}$ cm^{-2}. Further details of the results of this experiment can be found elsewhere in the published literature (Astrophysical Journal *(Letters), Volume 191, L43, 1974).*

DISCUSSION

SNYDER: What were the Swedish negative results?

CHAISSON: They reported negative results on the 7th and 9th. On our data we could see no evidence from the line on either of those days. Their limit in the IAU telegram was considerably below our detection on the previous dates, but it was probably higher than that.

FELDMAN: Was the CH turned off, or what?

CHAISSON: No. It decreased with intensity and with time. Their observations would be in agreement with us.

BELTON: Was the velocity offset the same as the OH?

CHAISSON: I think it was 0.5 km/s for OH. And it was 0.8 km/s for water in Bradford.

ULICH: I might also mention that CH_3CN data indicate a slight offset of about 0.5 km/s in the same direction.

CHAISSON: Right. To the blue side.

ANDREW: I noticed that the various line velocity widths seem to vary with frequency. And that the higher frequency was on a narrower line. Is this a resolution effect, or something more real?

CHAISSON: The millimeter lines observed by Ulich from those molecules are probably coming from the nucleus. Ours are coming from large daughter clouds and attribute the larger line to the beams.

THE $^{12}C/^{13}C$ RATIO IN COMET KOHOUTEK (1973f)

A. C. DANKS
Department of Astronomy
University of Texas

D. L. LAMBERT
McDonald Observatory

C. ARPIGNY
Institut d'Astrophysique
Université de Liège, Cointe-Ougrée

Photoelectric scans of the C_2 1–0 bandhead at 4737 Å in Comet Kohoutek (1973f) are presented at resolutions of 0.14 to 0.5 Å. The ratio $^{12}C/^{13}C = 115^{+30}_{-20}$ was determined. Within the experimental errors, this agrees with the terrestrial ratio $^{12}C/^{13}C = 89$.

Introduction

An isotopic abundance ratio may constitute a clue to the origin of comets. At present, the $^{12}C/^{13}C$ ratio is the only isotopic abundance ratio which has been derived for comets.

Previous estimates for this ratio have been made by Stawikowski and Greenstein (1964) for Comet Ikeya (1963I) and by Owen (1973) for Comet Tago-Sato-Kosaka (1969IX). The isotopic ratios found were $^{12}C/^{13}C = 70 \pm 15$ and 100 ± 20, respectively. Both these investigations were made with photographic spectra of moderate dispersion. The ratio is determined by comparison of the intensities of the $^{12}C^{12}C$ (1–0) P-branch bandhead at 4737.08 Å with the $^{12}C^{13}C$ (1–0) bandhead at 4745 Å. The isotopic shift is approximately 7 Å and places the $^{12}C^{13}C$ (1–0) bandhead in a relatively clear region of the spectrum.

The 4745 Å feature was first identified by Bobrovnikoff (1930). Swings (1943) had noted that the feature was absent in some comets, most notably

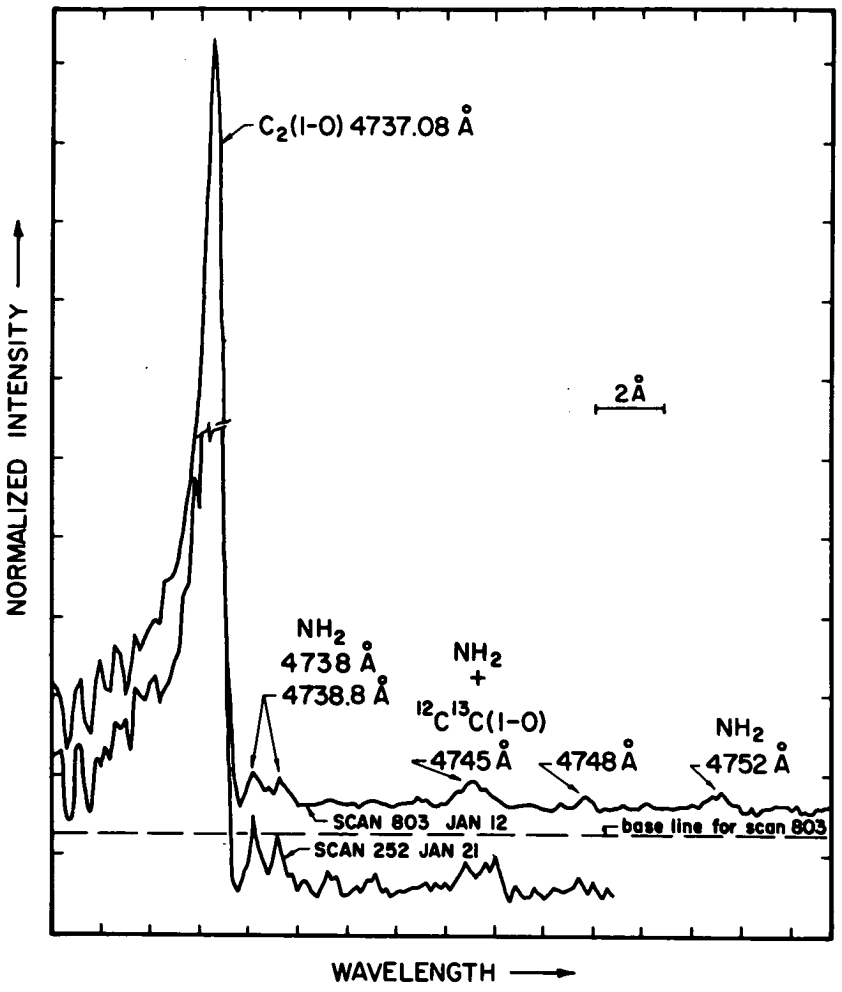

FIGURE 1.—*Medium resolution scans of Comet Kohoutek (1973f). The scans have been normalized to the same peak intensity for the* $^{12}C_2$ *bandhead at 4737 Å. The* $^{12}C^{13}C$ + NH_2 *blend is seen at 4745 Å. The increased strength on January 21 of the* NH_2 ($1_{10} - 2_{20}$) *complex at 4738.0 and 4738.8 Å is shown.*

Comet Cunningham (1940I). This is a tentative indication that cometary compositions may differ.

Observations

The spectrum shown in figure 1 was obtained with the 107-inch telescope at McDonald with the Tull (1972) coudé scanner. The resolution is 0.4 Å. The

$^{12}C^{12}C$ (1–0) and $^{12}C^{13}C$ (1–0) bandheads are indicated. In addition, there is the previously reported unidentified feature at 4748 Å. The other features at 4738.0, 4738.8, and 4752 belong to the NH_2 (0, 14, 0) system. A measure of the NH_2/C_2 intensity ratio is provided by the 4738.0 and 4738.8Å NH_2 lines.

The extraction of a $^{12}C/^{13}C$ ratio from $^{12}C^{12}C$ (1–0) and $^{12}C^{13}C$ (1–0) bands is complicated because the $^{12}C/^{13}C$ (1–0) band is blended with several NH_2 lines. In order to try to correct for the NH_2 contribution, a series of high-resolution scans were made of the 4745 Å feature and are shown in figure 2. The high-resolution scans were made with the echelle mode and are at a resolution of 0.1 Å. The $^{12}C^{13}C$ (1–0) bandhead occurs at 4744.69 Å. The NH_2 blending lines are at 4744.28 (0.49), 4744.46 (0.64), 4744.84 (1.00), and 4745.19 (0.67) Å. The number in parentheses is the relative absorption strength of the line as estimated from a tracing reproduced in Owen (1973). The last three lines are from the (0, 14, 0) band and are classified by Dressler and Ramsay (1959). This 4744.28 Å line probably belongs to the (1, 10, 0) band (Ramsay, 1974). This is the first time that these lines have been resolved in a comet.

The ratio NH_2/C_2 was approximately constant from January 4 to January 12. The high-resolution scans were made between January 14 and January 21. A marked increase in NH_2 relative to C_2 occurred between January 12 and 21, as can be seen in figure 1.

The $^{12}C/^{13}C$ Ratio

The low-resolution scans from January 4 to January 12 were co-added to improve their S/N; the relative Doppler shifts were taken into account before the addition was carried out. An attempt was made to synthesize the observed spectrum. For the $^{12}C^{12}C$ (1–0) bandhead, wavelengths were taken from Phillips and Davis (1968). The relative rotational line intensities were calculated, assuming a Boltzmann distribution. The generated spectrum was convolved with the instrumental profile. The best fit obtained was for a temperature of 3000 K. The wavelengths for the $^{12}C^{13}C$ (1–0) bandhead were calculated along with their relative intensities, assuming a temperature of 3000 K. A composite of the $4NH_2$ lines + $^{12}C^{13}C$ (1–0) bandhead was computed and the ratio of $^{12}C^{13}C/NH_2$ was adjusted until the best fit to the observed profile was obtained. The key assumption is that NH_2 lines are present with their assumed relative intensities. The best fit obtained—to the mean profile—is shown in figure 3. The ratio $^{12}C^{13}C/(^{12}C^{13}C + NH_2)$ was 42 percent and values of 33 percent and 53 percent give inferior fits. The ratio of $^{12}C/^{13}C$ provided by the two best fitting synthetic profiles was 115^{+30}_{-20}.

The high-resolution scans, however look like pure NH_2. The synthetic spectrum for these scans indicated a $^{12}C^{13}C/(^{12}C^{13}C + NH_2)$ of 13 percent which is equivalent to a ratio of $^{12}C/^{13}C = 370$. The resolution of this incon-

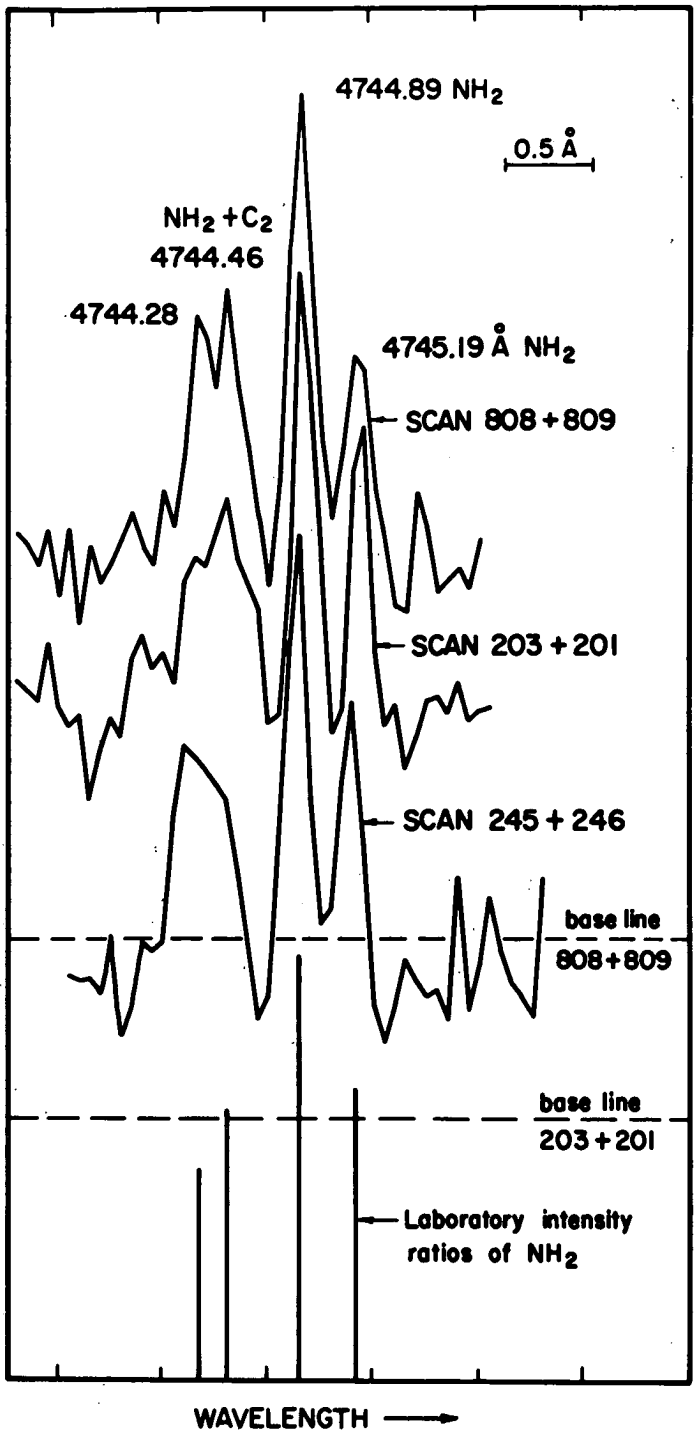
4744.89 NH2
0.5 Å
NH2 + C2
4744.46
4744.28
4745.19 Å NH2
SCAN 808 + 809
SCAN 203 + 201
SCAN 245 + 246
base line
808 + 809
base line
203 + 201
Laboratory intensity
ratios of NH2
WAVELENGTH

sistency between the high- and low-resolution scans lies in the increased intensity of NH_2 relative to C_2 during the period when the high-resolution scans were made. The increase shown between January 12 and 21 is approximately a factor of 3 which would make the high-resolution scans consistent with the medium-resolution scans.

Conclusion

On the basis of the medium-resolution scans, the $^{12}C/^{13}C$ ratio for Comet Kohoutek (1973f) is found to be $^{12}C/^{13}C = 115^{+30}_{-20}$ which is not significantly different from the terrestrial value $^{12}C/^{13}C = 89$.

This study demonstrates the limitations imposed by the NH_2 blends. The moderate spectral resolution enabled a reasonably satisfactory treatment of the NH_2 blends. Higher resolution should be possible in future comets with our projected instrumental improvements. Nonetheless, consideration might be usefully given to alternative methods for obtaining $^{12}C/^{13}C$ ratio. The CN(0, 0) Violet system is an attractive possibility. A carefully chosen ^{13}CN rotational line in the (0, 0) system could be picked out in the Q branch gap of the superimposed CN (1, 1) system shown in figure 4. The line separation in this region is sufficiently large to resolve them in a bright comet. We show lines up to N(20), as levels for $N > 20$ are not likely to carry an appreciable population. Resonance-fluorescence would have to be taken into account; but this has already been treated by Arpigny (1964).

NOTE: A full discussion of this problem has been accepted for publication in the *Astrophysical Journal* (1974) 194, 745.

ACKNOWLEDGMENTS

We are indebted to Drs. E. Barker and R. Beer, and to Mr. D. Dearborn and Miss A. Cousins for assistance at the telescope; to Dr. R. G. Tull for advice on the instrumentation; and to Drs. J. L. Greenstein, G. H. Herbig, T. C. Owen, and D. A. Ramsay for helpful discussions. A. C. Danks wishes to thank the Lindemann Trust for a fellowship administered by the English Speaking Union. C. Arpigny is grateful to the Belgian Ministère de l'Education Nationale for financial support. This work was supported in part by the National Aeronautics and Space Administration under grant NGR 44–012–152.

FIGURE 2.—*High-resolution scans of the $^{12}C^{13}C$ + NH_2 4745 Å blend in Comet Kohoutek (1973f). The close similarity of the comet spectrum to the NH_2 laboratory spectrum is apparent. The two NH_2 lines at the red end of the complex are completely beyond the blue degraded $^{12}C^{13}C$ 1–0 bandhead.*

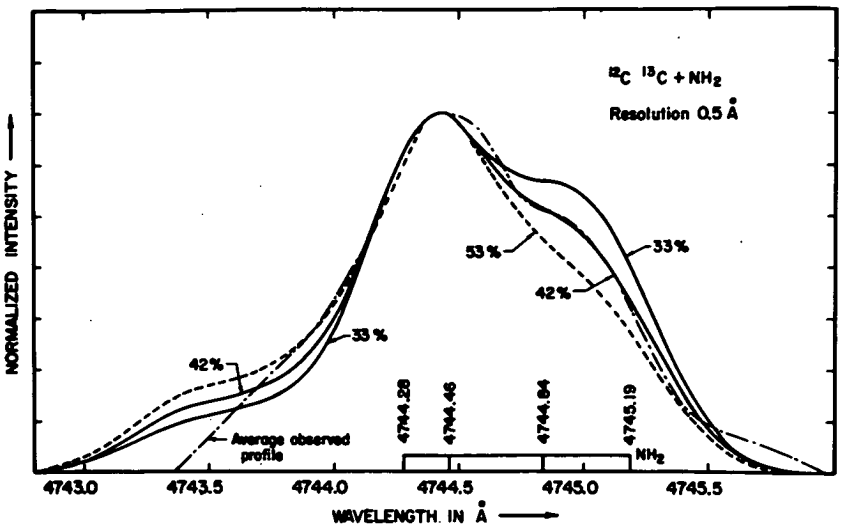

FIGURE 3.—*The observed and synthesized 4745 Å blend of $^{12}C^{13}$ + NH_2. Positions of the NH_2 lines are shown; their assumed relative intensities are indicated in figure 2. The blue degraded $^{12}C^{13}C$ + 1–0 bandhead extends to 4744 Å. The best fitting synthetic profile is that labeled 42 percent.*

REFERENCES

ARPIGNY, C.: 1964, Ann. Astrophysics 27, 393.
BOBROVNIKOFF, N. T.: 1930, Pub. A.S.P. 42, 119.
DRESSLER, K.; and RAMSAY, D. A.: 1959, Phil. Trans. Rov. Soc., London, A. 251, 553.
OWEN, T.: 1973, Ap. J. 184, 33.
PHILLIPS, J. G.; and DAVIS, S. P.: 1968, The Swan System of the C_2 Molecule. Berkeley: University of California Press.
RAMSAY, D. A.: 1974 (private communication).
STAWIKOWSKI, A.; and GREENSTEIN, J. L.: 1964, Ap. J. 140, 1280.
SWINGS, P.: 1943, M.N.R.A.S. 103, 86.
TULL, R. G.: 1972, Proceedings ESO/CERN Conference on Auxiliary Instrumentation for Large Telescopes. Geneva, May 2–5, p. 259.

DISCUSSION

DONN: Did you use the same temperature for the $^{12}C/^{13}C$?

DANKS: Yes.

DONN: There is some danger in this if the temperature is not at the thermodynamic temperature but something approximated by radiative equilibrium. This depends on the solar spectrum. The distributions may not be the same.

DANKS: It seems that in past studies C_2 has not been very sensitive to any resonance-fluoresence mechanism. There are no strong Franhoufer lines in the

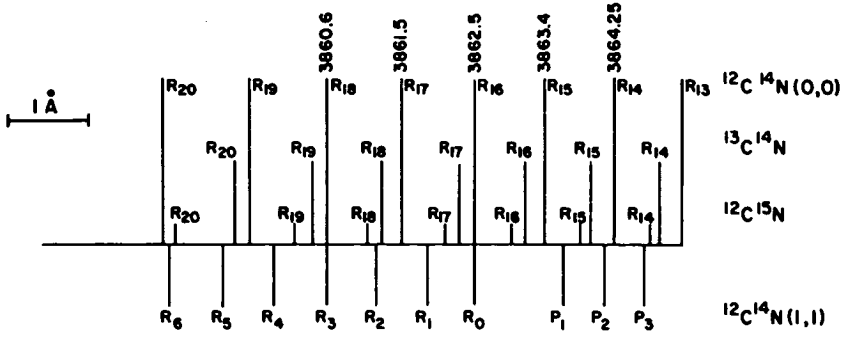

FIGURE 4.—*Approximate line separations in the CN (0, 0) Violet band. The superimposed $^{12}C^{14}N$ (1,1) band is also shown.*

region of $^{12}C/^{13}C$ and I don't think the transition probability is going to be very different from that of $^{12}C/^{12}C$. The best temperature fit there was 3000°, but 4500° would not have been very different.

PAGE: Why did NH_2 increase by a factor of 3 in 10 days?

DANKS: I wish I knew; but it is not impossible. You would expect the ratio of NH_2 to C_2 to change. I can't explain it.

MARAN: Can this allow you to say something about the comet's being the same age as other objects?

DANKS: If the ratio is terrestrial, it does not say very much. Within the experimental error it is similar to the terrestrial value.

WEHINGER: Did you look at any of the other $^{12}C/^{13}C$ bandheads?

DANKS: No. That is not quite as simple because it is going to be shifted into a region which is more complicated. You have to separate it from other lines. There are other emissions in this region. We also considered the CN (2–0) red system and we thought if we could take one rotational line we might not only get ^{12}CN and ^{13}CN but perhaps results from the C_2.

SEKANINA: How certain are you in using or eliminating the continuum? Can it be in part responsible for the discrepancy?

DANKS: I feel certain that we have done the best job possible in this region. There are two faint Fe–I lines in the region of the $^{12}C/^{13}C$ bandhead. We can account for these, and the background looks fairly smooth.

*ON THE STRUCTURE OF THE NUCLEUS OF COMET KOHOUTEK (1973f)**

W. F. HUEBNER
University of California
Los Alamos Scientific Laboratory

Detection of some mother molecules in Comet Kohoutek and the multiple Doppler shifts in the emission spectra of these molecules yield new information about the detailed chemical and physical structure and the accretion mechanism of the nucleus. The more volatile frozen gases vaporize first and rather uniformly from the surface layer of the comet during its approach to the Sun. This relatively quiescent phase occurs at heliocentric distances $r > 0.5$ AU. The depletion of volatiles changes the chemical composition of the surface layer into a conglomerate of coarse-grained refractories (that were too big to be dragged into the coma by the escaping gases) and less volatile frozen gases, predominantly water. This fractionation accentuates unevenness in the surface structure and exposes materials which can acquire somewhat higher equilibrium temperatures. As the comet continues to approach the Sun, it is exposed to more intense solar radiation and some of the heat is conducted below the surface. Jets form if volatile material is concentrated in pockets to which heat can penetrate. The intensity, duration, and magnitude of the Doppler-shifted spectra permit very crude estimates for the size of such pockets. It appears that the nucleus is heterogeneous in composition and structure on a scale of about 10 m. If Kohoutek is a typical comet, then this suggests that comet nuclei accrete cometesimals of this size.

* Work performed, in part, under the auspices of the U. S. Atomic Energy Commission.

Comet Kohoutek has been a very rewarding astronomical object. The wealth of observational data obtained admits some new conclusions about the detailed chemical and physical structure of its nucleus. A number of models for the physical structure of the nucleus have been suggested—all within the framework of the icy conglomerate composition proposed by Whipple (1950, 1951, 1955). Among these models are the homogeneous nucleus, the heterogeneous nucleus, the "onion skin" nucleus composed of layers of different composition, and the spotted nucleus (Shul'man, 1970). The observational data based on brightness of the comet as a function of heliocentric distance (reduced to 1 AU geocentric distance) linked to gas production rates; the development of the dust coma, tail, and spikes; and particularly the microwave detection of some mother molecules and the associated Doppler shifts of their spectra favor the heterogeneous model of the nucleus.

First, I want to discuss the gas production rate as a function of heliocentric distance. Taking all the pre-perihelion brightness data as published in the IAU Circulars, reducing the data to 1 AU geocentric distance, and fitting these to the gas production rates as obtained from the principle of energy balance (Huebner, 1965a; Delsemme 1966) as outlined by Huebner (1965b), we find that the average latent heat of vaporization of the frozen gases in the surface layer is about 4 to 7 kcal/mole. The range of these values is determined primarily by the scatter of the brightness data, and the uncertainties of the physical properties such as visual albedo, infrared emissivity, heat conductivity, and spin of the nucleus. Applying the same procedure to the data after perihelion we find that the average latent heat of vaporization is about 7 to 10 kcal/mole. If the physical properties are not significantly altered during perihelion passage, then the composition of the frozen gases in the surface layer must have changed. As pointed out in earlier papers at this meeting by Keller and Sekanina, Kohoutek produced a dust coma at large heliocentric distances before perihelion. The dust production is closely coupled to the gas production rates through drag forces. Submillimeter dust grains had to be dragged into the coma at $\sim$ 4 AU heliocentric distance to account for the observed spikes during perihelion passage. The lift-off forces for such grains require that the latent heat of the frozen gases be about 4 kcal/mole (Sekanina, 1974). This value is in good agreement with the above deductions based on the visual brightness of the comet. A change of $\sim$ 2 kcal/mole for the latent heat of vaporization from before perihelion to after perihelion is not very unusual (see, e.g., Huebner, 1965a). It indicates depletion of the more volatile components of the frozen gases in the surface layer while the comet moved around the Sun.

Secondly, I want to discuss the radio observations before perihelion of the comet at heliocentric distances between 0.9 and 0.8 AU. Ulich and Conklin (1974) detected methyl cyanide while the comet was at these heliocentric distances. The observed spectrum indicates a Doppler shift of less than 0.5 km/s

with respect to the rest frame of the nucleus. Methyl cyanide has a latent heat of vaporization of about 8 kcal/mole. The observation indicates rather uniform continuous outgassing of the surface layer. As reported earlier in this session by Snyder et al., hydrogen cyanide was detected in the comet before as well as after perihelion at heliocentric distances between 0.5 and 0.3 AU. The observed spectrum had many Doppler shifts. The Doppler shifts varied in frequency as well as in intensity. There was no visible abatement of the intensity after perihelion as compared with intensity before perihelion. The combined spectrum obtained on December 15 and 16 and the spectra obtained on January 3 and on January 6 are presented in figure 1. The bars above the spectrum indicate triplet hyperfine components belonging to the same Doppler shift. These Doppler shifts indicate directed jets with velocity components up to $\sim$ 3.5 km/s in the line of sight. The bar with the arrows pointing downward corresponds to the hyperfine triplets with zero Doppler shift in the rest frame of the comet. This could be interpreted as a quiescent outgassing. It is more likely, however, to represent jets of neutral gas, just like all the other Doppler shifts, but in a direction perpendicular to the plane of observation. The "quiescent" HCN spectrum is present in each observation to within the width of one channel of the spectrum analyzer (100 kHz or $\sim$ 0.34 km/s). The more intense Doppler-shifted spectra appear to persist for at least several hours, but less than 24 hours. Jets have been observed visually in many comets (see, e.g., Rahe, 1966; Rahe and Donn, 1969, 1971) but they were not necessarily composed of neutral gases and their stream velocities had not been measured.

An explanation consistent with observations is that the jets are formed by exploding pockets of volatile gases somewhat below the surface of the nucleus. Since the comet is close to the Sun (less than 0.5 AU) and the surface layer has been depleted of the more volatile components (leaving primarily dust, water, and clathrates in that layer) the equilibrium temperature will rise somewhat and the temperature gradient toward the interior of the nucleus will become accentuated. As heat penetrates into the nucleus it will heat up pockets of the more volatile gases which will then explode by fracturing the delicate structure that surrounds them. The escape velocity of the gas for the adiabatic case is given by Lelevier (1965) as

$$v_E = 2c/(\gamma - 1), \tag{1}$$

where c is the speed of sound (approximately equal to the thermal velocity of the ambient coma, about 0.4 km/s) and γ is the ratio of the specific heats. Typically $\gamma \approx 1.1$ to 1.35 for polyatomic molecules at low temperatures. For HCN, $\gamma \approx 1.25$ and the escape velocity is about 8 times the thermal velocity, which is consistent with the observed 3.5 km/s. From the column density of the stronger Doppler components in the line of sight (as obtained from the antenna temperature), the escape velocity, and the approximate duration of

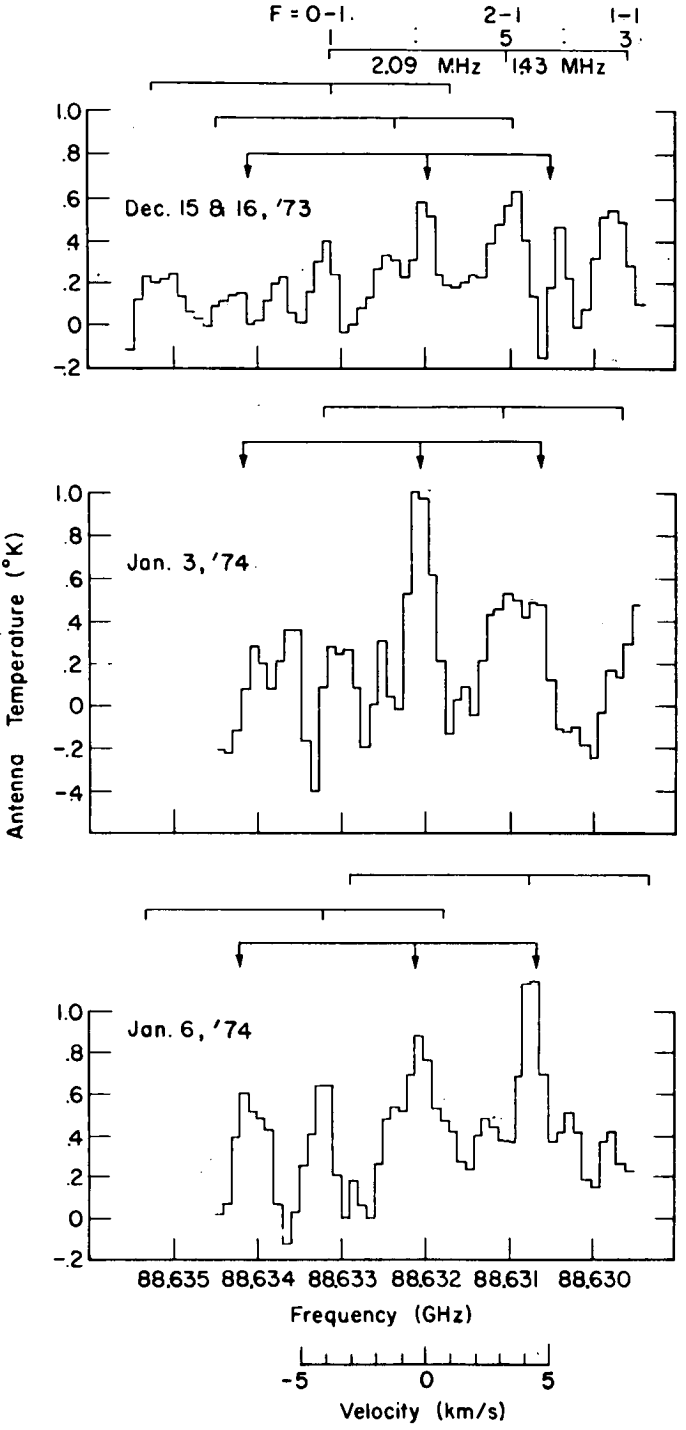
F = 0-1
2-1
1-1
1
5
3
2.09 MHz
1.43 MHz
Dec. 15 & 16, '73
Jan. 3, '74
Jan. 6, '74
Antenna Temperature (°K)
1.0
.8
.6
.4
.2
0
-.2
-.4
88.635 88.634 88.633 88.632 88.631 88.630
Frequency (GHz)
-5
0
5
Velocity (km/s)

the jets, one can estimate the amount of gas enclosed in these pockets. The volume one arrives at in this manner is of the order of several thousand m^3 per pocket. Only large pockets will produce clearly observable jets. Finally, as the comet moves beyond 0.5 AU heliocentric distance after perihelion, no line emission has been detected in the radio range (Simon, 1974). This indicates that the outgassing of volatiles has stopped, and that the interior layers just below the surface have cooled off and no pockets can be exploded.

In summary, the impression one obtains from the observations is illustrated in figure 2. As the comet approaches the Sun at heliocentric distances larger than 1 AU, the surface layer is depleted of the more volatile components leaving mostly water, clathrates, and dust in it. Some icy grains and dust are dragged into the comet's coma by escaping volatile gases. Between 1 and 0.5 AU heliocentric distance, some of the pockets in the surface layer are depleted and the surface layer begins to warm up to a somewhat higher equilibrium temperature. The temperature gradient toward the interior develops and heat is conducted into the layers just below the surface. This then causes pockets of frozen volatile gases just below the surface layer to vaporize, explode, and form jets as the comet continues to approach the Sun. Jets appear to form in random directions. This does not necessarily mean that they have to issue uniformly or nearly uniformly from the surface of the nucleus. They could also originate primarily from the subsolar side of the nucleus but in different directions determined by surface irregularities. Some larger dust grains accumulate on the surface. They will temporarily shield the frozen gases from the solar radiation, but they will also form hot spots which can lead to flares. The peak of the temperature distribution on the surface must be reached during, or very shortly after, perihelion passage. This peak will diffuse inward and broaden as time passes; thus heat can still penetrate into the surface for some time after perihelion passage, giving rise to further jets. At distances larger than about 0.5 AU, the temperature distribution has flattened out sufficiently and the surface layer has been depleted to some depth of all volatiles, including those in pockets, to such an extent that jets can no longer form. If Comet Kohoutek is a typical comet, then the heterogeneous model of the nucleus suggests that comets accrete cometesimals of varying composition and of linear dimensions of the order of a few times 10 m.

Not nearly as much detailed information has been obtained about the chemical constituents of the comet other than water. Only a few mother molecules have been detected: CH_3CN and HCN. It must be kept in mind that the mol-

FIGURE 1.—*Emission spectrum of the HCN $J = 1 - 0$ transition observed in Comet Kohoutek (1973f) before perihelion (December 15 and 16, 1973) and after perihelion (January 3 and 6, 1974). Each horizontal bar connects hyperfine triplet components ($F = 0 - 1$, $2 - 1$, and $1 - 1$) belonging to the same Doppler-shifted jet. The corresponding theoretical intensity ratios are indicated above the top bar. Bars with arrows indicate the "quiescent" emission triplet.*

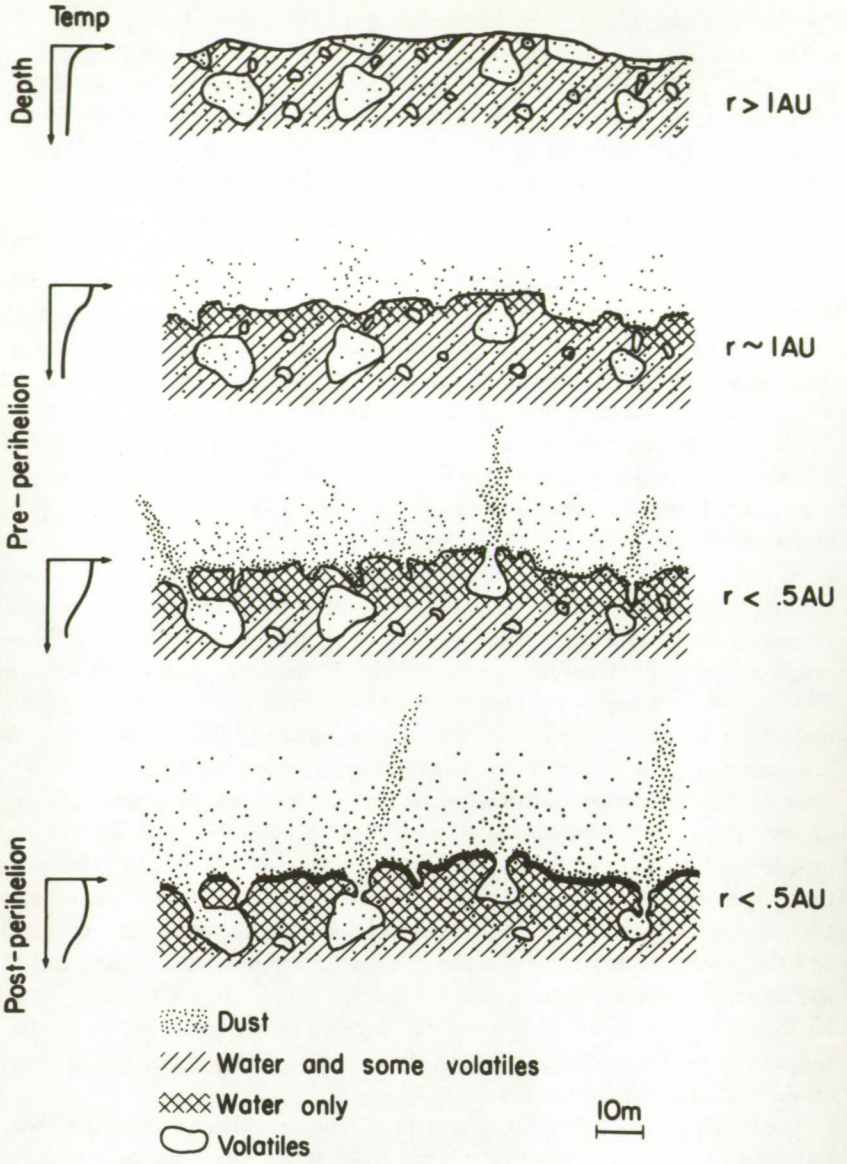

FIGURE 2.—*A portion of a cross section of the heterogeneous model of a comet nucleus. At some heliocentric distance $r > 1$ AU (top of figure), the out-gassing of the volatile components begins. The temperature profile on the left indicates a rise of the equilibrium temperature at the nuclear surface. At $r \sim 1$ AU, volatiles have been depleted from the surface, heat begins to penetrate. At $r < 0.5$ AU heat has penetrated to pockets of volatiles and causes them to erupt in jets. After perihelion, but*

ecules have very strong transitions in the radio range, which make their detection easy, and it was for this reason that the search had been concentrated on these species (Huebner, 1971). There may be many other molecules which have weaker transitions, but this does not reflect on their abundance in comets. The relatively high abundance of CH_3CN (several ten times higher than HCN) computed from the observed antenna temperature, as reported earlier in this session by Ulich and Conklin, may be a consequence of the assumed equilibrium model. Since CH_3CN was detected in the $v_8 = 1$ state which is about 500 K above the ground state, non-equilibrium processes may play an important role. This requires further investigation.

ACKNOWLEDGMENT

It is a pleasure to thank Dr. J. F. Barnes for stimulating discussions about the explosive release of the trapped volatiles.

REFERENCES

DELSEMME, A. H.: 1966, Mém. Soc. Roy. Sci., Liège, Sér. 5, 12, 77.
HUEBNER, W. F.: 1965a, Z. Astrophys. 63, 22.
HUEBNER, W. F.: 1965b, Sitz.-Ber. Bayer. Akad. Wiss., November 1965, 147.
HUEBNER, W. F.: 1971, Bull. A.A.S. 3, 500.
LELEVIER, R.: 1965, Lectures on Hydrodynamics and Shock Waves, Lawrence Radiation Laboratory report UCRL–4333 Rev. 1.
RAHE, J.: 1966, Mém. Soc. Roy. Sci., Liège, Sér. 5, 12, 141.
RAHE, J.; and DONN, B.: 1969, Astron. J. 74, 256.
RAHE, J.; and DONN, B.: 1971, Sky Tel. 41, 2.
SEKANINA, Z.: 1974, private communication.
SHUL'MAN, L. M.: 1970, The Evolution of Cometary Nuclei, IAU Symposium No. 45, 271.
SIMON, M.: 1974, private communication.
ULICH, B. L.; and CONKLIN, E. K.: 1974, Nature 248, 122.
WHIPPLE, F. L.: 1950, Astrophys. J. 111, 375.
WHIPPLE, F. L.: 1951, Astrophys. J. 113, 464.
WHIPPLE, F. L.: 1955, Astrophys. J. 121, 750.

DISCUSSION

SEKANINA: Most of the energy is re-radiated. The production rate depends on the albedo. Production as a change in albedo could, for example, mean partial depletion of dust and a decrease in the production rate of water.

---

still at small heliocentric distances ($r < 0.5$ AU) the temperature profile broadens and heat penetrates still somewhat deeper, but the temperature begins to decrease at the surface. A few more pockets of volatiles explode. Coarse-grained dust (indicated by a black surface contour) accumulates. At later times only frozen gases (mostly water and clathrates) from the surface vaporize, causing a dimming of the comet when its brightness is compared with that at the same heliocentric distance before perihelion.

DELSEMME: Latent heat may not be the same as actual latent heat of what is vaporizing, because of the existence of icy grains, which makes a big difference. We have no good way of measuring the actual latent heat. It does not exclude at all the vaporization of water.

HUEBNER: The latent heat which I have indicated here is an average value. A better way would be to have the detailed spectra, follow the brightness flow of the detailed spectra for each species, and then do a fit.

HIGH-RESOLUTION SPECTROPHOTOMETRY OF SELECTED FEATURES IN THE 1.1-MICRON SPECTRUM OF COMET KOHOUTEK (1973f) [SUMMARY]

DAVID D. MEISEL*
Department of Physics and Astronomy
State University College

RICHARD A. BERG
Department of Physics and Astronomy
and the C.E.K. Mees Observatory
University of Rochester

A pressure-scanned Fabry-Perot interferometer with complete blocking of overlapping orders was used on the C.E.K. Mees Observatory (University of Rochester) 24-inch reflector at Bristol, New York, to observe Comet Kohoutek (1973f). Selected regions in the 1.1-μ near-infrared spectrum were scanned with a resolution of 1.2 Å half-power-full-width. Profile deconvolution as carried out with a newly developed Fourier transform, nonlinear sampling, and transform inversion procedure, enabled weak spectral line emissions to be detected against the comet Fraunhofer continuum on January 4.95, 1974 (UT), and January 7.95, 1974 (UT).

Two radicals, CN(0–0)[A $^2\Pi$–X $^2\Sigma$] and OH(5–2)[X $^2\Pi$] were observed, but searches for He I (λ10830), H_2O (000–012), and CH_4 $3\nu_3$ R (J = 1) were negative although it is likely that our 54-arc-seconds diaphragm probably included most of the coma that is likely to contain neutral molecules (Potter and Del Duca, 1964).

Central intensities (or upper limits) were derived for three possible cases for the change of intensity within the Fabry-Perot diaphragm. Limits to molecular production rates for CH_4 and H_2O were not derived because of the difficulties in assessing the contribution of collisional effects in the regions near the comet nucleus.

---

* Associate of the C.E.K. Mees Observatory.

Although a quantitative analysis of the OH infrared emission has not yet been carried out, it is plausible that the OH (5–2) Q_1 line was selectively excited because of pumping by the solar chromospheric He I (λ10830) line. This interpretation is reinforced by 18 cm OH radio observations (Biraud, 1974) which indicated that solar UV pumping of OH was near zero at the time of the infrared OH detection (Jan. 7.95, 1974).

NOTE: The observations were published in detail in *Icarus* ((1974) 23, 454). Equipment and data reduction procedures will be published elsewhere.

ACKNOWLEDGMENT

This work was sponsored under NASA Grant NGR 33219002.

REFERENCES

BIRAUD, F.; BOURGOIS, G.; CROVISIER, J.; FILLIT, R.; GERARD, E.; and KAZES, I.: OH Observations of Comet Kohoutek at 18 cm. Comet Kohoutek Workshop, MSFC, June 13–14, 1974.

POTTER, A. E.; and DEL DUCA, D.: 1964, Icarus 3, 103.

AN UPPER LIMIT FOR METHANE PRODUCTION FROM COMET KOHOUTEK BY HIGH-RESOLUTION TILTING-FILTER PHOTOMETRY AT 3.3 μ

A. E. ROCHE
W. C. WELLS
Lockheed Palo Alto Research Laboratory

C. B. COSMOVICI
Instituto di Fisica
Universita di Lecce

S. DRAPATZ
K. W. MICHEL
Max-Planck-Institut für Physik und Astrophysik

We have established an upper limit for the methane production from Comet Kohoutek(1973f) by studying the fluorescence radiation from the P2, P3, and P9 lines at 3.3 μ. The measurements were made on flights aboard the NASA CV990 aircraft, with a new and unique high-resolution, high-throughput tilting-filter photometer. The photometer (fig. 1) employed three dielectric interference blocking filters on a filter wheel and a 0.2-mm-thick solid spaced Fabry-Perot etalon with a resolution of 3.7 Å (FWHM), finesse of 43 and 42 percent peak transmission (fig. 2). The etalon had a tilt range of 6° to give a 50 Å scan. The photometer was mounted on a 12-inch Dahl-Kirkham $f/30$ telescope, and the comet was tracked with a gyrostabilized heliostat mirror. Observations were made on flights on a line from Los Angeles to Vancouver at an altitude of 40 000 feet where the Doppler-shifted comet emission lines reached the detector with little or no attenuation by atmospheric methane. Wavelength calibration was first carried out at Kitt Peak Solar Observatory. Further precision calibration was done in our laboratory and in flight by observation of methane in absorption (fig. 3). The instrument was calibrated absolutely in the laboratory and by observing the thermal emission from Venus. On January 8, 1974 (at 2 UT), our measurements indicated a production rate upper limit of $Q \leq 10^{29}$ molecules/second steradian.

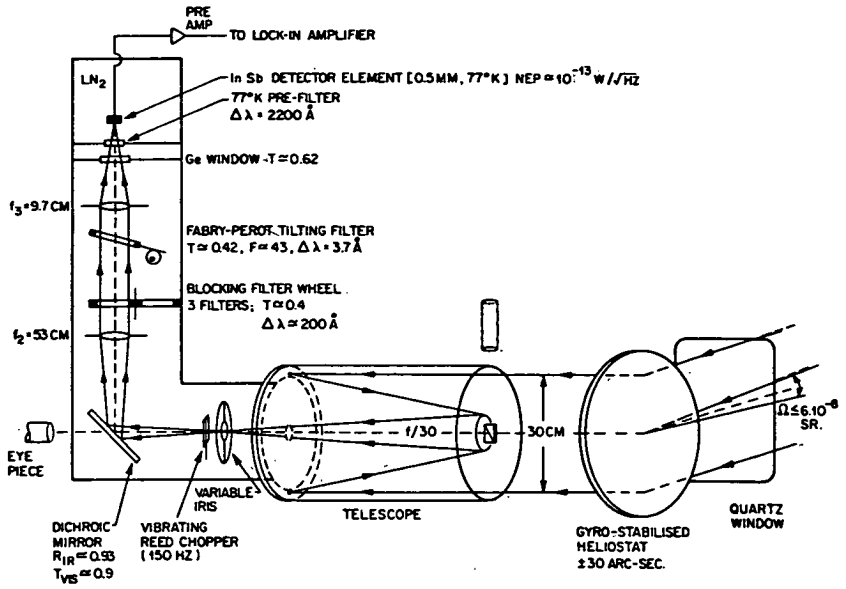

FIGURE 1.—*Schematic of the tilting filter photometer interfaced with the f/30 telescope, and helostat mirror.*

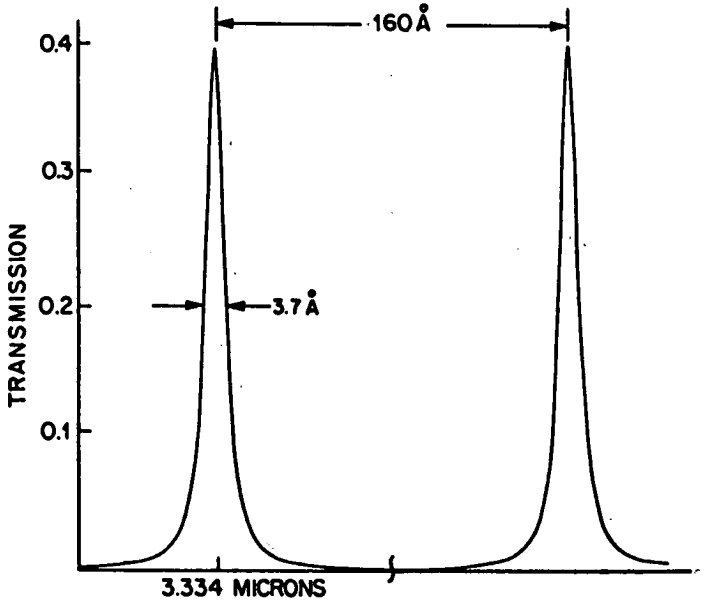

FIGURE 2.—*Two transmission band profiles of the solid-spaced Fabry-Perot interference filter showing its bandwidth (~ 3.7Å) and free spectral range (~ 160Å).*

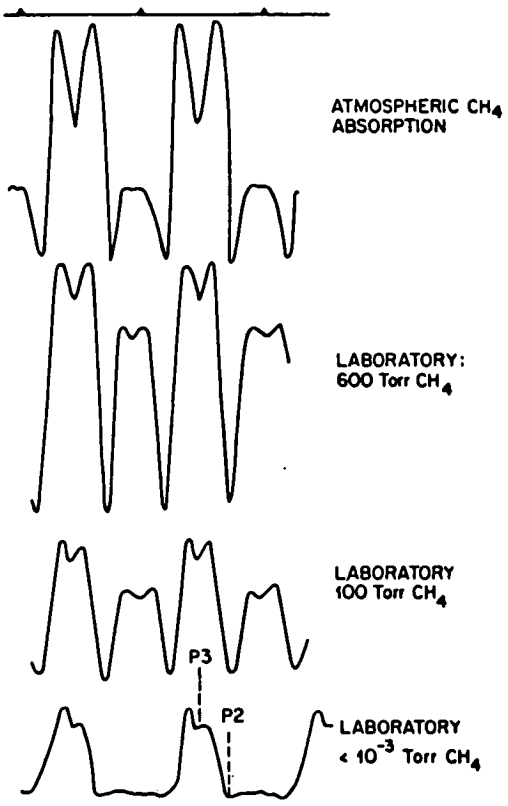

FIGURE 3.—*Typical absorption line spectra obtained by tilt-scanning the narrow band filter in the laboratory (a standard source and absorption cell) and in flight (absorption of solar radiation by atmospheric methane).*

DISCUSSION

HUEBNER: We flew the AEC aircraft with IR equipment from the time of December 16 to January 16. We also did not see methane.

A SEARCH FOR EXTREME ULTRAVIOLET RADIATION FROM COMET KOHOUTEK

GUENTER R. RIEGLER
Bendix Aerospace Systems

GORDON P. GARMIRE
California Institute of Technology

As a part of Operation Kohoutek, an extreme ultraviolet photometer experiment was flown on an Aerobee 200 sounding rocket above the White Sands Missile Range on January 5, 1974 (0150 UT). The experiment was mounted piggyback on the Johns Hopkins University payload, NASA 26.023 UG. The same photometer had been flown previously for airglow studies (Riegler and Garmire, 1974a). The purpose of the experiment was to search for helium on Comet Kohoutek by detecting resonantly scattered solar 584 Å radiation. Helium is assumed to have been trapped along with local matter during the formation of the comet, and released during the evaporation of the outer layers under the influence of solar heating.

The photometer contains two concentric gold-coated paraboloid mirrors which act as grazing-incidence concentrators. A 1500-Å-thick tin filter defines a bandpass from 550 Å to 800 Å. An aperture stop defined an effective field of view with 1° full width at half maximum. The response to periodic exposure to a radioactive calibration source verified that the photometer performed well during the flight.

Observations of Comet Kohoutek at extreme ultraviolet wavelengths were severely compromised by atmospheric photoelectric absorption along the line of sight. The peak altitude achieved during the flight, 232 km, was significantly lower than the altitude anticipated during the initiation of this project. As a result, the transmission of the intervening atmosphere for 90° zenith angle near the peak altitude was only 0.045. Including all efficiency factors and atmospheric absorption, the effective on-axis collecting area of the photometer was $A = 0.021$ cm^2.

The observed counting rate distribution as a function of altitude is consistent with the response to the atmospheric 584 Å helium twilight airglow alone. Using standard statistical arguments, we therefore use the one-standard

deviation of the counting rate at apogee to derive an upper limit to the signal from Comet Kohoutek. This upper limit can be interpreted in terms of an upper limit to the production rate of helium on Kohoutek.

For simplicity we assume that the helium distribution follows a r^{-2} law where r is the distance from the center of the nucleus. The upper limit to the production rate of helium atoms ranges from $Q = 2.1 \times 10^{29}$ He/s for an average temperature $T = 100$ K to $Q = 8.6 \times 10^{29}$ He/s for $T = 1000$ K. Assuming a hydrogen production rate of $Q' = 8.6 \times 10^{29}$ H/s (scaled from an observation by Opal and Carruthers, 1974), we thus obtain upper limits to the helium/hydrogen production rate ratio between 0.25 and 1.0 for helium temperatures between 100 K and 1000 K, respectively.

Details of the experiment, the calculations, and the uncertainties involved have been given elsewhere (Riegler and Garmire 1974b).

ACKNOWLEDGMENT

This work was performed under National Aeronautics and Space Administration grant NGR 05–002–284.

REFERENCES

OPAL, C.; and CARRUTHERS, C.: 1974, preprint.
RIEGLER, G. R.; and GARMIRE, G. P.: 1974a, J. Geophys. Res. 79, 226.
RIEGLER, G. R.; and GARMIRE, G. P.: 1974b, submitted to Icarus.

ULTRAVIOLET (2558 Å) PHOTOGRAPHY OF THE COMET KOHOUTEK USING S-183 ON SKY-LAB

GEORGES COURTES
MICHEL LAGET
ANDRE VUILLEMIN
Laboratoire d'Astronomie Spatiale

HARRY L. ATKINS
Space Sciences Laboratory
NASA, Marshall Space Flight Center

Two 7° × 9° photographs (λ_{eff} = 2558 Å, $\Delta\lambda$ = 356 Å) were taken on Skylab 4, with S-183. One of these photographs taken on January 10, 1974 (0^h UT a = 92°, Θ = 30°) was used to estimate the flux in conjunction with the nearby stars. An average value of 1.8 × 10^{-8} erg cm^{-2} s^{-1} is deduced. An angular diameter of 4 arc-minutes was detected.

Introduction

S-183 was designed to take photographs in three bandpasses centered at 1878 Å and 2970 Å with a half-maximum bandwidth of 636 Å, and at 2558 Å with an half-maximum bandwidth of 356 Å. The proposed plan of observation of Comet Kohoutek was to measure the intensities of the 3098 Å OH emission line and the scattered ultraviolet solar light through the coma and into the dust tail at 1878 Å and 2558 Å. The main spectrograph section of the experiment did not work because of mechanical malfunctions. However, the 2558-Å bandpass did operate and the present note is relative to a photograph taken January 10, 1974, at 0^h 03^m 36^s

Earth-Comet-Sun angle = 92°
Sun-Earth-Comet angle = 30°

Observational Data

The picture of the comet was recorded with a Maurer camera loaded with 16mm 103a-O(film), equipped with a Schmidt-Cassegrain telescope (λ_{eff} = 2558 Å, $F/3$, f = 74 mm). The bandpass was defined by the mirror coatings. The measured transmission during the preflight calibration is given by figure 1. Postflight measurements (2000–5000 Å) have shown the reflectivity to be the same. The secondary transmission band located at 3100 Å has approximately 2-percent transmission. Figure 2 shows the comet against the

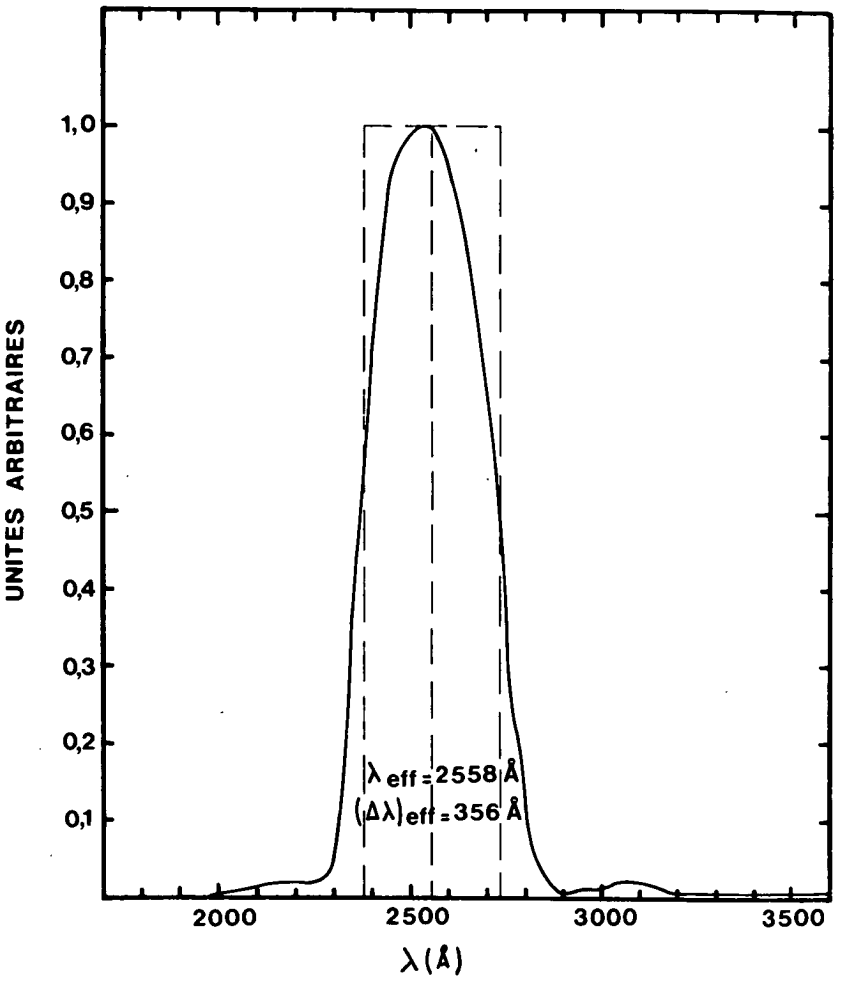

FIGURE 1.—*Bandpass of the observations.*

background field stars, and another star field obtained with the same exposure time (5 minutes). The comet appears as a bright round-shaped star. The letter near the stars and the first number refer to the spectral type. The last two numbers refer to the visual magnitude. The tail is not detected. A microdensitometer scan of the stellar image with a spot of 15 × 200 μ shows a triangular profile. According to the spread function of the stars and the maximum optical density of the comet, the angular diameter can be estimated from 3.5 to 4.5 arc-minutes. In the focal plane, 40 μ is equal to 1.85 arc-minutes.

Figure 3a represents an isodensity contour. The slightly elliptical shape seems to be related to the direction of the tail. Figure 3b illustrates a microdensitometer scan across the maximum.

Most of the stars recorded on figure 2 have been identified in terms of visual magnitude and spectral type. Only a few have additional data such as B–V and these indicate an insignificant amount of reddening (E(B–V) $\approx$ .05).

To estimate the flux scattered and/or reflected by the coma, we used the point spread function plus diffusion of the stars as absolute standards for calibration. For each identified star we computed the flux by using the theoretical models of Carbon and Gingerich (1969) integrated over the bandpass of the telescope. The reddening was not included. In addition, a comparison of focused and slightly out-of-focus star images was used to give a maximum and minimum value of the flux.

This method was used to deduce the flux F of the comet in the 2558-Å bandpass. This value was found to be

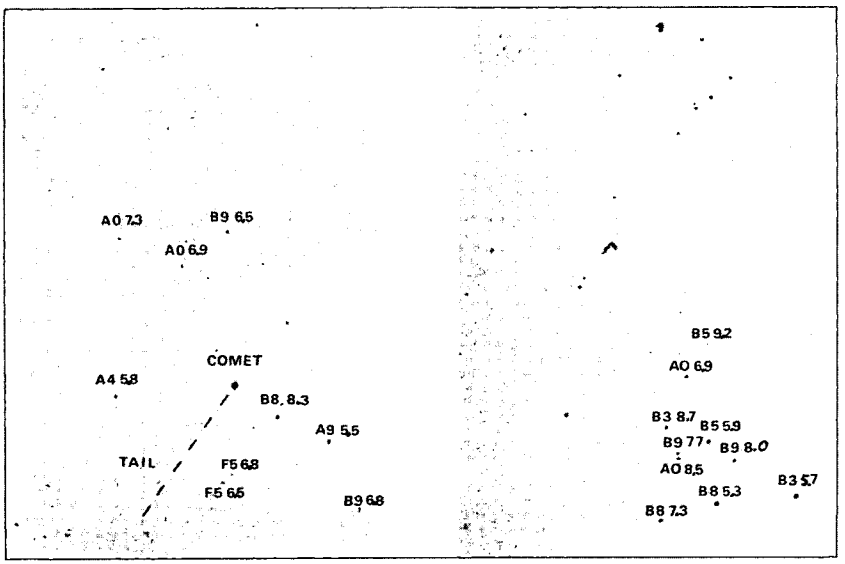

FIGURE 2.—*UV (λ_{eff} = 2558 Å) photography of Comet Kohoutek and reference stars.*

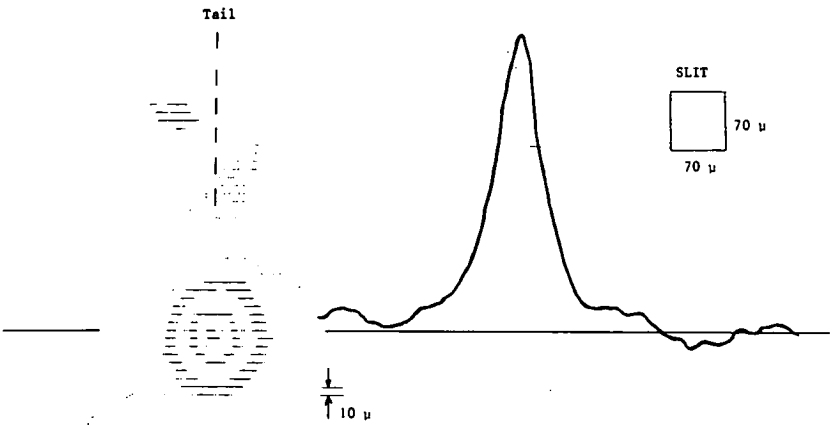

FIGURE 3.—*Microdensitometer scan of Comet Kohoutek.*

$$10^{-8} < F \text{ (erg cm}^{-2} \text{ s}^{-1}) < 2.5\ 10^{-8}$$

Further measurements derived from calibration indicate that the OH emission constitutes about 10 percent of the measured flux. In addition, if one assumes that the continuum in the visible and in the ultraviolet has a solar type spectral distribution, then 21 percent of the measured flux is due to an average transmission of the multilayer filter of 0.03 percent over the spectral range 3500–5500 Å.

REFERENCES

HARVEY, G. A.: 1974, Ultraviolet Hydroxyl Observations of Comet Kohoutek on January 24 1974, Comet Kohoutek Workshop Paper.

CARBON, D. F.; and GINGERICH, O.: 1969, Theory and Observation of Normal Stellar Atmospheres. Proceedings of the Third Harvard-Smithsonian Conference on Stellar Atmospheres. Ed. O. Gingerich, The MIT Press, Cambridge Mass., 377.

SESSION IV:

OBSERVATIONS OF COMET KOHOUTEK AT WAVELENGTHS FROM 0.55 MICRON TO 18 MICRONS

EDWARD P. NEY
School of Physics and Astronomy
University of Minnesota

Since I have a limited time, I will say very little about the observational details in order to concentrate on the results. In essence our observations were obtained on the 30-inch telescope at O'Brien Observatory outside Minneapolis with a bolometer operating at 1.1°K, and refer to a diaphragm size of 27 × 27 arc-seconds. Sky cancellation was accomplished by the use of a chopping secondary. A second telescope was used to measure the comet in a one-minute beam.

The broadband filters have $\lambda/\Delta\lambda = 10$ and define 12 wavelengths from 0.5 microns to 18 microns. The comet was acquired in daylight and observed near the meridian. Since the same detector was used at all wavelengths, the measurements were made at the same position on the comet, which was automatically tracked by the telescope.

Figure 1 shows the circumstances of the observations. The Sun-comet distance varied from 0.15 to 1 AU, and the comet-Earth distance was usually near 1 AU.

Figure 2 shows Mars, Vesta, and Ceres. Figure 3 shows Comet Kohoutek and Mercury. The quantity plotted is λF_λ, the product of the monochromatic intensity and wavelength. This kind of plot is useful because a horizontal line represents equal energy/octave. Two black bodies which have the same maximum λF_λ represent the same total energy. At short wavelengths the planets and the comet simply reflect or scatter sunlight and the short wavelength data fit a solar 6000° black body. At long wavelengths the black body curve is the thermal radiation from the dust. The principal difference between the planets and the comet is the presence of the silicate signature at 10 and 20 microns in the comet and the fact that the comet temperature is higher than a black body at the given distance from the Sun. The visual albedo is given by the relative height of the scattered light curve and the thermal radiation curve.

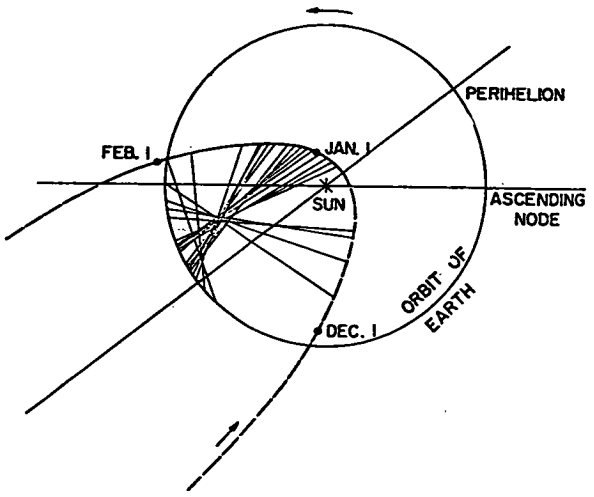

FIGURE 1.—*Wavelength observations of Comet Kohoutek, showing circumstances of the observations.*

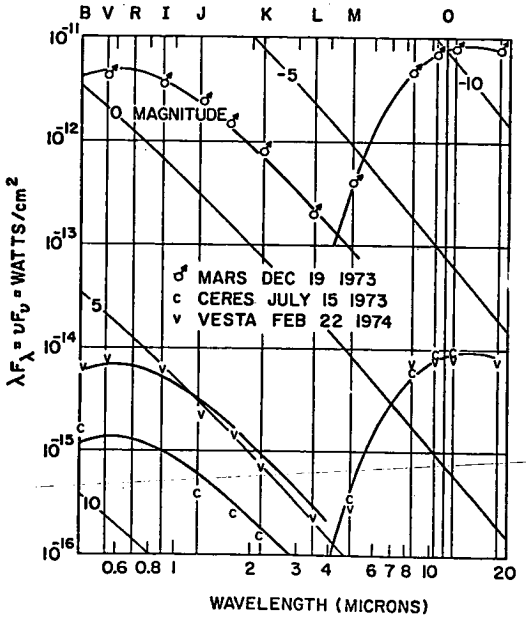

FIGURE 2.— *Wavelength observations of three planets—Mars, Vesta, and Ceres.*

Figure 4 shows Comet Bennett and Comet Kohoutek at the same distance from the Sun. The silicate signature was first discovered in Comet Bennett in 1970 and it was not possible to look for it in another comet until Kohoutek.

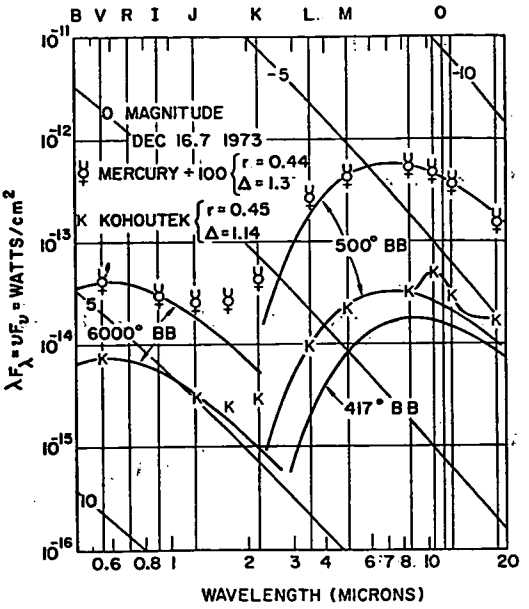

FIGURE 3.—*Wavelength observations showing Comet Kohoutek and the planet Mercury.*

Figure 4 also shows that the dust in Bennett had a higher albedo, a higher temperature, and a more pronounced silicate signature. The grey body temperature at this distance from the Sun is also shown. The coma, tail, and sunward spike were observed between December 29 and January 7.

Figure 5 shows the geometry on New Year's Day. The numbers refer to the relative surface brightness of the comet. Figure 6 shows the energy spectra of the coma, tail and anti-tail. The coma and tail show the silicate signature and seem hot. The anti-tail is a perfect black body at the black body temperature.

These curves show a great deal about the nature of the particles. The opacity of silicates at 10 microns is 1000 cm^2/g. For a single grain to be optically thin requires that its diameter be less than three microns. The average coma optical depth is very small ($\tau \approx 10^{-4}$). The presence of these small particles, which are smaller than the wavelength at the Planckian maximum causes the temperature excess. Because the scattered sunlight shows solar colors, we can infer that the important particles are not Rayleigh scattering and are therefore larger than 0.2 micron. The albedo of the grains is 0.18 ± 0.02. The fact that the brightness versus beam size is the same at visual and infrared wavelengths indicates that the same particles are responsible for the scattered sunlight and the thermal radiation.

In the anti-tail the situation is quite different. Either these particles are

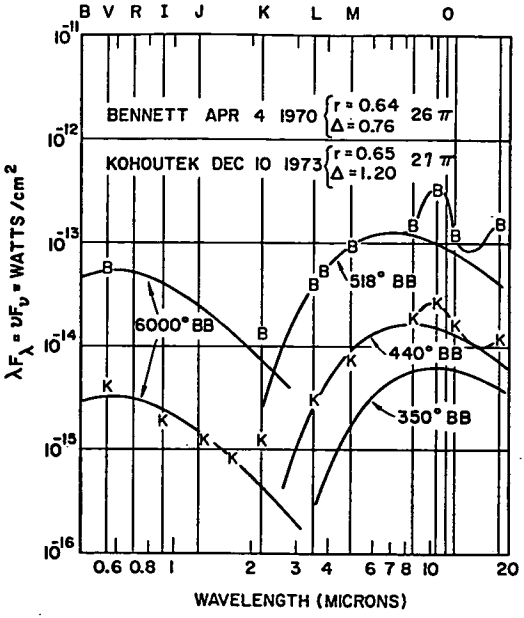

FIGURE 4.—*Wavelength observations comparing Comet Bennett and Comet Kohoutek at the same distance from the Sun.*

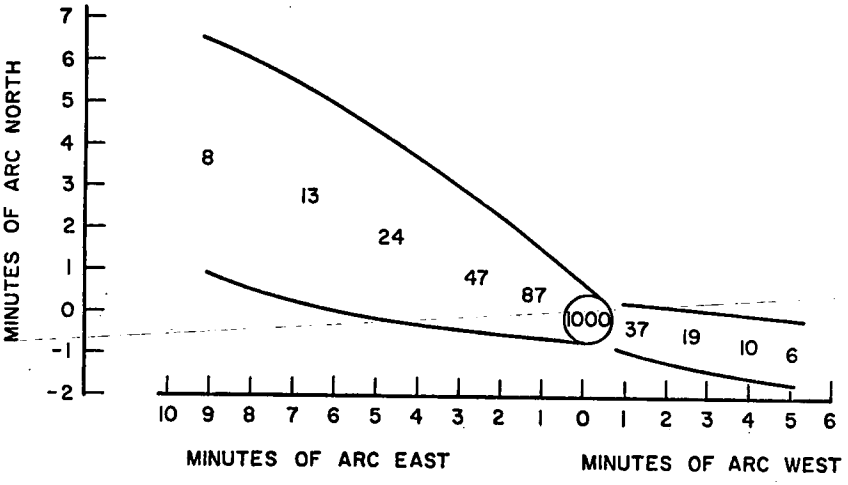

FIGURE 5.—*Geometry of Comet Kohoutek on New Year's Day. The numbers refer to the relative surface brightness of the comet.*

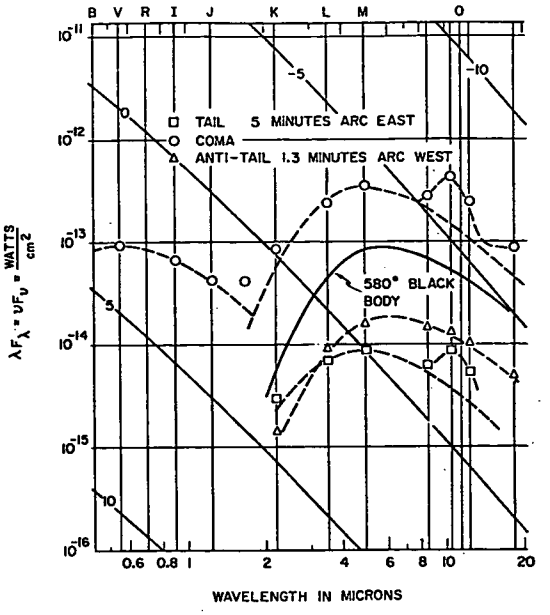

FIGURE 6.—*Wavelength observations showing the energy spectra of the coma, tail, and anti-tail of Comet Kohoutek.*

large compared with 20 microns or are of a different material. The elegant analysis of Sekanina gives credence to the postulate that they are large particles in orbit. According to his analysis, they should be particles ejected more than 25 days before the observation and having a ratio of radiation pressure to gravity of 0.01 to 0.02.

Figure 7 shows a set of observations between $r = 0.15$ and $r = 0.95$ AU all corrected to $\Delta = 1$.

The super heat of the coma varies from 15 to 20 percent, and the albedo is 0.18 ± 0.02. The silicate bump is always present.

Figure 8 shows Comet Kohoutek pre- and post-perihelion, and Bradfield post-perihelion at the same distance from the Sun. Kohoutek is dimmer after perihelion than before. Both comets have the silicate feature and the temperature excess.

However, Bradfield suffered some drastic changes. Between March 21 and April 5, it lost the silicate signature and its albedo dropped. It seems likely that the particle size increased.

Figure 9 shows all four comets that we have observed as a function of radial distance from the Sun. The period in which the dust bump disappeared in Bradfield is during the short horizontal section of the curve at $r \cong 0.6$ AU. Subsequently this comet dimmed drastically and the dust virtually disap-

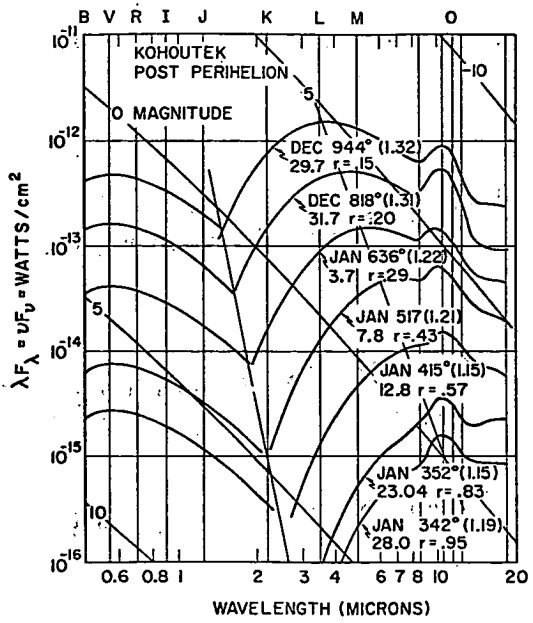

FIGURE 7.—*Wavelength observations of Comet Kohoutek, showing a set of observations between r = .15 and r = .95 AU, all corrected to Δ = 1.*

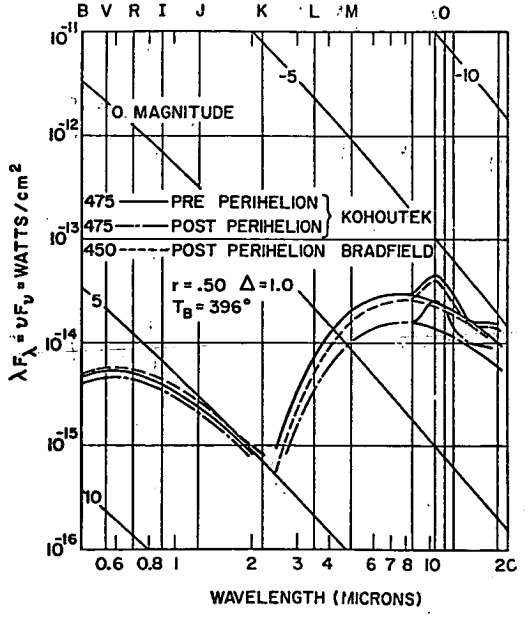

FIGURE 8.—*Wavelength observations showing Comet Kohoutek pre- and post-perihelion, and Comet Bradfield post-perihelion at the same distance from the Sun.*

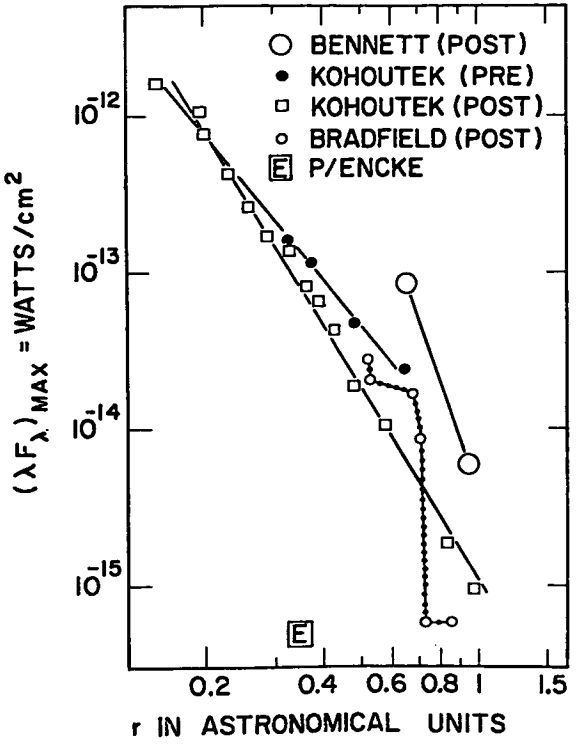

FIGURE 9.—*Comets Bennett, Kohoutek, Bradfield, and P/Encke observed as a function of radial distance from the Sun.*

peared. The nucleus appeared stellar and 10 to 10.5^m, indicating a nuclear diameter of about 10 km.

Figure 9 shows that Bradfield and Kohoutek were similar comets, that Bennett was about five times brighter, and that Encke is about 100 times dimmer. If the comets are otherwise similar, Kohoutek and Bradfield are about 10 km in diameter, Bennett 20 to 30 km, and Encke about 1 km.

REFERENCES

MAAS, R.; NEY, E. P.; and WOOLF, N. J.: 1970, The 10-Micron Emission Peak of Comet Bennett 1969i, Ap. J. (Letters) 160, L101.

NEY, E. P.: 1974, Infrared Observations of Comet Kohoutek Near Perihelion, Ap. J. (Letters) 189, L141.

O'DELL, C. R.: 1971, Nature of Particulate Matter in Comets as Determined from Infrared Observations, Ap. J. 166, 675.

RIEKE, G. H.; and LEE, T. A.: 1974, Photometry of Comet Kohoutek (1973f), Nature 248, 737.

SEKANINA, Z.: 1974, I.A.U. Circular 2580 and Sky and Telescope 47, No. 6, 374.

INFRARED OBSERVATIONS OF COMET KOHOUTEK

G. H. RIEKE
F. J. LOW
T. A. LEE
W. WISNIEWSKI
University of Arizona

Because the infrared radiation of comets is dominated by thermal emission of dust grains, infrared photometry is a powerful tool for studying cometary dust. However, since the techniques for infrared observing have developed fairly recently, very few comets have been observed in this spectral region. The extensive record of the behavior of Comet Kohoutek(1973f) in the infrared is unique and should result in a substantial increase in our understanding of these objects.

Photometry of Comet Kohoutek before perihelion passage has already been described (Rieke and Lee, 1974). In contrast to the behavior after perihelion passage, which will be described in detail below, during this period the comet evolved without abrupt changes and along lines suggested by the much less detailed infrared studies of earlier comets. The nucleus of the comet was not exceptionally large and, compared with Comet Bennett(1969i), Comet Kohoutek ejected relatively little dust. These two facts adequately explain why Comet Kohoutek was much fainter than the early predictions. The spectrum did not show a "silicate" emission feature until the comet came within 1.5 AU of the Sun. Within this heliocentric distance, the absorption efficiency of the dust grains in the visible remained constant at about 80 percent. The infrared color temperature exceeded the temperature that would be attained by gray, conducting spheres at the same heliocentric distances, indicating that the emissivity of the dust grains was substantially less than 80 percent in the middle infrared.

More recent photometry of Comets Kohoutek and Bradfield(1974b) is summarized in tables I, II, and III. The measurements were carried out under procedures described in the previous article. Because a system of winter storms coincided with perihelion passage, we have no measurements of Comet Kohoutek near this time. Fortunately, the observations described by Ney at this

Table I.—*Photoelectric Photometry of Comet Kohoutek(1973f)*

Date (UT)	r (AU)	Diaphragms (")					Magnitudes				
		12	31	62	112	157	U	B	V	R	I
Jan 16.1	0.66					×		6.20	5.76	6.53	
					×		6.19	6.53	6.02	6.75	
				×			7.02	7.28	6.75	7.33	
			×				8.24	8.46	7.92	8.29	7.84
		×						10.91	10.04	10.04	
Jan 23.1	0.73					×		7.27	6.66	7.40	
			×				9.58	9.78	9.18	9.36	9.02
		×						12.10	11.58		
Jan 28.1	0.95					×		7.98	7.41	8.14	
			×				10.32	10.51	9.96	10.19	9.75
		×						12.71	12.23		

workshop cover the interval near perihelion thoroughly, with a slight overlap with out data at either end. The combination of both sets of data provides a complete record of the photometric behavior of Comet Kohoutek. In comparing Ney's infrared data with ours, one should make allowance for some small differences in observing procedure and calibration. Ney used a 20-arc-sec square aperture. In addition to the normal corrections for beam size, a correction of about 15 percent to allow for the different beam shape should be made.* In addition, Ney's calibration is about 15 percent brighter than ours. Finally, the separation between the measurement and reference beams is larger for Ney's work, also making the comet appear brighter. The correction to be applied for this difference depends on a number of experimental details, but from scans of the central region of the comet (Rieke and Lee, 1974) we estimate it to be 5 to 10 percent. Therefore, for comparison with Ney's photometry, our measurements should be multiplied by a factor of about 1.45, or brightened by 0.4 magnitude. Observations similar to Ney's were also made by Gatley et al. (1974).

Infrared photometry of three comets at heliocentric distances near 0.6 AU is shown in figure 1. Although the spectra are similar, closer inspection shows significant differences in the strength of the "silicate" emission at 10μ (3×10^{13} Hz), with Comet Bennett having the most pronounced spectral feature. Between 3 and 5μ, the color temperature of Comet Bradfield is only slightly above the equilibrium temperature for gray, conducting spheres, while the color temperature of Comet Bennett over this spectral range substantially exceeds the equilibrium temperature. Comet Kohoutek is intermediate in this regard.

* (Editor's comment: Ney communicated to the editor that a 27-arc-sec square aperture was used, a correction to the data presented at the workshop.)

Table II.—*Infrared Photometry of Comets Kohoutek(1973f) and Bradfield(1974b)*

Date (UT)	Diaphragms			Fluxes (10^{-26} Wm^{-2} Hz^{-1})									
	13.5	5.5	4.2	2.2 μ (0.6)	3.6 (0.9)	5.0 (1.0)	8.8 (1.0)	10.3 (1.2)	10.6 (5.0)	11.6 (0.8)	12.6 (1.0)	21 (8)	22.5 (5)
Jan 16.1*	×			0.85	5.5	20	95	150		142	114	156	171
Jan 25.1*		×		0.05	0.28	1.0	9.4	12.7			13.9	20	17
Jan 28.1*		×			0.17	0.8	7.2	9.9	10.2	11.1	10.3	18	15
Feb 8.1*			×		<0.06	0.2	1.4	2.6		3.1	3.0	6.1	3.9
Feb 17.1*		×						0.8	0.9	1.1	0.9		
Mar 16.1†		×			8	29	123	160	168	173	95		
Mar 17.1†		×			10	39	146	176	177		85	66**	45**

*Comet 1973f.

†Comet 1974b.

**Normalization relative to shorter wavelength results is uncertain because of high extinction.

Table III.—*Additional Infrared Photometry of Comet Kohoutek*

Date (UT)	Diaphragm (arc sec)	Wavelength (μ)	Bandpass (μ)	Flux (10^{-26} W m^{-2} Hz^{-1})
Jan 16.1	13.5	3.05	0.1	5.5
Jan 16.1	13.5	3.85	0.5	6.8
Jan 16.1	13.5	4.8	0.6	17
Jan 28.1	5.5	17	2	22

The behavior of Comet Kohoutek after perihelion passage is shown in figure 2. The infrared photometry is compared with photometry before perihelion passage at comparable heliocentric distances. Because of the reduced geocentric distance of the comet, it would be expected to be about 20 percent brighter after perihelion passage. This correction has not been applied to the data in figure 2. Slight variations in the width and height of the 10μ emission feature were suggested by the pre-perihelion passage measurements but the more recent data show a much larger and definitely significant change between 0.66 and 0.88 AU heliocentric distances. At the same time, changes appear to have taken place near 20μ (1.5×10^{13} Hz). In contrast to the behavior before perihelion passage, the albedo of the dust grains may have fluctuated, with the largest departure from the mean value occurring on January 16 (0.66 AU).

Thus, observations at comparable heliocentric distance show variations in the infrared spectra both from comet to comet and, in the case of Comet Kohoutek, as a function of time. Changes have also been seen in the albedo of the dust grains. It appears that the nature of the dust ejected by the nucleus is different for different comets and can even change with time as a given comet evolves. These changes can occur rapidly, with time scales of less than one week and over changes in heliocentric distance less than 0.2 AU.

Both in the infrared and visible, Comet Kohoutek faded rapidly as it left the Sun. After January 16, it was substantially fainter at all wavelengths than it had been at the same heliocentric distances approaching the Sun. However, the brightness in the U, B, and V bands, which are dominated by gaseous emission lines, did not decrease as dramatically as at the wavelengths dominated by reflection and emission by dust.

Although other possibilities may exist, the simplest explanation of the changes we have observed in Comet Kohoutek is that the nucleus contains pockets or layers of frozen gas and dust with different properties. As these pockets or layers are exhausted and new ones exposed, the composition of the comet ejecta can undergo abrupt changes. The initial predictions that Comet Kohoutek would be spectacular were based on its being relatively bright when it was far from the Sun. However, the brightening was anomalous and the diameter of the nucleus was overestimated (Rieke and Lee, 1974). Mendis and

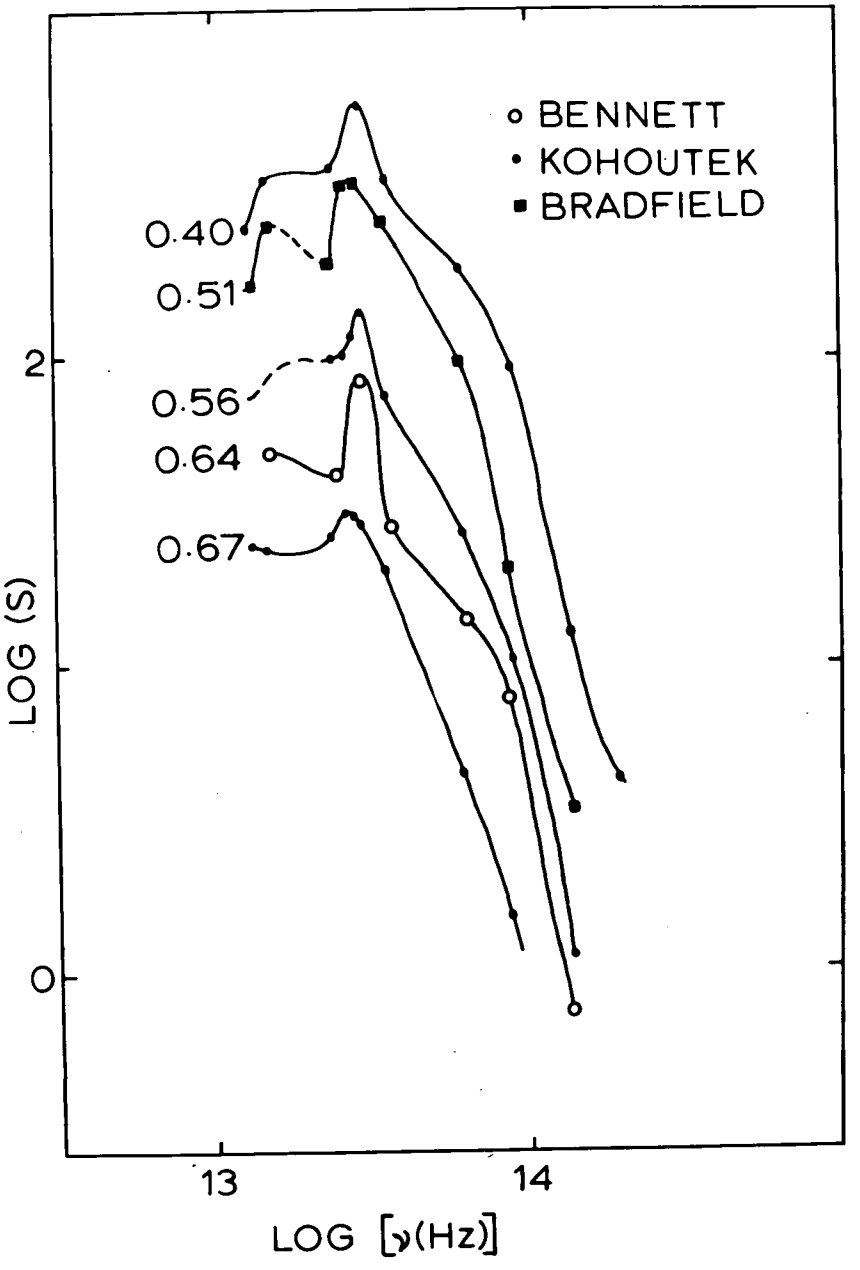

FIGURE 1.—*Infrared photometry of three comets. The spectra are labeled with the heliocentric distances in AU. The data for Comet Bennett are from Maas et al. (1970). The observations of Comet Kohoutek were before perihelion passage. The flux values have been arbitrarily renormalized to facilitate comparison of the spectra.*

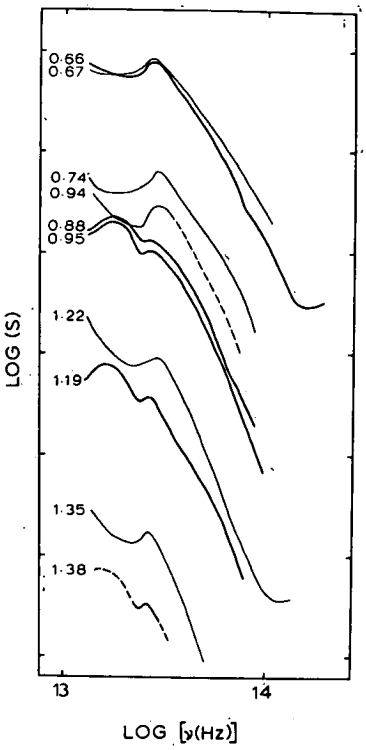

FIGURE 2.—*Comparison of infrared observations of Comet Kohoutek before and after perihelion passage. The spectra are labeled with the heliocentric distance in AU and the observations after perihelion passage are indicated with the heavier line. The trick marks in log (S) are at intervals of one. The four groups of spectra have been renormalized to avoid confusion, but there has been no renormalization within each group.*

Ip (1974) have suggested that this brightening was caused by the exposure of a layer or pocket of volatile material which quickly evaporated from the nucleus.

Therefore, the hypothesis that cometary nuclei contain layers or pockets of different compositions can explain many of the phenomena exhibited by Comet Kohoutek. Abrupt changes and unpredictable behavior have been observed in many other comets, indicating that their nuclei are similar to Comet Kohoutek in this respect. This possibility should be given serious consideration in future studies of the origin and nature of comets.

The infrared observations show that silicates play a role in cometary dust. However, the 10-μ emission feature is much weaker in Comet Kohoutek than would be expected from silicate grains unless appreciable numbers of the grains are larger than 5μ in diameter (Hunt and Logan 1972). The presence of many large silicate grains would be hard to reconcile with the elevated brightness temperature in the 3- to 5-μ region and with theories regarding the

development of type II (dust) tails. It is more likely that cometary dust contains other materials besides silicates.

The changes in the infrared spectrum might be caused by changes in the size distribution or composition of the grains. In the case of Comet Kohoutek, the development of an anti-tail and the infrared spectrum of the anti-tail described by Ney at this workshop show the presence of large grains. However, if the grain diameter is the only variable, the elevation of the 3- to 5-μ color temperature should be correlated with the strength of the 10-μ emission feature. Such a correlation is not apparent for Comet Kohoutek and is clearly absent in the three-comet comparison shown in figure 1. Therefore, variations in the composition of the dust probably account for some of the infrared behavior of comets.

In summary, our observations indicate the following:

1. The absorption efficiency of the dust in Comet Kohoutek was about 80 percent. The infrared spectrum showed weak silicate emission features at 10 and 18 μ, and an elevated color temperature between 3 and 5 μ.

2. Although silicates are the only material definitely identified in cometary dust, significant amounts of other materials are probably also present.

3. The infrared spectra, and therefore the nature of the dust, varies from comet to comet.

4. Rapid changes in the infrared spectrum of Comet Kohoutek indicate that material of different compositions is found in layers or pockets in the nucleus.

ACKNOWLEDGMENTS

We thank K. L. Day for helpful discussions. This work was supported by NASA and the NSF.

REFERENCES

GATLEY, I.; BECKLIN, E. E.; NEUGEBAUER, G.; and WERNER, M. W.: 1974, Icarus, 23, 251.
HUNT, G. R.; and LOGAN, L. M.: 1972, App. Optics 11, 142.
MAAS, R. W.; NEY, E. P.; and WOOLF, N. J.: 1970, Ap.J. (Letters) 160, L101.
MENDIS, D. A.; and IP, W–H.: 1974, Nature 249, 536.
RIEKE, G. H.; and LEE, T. A.: 1974, Nature 248, 737.

DISCUSSION

OPAL: How much water would you say is in amorphous silicates, and is there a transition due to the elimination of the water by evaporation?

RIEKE: I don't think anyone knows what structure the silicate has. It appears not be be critical. There is some evidence that similar materials do exist in meteors. The transition involves both driving off the water and a change in the crystalline nature of the material.

HENIZE: I found a significant change in the dust nature in mid-January; can you pin that down for us?

RIEKE: The first observation was on January 16. It appeared to have changed in photometric observations 4 days later.

HENIZE: On the 16th, did you find that things were different than in December?

RIEKE: No. On the 16th it was slightly fainter when corrected for geometry. It appeared to be very similar.

DONN: There is strong evidence for the silicate theory and there is a lot of talk about icy grains at larger distances. Does anyone have any indication of the ice absorption at 3 microns or any other indication of the molecular material or the grains?

RIEKE: Unfortunately the comet is very faint at 3 microns, where you might expect to find ice. We should have found ice if it was there.

PHOTOGRAPHIC PHOTOMETRY FROM SKYLAB

P. D. CRAVEN
R. V. HEMBREE
C. A. LUNDQUIST
Marshall Space Flight Center

Early Skylab plans for observations of Comet Kohoutek showed that observation opportunities would have to be distributed between the major instruments, and that for each instrument these opportunities typically would be separated by several days. This observation pattern stimulated consideration of a schedule of frequent comet photographs through the spacecraft windows, using existing cameras. A conceptually simple photographic effort could provide a baseline record of gross comet behavior. A plan for such a schedule of photographic photometry was adopted and designated Experiment S–233.

Table I lists the characteristics of the selected photographic system. Kodak 3401 film was chosen on the basis of availability, resolution, speed, predicted radiation effects, and other pertinent factors. Spectral transmission of the window and lens and the spectral sensitivity of the film are such that the spectral response of the system covers approximately the range from 4000 to 7000 Å. The large field of view minimized pointing requirements for the astronauts and ensured adequate numbers of star images for reference purposes.

Each standard set of photographs contained three frames, exposed as shown in table II. When possible, such a set was taken approximately every 12 hours. One calibration sequence of six frames of a selected star field was obtained for each film cassette.

The exposures focused on infinity were intended primarily to record the gross characteristics of the comet tail. The defocused frames were taken so that the integrated coma magnitude could be measured by microdensitometry relative to images of stars of known magnitude and spectral class.

The best data were obtained during periods when the spacecraft motion was stable, which required that the automatic momentum dump system not be operating. However, modest spacecraft motion does not prevent photometry from the photographs. The four cassettes of film yielded about 90 usable comet photographs, of which about one-third are focused on infinity. The last pre-perihelion observation was on December 22, 1973, and the first post-

Table I.—*Photographic System*

CAMERA:	35-mm Nikon with remote shutter control. Camera body taped to items of spacecraft structure for stability. Manual operation.
LENS:	55 mm; *f*/1.2; adjustable focus 36 x 24 deg field of view
FILM:	Kodak Plus-X Aerial 3401 (thin base) 4 film cassettes, 60 exposures per cassette

Table II.—*Exposure Sequence*

STANDARD OBSERVATION SEQUENCE	
60-s exposure	15-ft focus
120-s exposure	infinity focus
60-s exposure	15-ft focus
CALIBRATION SEQUENCE	
Unexposed	
10-s exposure	15-ft focus
30-s exposure	15-ft focus
60-s exposure	15-ft focus
120-s exposure	15-ft focus
120-s exposure	infinity focus

perihelion observation was on January 8, 1974. The most prevalent causes of unusable frames were failure to have the comet in the field of view and excessive spacecraft motion.

Only preliminary results are available at this date, three months after the Skylab film was returned to Earth and processed at the Johnson Space Center. These results are derived from trial analysis procedures using third-generation duplicate films. These analyses used two different microdensitometers and several numerical techniques. The original first-generation films will be used in the final analyses after optimum procedures have been established.

Preliminary determinations of coma integrated magnitudes confirm that for equal heliocentric distances the comet was about two magnitudes dimmer after perihelion than before perihelion.

ACKNOWLEDGMENT

The authors gratefully acknowledge the help of those people who have diligently assisted in the performance and data analysis of this experiment, particularly the Skylab 4 astronauts, the personnel in Mission Control, and personnel of Computer Sciences Corporation.

THE DETECTION OF CONTINUUM MICROWAVE EMISSION FROM COMET KOHOUTEK (1973f)

STEPHEN P. MARAN*
ROBERT W. HOBBS*
JOHN C. BRANDT
Laboratory for Solar Physics and Astrophysics

WILLIAM J. WEBSTER, JR.*
Atmospheric and Hydrospheric Applications Division

K. S. KRISHNA SWAMY †
Laboratory for Optical Astronomy
NASA-Goddard Space Flight Center

We observed the comet on January 10 and 11, 1974, with both the interferometer and the 140-foot (43-meter) radio telescope at the National Radio Astronomy Observatory. In both cases, a positive result was obtained. The 140-foot telescope observation, made at wavelength 2.8 cm, yielded a flux density of (0.034 ± 0.013 standard error) flux units. Taken by itself, it would constitute only another "probable detection" in the long history of attempts to detect continuum radio emission from comets, and in fact we shall not discuss this measurement further here.

On the other hand, our interferometer observations, at wavelength 3.71 cm yielded a flux density of (0.78 ± 0.001 formal standard error) flux units and therefore constitute a very definite detection. Allowing for an uncertainty of about 25 percent in the absolute calibration of the interferometer flux density scale, we can quote a value of (0.08 ± 0.02) flux units for the 3.71–cm emission of the comet on January 10 and 11. Our data on the measured fringe amplitude as a function of baseline, obtained during an interval of 9 hours, with a maximum baseline of 2.7 km, show that this emission arose

* Visiting Astronomer, National Radio Astronomy Observatory. The NRAO is operated by Associated Universities, Inc. under contract to the National Science Foundation.
† National Research Council Resident Research Associate.

from a region located within a few arc-seconds of the location of the nucleus and having a diameter that was certainly less than 2.8 arc-seconds (1700 km) and very possibly less than 1.4 arc-seconds (850 km). These limits correspond to brightness temperatures of more than (240 ± 60) K and more than (980 ± 250) K, respectively.

If the lower temperature limit and larger diameter apply, the observations fit what we might expect in terms of thermal radio emission from the grains in the icy grain halo that Delsemme has postulated to exist in comets. On the other hand, if the higher temperature and smaller diameter apply, we would require the presence of a dust component that is more volatile than the dust studied by the infrared observers, since it is limited to a region of only several hundreds of kilometers. In either case, we would expect that the source of the microwave continuum emission must also appear in scattered visible light as a "false nucleus." Dr. E. Roemer (private communication to John C. Brandt) has stated that the existence of a false nucleus of a few arc-seconds diameter on January 10 and 11 would not contradict the visual observations known to her.

We should note that continuum emission from this comet has been observed at millimeter wavelengths by Akabane and Chikada (preprint) and by Vidal-Madjar and colleagues (private communication). Akabane and Chikada have proposed a thermal bremsstrahlung mechanism as an alternative to thermal emission from grains. W. Altenhoff and B. Andrew have both advised us in private communications of unsuccessful attempts to detect the microwave emission from this comet.

ACKNOWLEDGMENTS

We thank T. Clark, B. Marsden, and D. Yeomans for ephemerides; B. Andrew and W. Jackson for valuable comments; and K. Akabane, W. Altenhoff, B. Andrew, and A. Vidal-Madjar for communicating information in advance of publication.

DISCUSSION

WHIPPLE: How effective is your dust in radiating?

MARAN: We found that we needed fairly dirty or very dirty ice grains of size range 0.6 to 6 mm to explain our 300° temperature. We have not yet looked at what we need in the way of dust that does not have any ice. The observation implies that in visible light there should be a false nucleus of at least an arc-second in diameter, possibly several arc-seconds. Dr. Roemer has told Brandt that there was no optical contradiction on that date.

WEHINGER: On January 10 and several dates around that time, the brightest part of the comet—the false nucleus—is about 2 seconds of arc in diameter.

DELSEMME: I assume you don't exclude a mixture of icy grains and dust?

MARAN: Oh, no, not at all.

MENDIS: I wish to make a comment about the radius. It is well known that if you have small grains you can probably get frequency dependence, but it may be possible to get a much higher temperature if you have fairy-castle-like structures of 1 micron.

MARAN: I understand, but do you think it can radiate effectively at 4 centimeters?

MENDIS: Possibly.

CHAISSON: As a comment, on the 10th, we were transmitting a signal at the same wavelength. I don't think you picked it up.

UPPER LIMITS ON THE RADAR CROSS SECTION OF COMET KOHOUTEK

E. J. CHAISSON
Center for Astrophysics
Harvard College Observatory and Smithsonian Astrophysical Observatory

R. P. INGALLS
A. E. E. ROGERS
NEROC Haystack Observatory

I. I. SHAPIRO
Department of Earth and Planetary Sciences and
Department of Physics
Massachusetts Institute of Technology

An attempt to observe radar echoes from Comet Kohoutek was made at a radio frequency of 7840 MHz ($\lambda \simeq 3.8$ cm) on January 12, 1974. The Haystack Observatory radar in Massachusetts was used. A search for an echo over a range of bandwidths covering 2 Hz to 66 kHz yielded no positive result. The upper limit on the radar cross section is therefore approximately $10^4 B^{1/2} km^2$, where B is the (unknown) bandwidth of the echo in Hertz. For $B \simeq 100$ Hz, it follows that (1) the nucleus, if a perfect spherical reflector, must be less than 250 km in diameter, and (2) the density of any millimeter-sized particles must be less than 1 m^{-3} for a coma of diameter 10^4 km.

On January 12, 1974, we attempted to observe radar echoes from Comet Kohoutek. We used the Haystack Observatory radar system to transmit a signal at a radio frequency of 7840 MHz ($\lambda \simeq 3.8$ cm). About two minutes before the echo was expected, the system was reconfigured for reception. The relevant parameters of the radar system are given in table I.

Table I.—*Radar Characteristics for Comet Kohoutek Observations on January 12, 1974*

Radar Frequency:	$f = 7840$ MHz
Radar Wavelength:	$\lambda \cong 3.8$ cm
Effective Antenna Area:	$A \cong 470$ m^2
Transmitted Power:	$P \cong 200$ kw
System Temperature:	$T \cong 50$ K
Integration Time for Echo:	$t \cong 5 \times 10^3$ s
Earth-Comet Distance:	$R \cong 1.24 \times 10^{11}$ m
Ephemeris Round-Trip Time-of-Flight for Echo Received at 16:00 UT:	$\tau \cong 812.246$ s
Ephemeris Doppler Shift for Echo Received at 16:00 UT:	$\Delta f \cong 498\,938$ Hz

The transmit/receive cycle, or "run," was repeated several times during the period of visibility of the comet. The results from these runs were "stacked" in accord with the ephemeris we produced from the initial conditions then available for Kohoutek's orbit (B. Marsden, private communication, 1973). Comparison "noise-only" runs were subtracted before further processing to attempt to remove any slope and "ripple" in the power spectrum that might be caused by the instrumentation. Since neither the bandwidth nor the center frequency of the radar echo was known precisely, we searched, at various resolutions, the spectral region within ± 33 kHz of the expected frequency of the echo. For the frequency interval within ± 925 Hz, the spectral analysis was performed with 2-Hz resolution and utilized a multi-bit Fourier technique normally used for planetary radar experiments. For the extended frequency interval, bandwidths of 12 kHz and 66 kHz were searched with resolutions of 0.2 kHz and 1 kHz, respectively. For this latter analysis, we used the one-bit digital autocorrelator normally employed at Haystack for observation of spectral-line emissions from the interstellar medium. The procedures used in both analyses were tested thoroughly by observing strong echoes from the planet Venus.

No echo was apparent in any of the spectra obtained from the observations of the comet. We can infer from this result an upper limit on the radar cross section, σ, of the comet by means of the radar equation:

$$\sigma = \frac{4\pi\lambda^2 R^4 kT(S/N)B^{1/2}}{PA^2 t^{1/2}} . \qquad (1)$$

where S/N denotes the signal-to-noise ratio, B the echo bandwidth and k Boltzmann's constant. The other quantities on the right side of Equation (1) are defined in table I. If we take $(S/N) = 5$, a conservative value, the upper limit on the cross section is 5×10^3 km^2 Hz$^{1/2}$ for the frequency interval of ± 925 Hz; however, for the extended frequency interval, this limit must be increased by approximately a factor of 2 to 10^4 km^2 Hz$^{1/2}$ to account for the clipping correction inherent in the one-bit autocorrelation spectral analysis.

We recognized from the start that the sensitivity of the Haystack radar system was insufficient to have detected an echo from the comet nucleus (hard target) were it no larger than the usually accepted estimate of a few tens of kilometers. However, we reasoned that a high-frequency echo might be observed from Rayleigh scattering in the considerably larger comet coma (soft target). Under the assumption that the particles in the coma are much smaller than the wavelength, λ, of the radio signals, the radar cross section is given approximately by $N4\pi(2\pi)^4(a^6/\lambda^4) \mid [m^2 - 1]/[m^2 + 2] \mid^2$ where a is the radius, N the number, and m the complex index of refraction of the particles.

In the absence of a definitive echo, its spectral width and shape are of course unknown. However, as an illustrative example, if we assume a flat spectrum of 100-Hz width, then we can conclude that (1) the density of millimeter-sized particles in a coma of diameter 10^4 km must be less than 1 m^{-3} (we ignore the small effects of "shadowing" and the possibility of an anomalously small index of refraction); and (2) the diameter of the nucleus of the comet, if considered to be a perfectly reflecting solid-body target, must be less than about 250 km.

ACKNOWLEDGMENT

Radar Astronomy at the Haystack Observatory of the Northeast Radio Observatory Corporation is supported by the National Aeronautics and Space Administration, Grant NGR–22–174–003, and by the National Science Foundation, Grant GP–25865.

AN ANALYSIS OF THE VISUAL MAGNITUDE OF COMET KOHOUTEK

W. A. DEUTSCHMAN
Center for Astrophysics

An analysis of 212 pre-perihelion and 230 post-perihelion visual magnitude observations of Comet Kohoutek shows that the magnitude is best represented by Levin's formula: $M^* = A + B \sqrt{R}$ *and not the usual power law* $M^* = M_0 + 2.5n \log (R)$. *Furthermore, the absolute magnitude of the comet at unit distance from both the Earth and Sun is 1.3 magnitudes fainter after perihelion than before perihelion. The paper also discussed the procedures necessary to intercompare magnitudes derived by different observers using different techniques.*

DISCUSSION

KELLER: Did you investigate the connection with lunar phase and low horizon in respect to the scattering of data?

DEUTSCHMAN: In regard to lunar phase, I tossed all that data out. No, I did not toss out the data that was near the horizon because that was about all we had in early January (2, 3, and 4). It was low in the sky and it is there.

MARAN: What magnitude did they give at perihelion? Have you looked at the recent, far-out 18-magnitude estimate from Dr. Roemer and what index that should give you?

DEUTSCHMAN: No, I have not looked at the 18-magnitude observation. At perihelion the magnitude is somewhere between +1 or 2. At that particular period the Skylab astronauts were talking about −0.5 to −1. There is a discrepancy there between the extrapolations.

You have to be a little bit careful in terms of using data that is taken strictly for position and is exposed only for that central condensation, since they are approximately two magnitudes too faint.

HENIZE: I wish to show my own slide of a curve. It is from visual estimates using defocused binoculars. I made one set of estimates and the other was made completely independently by Diggs. Our slopes were so comparable that it looked as if we had a lot of good data. It does require an 0.6 magnitude adjustment between us. The main thing I mean to point out is that we had a nice slope down to the 16th of January. If you put this on the magnitude-log r curve it gives you a slope of about 3.8 and it extrapolates to -0.8 at perihelion with a very smooth decline from perihelion down to the 16th of January. On the 16th of January it is suggested there is a standstill for approximately 3 nights.

PHYSICAL INTERPRETATION OF THE BRIGHTNESS VARIATION OF COMET KOHOUTEK

A. H. DELSEMME
Department of Physics and Astronomy
The University of Toledo

The brightness variation of Comet Kohoutek before perihelion is used in connection with the theory of vaporization of the cometary nucleus, to establish that the vaporization was probably not controlled by water, but possibly by a mixture of water with a more volatile major constituent like CO_2. *A large fraction of very volatile molecules like* CH_4 *or CO is very unlikely, if the magnitudes published at discovery are meaningful. At the time of this writing it is too early to understand the meaning of the brightness law* after *perihelion.*

Use of the Brightness Law

Use of the law of cometary brightness (i.e., the dependence of the total brightness of a comet on its heliocentric distance) is one of the simplest ways to get some idea about the production law (i.e., the dependence of the production rate of gas and dust on distance).

More information on this production law may be deduced from a study of the dependence on distance of either the nongravitational force (Delsemme, 1972, Marsden et al., 1973) or better, the monochromatic brightness of the different neutral radicals observed in the coma (Mayer and O'Dell, 1968). The meaning of these two latter approaches can be more easily clarified than that of the total brightness law, which unfortunately mixes the light reflected by the dust with the light emitted by fluorescence of the different radicals. However, the brightness law is much easier to establish and therefore is still widely used for all comets, whereas the law of monochromatic brightness has been scantily used so far, with incomplete results for only one or two comets. In the same way, the law of dependence on distance of the nongravitational

force can be approximately established only for short-period comets, when several returns have been observed.

When the brightness law is used to approximate the production law, three assumptions are made. First, it is assumed that the gas production is in proportion to the light emitted by the fluorescence of the observed radicals. This is basically true, because if the fluorescent intensity varies with r^{-2} (r = heliocentric distance), this factor cancels out, since the observed molecule decays by photodissociation or ionization with a lifetime τ proportional to r^2. However, as the molecule leaves the nuclear region with a velocity v, it decays in the coma with an exponential scale length $v\tau$. But the instrumental field of view may be limited by a diaphragm or more simply—in particular, for visual observations—by the sky brightness. The cancellation of the factors r^2 and r^{-2} takes place only if we see all the emitting molecules, that is, if the field of view is in practice six or seven times larger than the scale length (Delsemme, 1973b). For visual observations, C_2 is likely to prevail. At 1 AU, the scale length for C_2 decay is 9×10^4 km; therefore, the light coming from distances up to 5×10^5 km from the nucleus must be taken into account; otherwise, a correcting term must be added (Delsemme, 1973b).

The second assumption is that the radicals observed in visible light are in proportion to the major constituents, in particular to OH and H. So far, we have all reasons to believe that it is about true (Delsemme and Miller, 1970).

The third assumption is that the fraction of the total light coming from the dust (continuum) does not vary widely. This is rather likely, because we believe that the dust is dragged away by the vaporizing gases in approximate proportion to them. The major assumption is, therefore, that the grain size distribution does not vary much, at least for the smallest sizes which are the major constituents of the reflected light.

Despite all these difficulties, my thesis here is that the total brightness law can lead to results which are significant enough to gain some physical insight on the release of gas and dust. This is true in particular when we can neglect (or smooth out) the activity outbursts, and if we can establish, during the approach of the comet, at what distance from the Sun the radiative steady state of the nucleus is progressively superseded by the vaporization steady state.

The Vaporization Theory

For this purpose, we must rely on a model; and before going further, we must clarify a misunderstanding which comes from the fact that several authors publishing cometary light curves, still use Levin's formula (1943) to fit in a theoretical curve with the observations. Its appeal obviously lies in its simplicity; but it has an accurate physical meaning that cannot be dissociated from it. That formula implies that the nuclear temperature is set by a purely radiative equilibrium, that is, that the latent heat of vaporization of the gas re-

leased is negligible compared with the heat radiated away in the infrared by the nucleus.

This was quite acceptable in the 1940's, when the total amount of gas liberated by a comet was unknown. Bobrovnikoff (1951) showed, however, that the 4477 observations he discusses are not better represented by Levin's formula than by the empirical formula that uses a constant n for the exponent of r, the heliocentric distance. But the large gas production stemming from Whipple's (1950) icy conglomerate model of the cometary nucleus, is the best reason to reject Levin's formula on theoretical grounds. Numerical models for the vaporization of large amounts of gases from the nucleus were computed independently by Huebner (1965) for water; and by the author (Delsemme, 1965) for water as well as for the solid hydrates of gases (clathrates and ionic hydrates). These models made clear that the temperature of the nucleus depends on two different types of steady states.

For water and for the solid hydrates of gases, the radiative equilibrium takes over at a distance larger than 3 or 4 AU, and Levin's law can be formally used as a limit at much larger distances; however, we do not have many comets whose brightness curve is known at distances much larger than 3 or 4 AU. For the shortest heliocentric distances, that is, for less than 1 AU, the vaporization steady state is overwhelming; the temperature is set by it, and not at all by the radiative term that becomes negligible; and the production law becomes an inverse-square law of the heliocentric distance. For intermediate distances, that is, from 1 to 3 AU, if the production law is described by a log-log diagram (fig. 1) the slope of the curve for water plunges from -2 (inverse-square law) to values larger than -20, around 2 or 3 AU, its accurate position depending on the albedos of the cometary nucleus in visible light and in the infrared (Delsemme and Miller, 1971). If the vaporization were controlled by snows of gases more volatile than water (see fig. 1 for example), the heliocentric distance where the vaporization takes over would be at some 7 AU for NH_3, 10 AU for CO_2, 70 AU for CH_4, and 140 AU for CO or for N_2. However, in the presence of water snows, up to 15 percent of these gases could be absorbed in the water snows, the limit leading to ionic hydrates or clathrates; and consequently water would still control the vaporization up to this limit. It is therefore likely that those comets that show a large production rate of CO^+ at rather large heliocentric distances, like Morehouse (1908III) or Humason (1962VIII), have an amount of gas more volatile than water, in excess of this limit of 15 percent and therefore not bound in clathrates. The nature of these volatile snows is suggested by the vaporization behavior of CO_2 (appearance at 10 AU) rather than that of CO (appearance of 70 AU?).

For most of the ordinary comets, however, the vaporization model seems to predict the correct distance for the appearance of the coma, if water controls the vaporization; that is, if no more than 15 percent of more volatile gases

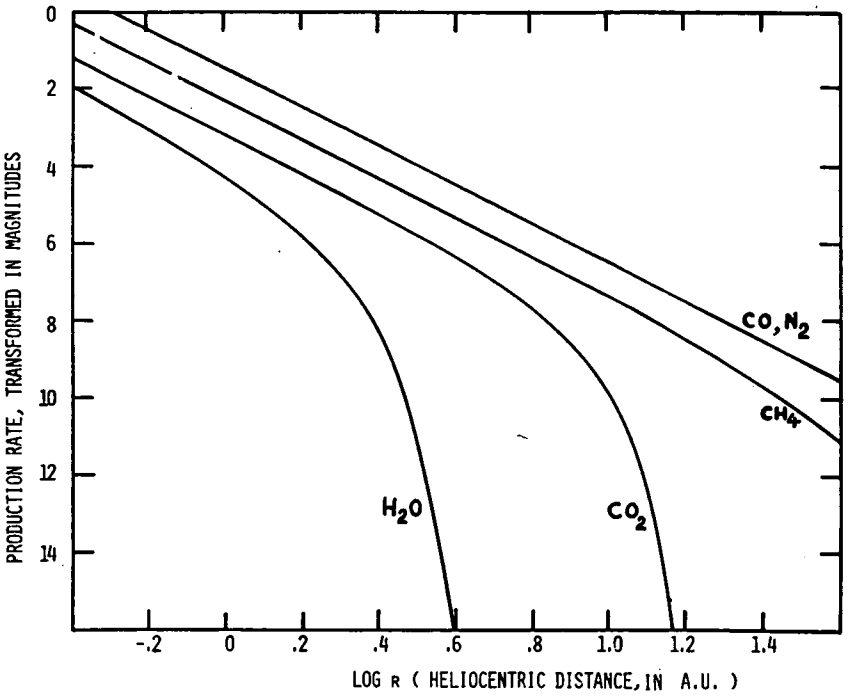

FIGURE 1.—*Vaporization rates (transformed in magnitudes for easy comparison) for various snows, as a function of the heliocentric distance, computed for the steady-state temperature of a rotating cometary nucleus with the same albedo in the visible and in the infrared. The curve for H_2O also stands for the solid hydrates of gas (clathrates). The volatile gases emprisoned in the clathrate cavities are limited to 15 percent of the amount of water. A sensible variation of the albedos may shift the curves by some ±0.2 in log r units.*

are present. In order to accept the vaporization model, large gas productions had to be observed. These large gas productions were definitely established only when a huge hydrogen coma was discovered by the OAO in the three bright comets of 1970. Since 1970, it has therefore become very difficult to believe in the desorption of small amounts of gases at short heliocentric distances, and therefore Levin's formula can no longer be used. This has been emphasized by Levin himself (Levin, 1972).

The Case of Comet Kohoutek

We can now use the vaporization theory to understand the meaning of the brightness curve of Comet Kohoutek. For this purpose, all the observed m_1 magnitudes collected from the IAU circulars have been reduced for a geocentric distance of 1 astronomical unit (AU) and plotted in figure 2. The upper curve goes from right to left before perihelion, whereas the lower curve goes

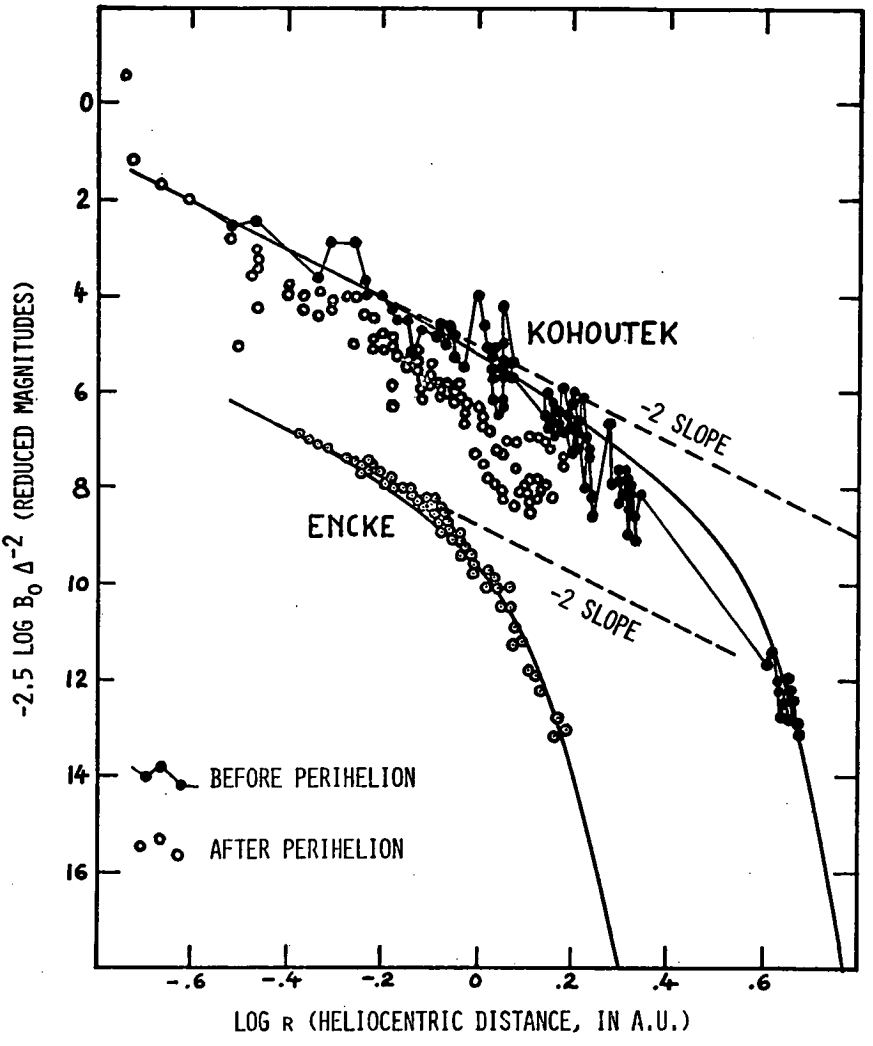

FIGURE 2.—*The brightness curve of Comet Kohoutek, before and after perihelion, compared with that of Comet Encke. The two solid lines both represent the H_2O curve of figure 1, shifted by two opposite variations of the albedos. No sensible albedo could shift the CO_2 curve enough to explain the light curve of Comet Kohoutek, but a slight excess of free CO_2 (above the 15 percent stabilized by the solid hydrates) could be used to explain the behavior of Comet Kohoutek before perihelion.*

from left to right after perihelion. For comparison, the light curves of Comet Encke, from Beyer (1950a, b; 1955; 1962) have also been plotted on the same diagram. For Encke, the two passages of 1947 and 1951 superpose rather well, with a slight vertical shift, on that of 1961.

It is clear from the onset the Comet Encke's results are homogeneous mainly because they come from a single observer, whereas each point of the light curve of Comet Kohoutek should be discussed for three possible corrections: the entrance pupil correction (Bobrovnikoff, 1941; Meisel, 1970; Morris, 1973); the field diaphragm correction (Delsemme, 1973b) (as mentioned before, in the absence of any field diaphragm, this correction comes from the sky brightness); and the correction from the variable personal equation of each individual observer. As it is impossible to assess what correction each observer has used, it is not worth trying to "improve" on figure 2.

At any rate, we are not interested here in small variations in the activity of the comet, but rather in the general trend, namely, in establishing the heliocentric distance for the onset of vaporization. In this respect, the most important information is the fact that the brightness at discovery (beyond 4 AU) was more than 4 magnitudes fainter than that extrapolated from the inverse-square law (slope–2 on fig. 2). A careful discussion of these results is needed here, because the brightnesses just after discovery have an influence on the final conclusions.

It could be argued that all the points at the extreme right of figure 2 (for $\log r \geq 0.6$) are biased: because they were obtained by long-focus instruments, they would represent the brightness of the central condensation (IAU circulars m_2) and not the total brightness of the coma (IAU circulars m_1).

But the magnitudes m_2 have all been rejected from figure 1 and the magnitudes m_1 only have been used. In particular, the discovery plates were obtained by Dr. Kohoutek with the 32-inch Schmidt telescope at Hamburg Observatory, which could hardly be called a long-focus instrument. As a matter of fact, the two fuzzy spots representing the comet had a diameter of 7 arc-seconds (*Sky and Telescope* 46, 91, August 1973) corresponding to a coma diameter of some 20 000 km, which could hardly be called the "central condensation." The first m_2 magnitudes were reported for the end of April by T. Seki (IAU Circular No. 2537) and were indeed one magnitude fainter than m_1 at that time. It must, however, be admitted that the separation of m_1 and m_2 is often difficult to establish with large instruments for faraway comets. Short exposure times include some coma light into the central condensation, because of the small scale on the plate. Long exposure times miss part of the outer coma, because of the intrinsic faintness of the comet.

On figure 2, the actual magnitudes just after discovery could therefore be somewhat brighter than shown, whereas they could certainly not be fainter. On the other hand, there is already an indication near $\log r = 0.2$ to 0.3, that the -2 slope is not yet reached.

If we first accept that the m_1 magnitudes can be taken at their face value, we can fit a model to the data. In figure 2, the vaporization of water (solid continuous curve) has been fitted to Comets Encke and Kohoutek, by changing the albedos of the vaporizing nucleus.

There are difficulties, however. The large drop in the slope takes place around 1.4 AU for Encke, and only near 4.0 AU for Kohoutek. The fitting of the curve for water vaporization implies that, for an infrared albedo $A_1 = 0.10$, the visible albedo must be $A_0 = 0.74$ for Encke, whereas $A_1 > A_0$ for Kohoutek; for instance, $A_1 = 0.64$ and $A_0 = 0.10$ is a possible solution.

The anomalous albedo A_0 for Encke does not make sense, as white snow reaches $A_0 = 0.7$ only. This strengthens the conclusions of Delsemme and Rud (1973) that Encke cannot be explained by a homogeneous nucleus steadily covered with water snows. The present results would be explained by water-ice glaciers covering some 10 percent of the surface area, whereas the rest of the area would be much darker. This is rather consistent with the history of Encke's decay for the last two centuries.

As far as Comet Kohoutek is concerned, it seems more likely that $A_1 = 0.64$ is much too high to be acceptable. Besides, if the actual magnitudes just after discovery were somewhat brighter than reported, A_1 would become even larger for the water model.

The only alternate explanation is the presence of another major constituent more volatile than water, like CO_2, that changes the vaporization pattern, but could be fitted to the drop of the light-curve near 4.0 AU. However, the fact that the brightnesses just after discovery were much lower than those extrapolated from the inverse-square law seems to imply the absence of a large fraction of a very volatile component, like CH_4, CO, or N_2. In this context, a "large fraction" means much larger than the amount that could be trapped in the cavities of the solid hydrates, that is, approximately 15 percent.

An even more volatile constituent like CO could control the vaporizations, only if the m_1 magnitudes were in error by more than four magnitudes, which seems to be rather unlikely.

The present conclusion has the interesting consequence of suggesting larger "parent" molecules like CO_2, and N_2H_4 for the tail ions CO^+ and N_2^+.

At the time of this writing, Comet Kohoutek is still being observed, and the complete light curve after perihelion cannot yet be compared with models. A discussion of the fact that its total brightness faded by more than one magnitude after perihelion (see fig. 2) is therefore to be reserved for the future.

ACKNOWLEDGMENTS

The author thanks David Rud who has computed the reduced magnitudes of Comet Kohoutek. NSF Grant GP 39259 is gratefully acknowledged.

REFERENCES

BEYER, M.: 1950, Astron. Nachr. 278, 217; and 279, 49.
BEYER, M.: 1955, Astron. Nachr. 282, 145.
BEYER, M.: 1962, Astron. Nachr. 286, 219.
BOBROVNIKOFF, N. T.: 1941, Contr. Perkins Obs. Nos. 15 and 16.
BOBROVNIKOFF, N. T.: 1951, Astrophysics (ed., J. A. Hynek) p. 302. McGraw Hill, New York.
DELSEMME, A. H.: 1965, Internat. Colloq. Astrophys., Liege, 13, 77; also in Mem. Soc. Roy. Sci., Liege, 12, 77 (1966).
DELSEMME, A. H.: 1972, The Origin of the Solar System, (ed., H. Reeves) p. 305. CNRS, Paris.
DELSEMME, A. H.: 1973a, Space Science Reviews 15, 89.
DELSEMME, A. H.: 1973b, Astrophys. Letters, 14, 163.
DELSEMME, A. H.; and MILLER, D. C.: 1970, Planet. Space Sci. 18, 717.
DELSEMME, A. H.; and MILLER, D. C.: 1971, Planet. Space Sci., 19, 1229 and 1259.
HUEBNER, W. F.: 1965, Z. Astrophys. 63, 22.
LEVIN, B. J.: 1943, Astron. Zu. 21, 48.
LEVIN, B. J.: 1972, Proc. IAU Symposium No. 45, (ed., G. A. Chebotarev et al.) p. 262. Reidel, Dordrecht-Holland, 1972.
MARSDEN, B. G.; SEKANINA, Z.; and YEOMANS, D. K.: 1973, Astron. J. 78, 211.
MAYER, P.; and O'DELL, C. R.: 1968, Astrophys. J. 153, 951.
MEISEL, D. D.: 1970, Astron. J. 75, 252.
MORRIS, C. S.: 1973, Publ. Astron. Soc. Pacific 85, 470.
WHIPPLE, F.: 1950, Astrophys. J. 111, 375.
WHIPPLE, F.: 1951, Astrophys. J. 113, 464.

DISCUSSION

DUBIN: In the case of the general formulas, they do show asymmetry with respect to radial distance. In the case of Comet Kohoutek, there is a clear asymmetry of maybe one to two magnitudes between pre- and post-perihelion. How do you take that into account without having a lot of dust?

DELSEMME: We don't know the detailed materials but there are several possible explanations. The one I favor is to imagine that we have any icy grain halo during the pre-perihelion approach and this icy grain halo has disappeared when it goes away. So the cross-sectional area for vaporization has diminished drastically. It is true that the vaporization curve does not rule out large quantities of materials which are roughly at the same order of magnitude as water for the vaporizations. This is typically true for HCN and CH_3CN. However, I have other arguments and I believe that so far CH_3CN has been underestimated. And I preliminarily calculate 1 to 2 percent water only.

I believe that amorphous ice is an excellent suggestion that certainly might work at rather large solar distances. However, because of its transition temperature I doubt if it really does exist at distances that are less than half an astronomical unit.

VOICE: Its transition temperature is about 140 K, which corresponds to 2.5.

DELSEMME: Then we agree, it is a very good suggestion. I quite agree on that point.

DONN: As I recall, then Comet Halley was recovered in 1909 it appeared about 3 AU with a rather diffuse structure and was not stellar at all. At this distance there was sufficient gas emission to cause a dust cloud. So we have evidence, even in a comet that has made as many returns to the Sun as Halley has, that it can have several gas ejections at very large distances. In order to get water to control vaporizations of the release from the nucleus it need not necessarily be clathrate but just a large excess of water would again have the same effect. A laboratory example of this thing is that using water and nonvolatile materials is to trap and pump by putting an excess and freezing them out. Nonvolatile material will condense and trap the volatile material.

DELSEMME: Certainly. The clathrate suggestion is there, not to explain a different vaporization rate of ice. On the contrary, it is there to suggest that up to 15 percent of other elements could be vaporized in proportion with ice. Of course, if you reach thermal equilibrium and if you start from a mixture of many gases and water ice you finish by having the clathrates, or at least you have the gases absorbed in the ices, which is formally the same as the clathrate model. If you don't have enough gas, you make absorptions.

ON PREDICTING THE BRIGHTNESS OF COMETS

E. J. ÖPIK
Department of Physics and Astronomy
University of Maryland

Comet Kohoutek actually presented a typical example of normal variation of cometary brightness as it depends on the distances from the Sun and the observer. Some nonfulfilled expectations in this respect were entirely due to an early prediction which was made without regard to known facts of cometary physics and observation (Öpik, 1972 and 1973). In a minor degree, misunderstandings of a similar kind are still obsessing current photometric predictions in cometary ephemerides.

Namely, regarding the effect of geocentric distance (Δ), the inverse-square law is still traditionally in use with the published ephemerides despite the incorrectness of this procedure having been pointed out more than a decade ago (Öpik, 1963). It is true that the total apparent brightness of a comet, from nucleus to the outer boundary of coma and tail (which goes, so to speak, out to infinity), should vary inversely as the square of the geocentric distance. However, in making his estimate of stellar magnitude, the observer reckons only with a central condensation around the nucleus which appears to be starlike enough to be compared with stellar images, and disregards the washed-out extended nebular envelope. The diameter of the effective starlike image corresponds to his photometric resolving power. The smaller the geocentric distance—or the larger the magnifying power of the telescope which serves as an interchangeable equivalent for reducing the distance—the smaller the linear radius of the sphere around the cometary nucleus which contributes to the photometric estimate; and the estimated subjective brightness will contain an additional factor increasing with the distance (or decreasing with the magnifying power of the telescope). At a uniform velocity of expansion of the cometary gases, or an inverse-square law of gas density around the nucleus, the additional factor is proportional to the first power of the distance Δ, so that the subjective photometric law becomes

$$\frac{1}{\Delta^2}\cdot\Delta=\frac{1}{\Delta},$$

or essentially an inverse first-power law.

The same refers to photographically estimated cometary stellar magnitudes, unless the total brightness to a fixed linear distance from the nucleus is found by integrating surface brightness measurements of the coma. This, however, is never done.

Strangely enough, an equivalent of this effect has been investigated with respect to the resolving power of telescopes as depending on aperture (Bobrovnikoff, 1941 and 1942), but never has been applied in the traditional treatment of the effect of geocentric distance.

Although for most comets observed in the inner solar system, the range in geocentric distance is usually not very large and its erroneous treatment not of too much consequence, for one like Comet Kohoutek discovered early at a large distance from the Sun, say at 4–6 astronomical units (AU), the error from this cause alone could amount to an overestimate of the perihelion brightness by a factor of from 3 to 5.

As to the effect of heliocentric distance (r), the theoretically expected inverse power is somewhere around $n = 4$ (a power of 2 for the rate of evaporation and another equal power for the intensity of illumination). Statistical analyses (Oort and Schmidt, 1951; Vanysek, 1952) have indeed confirmed this expectation; when reduced to the correct law of geocentric distance (Öpik, 1973, p. 387), which but slightly affects the results, the statistics lead to an inverse power of $n = 4.1$ or 4.2 for all cometary apparition, and to $n = 3.9$ or 3.7 for the "new" first apparitions with their nearly parabolic orbits.

Through use of an exaggerated value of $n = 6$ for the inverse power of heliocentric distance, and because of the large range in distance, the perihelion brightness of Comet Kohoutek was overestimated by a factor of 900 and, with the traditional incorrect allowance for geocentric distance, the overestimate amounted to a total brightness ratio of 2800 (Öpik, 1972 and 1973) or 8.6 magnitudes.

Of course, the composition of cometary gases may vary with heliocentric distance, and this may have an effect on the brightness variation. Thus, water ice, responsible for a considerable fraction (perhaps about 40 percent of gases or 20 percent of the total mass loss) of the evaporate in solar vicinity, would not yield vapors at large distances—somewhere near Jupiter or farther out. One may ask whether this could increase the average heliocentric exponent when starting the prediction from a large distance. Actually, from obvious physical considerations, the absence of the water vapor component at low temperatures would act in the opposite direction, tending to depress the exponent below the standard values of 4. This also appears to be reflected in the lower empirical value of n for the "new" comets.

Indeed, when water ice is not evaporated, a larger fraction of solar heat is spent on the evaporation of those constituents of Whipple's icy conglomerate —the cometary "clathrate"—which yield the "photogenic" molecules, C_2, CN,

and CO^+. Also, the latent heat of vaporization of their parent materials is less than that of H_2O, which again favors release of more luminescent material at large heliocentric distances, in proportion to the received solar heat. Moreover, the solid water ice, while losing its enclosed more volatile gases, would separate as snowflakes or "ice dust," similar to the meteoric dustballs but of higher reflectivity. The separation as snowflakes would thus increase the total brightness yield at large heliocentric distances, while evaporation of H_2O would depress it at smaller distances from the Sun. With the numerical data as assumed by Öpik (1963), it can be shown that released snow-dust, if amounting to 40 percent of the total mass of the ices, could lead to a twofold increase in the brightness of the cometary coma, if consisting of compact particles of about 0.04 cm in diameter, or of snowflakes with a mass load of 0.027 gram per cm^2 of cross section. The reflecting area, or the increase in brightness, is of course inversely proportional to the mass load. Thus, if anything, when extrapolating the brightness of a comet discovered at a large heliocentric distance, one should use an exponent of $n < 4$, and not one larger than the "classical" value of 4. There is urgent need now to change the routine of photometric predictions in cometary ephemerides and to apply a revised formula for apparent magnitude,

$$m = m_o - 2.5 \log \Delta - 10 \log r$$

with 2.5 instead of the traditional coefficient 5 in the second term.

At the same time we could say that the misjudged prediction for Comet Kohoutek has turned out as a bonus, resulting in an unparalleled harvest of observations which no other comet could match.

REFERENCES

Öpik, E. J.: December 1972, Irish Astron. J. 10, back page of plate: note dated September 6, 1973.

Öpik, E. J.: 1963, Photometry, Dimensions, and Ablation Rate of Comets, Irish Astron. J. 6, 93–112; Armagh Observ. Contrib. No. 42.

Bobrovnikoff, N. T.: 1941, Investigations of the Brightness of Comets, Perkins Observatory Contrib. 2, 49–187; and 1942, 189–300.

Oort, J. H.; and Schmidt, M.: 1951, Bull. Astron. Inst. Netherl. 11, 259.

Vanysek, V.: 1952, Contrib. Astron. Inst. Masaryk Univ. Brno 1, 1.

Öpik, E. J.: 1973, Comets and the Formation of Planets, Astrophys. and Space Sci. 21, 307–398; Armagh Obs. Contrib. No. 83.

DYNAMICAL AND COLORIMETRIC STUDY OF THE DUST TAIL OF COMET KOHOUTEK

B. J. JAMBOR
Martin Marietta Corporation
Denver, Colorado

The yellow color starting away from the coma and the orange seen by the astronauts in the tail of Comet Kohoutek 1.3 and 2 days, respectively, after perihelion can be explained as scattering on dust particles of size 0.5 micron and of basaltic nature. The sodium enhancement can produce yellow if the atoms are released by small metal or graphite particles, but it does not explain the absence of color near the coma, nor the change to orange. The dust scattering explanation would put limits to the applicability of the Finson-Probstein dynamical calculations in the case of small particles.

The Skylab astronauts observed Comet Kohoutek during extravehicular activity (EVA) 1.3 days after perihelion, reporting a well-developed anti-tail, a broad fanned-out tail with a yellow color starting at a distance away from the coma, not in it. The next day, +2 days after perihelion, they observed it again and reported a similar general appearance, but the color was then orange. From the reported length of the tail proper, about 3°, it is seen that the color extended to regions about 6×10^6 km. These observations are described in the voice transcripts of the Skylab mission, the sketches made by the astronauts, and the colored drawings made under the supervision of the astronauts. The use of visual observations, although rare today, is nevertheless the basis of all astronomy—and, in particular, of early cometary astronomy. The astronauts are well-trained observers and scientists in their own right. The normal human eye is by far the most sensitive and precise discriminator of color over an enormous range of brightness and its response is carefully calibrated and documented. It is not inaccurate and purely of a subjective nature to base theoretical calculations on visual observations confirmed by two well-trained scientists

observing at the same time. Therefore, we use their report of color as true and unbiased in the following analysis.

Sodium Enhancement

The intensity of sodium lines is strongly distance-dependent, and sodium emission is expected and indeed was reported for Kohoutek. However, all observers agree that the lines are strongest near the coma and the farthest extension in the tail reported was 5×10^4 km (Wehinger, 1974). A release of the NaI by dust grains far away from the coma is required to bring it to 6×10^6 km. As will be shown later, the only particles which could be present in the normal tail on that day (+ 1.3) are very small ones: 0.1 micron or smaller. The lifetime of such particles can be calculated (Huebner, 1970). The only particles of that size that could survive long enough to reach those distances under the assumption of motion in a gravitational field weakened by radiation pressure are, of necessity, iron or graphite. The sodium assumption can explain the yellow color but not the appearance of color away from the nucleus, nor the change to orange the next day.

Scattering by Dust

The fact that grains are necessarily involved in the production of the color, even if only in the role of NaI producers, raises the question of their true contribution. Can the grains by themselves be responsible? To investigate this, we can calculate the color of the light scattered by particles of different sizes at any angles. The nature of the particles is described by their complex index of refraction. The technique used is described by Kerker (1969). Three standard primaries X, Y, Z, adopted by the Commission Internationale de l'Eclairage (CIE), are used. Any color is a mixture of these. We obtain the chromaticity, which describes the hue and purity by calculating

$$x = X/(X+Y+Z)$$

$$y = Y/(X+Y+Z)$$

and then using a chromaticity diagram which gives us both the hue and the purity.

For the case of scattering spheres for example:

$$X = (1/4\pi^2 r^2) \int_0^{00} \lambda^2 \bar{x}_\lambda P_\lambda i(m, a, \lambda)\, d\lambda$$

where r is the distance, x_λ is one of the tristimulus color-matching values given by CIE, $P_\lambda d\lambda$ is the fraction of incident energy contained in the spectral band between λ and $\lambda + d\lambda$, and $i(m, a, \lambda)$ is the dimensionless parameter describing the scattering. Similar expressions are obtained for Y and Z. In our

special case, the color-matching functions x_λ, y_λ, z_λ were chosen to be those given for colors of large angular areas (4 degrees and up) by the 1964 CIE Supplementary Standard Observer for Colorimetry. The $P_\lambda d\lambda$ fraction of solar energy was taken from tables given by Thekaekara (1970). The chromaticity was read off a chromaticity diagram to obtain the dominant wavelength of the pure spectral color and the purity of ratio of pure spectral color to achromatic white. The purity of hues adopted was as follows: pale (p) for 0. to 0.249; medium (m) for 0.250 to 0.499; bright (b) for 0.500 to 0.749; and brilliant (br) for 0.750 to 1. (Kerker, 1969).

An attempt was made to match the color of the dust tail on days +1.3 and +2 when the solar scattering angles from the nucleus were 135° and 124°, respectively. The color was yellow on the first day and started about 2° in the tail. The next day, the color was orange. The anti-tail looked whitish on both days. Tristimulus values X,Y,Z were calculated by using the solar spectrum from 0.38 to 0.76 μm and scattering by spheres of various sizes. The tail was assumed to be optically thin so that single scattering only was involved. Scattering on both single sizes and distributions of sizes, chosen to be Zeroth Order Logarithmic (Z.O.L.D.) (Kerker, 1969), were investigated. The fact that any color at all was observed indicates that a rather narrow distribution of sizes was present in the tail. For increasing polydispersity, described by the scatter parameter σ_o in a Z.O.L.D. distribution, the color is washed out by the mixture of different colors due to different sizes. Narrow size distributions of $\sigma_o = 0.01$ to $\sigma_o = 0.07$ are required to conserve the colors which blend to achromatic white for $\sigma_o = 0.15$ to $\sigma_o = 0.2$. Before such modeling can be done, it is well to calculate what size of dust can be present in the region of the tail observed.

Synchronic Method

The synchronic method of Finson and Probstein (1968) was chosen to map the two tails. The parameter 1-μ expressed as

$$1-\mu=\frac{1.19\times10^{-4}Q_{r.p}}{\rho d}\ (\mathrm{g\ cm^{-2}})$$

in terms of the efficiency of radiation pressure $Q_{r.p}$, the density ρ of the grain, and its diameter d, is the ratio of repulsive solar pressure to solar gravitational attraction.

Figures 1 and 2 show, as seen from the Earth, the position of the particles emitted at various times before the date of observation (synchrones). A few values of $1-\mu$ are indicated on the synchrones. The dates of observation are December 29.7 (1.3 days) and December 30.4 (+2 days). The synchrones show a tendency to rotate counterclockwise. The figure shows that for all particles with $1-\mu < 1$, this tail is mostly in the solar direction. All particles emitted 4 days or more before perihelion are in the "anti-tail." Dust emission

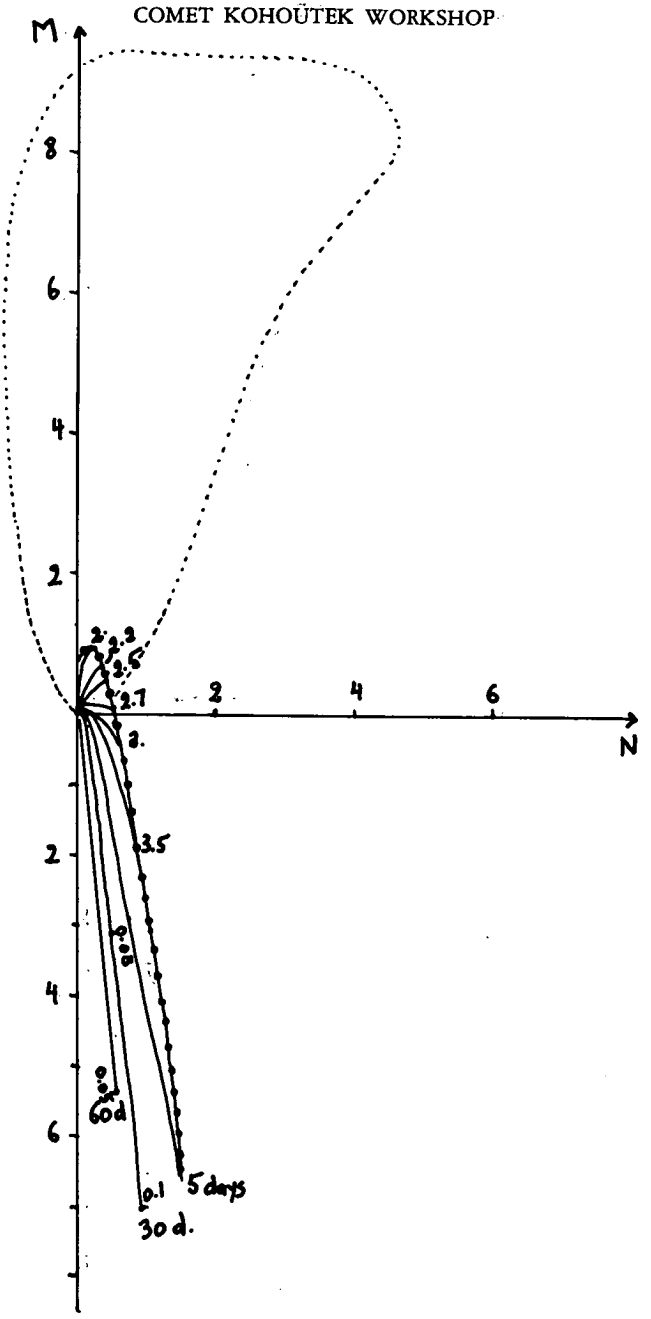

FIGURE 1.—*Comet Kohoutek, synchrones +1.3 days. Unit scale: 10^6km. The M axis is radially away from the Sun. The date of the synchrones is indicated at the end of each one. The end point of the synchrones, the curve with the small circles, is the 1-μ = 0.99 syndyne. The portion of the tail drawn in dotted line is made up of particles expected to be under a net repulsive force (1-μ > 1) and showed a yellow color starting away from the coma. Some values of 1-μ are indicated along synchrones.*

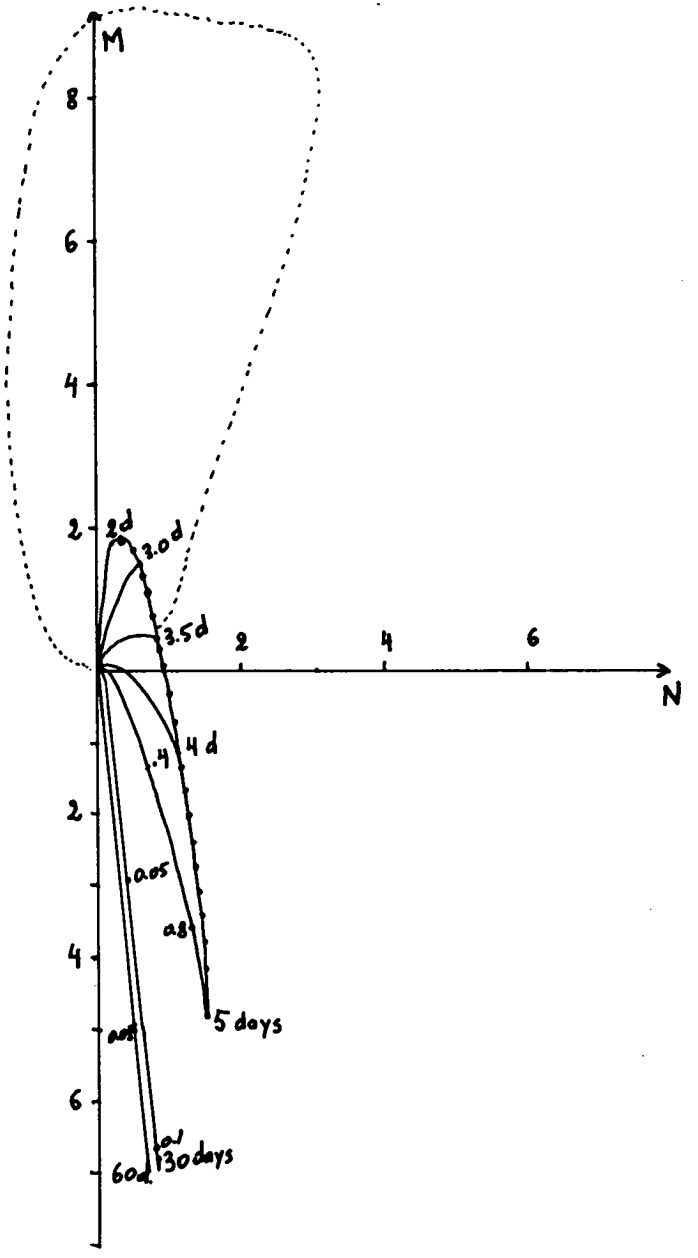

FIGURE 2.—*Comet Kohoutek, synchrones, +2 days. Notice the rotation of synchrones as compared to figure 1. The 1-μ = 0.99 syndyne extends further in the +M direction. The tail in the dotted line region was observed to be orange.*

as recent as one or two days is within 1 or 2 $\times$ 10^{16} km of the nucleus for 1 $-$ μ $<$ 1. The normal tail is, therefore, made up of particles emitted recently and with 1 $-$ μ larger than one. For iron or graphite the sizes involved are all smaller than 0.1 μm.

Results of Colorimetry

The simple fact that we see any color indicates a very narrow-size distribution, as discussed above. In the anti-tail and near the coma region, the mixture of different sizes washes out the color and white is a result. The reason we can give credit to the determination of size and the nature of particles by using colorimetry is precisely because of the wide separation of synchrones in the tail region, resulting also in a separation of sizes; i.e., a very narrow-size distribution. The results are shown in tables I and II which correspond to the two days of observation. The angles of scattering start at the nucleus and extend four degrees in the tail. It is seen that particles 0.3 μm are, in general, too small and give bluish or pale whitish colors. Particles 0.1 μm or smaller (not shown) tend toward blue colors. Even smaller particles approximate Rayleigh scattering and would give a uniform blue at all angles. Ice would not survive for long but was tried in any case. Neither ice, nor strongly absorbing particles like carbon (graphite) and iron, can match the colors. The best fit is given, on both days, by basaltic glass $m = 1.57 - 0.0005i$. Next best is pure SiO_2 $m = 1.55$, followed by SiO_2 with slight absorption. The color changes from yellow on 1.3 days to orange on day $+2$ if we take 0.4 μm for the size in the first case and 0.4 μm and 0.6 μm in the second. These sizes correspond to 1 $-$ μ $\sim$ 0.8. We have, therefore, an apparent contradiction between the good match obtained from colorimetry, and the dynamical calculations which would put these particles much closer to the nucleus. Which one is correct? For particles below 1 μm the shape of the scatterer (cube, cylinder, etc.) has little to do with the end result, and the Mie theory using spheres is accurate (Carabine et al., 1971). The Finson-Probstein theory (1968) applied to Arend-Roland, to Bennett (Sekanina and Miller, 1973) and to Seki-Lines (Jambor, 1973) did not need particles of a size corresponding to 1 $-$ μ larger than 0.6 in great number; although these were present in some cases, the peak of distribution corresponded to larger sizes. Comet Kohoutek is different, with the spreading of synchrones resulting in a narrow-size distribution of small particles. Using only small particles here is a necessity. An independent check on the calculations using colorimetry, a proven technique, shows a discrepancy. Another comet which showed similar spreading out of synchrones is Ikeya-Seki, the Sun-grazing comet, 9 days after perihelion. The dust tail showed enormous length (30°) and fine structure in the form of whorls.

The yellow color can, therefore, be due to atomic sodium released by metallic or graphite dust grains that are under a repulsive force. But neither the fact that the color started away from the coma, nor that it changed to orange the

Table I.—*Colorimetry of the Dust Tail of Comet Kohoutek: +1.3 days*

Size (microns)	Ice				Carbon	SiO_2, $m = 1.55$				SiO_2, $m = 1.55 - .15i$				Basaltic Glass				Iron
0.3	Bp	Bp	Bp	Bp	W	Bp	Bp	Bp	Bp	Yp	W	W	W	Bp	Bp	Bp	Bp	W
0.4	Yp	GYm	GYm	Gm	W	Ym	Ym	Ym	Yp	Ym	Ym	Ym	Ym	Yb	Ym	Ym	Ym	W
0.6	W	W	W	W	W	Gb	Bm	Bm	Bp	W	W	W	W	Gm	GBp	Bp	Bp	W
2.5	W	W	W	W	W	Pp	W	Yp	Yp	W	W	W	W	Yp	W	Bp	Gp	W
10.0	W	W	W	W	W	Bp	Yp	Yp	W	W	W	W	W	Bp	W	Yp	W	W
Angle	135	137	138	139	All	135	137	138	139	135	137	138	139	135	137	138	139	All

Note: The symbols used in the table are as follows: B = Blue, G = Green, O = Orange, P = Purple, R = Red, W = White, Y = Yellow, p = pale, m = medium, b = bright.

Table II.—*Colorimetry of the Dust Tail of Comet Kohoutek: +2 days.*

Size (microns)	Ice				Carbon	SiO_2, $m = 1.55$				SiO_2, $m = 1.55 - .15i$				Basaltic Glass				Iron
0.3	W	W	W	W	W	Gp	Yp	Gp	Gp	Yp	Yp	Yp	Yp	GYp	GYp	Gp	Gp	W
0.4	Pp	Pp	Op	Yp	W	Pp	Op	Yp	YOm	Yp	Yp	Yp	Yp	Pp	Pp	Op	Om	W
0.6	Yp	Op	Ym	Ym	W	Om	Om	YOb	YOm	Op	Op	Op	Yp	Pm	Rm	Om	Ob	W
2.5	W	W	W	W	W	W	Yp	Yp	YGp	W	W	W	W	Yp	Yp	Yp	GYp	W
10.0	W	W	W	W	W	Yp	Op	W	Yp	W	W	W	W	W	W	W	W	W
Angle	124	126	127	128	All	124	126	127	128	124	126	127	128	124	126	127	128	All

Note: The symbols used in the table are as follows: B = Blue, G = Green, O = Orange, P = Purple, R = Red, W = White, Y = Yellow, p = pale, m = medium, b = bright.

next day, is thus explained. Both of these observations are easily and naturally explained by assuming grains like basalt of size 0.5 μm, and the change in angle of scattering. This assumption, however, apparently goes against a pure Finson-Probstein interpretation of this part of the dust tail. Some other force, perhaps due to electrostatic charging of the grains, must be acting to bring these particles to the large distances in a relatively short period of time.

REFERENCES

CARABINE, M. D.; MADDOCK, J. E. L.; and MOOR, A. P.: 1971, Nature Physical Science 231, 18.

FINSON, M. L.; and PROBSTEIN, R. F.: 1968, Ap. J. 154, 327.

HUEBNER, W. F.: 1970, Astron & Astrophys 5, 286.

JAMBOR, B. J.: 1973, Ap. J. 185, 727.

KERKER, M.: 1969, The Scattering of Light. Academic Press, New York.

SEKANINA, Z.; and MILLER, F. D.: 1973, Science 179, 565.

THEKAEKARA, M. P.: 1970, The Solar Constant and the Solar Spectrum Measured From a Research Aircraft, NASA TR–R–351.

WEHINGER, P. A.: 1974, Comet Kohoutek Workshop, P. —

SESSION V:

NOTE: In session V of the workshop, four summary talks were presented. Each of the four speakers had the freedom to say whatever interested him about Comet Kohoutek, plus his own work and the proceedings of the workshop. The discussion following these speeches is presented on page 241.

Shown in the photograph (left to right) are A. H. Delsemme, F. L. Whipple, C. R. O'Dell, J. C. Brandt, and G. H. Herbig.

MOLECULAR PROCESSES IN THE COMETARY COMA AND TAIL

A. H. DELSEMME
Department of Physics and Astronomy
The University of Toledo

A missing link for understanding the molecular processes in the cometary coma and tail, was the nature of the parent molecules vaporizing from the nucleus. A major step forward has been brought about by the first identification of three neutral parent molecules: hydrocyanic acid and methyl cyanide in Comet Kohoutek, water in Comet Bradfield. The discovery of the atomic resonance lines of C and O in Comet Kohoutek will also play a fundamental role in our understanding of the cometary phenomena, in particular when the meaning of their production rates will have become well understood.

The major feature that seems to emerge from the new results is the large depletion of hydrogen of the volatile fraction, as compared with a mixture of cosmic abundances. In particular, the H/O ratio points to an oxidation-reduction equilibrium very much like that of carbonaceous chondrites.

Most of the molecular processes taking place in the cometary coma are not yet quantitatively understood. Our present knowledge mainly stems from the spectroscopy of the coma. The monochromatic emissions of light that are observed in the coma tell the story of one single step (namely, the resonance-fluorescence) in a very long chain of unobserved processes that we must reconstruct without enough clues.

Let us try to describe at least qualitatively this sequence of processes that we do not see. First, the production rate of gas and dust is set by the vaporization rate of the nucleus (Delsemme and Miller, 1971a) that we can visual-

ize as an icy conglomerate (Whipple, 1950). The brightness law of the comet versus its heliocentric distance confirms the existence of a vaporization equilibrium (Delsemme, 1965; Huebner, 1965); the production rates of the major constituents (like H and OH) set the size of the nucleus as well as its albedo (Delsemme and Rud, 1973).

The dust is dragged away by the vaporizing gases. The gas drag provides the terminal velocity of the dust (Finson and Probstein, 1968) and the observed distribution in the dust tail sets the size of the dust (Bessel, 1836; Bredichin, 1903). The hydrodynamics of the gas drag provides a confirmation of the production rate of gas (Finson and Probstein, 1968). Volatile grains like hail grains or snowflakes are also probably dragged away by the vaporizing gases, and form a transient icy halo (Delsemme and Wenger, 1970; Delsemme and Miller, 1971b).

So far, so good: the gas vaporizes from the nucleus and is steadily lost in space. Outside a small region surrounding the nucleus, no molecular collisions take place (Malaise, 1970). Outside this region, the molecules interact only with the flux of solar light and solar wind, which is going either to excite them or to dissociate or ionize them, according to their individual behavior (it depends on their cross sections for collisions with ions or with photons). As far as photons are concerned, the dissociation, for wavelengths shorter than a threshold set, takes place by the binding energy of the bond to be broken; most of them are in the ultraviolet. For the same reason, most of the ionization energies correspond to the extreme ultraviolet.

The ultraviolet end of the solar spectrum is now rather well known, and is rather constant, and its flux (with due consideration to the variation of Lyman-α) can be used to predict the lifetimes of the possible molecules for photodissociation and/or photoionization. However, none of these parent molecules were known until recently—only their dissociation or ionization products. But comparison of the predicted and the observed lifetimes (Potter and Del Duca, 1964) has not been very successful so far. I have recently rediscussed all observed photometric profiles in the monochromatic light of each radical (Delsemme, 1973a). They are compared in table I with some of the possible parent molecules.

The fact that identifications remain difficult in most cases suggests that we have neglected a possible source of dissociation. The primary agent that we have neglected so far is the solar wind. However, dissociations by charge-exchange collisions with protons or electrons, leading finally to neutral molecules, are less likely than straightforward ionizations, but some are possible through a chain of several steps. Many of them are poorly known, but some have been studied (Cherednichenko, 1965). The probable existence of a shock wave in the flow of the solar wind, ahead of the comet (Alfvén, 1957, Biermann et al., 1967), changes the energy of those protons and electrons that are going to reach the vicinity of the nucleus, and may therefore affect their

Table I.—*Comparison of Observed Photometric Profiles in the Monochromatic Light of Each Radical*

	LOG OBSERVED SCALE LENGTHS (IN KM) REDUCED FOR 1 A.U.		PROPOSED IDENTIFICATION	
	Light Emitter	Its Parent	Parent	Scale Length (predicted from photodissociation)
CN	5.17 ± 0.04	4.1 ± 0.1	$CH_3—CN$	6.4 ± 0.1
			H—CN	n.a.
			CH≡C—CN	4.6 ± 0.1
C_2	4.82 ± 0.06	4.0 ± 0.2	C_2H_4	4.0 ± 0.1
			C_2H_2	5.0 ± 0.1
C_3	4.6 ± 0.3	3.3 ± 0.3	$CH_3—C≡CH$	n.a.
CH	4.5 ± 0.3	3.2 ± 0.3	CH_4	4.8 ± 0.1
OH	3.4 ± 1.0	4.7 ± 1.0	H_2O	4.7 ± 0.1
			H_2O_2	3.6 ± 0.1
H	7.3 ± 0.2	n.a. (optical depth)	H_2O	4.7 ± 0.1

charge-exchange process with the parent molecules. These phenomena are less quantitatively understood than the flux of solar photons because they are more complex. Explaining quantitatively the production rates of the ions observed in the tail meets the same difficulty for the same reasons.

Whatever the dissociation or ionization mechanism, when a radical has been produced that can be excited by the solar light, we observe its bands in emission in the cometary spectra. We usually can explain their intensities by a fluorescence mechanism, by taking into account the accurate flux of photons available in the solar spectrum at all those wavelengths that are needed for the excitation, properly corrected for the radial velocity of the comet. We have even enough high-dispersion spectra to try to explain minute differences in terms of collisional effects in the vicinity of the nucleus (Malaise, 1970) or radial velocity differences from different parts of the coma (Greenstein, 1958).

The only known exception is the 6300 Å red line of forbidden oxygen, that had to be explained by another mechanism (Biermann and Trefftz, 1964), its excitation stemming from the dissociation of its parent molecules, and not directly from the solar light.

The decays of the observed radicals can be assessed from their photometric profiles. We have not yet succeeded in explaining all of them quantitatively, but at least we believe that we understand them qualitatively, as being further dissociated or ionized by the solar light and/or by the solar wind.

The major problem that we were facing, before Comet Kohoutek, was therefore identification of the parent molecules, to bridge the gap between the

vaporization of the nucleus and the presence of neutral and ionized radicals in the coma and tail.

Circumstantial evidence suggested that *water* was controlling the vaporizations (Delsemme, 1973b) but no neutral parent molecule has ever been positively identified. After Comets Kohoutek and Bradfield, three of them have been found, namely H_2O (Jackson, Clark, and Donn, 1974, in Bradfield), HCN and CH_3CN (Ulich and Conklin, 1973; Snyder, Buhl, and Huebner, 1974, in Kohoutek), without mentioning the spectacular identification of the H_2O^+ ion in Comet Kohoutek (Herzberg and Lew, 1974).

The list of the atoms or molecules that have now been observed in comets is given in table II.

There is not much doubt left that H_2O is the parent molecule which explains the bulk of H and OH (although minor contributions to H and OH are still possible from the photodissociation of minor constituents); whereas the molecular bands of H_2O^+ do not show the bulk of water.

From the photoionization and photoionization thresholds of water, which are 12.62 and 5.114 eV, respectively (Herzberg, 1966), some 99.9 percent of H_2O should dissociate, whereas some 0.1 percent should photoionize into H_2O^+, although ionization by the solar wind could multiply the share of H_2O^+ by more than one order of magnitude.

However, the most significant discovery, whose importance has not yet been properly assessed, is probably the identification of the resonance lines of carbon and oxygen, in the far ultraviolet spectrum, by two Aerobee rockets (Feldman, Tanacs, Fastie, and Donn, 1974) (Opal and Carruthers, 1974). The C line at 1657 Å is approximately four times stronger than the 0 line at 1304 Å. The number of solar photons available is approximately 10 times as large at 1657 Å as at 1304 Å. Taking transition probabilities and lifetimes into account, Feldman and his associates think that the production rate of carbon could be of the order of 0.4 that of oxygen, suggesting a production rate of CO or CO_2 of the same order of magnitude as that of water. But CO is excluded and the presence of CO_2 is suggested by the light curve of Kohoutek (Delsemme, 1974).

In order to determine the production rate of OH, its scale length must be

Table II.—*List of Atoms or Molecules Observed in Comets*

Stable Molecules		Radicals or Atoms
Neutral	Ionized	
H_2O	H_2O^+	H, O, OH, OH^+
HCN	CO^+	CN
CH_3CN	CO_2^+	C, C_2, C_3, CH, CH^+
	N_2^+	NH, NH_2
		Metals

measured to obtain its lifetime for dissociation. Blamont and Festou (1974), using the monochromatic photograph of OH at 3090 Å, find a surprisingly short scale length of $(6 \pm 1.5) \times 10^4$ km for OH, when Kohoutek was at a heliocentric distance of 0.62 AU. (The photograph was obtained at high altitude from the Convair 900 airplane used by Ames Research Center.) Such a scale length brings up the production rate of OH in the vicinity of that of the hydrogen cloud detected in Lyman-α.

The picture that seems to emerge for the chemical constitution of the volatile fraction of the nucleus is therefore a mixture of water and carbon dioxide, as major constituents, with one or two percent of HCN and CH_3CN, and of those parent molecules (C_2H_2, C_3H_4, etc.) still needed to explain the other spectral features like C_2 and C_3.

The major departure of these findings from the early model of the nucleus, qualitatively proposed by Whipple (1951) and quantitatively discussed by Delsemme (1965), is the disappearance of those molecules, like CH_4 or NH_3, containing large amounts of hydrogen, and their substitution by molecules with less or no hydrogen. This trend is suggested by the reactions of table III. The present table III evidence (table II) points to the presence of those molecules that are rather on the right-hand side of the reactions of table III, that is, that have lost some hydrogen. Standing in contrast, a search for CH_4 in Kohoutek was unsuccessful (Roche et al., 1974). One of the major conclusions that can be drawn from the preliminary results seems to be that the redox potential of the chemical mixture found in a "new" cometary nucleus, is far away from that of the primeval cosmic mixture because of the absence, not only of the free hydrogen excess, but also of a large fraction of the hydrogen that would be bound in molecules, if the primeval cosmic mixture had cooled down to a low-temperature thermodynamic equilibrium, as exemplified by the right-hand part of figure 1. As figure 1 was drawn before the discovery of HCN and CH_3CN, these two molecules had not been considered in the equilibrium; however, the trend remains clear that at equilibrium the ratio H/O should probably be larger than 2 but not much larger than 3 in the vola-

Table III.—*Trend Toward Disappearance of Hydrogen in Molecules of Comet Nucleus*

$CH_4 + NH_3$	→	$HCN + 3H_2$	(1)
$\frac{1}{2}C_2H_4 + NH_3$	→	$HCN + 2H_2$	(2)
$C_2H_2 + NH_3$	→	$CH_3CN + H_2$	(3)
$CH_4 + H_2O$	→	$CO + 3H_2$	(4)
$CH_4 + 2H_2O$	→	$CO_2 + 4H_2$	(5)
$2NH_3$	→	$N_2 + 3H_2$	(6)

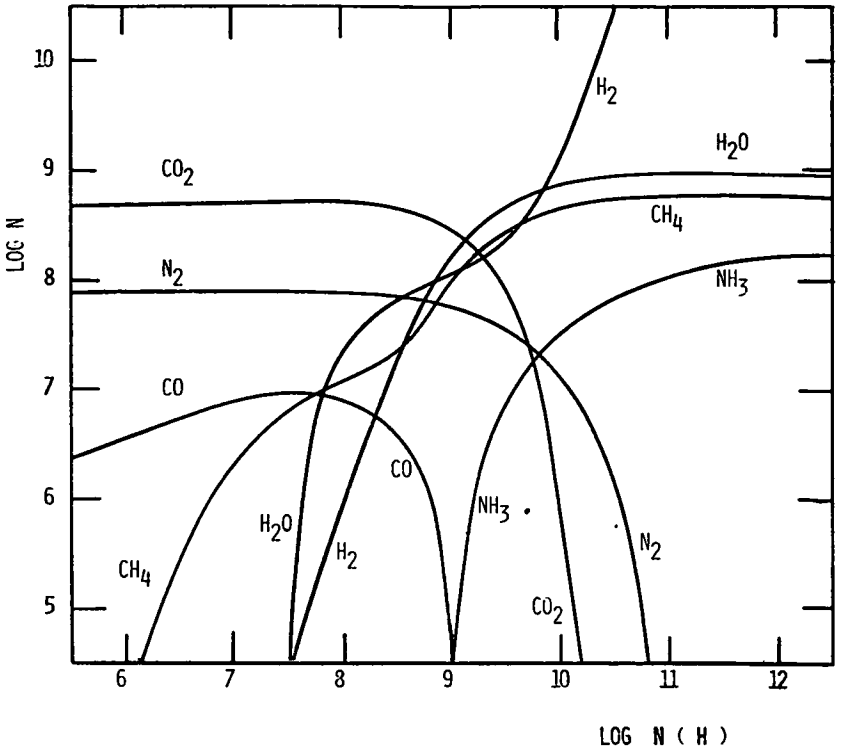

FIGURE 1.—*Thermodynamic equilibrium at 300 K and 10^{-4} bars of a cosmic mixture depleted in hydrogen only. Log N(H) represents the total amount of hydrogen available, with Log N(H) = 12 representing its cosmic abundance. Log N represents the abundance of the respective molecular species. The equilibria leading to HCN and CH_3CN have not been included.*

tile fraction, to simultaneously observe water and CO_2. This suggests a chemical fractionation in the early solar system.

Of course, thermodynamic equilibrium is unlikely to be reached and must be considered as a trend only, that can be modified by different factors influencing the reaction kinetics, as exemplified by the FTT reactions proposed by Anders to explain the hydrocarbons observed in the carbonaceous chondrites; the same type of reaction would probably be needed to explain the parent molecules of C_2 and C_3. If the cometary stuff was made in deep space, where triple molecular collisions are notoriously absent, and where the radiation field is a diluted mixture of two Planckian distributions, roughly at 100 and 10 000 K, it is clear that the thermodynamic equilibrium has no meaning, and that the depletion in hydrogen may simply translate the fact that hydrogen cannot easily stick for aeons on interstellar grains.

However, if Herbig's ideas (1970) make sense, comets as well as interstellar molecules could have been formed in the primeval solar nebula (and other primeval "stellar" nebulae) and the clues we have just found about the present redox potential of the cometary nuclei may simply mean that comets were made at the confines of the solar nebula, at a time when the T Tauri wind had already not only blown away all hydrogen excess, but also dissociated a fraction of the most abundant hydrogen-bearing molecules like CH_4 and NH_3.

ACKNOWLEDGMENT

NSF Grant GP 39259 is gratefully acknowledged.

REFERENCES

ALFVÉN, H.: 1957, Tellus 9, 92.
ANDERS, E.: 1971, Ann. Rev. Astron. Astrophys. 9, 1.
BESSEL, W.: 1836, Astron. Nachr. 13, 185, 345.
BIERMANN, L.; BROSOWSKI, B.; and SCHMIDT, H. U.: 1967, Solar Phys. 1, 254.
BIERMANN, L.; and TREFFTZ, E.: 1964, Z. Astrophys. 59, 1.
BLAMONT, J.; and FESTOU, M.: 1974, C. R. Acad. Sci. Paris 278, Ser B, 479.
BREDICHIN: 1903, quoted by R. Jaegermann in Kometenformen, St. Petersburg.
CHEREDNICHENKO: 1965, Physics of Comets and Meteors (ed., V. P. Konopleva, translated by NASA TFF–340) p. 31. U.S. Dept. of Commerce.
DELSEMME, A. H.: 1966, 13th Internat. Colloq. Astrophys., Liege, 1965, Proceedings in Mem. Soc. r. Sci. Liege 12, 77.
DELSEMME, A. H.: 1973a, Commission 15 Meeting, IAU Sydney, August 1973.
DELSEMME, A. H.: 1973b, Space Sci. Reviews 15, 89.
DELSEMME, A. H.: 1974, Proceedings, Comet Kohoutek Workshop, Huntsville, June 1974, p. 195.
DELSEMME, A. H.; and MILLER, D.: 1971a, Planet. Space Sci. 19, 1229.
DELSEMME, A. H.; and MILLER, D.: 1971b, Planet. Space Sci. 19, 1259.
DELSEMME, A. H.; and RUD, D.: 1973, Astron. Astrophys. 28, 1.
DELSEMME, A. H.; and WENGER, A.: 1970, Planet. Space Sci. 18, 709.
FELDMAN, P. D.; TAKACS, P. Z.; FASTIE, W. G.; and DONN, B.: 1974 (submitted to Science).
FINSON, M. L.; and PROBSTEIN, R. F.: 1968, Astrophys. J. 154, 327 and 353.
GREENSTEIN, J. L.: 1958, Astrophys. J. 128, 106.
HERBIG, G. H.: 1970, 16th Internat. Colloq. Astrophys., Liege 1969, Proceedings in Mem. Soc. r. Sci. Liege 19, 13.
HERZBERG, G.: 1966, Electronic Spectra of Polyatomic Molecules, p. 585. Van Nostrand, New York.
HERZBERG, G., and LEW, H.: 1974, Astron. Astrophys. 31, 123.
HUEBNER, W. F.: 1965, Z. Astrophys. 63, 22.
JACKSON, W. M.; CLARK, T.; and DONN, B.: 1974, I.A.U. Circular No. 2674, May 24, 1970.
MALAISE, D.: 1970, Astron. Astrophys. 5, 209.
OPAL, C., and CARRUTHERS, G.: 1974, IAU Circular No. 2618, January 15, 1974.
POTTER, A. E., and DEL DUCA, B.: 1964, Icarus 3, 103.
ROCHE, A. E.: TITLE, A. M.; WELLS, W. C.; BIERMANN, L.; DRAPATZ, S.

W.; MICHEL, K. W.; and COSMOVICI, C. B.: 1974 (preprint). (See also IAU Circular No. 2621, January 18, 1974.
SNYDER, L.; BUHL, D.; and HUEBNER, W.: 1974, IAU Circular No. 2616, January 8, 1974.
ULICH, B. L.; and CONKLIN, E. K.: 1973, Nature 248, 121.
WHIPPLE, F.: 1950, Astrophys. J. 111, 375.
WHIPPLE, F.: 1951, Astrophys. J. 113, 464.

IMPLICATIONS FOR MODELS AND ORIGIN OF THE NUCLEUS

FRED L. WHIPPLE
Center for Astrophysics

The new discoveries resulting from the massive observational program supported by NASA for Comet Kohoutek are both highly impressive and highly important. Schematic listings of these new discoveries appear in table I for the radio, and in table II for the ultraviolet (UV), optical, and infrared (IR) regions of the spectra. I wish to congratulate the observers for their ingenuity and tenacity.

Of vital significance is the extreme coverage of the spectrum from the far UV well into the radio regions, both before and after perihelion passage. When the reductions and theoretical analyses are complete, we will have by far the best measures ever obtained for the composition of a comet. It is too early to assume these results and attempt to evaluate them.

Critical to the understanding of the cometary nucleus is the amazing abundance of carbon, especially in the newly discovered compounds CH_3CN and HCN. Of comparable importance is the increased understanding of the "dust" content and evidence for sublimation of dust particles.

Comet Kohoutek appears to be a truly "new" comet, in the Oort-Schmidt sense. Thus I attribute its luminosity fall-off, post-perihelion versus pre-perihelion, primarily to an extremely loose consolidation of the outmost layers, compared with somewhat increased consolidation at deeper layers, several meters below the original surface. Only in an extremely porous, loose material could the highly volatile elements blow out icy grains significantly at five astronomical units' distance from the Sun. Here the material loss rate and, therefore, the luminosity must have far exceeded any theoretical expectations based on sublimation energy calculations. After perihelion, the loss rates may have more closely approximated those expected from pure gas sublimation and resultant dust grain ejection. Any calculation of the nucleus dimensions based on luminosity and mass loss are thus highly suspect, either before or after perihelion.

The following basic facts and deductions about the nature of cometary nuclei may be confidently accepted:

1. *Comets are members of the solar system.* No evidence exists for orbits of interstellar origin (Marsden and Sekanina, 1973).

2. *Comets have been stored for an unknown length of time in very large orbits in the Öpik-Oort cloud out to solar distances of tens of thousands of astronomical units (Öpik, 1932; Oort, 1950).* Perhaps 10^{11} comets with a total mass comparable to that of the Earth still remain, as Oort suggested.

3. *The basic cometary entity is a discrete nucleus (rarely, if ever, double) of kilometer dimensions consisting of ices and clathrates, including specifically* H_2O, CH_3CN, HCN, CO_2 *and probably CO.* Other parent molecules of the abundant H, C, N, and O atoms mixed in an unknown fashion with a comparable amount of heavier elements as meteoric solids must occur in comets because of the observed radicals, molecules, and ions, C, C_2, C_3, CH, CN, NH, NH_2, N_2^+, CO^+, and CH^+ (Whipple, 1950, 1951; Delsemme and Swings, 1952; Swings, 1965).

4. *Cometary meteoroids are fragile and of low density (McCrosky, 1955, 1958; Jacchia, 1955).*

5. *The comet nuclei as a whole must have never been heated much above a temperature of about 100 K for a long period of time*; otherwise new comets could not show so much activity at large solar distances (Kohoutek (1973f), for example). Possible internal heating by radioactivity, and temporary external heating by supernovae, for example, are not excluded.

6. *Comets were formed in regions of low temperature, probably much below 100 K.*

7. *Comet nuclei are generally rotating, but in no apparent systematic fashion and with unknown periods* in the range from about 3^h to a few weeks.

Table I.—*New Radio Results*

Methyl Cyanide	CH_3CN
Hydrogen Cyanide	HCN
Continuum at $\lambda = 3.7$ and 2.8 cm	
OH absorption, then emission	
CH emission	
Possible: Silicon Monoxide, SiO	
Negative Observation: NH_3, CH_4	

Table II.—*New Ultraviolet (UV) Optical, and Infrared (IR) Results*

Water Ion (Red)	H_2O^+
OH Half-Life = $8.^h5$ at 0.62 AU	
Carbon Atom (UV)	C and CO
Strong IR (many obs.)	
Anti-tail Prediction and Skylab Discovery, then IR	
Negative Observation: H_e (Far UV)	

Periods of rotation are based on nongravitational motions and the delayed jet action of the icy nucleus.

8. *The nuclei, at least of three tidally split comets, show evidence of a weak internal compressive strength on the order of 10^4 to 10^6 dyne cm^{-3} (Öpik, 1966) and evidence of little internal cohesive strength.*

9. *The surface material of active comets must be extremely friable and porous* to permit the ejection by vapor pressure of solids and ices at great solar distances. The evidence for clathrates by Delsemme and Swings (1952), coupled with the probable ejection of ice grains at great solar distances (Huebner and Weigert, 1966), supports this deduction.

The following probable limits of cometary knowledge or negative conclusions appear valid:

1. *Roughly a solar abundance of elements may reasonably be assumed for the original material from which comets evolved.* Note Millman's evidence (1972) regarding the relative abundances of Na, Mg, Ca, and Fe in cometary meteor spectra and the solar value of the $^{12}C/^{13}C$ ratio.

2. *The material in the region of comet formation (with roughly solar abundances of elements) could not have cooled slowly in quasi-equilibrium conditions from high temperatures.* The significant abundances of CO, CO_2 C_2, C_3, and now CH_3CN and HCN in comets, along with the low density and friability of the cometary meteoroids, indicate non-equilibrium cooling in which the carbon did not combine almost entirely into CH_4 and the meteoroids generally did not have time to aggregate into more coherent high-density solids before they agglomerated with ices.

3. *The existence of an original plane of formation of comets beyond some 3000 to 5000 AU appears to be unknowable.* The perturbations by passing stars would have so disturbed the orbits that the lack of evidence for a common plane in the motions of new comets tells nothing about the place or plane of origin (Oort, 1950) (note exception in 4 below).

4. *That the comets formed concurrently with the solar system some 4.6×10^9 years ago is an assumption* based on the lack of a tenable theory for more recent or current formation. The lack of evidence for a common plane of motion implies an origin remote in time or, if recent, no common plane of origin.

5. *The highly variable ratio of dust to gas observed from comet to comet proves a large variation in particle-size-distribution* but has not yet been shown to measure a true variation in the dust/gas mass ratio. P/Encke, for example, shows a low dust/gas ratio in its spectrum but has contributed enormously to the interplanetary meteoroid population.

The above evidence points conclusively to the origin of comets by the growth and agglomeration of small particles from gas (and dust?) at very low temperatures. But where? If concurrently with the origin of the solar sys-

tem (and necessarily associated with it gravitationally) two locations in space are, a priori, possible:

1. In the other regions of the forming planetary system beyond proto-Saturn (Kuiper, 1951; Whipple, 1951).

2. In interstellar clouds gravitationally associated with the forming solar system but at proto-solar distances out to a moderate fraction of a parsec, that is to say, in orbits like those in the Öpik-Oort cloud of present day comets (Whipple, 1951; McCrea, 1960; Cameron, 1961).

There can be little doubt that comets were the building blocks for the great outer planets, Uranus and Neptune. The mean densities of these planets are consistent with their origin largely from the accretion of comets, assumed to consist of the compounds possible, excluding H_2, in a solar mix of elements. This process of building Uranus and Neptune is precisely analogous to building the terrestrial planets from planetesimals. Temperature was the controlling factor, being too high within the orbit of proto-Jupiter for water to freeze. For this reason Oort's (1950) suggestion that the comets formed within the Jupiter region appears unlikely because asteroids clearly formed there. Similarly, Öpik's requirement for solid H_2 in the proto-Jupiter region appears untenable. Nevertheless, Oort's idea that comets were thrown out from the inner regions of the solar system by planetary perturbations is highly significant.

Thus the possible origin of the presently observed comets in the Uranus-Neptune region rests solely on the premise that the major planets (or proto-planets) could indeed throw the comets into stable orbits with aphelia out to some 50 000 AU or more. Approximately an Earth mass of comets in large orbits appears to be required as an end product but a hundred Earth masses may originally have been involved. Öpik (1965, 1973) is doubtful about the process unless the comets formed near Jupiter; Everhart (1973) finds it highly unlikely, while Levin (1972) provides the angular momentum from proto-Uranus and proto-Neptune by forming these planets at very great solar distances (up to 200 AU) from a very large nebular mass and drawing them into their present orbits by the ejection of comets (mostly to infinity).

Alternative 2, of forming the comets directly in the orbits of the Öpik-Oort cloud is highly attractive except for the difficulty of agglomerating kilometer-sized bodies in the low-density fragmented interstellar clouds. Such a possibility must be demonstrated before one can accept this tempting solution to the problem. Öpik (1973) finds the process quite impossible.

Let us now look to the comets themselves to see whether their structure can help us distinguish between the two possible regions of origin. Most conspicuous are the numerous carbon radicals, molecules, and ions, not in low-temperature equilibrium with excess hydrogen. The gas, if once hot, could not have cooled slowly. Note too the friability and low density (0.5 to < 0.01 g/cm^3) for meteoric "solids." We must conclude that the ices, earthy material, and clathrates are all accumulated simultaneously at very low temperatures.

More specifically, the ices, clathrates, and "solids" collected together inti-

mately in such a fashion that earthy molecules were somewhat bonded together in order to provide some degree of physical strength after the ices sublimated. Note that any sintering process to make the earthy grains coherent physically would remove the highly volatile substances necessary to provide the activity of Comet Kohoutek and other comets at great solar distances where the vapor pressure of H_2O is negligible. Thus the process of grain growth must have involved the "whisker" type of growth, commonly observed in laboratory crystals. *We can confidently visualize a comet as a complex lacy structure of "whiskers" and "snowflakes" that grew atom-by-atom and molecule-by-molecule while highly volatile molecules were trapped as clathrates.*

The temperature could have been sufficiently low for such cometary growth anywhere in space beyond perhaps 30 to 50 AU from the center of the proto-solar-system. Levin's concept (1972) of comet growth up to 200 AU is entirely consistent with such growth, as is alternative 2, fragmented interstellar clouds at far greater distances. The requirement of Safronov (1972) and Levin (1972) of excessive material (perhaps 30 to 100 times the present-day mass of Uranus and Neptune) to provide a reasonably rapid growth rate for Uranus and Nepture confirms Öpik's vehement denial that fragmented interstellar clouds may be capable of producing comets. Careful analysis of grain growth rates under imaginative sets of assumptions as to the nature and stability of such clouds is clearly needed. Note that a comet does not appear to be an aggregate of interstellar grains if, indeed, these grains are solids covered with icy mantles. Such grains might not cohere when exposed to solar radiation sublimating the ices, and thus would not provide the much larger meteoroids or the large dust particles in Comet Kohoutek.

At present then, we have no criterion to identify the unique region in space where comets formed—if, indeed, they all formed in the same general region. We need more precise knowledge concerning the identity and abundances of the more volatile parent molecules. Did CH_4, CO, Ar, or Ne, for example actually freeze out in comets? As Lewis (1972) shows, the mass percentages of such volatiles can be used as thermometers. Even the dimensions of comet nuclei are uncertain, while we have no knowledge whatsoever of their detailed structure. Are they layered? Do they contain "pockets" of ices or "pockets" of dust? How fast do they rotate? What produces comet bursts in luminosity?

Furthermore, we do not know whether comets generally or indeed any comets contain cores of asteroidal nature. It is tempting to identify many of the Apollo or Earth-orbit-crossing asteroids, as "burned out" comets. Proof of a truly asteroidal core for an old comet would require a further knowledge of the chemistry and structure of the core to ascertain whether meteoric material collected first or whether radioactive heating drove out the volatiles. Such knowledge would, of course, be invaluable in ascertaining the physical and chemical circumstances of the origin. No definitive answer is likely without such data.

It is clear that far more ground-based and space-based research on comets is

necessary. From Comet Kohoutek we see that a massive attack on one comet can produce extraordinary results. There are too many comets to permit an overall observational attack on each one; nevertheless we need to accumulate data on all observable comets. A reasonable program is to institute massive observing programs from time to time for especially selected comets, while accumulating basic data for all comets.

Only space missions to comets can give us the "quantum jump" in knowledge necessary to solve the most fundamental problems of comets. Equally, we need to study a few asteroids at their surfaces to understand their nature and to identify the sources of meteorites. Because meteorites have given us extraordinary insight regarding early conditions in the developing solar system, we can expect asteroid space missions to answer some basic direct questions, while "calibrating" our laboratory data on meteorites. Furthermore, the extraordinary successes in exploring the Moon and Mars have given us only limited data concerning the early phases of solar system formation because these bodies have been severely altered since they were originally agglomerated.

Space missions to comets and to asteroids are the essential next steps toward understanding how the solar system came into being. Such missions are entirely feasible in the present state of our space technology.

REFERENCES

CAMERON, A. G. W.: 1962, Icarus 1, 13–69.

DELSEMME, A. H.; and SWINGS, P.: 1952, Ann. d'Astrophys. 15, 1–6.

EVERHART, E.: 1973, A. J. 73, 329–337.

HEUBNER, W.; and WEIGERT, A.: 1966, Z. f. Astrophys. 64, 185–201.

JACCHIA, L. G.: 1955, Ap. J. 121, 521–527.

KUIPER, G. P.: 1951, Astrophysics (ed., J. A. Hynek) Ch. 8. McGraw-Hill Company, New York, London.

LEVIN, B.: 1972, On the Origin of the Solar System, a symposium at Nice, Centre National de la Recherche Scientifique, Paris.

LEWIS, J. S.: 1972, Icarus 16, 241.

MARSDEN, B. G.; and SEKANINA, Z.: 1973, A. J. 78, 1118–1124.

MCCREA, W. H.: 1960, Proc. Roy. Soc. (London) A256, 245–266.

MCCROSKY, R. E.: 1955, A. J. 60, 170.

MCCROSKY, R. E.: 1958, A. J. 63, 97–106.

MILLMAN, P. M.: 1972, Nobel Symposium 21, From Plasma to Planet (ed., A. Elvius) 156–166. Almquist and Wiksell, Stockholm.

OORT, J. H.: 1950, Bull. Astr. Inst. Neth. 11, 91–110.

ÖPIK, E. J.: 1932, Proc. Amer. Acad. Arts and Sci. 67, 169–183.

ÖPIK, E. J.: 1966, Irish Ast. J. 7, 141–161.

ÖPIK, E. J.: 1965, Mem. Soc. Roy. Sci. Liège, Ser. 5, 12, 523–574.

ÖPIK, E. J.: 1973, Ap. & Sp. Sci. 21, 307–398.

SAFRONOV, V. S.: 1972, Evolution of the Protoplanetary Cloud and Formation of the Earth and Planets, NASA, English Translation.

SWINGS, P.: 1965, Quarterly J. Roy. Ast. Soc. 6, 28–69.

WHIPPLE, F. L.: 1950, Ap. J. 111, 375.

WHIPPLE, F. L.: 1951, Ap. J. 113, 464–474.

SPECTROSCOPY OF THE COMA AND TAIL

GEORGE HERBIG
Lick Observatory

Rather than attempt to summarize all the important spectroscopic results presented here, I prefer to list several items in which I saw either observational confirmation of what cometary experts had assured me was true, or some puzzling observational information.

1. Direct demonstration that H_2O is ionized very near the nucleus, and that little volatile water remains in the dust that is swept back into the dust tail. I draw this conclusion from the spectrograms shown in the accompanying figure, which show a spectroscopic cut across the tails of Comet Kohoutek (1973f) and of Comet Bradfield (1974b). The line staggering (described in detail in the caption) shows that the dust continuum is accompanied by the cometary lines of NH_2 and C_2, while H_2O^+ is carried with the plasma. If any volatile H_2O remained in the dust, we should not expect such a clear separation of neutral molecules and the water ion.

2. Motions of about 5–10 km/s are seen in the nuclear regions, but far out in the plasma tail we have heard of structures that move at more than 200 km/s. If this represents material motion of the ions, one would like to know how rapidly they are accelerated to those velocities by the solar wind. On spectrograms like those shown in figure 1 of Comets Kohoutek and Bradfield, but admittedly only 1 to 3 minutes from the nucleus, there are no measurable Doppler shifts of the H_2O^+ lines with respect to the head. It is technically possible in the case of future comets to obtain spectrograms like these much farther out in the tail, so my question is "How far out must one observe in order for Doppler-shift measurements to constitute a critical test of the theory?"

3. It is presumed that H_2O is the molecular predecessor of H_2O^+, OH, OH^+, and H I. Presumably the NH_2 that was so prominent in the spectrum of Kohoutek (and of Bradfield) is the predecessor of NH. Now, CH and CH^+ also are present, but what is their parent molecule? If the photodissociation chain begins with CH_4, then CH_2 is an intermediate product. But the red bands of CH_2 have been well analyzed in the laboratory by Herzberg and Johns, so one knows precisely where to look for CH_2, but the bands are not

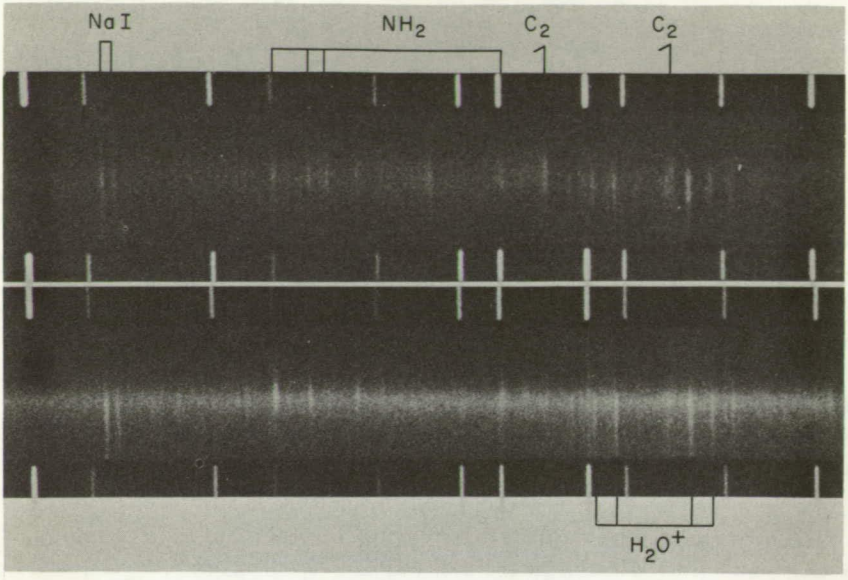

FIGURE 1.—*Above, the tail of Comet Kohoutek (1973f) about 1 minute from the head, on January 14, 1974; below, the tail of Comet Bradfield (1974b), also about 1 minute from the head, on March 20, 1974. In Comet Kohoutek, the dust and plasma tails crossed the slit at somewhat different heights, and the resulting offset of the neutral molecular lines (Ca_2, NH_2) and the dust continuum from the lines of H_2O^+ is apparent. The Na I lines may be stronger in the dust tail, but they extend across the plasma tail as well. In Comet Bradfield, the NH_2 features (and C_2 as well, although it is very weak) are strongest at the edge of the strong dust continuum, while H_2O^+ and Na I together extend into the plasma tail. The Ne I line at 6143 Å extends across the entire spectrum of Comet Bradfield; it is due to scattered artificial lighting. The original dispersion was 34 Å/mm. These plates were obtained with the coudé spectrograph of the 120-inch reflector, but fed by the 24-inch auxiliary telescope.*

found in Comet Kohoutek. Unless there is some photochemical explanation for a low abundance of CH_2 (for instance, a particularly short lifetime under cometary conditions), then one is inclined to think that CH and CH^+ may not come from methane.

4. Reference has often been made to the analogy between cometary and interstellar spectra. It is a rather good one—all the expected atoms, ions, and molecules that have been observed in interstellar absorption in the optical region occur also in cometary fluorescence (except Ti II). However, there is one large and possibly significant exception: the diffuse interstellar absorption bands were not found in Comet Kohoutek, either in emission or absorption. This may tell us something significant about the nature of cometary material.

5. Someone has suggested half-seriously that if one wanted to do experimental cometary chemistry, what a pity that apparently no spectroscopic obser-

vations were made of the urine dumps on the Apollo missions. With the dumps exposed to ultraviolet sunlight one would expect to have seen NH_2 and NH from urea, and possibly some of the products of H_2O.

PHYSICS OF THE TAIL

JOHN C. BRANDT
Laboratory for Solar Physics and Astrophysics
Goddard Space Flight Center

There are several unique things about the tail observations of Comet Kohoutek that deserve some mention, and then I will try to get into the physics of comet tails.

First of all, it is quite clear that the Skylab observations (see Gibson, this volume) through perihelion are unique and very valuable. They are particularly important in interpreting the so-called "sunward" component or the anti-tail. I am apprehensive of any attempt to use a series of observations that start out to be visual, and then suddenly become photographic. Luckily, the Skylab observations (both with the coronograph and the Nikon camera—see MacQueen and Lundquist, respectively, this volume) will enable us to bridge the gap and guard against "discovering" something that is an artifact of the observing method. The interpretation of the anti-tail, I am sure, will be rather well in hand after a few months of iteration. The basic Finson-Probstein model for dust tail formation which frees you from the old constraints of syndynames (one kind of particles emitted continuously) or synchrones (all kinds of particles emitted at one time) but allows the physics of different combinations of these, can surely account for it. The observations require particles with typical dimensions of 0.1 to 1 millimeter, a size roughly two orders of magnitude larger than the size of particles normally attributed to the dust tails (type 2) of comets. There appears to be good evidence that, for the larger particles, you must include the gravitational attraction of the nucleus (see Gary and O'Dell, this volume) and that perhaps some of the particles involved are volatile (see Sekinina, this volume). For example, sodium was observed well away from the head, at distances of about 5 million kilometers, and this may be evidence for vaporization of the volatile dust. Comet Kohoutek contained more large dust than "normal." Certainly after perihelion, and possibly before perihelion, there was less micron-size dust than normal. There was a healthy ion tail, which (personally) left nothing to be desired. There may be Skylab tail photographs (Page, this volume) that could be used to determine solar wind properties closer to the Sun than have been considered be-

fore. It will be helpful when we know the composition of the tails observed near perihelion. George Carruthers has suggested that there is a C^+ tail; this is a beautiful potential source of information.

It is too early to look for specific events in the ion tail that might be caused by features in the solar wind. Simply, the spacecraft data on solar wind velocities and densities are not fully available and when they are, we may have some exciting things to consider. On the other hand, I don't think that there is the one-to-one correlation between solar wind events and comet events that some people would like to find. Our "Swan" feature, for example, didn't have any obvious solar correlation or solar-wind correlation (see Brandt, this volume). I specifically do *not* mean the comet is not influenced by the solar wind! We have made some estimates of the magnetic field in the tail and find $\approx$ 100 γ (Brandt, this volume). If this value stands up, it will be an interesting input for the design of magnetometers for direct missions to comets.

I can give George Herbig (this volume) a tentative answer as to the spectroscopic observations needed to detect the Doppler shifts of knots, etc., in comet tails. Speeds of the order of 20–25 km/s are measured in tail features roughly $\frac{1}{2}°$ from the nucleus, and these speeds generally increase outward. Our results (Brandt, this volume) at about 7° give speeds between 200 and 250 km/s. However, mid-January would have been unprofitable because the tail axis of the comet was very close to face-on. The foreshortening factor was 1.00 during the time of our major sequence of observations. There is also an obvious tradeoff to consider, namely, that you will get better intensity but lower velocity near the head; and far from the head, you will get larger velocities, but the intensity will be down. This picture assumes that the inferred velocities of knots are real motions—and, personally, I have my doubts. The problem of the reality of the observed speeds in comet tail features is serious, and its direct resolution by spectroscopy would be a milestone.

The general question of magnetic fields in comets is confused. We go back to the suggestions by Alfvén in 1957. On his picture, the ionized particles in the cometary atmosphere load the solar wind or interplanetary magnetic field lines, which are being convected along at the solar wind speed. This process captures magnetic field from the solar wind. Whatever the origin of the cometary magnetic field, it is probably responsible for the fine structure in the rays that we see in CO^+. However, there are observations that are incompatible with this simple picture. For example, Wurm has maintained for years (and it certainly is true in Comet Morehouse) that the CO^+ is produced rather close to the nucleus, at a distance of about 500 km, and on the Sunward side. But what mechanism produces the ionization? And what force propels the CO^+ ions into and along the tail? Bessel, in his observations of Halley's Comet in 1835, describes a luminous cone which oscillated back and forth and which curled backward at the tip. It may have been a jet connected to the tail, because the tail appeared at the same time as the Sunward activity. There is a

possibility of having a magnetic field embedded in the nucleus, or recent suggestions have been made that any "seed" field (either from a small residual field or from the "captured" field) could be amplified because of turbulent, asymmetrical motions in the coma (Mendis and Alfvén, 1974). Perhaps this process builds up the structures that we know exist near the nucleus. Six months ago I thought that we understood basically how the magnetic field worked in comets. I am now convinced that we are not close to the truth, and that we have a great deal of work ahead of us.

It is fortunate that the discussion of comet tails was last in the reviews because there is no conceivable way that the physics of the tails can be effectively de-coupled from the physics of the coma and the physics of the nucleus. Surely, the CO^+ has its origin in the nucleus; and it is ionized and it passes through the coma. The cometary plasma is formed into rays which turn like a folding umbrella into the tail axis. The plasma travels down the tail and is eventually accelerated to the solar wind speed. How all this happens is simply not known at the present time.

DISCUSSIONS OF SESSION

CARRUTHERS: In your slide showing a thermodynamic equilibrium of a cosmic mixture depleted in hydrogen, CO_2 is always more abundant than CO. Is this not surprising?

DELSEMME: No, because I picked up an equilibrium temperature of 300 K. I believe that this temperature is rather representative of comet formation. Cosmothermometers indicate that accretion took place below 400 K for type I carbonaceous chondrites (Anders, 1971) *; this sets an upper limit for comets. CO_2 typically is a low-temperature product, whereas CO appears at higher temperatures (1000 K).

DONN: The equilibrium at that low temperature of 300 K is rather slow to establish. You probably freeze some non-equilibrium composition. The heliocentric distance of appearance of C_3 is very large; this seems to point out a very volatile parent molecule, which is probably related to this non-equilibrium composition.

DELSEMME: You are quite right. If I use the thermodynamic equilibrium picture, it is not because I believe in it; it is because, in the absence of enough information, it is the only possible mixture that is uniquely defined by the temperature, the pressure, and the redox ratio. I believe it is a useful standard which can indicate trends, and a careful comparison with the actual cometary snows will eventually tell us more about the deviations from equilibrium. This is what Anders has done for meteorites, and he has shown in particular that the complex hydrocarbons detected have probably been synthesized by catalytic reactions, probably due to the presence of silicate and/or iron dust. He has compared them to the Fischer-Tropsch synthesis, that uses a catalytic

* Anders, E.: 1971, Ann. Rev. Astron. Astrophys. 9, 1.

condensation of carbon monoxide and hydrogen to produce high molecular weight hydrocarbons and water:

$$n\mathrm{CO} + 2n\mathrm{H_2} \rightarrow (\mathrm{CH_2})_n + n\mathrm{H_2O}$$

Here n may vary from 2 to 20, with typically the major fraction near $n = 8$ in the industrial conditions leading to gasoline. Fischer-Tropsch-type reactions are exactly what we need to produce the hydrocarbons needed to explain C_2 and C_3 in comets. Hence, we must assume that an equilibrium near some 800–900 K has been determined quickly by the catalysis introduced by dust, and then quickly quenched to a cooler temperature. When we know the parent molecules of C_2 and C_3, and their abundances, we will try to reconstruct the whole picture.

PAGE: What is the depletion ratio for hydrogen that you require to explain the ccmetary observations?

DELSEMME: The cosmic abundance of hydrogen being log $n = 12$, I must come down in the range of log $n = 9$, which is a depletion of 1000 to 1. More accurately, I must come in the range of H/O larger than 2 but possibly smaller than 3.

LANE: With respect to specific data on the urine dump of Apollo—in a slightly similar vein, although it didn't dump urine, we had a hydrozene motor burn on Mariner 6 and 7 in interplanetary space. We very carefully examined these exhaust products and everything else. We found that the hydrogen was converted into ammonia, and the catalyst band was ejected. What we saw spectroscopically on the ultraviolet spectrometer were NH singlets, some NH triplets, N_2^+, and other things we could not identify; we did not have adequate spectral resolution. So, some of these experiments have been done and more are planned.

VOICE: We have a spectrum of a urine dump. It was attained between 1200 and 1700 Å on Apollo, with the ultraviolet spectrometer. It shows Lyman-alpha, and we had 10-Å resolution. There is some structure at longer wavelengths but I have not really been too interested until now. As far as 10-Å resolutions are concerned, it makes it very difficult to interpret; it was more like a continuum. I should add to what Lane said, that during the same period of Apollo 17, we observed fluorescence of hydrogen which was ejected during a hydrogen purge of fuel cells. That spectrum can be beautifully fit by the theory assuming that Lyman-β and Lyman-γ from the Sun produced the fluorescence; so it is a very powerful way to study what happens in this type of medium. The final comment I would have is that you cannot actually see a spectrum of urine in the vapor phase. It will probably freeze out in the vacuum of space; it's not clear what would happen.

When ammonia was released, interestingly enough, absolutely nothing was seen. That may still be significant. I don't remember the details of that operation.

DUBIN: Is water a dominant or well-known molecule in interstellar observations?

HERBIG: In dense clouds, yes. Not in interstellar space at large.

DUBIN: The question arises concerning the missing hydrogen: In the argument that Fred Whipple gave of the cooled condensation of comets, is it not possible that the hydroxyl or the oxygen atoms are captured at first, and then and then only can the hydrogen be captured chemically, thereby giving you the ratio you want? In other words, hydrogen by itself is not capturable unless you drop the temperatures of the comet to the Öpik value of 5 K. Any comments on that?

WHIPPLE: If I understand it correctly, in the dense clouds of interstellar space you have water but you also have all this carbon around (CO and many other forms). I think it is simply that you cannot avoid the hydrogen. You know that the H_2 is there in those clouds, even though the atom is often missing. I don't believe we can ever go to Delsemme's three hydrogen atoms. I don't think there is any place in interstellar space where so little hydrogen exists. For some reason, carbon likes carbon better than it likes hydrogen out there. Possibly it is the ultraviolet dissociation of the molecules from the high temperatures regime that causes the effect, but I should think there would be a lack of high-energy radiation. So there is something missing in our theory. I cannot answer your question, but we have evidence that refractory materials are tied up in the dust in these dense clouds. The calcium and lithium and so forth are missing from the gas, but there is still carbon around. And so it is a place to make comets. I can't see much difference between the outer fringes of the solar system, where there is no good reason to think that the temperature ever got very high, and interstellar clouds, except for the difference in density and the fall of material to a plane. I am quite happy with comets' being made in fragmented interstellar clouds near the solar nebula, if someone can figure out a method to form them large enough.

CARRUTHERS: Hydrogen and CO are the most abundant molecules in interstellar space, and it is well known there is a great deal of formaldehyde (H_2CO) in interstellar space in its combinations. In view of the fact that formaldehyde is not volatile and therefore is more likely to be present in comets, I am wondering if the upper limits on formaldehyde are sufficiently good to rule it out as the parent molecules of CO and possibly other molecules.

WHIPPLE: I wish I knew the answer.

DELSEMME: I think not, but I am not sure.

DONN: Whipple has emphasized the presence of carbon in comets, I think I would like to repeat a statement that Urey made several times when we worked together—that in comets you find carbon simultaneously in the oxidized (CO, CO_2) and reduced (CH) form. To him, this is very puzzling.

WHIPPLE: I remember that only too well, in the early days when I was talking about methane and ammonia. He said you just can't have them at the same time. And it is beginning to look as if he were absolutely right. I didn't deny it then; I just didn't know what the answer was, and still don't.

DELSEMME: The presence of CO_2^+ and N_2^+ in the ion tails (if they come from the ionization of the neutral molecules) simultaneously with water, implies a redox state in the nuclear snows set by log N(H) $\doteq$ 9 in my equilibrium diagram. This can be changed only if we are very far away from thermal equilibrium, which is certainly not to be excluded.

DONN: How much CH would you get in your equilibrium?

DELSEMME: CH itself is a radical that is not present in a thermodynamic equilibrium at 300 K. We should know its parent molecule. If it were CH_4, we would have at log N(H) = 9, approximately 60 percent CO_2, 30 percent H_2O, and 10 percent CH_4. This amount of CH_4 is small but not negligible, and it could explain CH; if higher hydrocarbons have been synthesized by a Fischer-Tropsch-type reaction, their total amount would remain in the same approximate abundance, producing the same amount of CH. My diagram fails to predict the amount of HCN only because it was computed before the discovery of HCN, and the reactions leading to HCN were (wrongly) neglected in the diagram. The HCN curve should approximately come in between N_2 and NH_3; HCN typically is a high-temperature product acting like CO, and not very important in a cool equilibrium.

HUEBNER: A few days ago, we computed a chemical equilibrium with 10 percent more oxygen than carbon, otherwise a rather standard cosmic mixture. At 10^{-4} atmosphere but at a higher temperature of 800°, the result was acetylene and HCN.

DELSEMME: This is a classical way of making acetylene in the industry. You heat methane or any other paraffin or olefin up to the 1000 K to 1500 K range and you make acetylene with a high yield. But you have to quench the

high-temperature equilibrium very fast because you also make higher acetylenes (like methylacetylene, ethylacetylene, diacetylene, allene, etc.) more slowly, and also many higher aromatics and much soot.

It happened that I developed such a technology in an industrial research laboratory in the late 1940's and early 1950's, and I still remember that 90 percent of the equilibrium yield was reached in 2 to 3 milliseconds at 1500 K for acetylene, whereas the higher hydrocarbons and soot took 10 to 100 times as long to appear in sizable yields. This was done at atmospheric pressure, without catalyst, the heat being brought by partial combustion of the hydrocarbons in oxygen. I suggested in 1952 (Colloque International d'Astrophysique, Liege, September 19–21, 1952, page 196 of the proceedings) that the quenching of such an equilibrium would give the molecules needed to explain the C_2 and C_3 observed in comets. In the same way, the fast quenching of a hot mixture containing nitrogen would yield a large amount of HCN. The production rate of HCN compared with that of water will tell presently whether the abundance of HCN requires non-equilibrium conditions.

KELLER: How certain are we that those species like CN, CH really do have or must have a parent molecule? Nobody doubts it. Are we completely certain about that, or can they be particles embedded in ice also?

WHIPPLE: My only comment on that is that some 20 years ago Urey and Donn suggested that radicals were indeed present in comets and produced activity like cometary bursts. When the radicals were heated up a little by sunlight, they produced exothermic chemical reactions. Is that a dead theory?

DONN: I think you might be able to get in a matrix at low temperature about 1 percent. Now at 1 percent the radicals are sufficient to account for this thing, if it is possible that some of these species may exist in radicals. If you need any more than that, except in a new comet, you have trouble seeing anything.

WHIPPLE: I was very impressed with George Herbig's spectra. We can only turn to observations for the final answers. But the interpretation is always a problem. I was not quite sure but I thought quite a few of those ions started right in the middle of the dust layer and then went into the tail. I hope he will do some photometry on that spectrum to find out for sure whether they might not originate in the dust.

APPENDIX 1. LIST OF PARTICIPANTS

T. F. Adams, Yerkes Observatory
B. Andrew, National Research Council of Canada
H. L. Atkins, NASA, Marshall Space Flight Center
L. Avery, National Research Council of Canada
R. J. Barry, Bendix Corporation, Denver
L. F. Belew, NASA, Marshall Space Flight Center
M. J. Belton, Kitt Peak National Observatory
J. E. Blamont, Centre National de la Recherche Scientifique d'Études Spatiales
J. J. Brainerd, University of Alabama, Huntsville
J. C. Brandt, NASA, Goddard Space Flight Center
F. M. Cameron, NASA, Marshall Space Flight Center
G. R. Carruthers, Naval Research Laboratory
E. J. Chaisson, Center for Astrophysics
J. I. Clark, USA, Redstone Arsenal
J. W. Clark, NASA, Marshall Space Flight Center
K. S. Clifton, NASA, Marshall Space Flight Center
H. J. Coons, NASA, Marshall Space Flight Center
P. D. Craven, NASA, Marshall Space Flight Center
J. Crovisier, Observatoire de Meudon
A. C. Danks, University of Texas
G. E. Daniels, NASA, Marshall Space Flight Center
W. A. Darbro, NASA, Marshall Space Flight Center
A. Deepak, NASA, Marshall Space Flight Center
A. C. deLoach, NASA, Marshall Space Flight Center
A. H. Delsemme, University of Toledo
W. A. Deutschman, Center for Astrophysics
B. Donn, NASA, Goddard Space Flight Center
J. Drake, Princeton University Observatory
M. Dryer, NOAA–ERL Space Environment Laboratory
M. Dubin, NASA Headquarters
B. J. Duncan, NASA, Marshall Space Flight Center
W. H. Ealy, NASA, Marshall Space Flight Center
T. D. Fay, NASA, Marshall Space Flight Center
P. D. Feldman, Johns Hopkins University
S. F. Fields, NASA, Marshall Space Flight Center
H. B. Floyd, NASA, Marshall Space Flight Center
J. A. Fountain, NASA, Marshall Space Flight Center
W. F. Fountain, NASA, Marshall Space Flight Center

L. D. Frederick, NASA, Marshall Space Flight Center
G. A. Gary, NASA, Marshall Space Flight Center
E. G. Gibson, NASA, Johnson Space Center
F. J. Giovane, Dudley Observatory
F. M. Graham, NASA, Marshall Space Flight Center
T. E. Hanes, NASA Headquarters
G. A. Harvey, NASA, Langley Research Center
A. Heiser, Dyer Observatory
R. V. Hembree, NASA, Marshall Space Flight Center
K. G. Henize, NASA, Johnson Space Center
G. Herbig, Lick Observatory
R. Hermann, University of Alabama—Huntsville
R. W. Hobbs, NASA, Goddard Space Flight Center
W. F. Huebner, Los Alamos Scientific Laboratory
D. A. Huppler, University of Wisconsin
R. Ise, NASA, Marshall Space Flight Center
B. J. Jambor, Martin Marietta Corporation, Denver
J. Jensen, Martin Marietta Corporation, Denver
H. U. Keller, University of Colorado
C. T. Kowal, California Institute of Technology
S. Kumar, Kitt Peak National Observatory
A. L. Lane, Jet Propulsion Laboratory
H. H. Lane, National Science Foundation
D. L. Lind, NASA, Johnson Space Center
W. R. Lucas, NASA, Marshall Space Flight Center
C. A. Lundquist, NASA, Marshall Space Flight Center
R. J. Mackin, Jr., Jet Propulsion Laboratory
S. P. Maran, NASA, Marshall Space Flight Center
M. J. Mayo, Altair Scientifics, Inc.
R. H. McElligott, Martin Marietta Aerospace, Huntsville
R. R. Meier, Naval Research Laboratory
D. D. Meisel, State University of New York—Geneseo
D. A. Mendis, University of California, San Diego
J. E. Michlovic, NASA, Marshall Space Flight Center
F. D. Miller, University of Michigan
R. W. Murphy, NASA, Marshall Space Flight Center
L. Newman, University of Alabama, Huntsville
R. J. Naumann, NASA, Marshall Space Flight Center
E. P. Ney, University of Minnesota
K. T. Nock, Jet Propulsion Laboratory
C. R. O'Dell, NASA, Marshall Space Flight Center
C. B. Opal, Naval Research Laboratory
E. J. Öpik, University of Maryland
R. P. Page, NASA, Marshall Space Flight Center
T. L. Page, NASA, Johnson Space Center
H. Pataschnick, Dudley Observatory
R. P. Rice, NASA, Marshall Space Flight Center
G. H. Rieke, University of Arizona
G. R. Riegler, Bendix Aerospace Systems, Ann Arbor
J. B. Plaster, USA, Redstone Arsenal
A. E. Roche, Lockheed Palo Alto Research Laboratory
G. Rupprecht, Bendix Corporation, Denver

S. W. Sauer, Martin Marietta, Huntsville
G. F. Schmitz, USA, Redstone Arsenal
E. S. Schorsten, NASA, Marshall Space Flight Center
S. R. Schrock, Martin Marietta Aerospace, Denver
Z. Sekenina, Center for Astrophysics
W. H. Sieber, NASA, Marshall Space Flight Center
W. C. Snoddy, NASA, Marshall Space Flight Center
L. E. Snyder, University of Colorado
K. J. Staas, Martin Marietta—Huntsville
E. S. Stuhlinger, NASA, Marshall Space Flight Center
G. E. Thomas, University of Colorado
N. H. Tolk, Bell Laboratories
B. L. Ulich, National Radio Astronomy Observatory
J. F. Valek, NASA, Kennedy Space Center
J. H. Waite, NASA, Marshall Space Flight Center
R. M. Wilson, NASA, Marshall Space Flight Center
W. Wamsteker, NASA, Marshall Space Flight Center
H. E. R. Watson, Northrop Services
J. R. Watkins, NASA, Marshall Space Flight Center
T. J. Wdowiak, NASA, Marshall Space Flight Center
D. W. Weedman, Dyer Observatory
P. A. Wehinger, Center for Astrophysics
G. S. West, NASA, Marshall Space Flight Center
W. C. Wells, Lockheed Palo Alto Research Laboratory
F. L. Whipple, Center for Astrophysics
C. E. Winkler, NASA, Marshall Space Flight Center
B. P. Woods, Bendix Corporation, Huntsville
S. T. Wu, University of Alabama, Huntsville
C. M. Yeates, Jet Propulsion Laboratory

APPENDIX 2. AUTHOR INDEX

C. Arpigny—137
H. L. Atkins—161
J. A. Ball—135
M. J. S. Belton—35
G. F. Benedict—129
R. A. Berg—153
J. H. Black—135
J. Blamont—81
F. Biraud—97
J. D. Bohlin—113
J. C. Brandt—15, 185, 237
A. L. Broadfoot—35
G. Bourgois—97
D. Buhl—123
G. R. Carruthers—107
E. J. Chaisson—135, 189
E. K. Conklin—119
C. B. Cosmovici—155
G. Courtes—161
P. D. Craven—183
J. Crovisier—97
A. C. Danks—137
A. H. Delsemme—195, 219
W. A. Deutschman—193
B. Donn—109
J. F. Drake—95
S. Drapatz—155
W. G. Fastie—109
P. D. Feldman—109
M. Festou—81
R. Fillit—97
G. P. Garmire—159
G. A. Gary—27
E. Gérard—97
E. G. Gibson—3
J. T. Gosling—19
G. A. Harvey—83
K. G. Henize—129
R. V. Hembree—183
G. Herbig—233
E. Hildner—19
R. W. Hobbs—185
W. F. Huebner—123, 145
D. H. Huppler—77
R. P. Ingalls—189
B. J. Jambor—209
E. B. Jenkins—95
I. Kazes—97
H. U. Keller—19, 113
C. Kowal—31
S. Kumar—35
M. Laget—161
D. L. Lambert—137
A. L. Lane—87, 129
T. A. Lee—175
A. E. Lilley—135
F. J. Low—175
C. A. Lundquist—183
S. P. Maran—185
R. M. MacQueen—19
M. B. McElroy—35
R. R. Meier—107
D. D. Meisel—153
F. H. Mies—87, 101
K. W. Michel—155
R. H. Munro—19
E. P. Ney—167
C. R. O'Dell—27
C. B. Opal—107
E. J. Öpik—205
T. L. Page—37
S. B. Parsons—129
H. Penfield—135
A. I. Poland—19
D. K. Prinz—107
G. R. Riegler—159

G. H. Rieke—175
F. L. Roesler—77
A. E. Roche—155
A. E. E. Rogers—189
C. L. Ross—19
F. Scherb—77
H. U. Schmidt—19
I. I. Shapiro—189
Z. Sekanina—21
A. N. Stockton—87
L. E. Snyder—123
K. S. K. Swamy—185
P. Z. Takacs—109
R. Tousey—113
J. T. Trauger—77
B. L. Ulich—119
A. Vuillemin—161
W. J. Webster, Jr.—185
P. A. Wehinger—103
W. C. Wells—155
F. L. Whipple—227
W. Wisniewski—175
J. D. Wray—129
S. Wyckoff—103

Comet Kohoutek Workshop Participants, Marshall Space Flight Center, June 13–14, 1974.

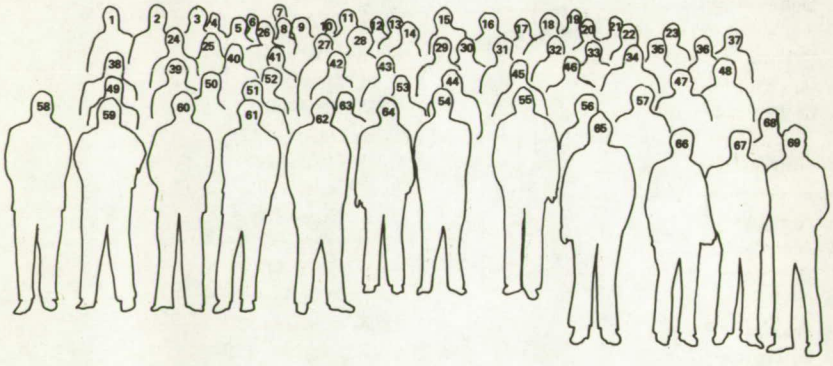

APPENDIX 3. COMET KOHOUTEK WORKSHOP PARTICIPANTS

PHOTOGRAPH IDENTIFICATION

1. B. Andrew
2. P. D. Feldman
3. C. B. Opal
4. G. R. Carruthers
5. M. J. S. Belton
6.
7. J. Jensen
8. G. Thomas
9. W. Wamsteker
10. J. A. Fountain
11. Z. Sekanina
12. J. E. Michlovic
13. E. P. Ney
14. H. L. Atkins
15. H. Patashnick
16. G. Rupprecht
17. W. F. Fountain
18. T. J. Wdowiak
19. W. F. Huebner
20. L. Avery
21. L. E. Snyder
22. A. E. Roche
23. F. D. Miller
24. G. Herbig
25. G. Schmitz
26. A. Deepak
27.
28. J. Crovisier
29. C. R. O'Dell
30. P. D. Craven
31. J. C. Brandt
32. R. J. Mackin, Jr.
33. A. Lane
34. H. U. Keller
35. J. Drake
36. J. E. Blamont
37. J. F. Valek
38. D. A. Mendis
39. W. A. Deutschman
40. B. Donn
41. R. Hermann
42. N. H. Tolk
43. P. A. Wehinger
44. C. A. Lundquist
45. D. D. Meisel
46. B. J. Jambor
47. W. C. Snoddy
48. F. J. Giovane
49. R. W. Hobbs
50. A. H. Delsemme
51. E. S. Stuhlinger
52. S. P. Maran
53. T. E. Hanes
54. F. L. Whipple
55. G. Schmidt
56. G. R. Riegler
57. A. C. deLoach
58. R. J. Barry
59. S. Fields
60. A. C. Danks
61. E. Chaisson
62. T. L. Page
63. M. Dryer
64. M. Dubin
65. B. L. Ulich
66. E. G. Gibson
67. H. H. Lane
68. C. T. Kowa
69. G. A. Gary

APPENDIX 4. COMPREHENSIVE EPHEMERIS OF COMET KOHOUTEK (1973f)

This ephemeris is based on the orbital calculations by Brian Marsden (Smithsonian Astrophysical Observatory) as published in International Astronomical Union Circular No. 2684. The observations included were over the interval from January 28, 1973, to March 16, 1974. The ephemeris computation was made by D. K. Yeomans (Computer Sciences Corporation) and was based on a two-body determination. It is included here as a cross-reference. For convenience, the ephemeris is tabulated for the interval from January 29, 1974, to July 31, 1974.

The ephemeris is based on the following ecliptic (1950.0) orbital elements.

T = 1973 Dec 28/10.3 Hr (JD 2442044.93067)
i = 14.2969°
Ω = 257.76560°
ω = 37.82380°
e = 1.0000078
q = 0.1424249 AU

Definitions:

J. D. Julian Day
R. A. Right Ascension*
Dec. Declination*
Delta Distance from Earth in Astronomical Units
R Distance from Sun in Astronomical Units
Theta Angular distance of comet from the Sun, as seen from Earth
Beta Angular distance of Sun from the Earth, as seen from the comet
Lat Ecliptic Latitude (1950)
Long Ecliptic Longitude (1950)

*R. A. and Dec. (1950) indicates equator and equinox of 1950.
R. A. and Dec. (date) indicates equator and equinox of date.

TWO BODY EPHEMERIS FOR COMET (1973F) KOHOUTEK

YR	MN	DY	HR	J.D.	R.A. 1950.0	DEC.	R.A. DATE	DEC.	DELTA	R	THETA	BETA	LAT	LONG
1973	1	29	0.0	2441711.5	8 53.428	2 10.78	8 54.624	2 5.48	4.1981	5.1517	163.91	3.04	-12.0	133.9
1973	1	30	0.0	2441712.5	8 52.602	2 13.36	8 53.798	2 8.07	4.1867	5.1411	164.35	2.96	-12.0	133.9
1973	1	31	0.0	2441713.5	8 51.770	2 16.02	8 52.967	2 10.75	4.1736	5.1306	164.70	2.90	-12.0	133.9
1973	2	1	0.0	2441714.5	8 50.933	2 18.76	8 52.131	2 13.51	4.1619	5.1200	164.96	2.86	-12.0	134.0
1973	2	2	0.0	2441715.5	8 50.092	2 21.58	8 51.290	2 16.35	4.1506	5.1093	165.13	2.84	-12.0	134.0
1973	2	3	0.0	2441716.5	8 49.247	2 24.47	8 50.446	2 19.27	4.1395	5.0987	165.20	2.83	-12.0	134.0
1973	2	4	0.0	2441717.5	8 48.399	2 27.44	8 49.598	2 22.26	4.1289	5.0881	165.17	2.84	-12.0	134.0
1973	2	5	0.0	2441718.5	8 47.548	2 30.49	8 48.748	2 25.32	4.1186	5.0775	165.04	2.87	-12.0	134.0
1973	2	6	0.0	2441719.5	8 46.694	2 33.61	8 47.895	2 28.46	4.1085	5.0668	164.81	2.92	-12.0	134.1
1973	2	7	0.0	2441720.5	8 45.839	2 36.79	8 47.039	2 31.67	4.0989	5.0563	164.49	2.99	-12.0	134.1
1973	2	8	0.0	2441721.5	8 44.982	2 40.05	8 46.183	2 34.95	4.0896	5.0455	164.08	3.07	-12.0	134.1
1973	2	9	0.0	2441722.5	8 44.124	2 43.38	8 45.325	2 38.30	4.0806	5.0348	163.59	3.17	-12.0	134.1
1973	2	10	0.0	2441723.5	8 43.265	2 46.77	8 44.467	2 41.71	4.0720	5.0241	163.03	3.29	-12.0	134.1
1973	2	11	0.0	2441724.5	8 42.406	2 50.22	8 43.609	2 45.18	4.0637	5.0134	162.40	3.41	-12.0	134.2
1973	2	12	0.0	2441725.5	8 41.548	2 53.74	8 42.752	2 48.72	4.0558	5.0027	161.71	3.55	-12.0	134.2
1973	2	13	0.0	2441726.5	8 40.691	2 57.31	8 41.895	2 52.32	4.0482	4.9920	160.97	3.70	-12.0	134.2
1973	2	14	0.0	2441727.5	8 39.835	3 0.95	8 41.040	2 55.97	4.0409	4.9812	160.18	3.85	-12.0	134.2
1973	2	15	0.0	2441728.5	8 38.981	3 4.64	8 40.186	2 59.68	4.0339	4.9705	159.35	4.02	-12.0	134.3
1973	2	16	0.0	2441729.5	8 38.129	3 8.38	8 39.335	3 3.45	4.0273	4.9597	158.49	4.19	-12.0	134.3
1973	2	17	0.0	2441730.5	8 37.280	3 12.18	8 38.487	3 7.27	4.0211	4.9489	157.59	4.37	-12.0	134.3
1973	2	18	0.0	2441731.5	8 36.434	3 16.02	8 37.642	3 11.13	4.0151	4.9382	156.66	4.55	-12.0	134.3
1973	2	19	0.0	2441732.5	8 35.592	3 19.92	8 36.801	3 15.05	4.0095	4.9274	155.71	4.73	-12.0	134.3
1973	2	20	0.0	2441733.5	8 34.755	3 23.85	8 35.963	3 19.01	4.0042	4.9166	154.74	4.92	-12.0	134.4
1973	2	21	0.0	2441734.5	8 33.921	3 27.84	8 35.131	3 23.01	3.9992	4.9057	153.75	5.12	-12.0	134.4
1973	2	22	0.0	2441735.5	8 33.093	3 31.86	8 34.303	3 27.06	3.9945	4.8949	152.74	5.31	-12.0	134.4
1973	2	23	0.0	2441736.5	8 32.270	3 35.93	8 33.481	3 31.14	3.9902	4.8841	151.72	5.51	-12.0	134.4
1973	2	24	0.0	2441737.5	8 31.454	3 40.03	8 32.665	3 35.27	3.9861	4.8732	150.69	5.71	-12.0	134.5
1973	2	25	0.0	2441738.5	8 30.643	3 44.16	8 31.856	3 39.42	3.9824	4.8623	149.64	5.91	-12.0	134.5
1973	2	26	0.0	2441739.5	8 29.840	3 48.33	8 31.053	3 43.61	3.9789	4.8515	148.58	6.11	-12.0	134.5
1973	2	27	0.0	2441740.5	8 29.044	3 52.53	8 30.257	3 47.83	3.9758	4.8406	147.52	6.31	-12.0	134.5

1973	2	28	0.0	2441741.5	8	28.255	3	56.76	8	29.470	3	52.08	3.9729	4.8297	146.45	6.51	-12.0	134.5
1973	3	1	0.0	2441742.5	8	27.476	4	1.01	8	28.690	3	56.35	3.9704	4.8188	145.37	6.71	-12.0	134.6
1973	3	2	0.0	2441743.5	8	26.704	4	5.29	8	27.920	4	0.65	3.9681	4.8078	144.29	6.91	-12.0	134.6
1973	3	3	0.0	2441744.5	8	25.941	4	9.69	8	27.158	4	4.97	3.9662	4.7969	143.20	7.11	-12.1	134.6
1973	3	4	0.0	2441745.5	8	25.188	4	13.90	8	26.406	4	9.30	3.9645	4.7860	142.11	7.31	-12.1	134.6
1973	3	5	0.0	2441746.5	8	24.445	4	18.23	8	25.663	4	13.65	3.9630	4.7750	141.01	7.51	-12.1	134.7
1973	3	6	0.0	2441747.5	8	23.712	4	22.58	8	24.931	4	18.02	3.9619	4.7640	139.92	7.71	-12.1	134.7
1973	3	7	0.0	2441748.5	8	22.990	4	26.93	8	24.210	4	22.39	3.9610	4.7530	138.82	7.90	-12.1	134.7
1973	3	8	0.0	2441749.5	8	22.279	4	31.30	8	23.500	4	26.78	3.9604	4.7420	137.72	8.10	-12.1	134.7
1973	3	9	0.0	2441750.5	8	21.579	4	35.67	8	22.801	4	31.17	3.9600	4.7310	136.62	8.29	-12.1	134.8
1973	3	10	0.0	2441751.5	8	20.891	4	40.04	8	22.113	4	35.56	3.9598	4.7200	135.51	8.48	-12.1	134.8
1973	3	11	0.0	2441752.5	8	20.215	4	44.42	8	21.438	4	39.95	3.9600	4.7090	134.41	8.67	-12.1	134.8
1973	3	12	0.0	2441753.5	8	19.552	4	48.80	8	20.775	4	44.35	3.9603	4.6979	133.31	8.85	-12.1	134.8
1973	3	13	0.0	2441754.5	8	18.901	4	53.17	8	20.125	4	48.74	3.9609	4.6869	132.21	9.04	-12.1	134.9
1973	3	14	0.0	2441755.5	8	18.263	4	57.54	8	19.488	4	53.13	3.9617	4.6758	131.11	9.22	-12.1	134.9
1973	3	15	0.0	2441756.5	8	17.638	5	1.90	8	18.863	4	57.50	3.9627	4.6647	130.01	9.40	-12.1	134.9
1973	3	16	0.0	2441757.5	8	17.026	5	6.25	8	18.252	5	1.87	3.9639	4.6536	128.91	9.57	-12.1	134.9
1973	3	17	0.0	2441758.5	8	16.428	5	10.60	8	17.655	5	6.23	3.9654	4.6425	127.82	9.75	-12.1	134.9
1973	3	18	0.0	2441759.5	8	15.844	5	14.93	8	17.072	5	10.58	3.9670	4.6314	126.72	9.92	-12.1	135.0
1973	3	19	0.0	2441760.5	8	15.274	5	19.24	8	16.502	5	14.91	3.9688	4.6202	125.63	10.09	-12.1	135.0
1973	3	20	0.0	2441761.5	8	14.718	5	23.54	8	15.947	5	19.22	3.9709	4.6091	124.54	10.25	-12.1	135.0
1973	3	21	0.0	2441762.5	8	14.176	5	27.82	8	15.407	5	23.52	3.9731	4.5979	123.45	10.41	-12.1	135.0
1973	3	22	0.0	2441763.5	8	13.650	5	32.09	8	14.881	5	27.80	3.9754	4.5868	122.37	10.57	-12.1	135.1
1973	3	23	0.0	2441764.5	8	13.138	5	36.33	8	14.369	5	32.05	3.9780	4.5756	121.28	10.73	-12.1	135.1
1973	3	24	0.0	2441765.5	8	12.641	5	40.54	8	13.873	5	36.28	3.9807	4.5644	120.20	10.88	-12.1	135.1
1973	3	25	0.0	2441766.5	8	12.159	5	44.74	8	13.392	5	40.49	3.9836	4.5532	119.13	11.03	-12.1	135.2
1973	3	26	0.0	2441767.5	8	11.693	5	48.90	8	12.927	5	44.67	3.9866	4.5419	118.05	11.18	-12.1	135.2
1973	3	27	0.0	2441768.5	8	11.242	5	53.04	8	12.476	5	48.82	3.9898	4.5307	116.98	11.32	-12.1	135.2
1973	3	28	0.0	2441769.5	8	10.806	5	57.15	8	12.042	5	52.94	3.9932	4.5194	115.91	11.46	-12.1	135.2
1973	3	29	0.0	2441770.5	8	10.387	6	1.22	8	11.623	5	57.03	3.9966	4.5082	114.85	11.59	-12.1	135.3
1973	3	30	0.0	2441771.5	8	9.983	6	5.27	8	11.220	6	1.08	4.0002	4.4969	113.78	11.73	-12.1	135.3
1973	3	31	0.0	2441772.5	8	9.596	6	9.28	8	10.833	6	5.10	4.0039	4.4856	112.73	11.86	-12.1	135.3

1973	4	1	0.0	2441773.5	8	9.224	6	13.25	8	10.462	6	9.08	4.0078	4.4743	111.67	11.98	-12.1 135.3
1973	4	2	0.0	2441774.5	8	8.869	6	17.19	8	10.108	6	13.03	4.0117	4.4629	110.68	12.10	-12.1 135.4
1973	4	3	0.0	2441775.5	8	8.530	6	21.08	8	9.770	6	16.93	4.0158	4.4516	109.57	12.22	-12.2 135.4
1973	4	4	0.0	2441776.5	8	8.207	6	24.94	8	9.448	6	20.80	4.0199	4.4403	108.63	12.33	-12.2 136.4
1973	4	5	0.0	2441777.5	8	7.901	6	28.75	8	9.142	6	24.62	4.0242	4.4289	107.49	12.44	-12.2 135.4
1973	4	6	0.0	2441778.5	8	7.611	6	32.52	8	8.853	6	28.40	4.0285	4.4175	106.46	12.56	-12.2 136.6
1973	4	7	0.0	2441779.5	8	7.338	6	36.25	8	8.580	6	32.13	4.0329	4.4061	105.42	12.65	-12.2 135.5
1973	4	8	0.0	2441780.5	8	7.081	6	39.93	8	8.324	6	35.82	4.0374	4.3947	104.40	12.76	-12.2 136.6
1973	4	9	0.0	2441781.5	8	6.841	6	43.56	8	8.085	6	39.46	4.0419	4.3833	103.37	12.85	-12.2 135.6
1973	4	10	0.0	2441782.5	8	6.617	6	47.15	8	7.862	6	43.05	4.0465	4.3718	102.36	12.94	-12.2 136.6
1973	4	11	0.0	2441783.5	8	6.410	6	50.69	8	7.655	6	46.60	4.0512	4.3604	101.34	13.02	-12.2 135.6
1973	4	12	0.0	2441784.5	8	6.219	6	54.18	8	7.465	6	50.09	4.0559	4.3489	100.33	13.11	-12.2 136.6
1973	4	13	0.0	2441785.5	8	6.045	6	57.62	8	7.291	6	53.53	4.0607	4.3374	99.32	13.19	-12.2 135.7
1973	4	14	0.0	2441786.5	8	5.887	7	1.00	8	7.134	6	56.93	4.0655	4.3260	98.32	13.26	-12.2 136.7
1973	4	15	0.0	2441787.5	8	5.745	7	4.34	8	6.993	7	0.26	4.0703	4.3144	97.32	13.34	-12.2 135.7
1973	4	16	0.0	2441788.5	8	5.620	7	7.62	8	6.868	7	3.55	4.0751	4.3029	96.33	13.40	-12.2 136.7
1973	4	17	0.0	2441789.5	8	5.510	7	10.85	8	6.759	7	6.75	4.0800	4.2914	95.34	13.47	-12.2 135.8
1973	4	18	0.0	2441790.5	8	5.417	7	14.03	8	6.666	7	9.96	4.0849	4.2798	94.35	13.53	-12.2 136.8
1973	4	19	0.0	2441791.5	8	5.340	7	17.15	8	6.590	7	13.08	4.0898	4.2683	93.37	13.59	-12.2 135.8
1973	4	20	0.0	2441792.5	8	5.279	7	20.21	8	6.530	7	16.15	4.0947	4.2567	92.39	13.64	-12.2 136.9
1973	4	21	0.0	2441793.5	8	5.235	7	23.22	8	6.485	7	19.16	4.0996	4.2451	91.42	13.69	-12.2 135.9
1973	4	22	0.0	2441794.5	8	5.206	7	26.18	8	6.457	7	22.11	4.1045	4.2334	90.45	13.74	-12.2 136.9
1973	4	23	0.0	2441795.5	8	5.193	7	29.07	8	6.445	7	25.01	4.1094	4.2218	89.49	13.78	-12.2 136.0
1973	4	24	0.0	2441796.5	8	5.195	7	31.91	8	6.448	7	27.84	4.1142	4.2102	88.53	13.82	-12.2 136.0
1973	4	25	0.0	2441797.5	8	5.214	7	34.69	8	6.467	7	30.62	4.1191	4.1985	87.57	13.85	-12.2 136.0
1973	4	26	0.0	2441798.5	8	5.248	7	37.41	8	6.502	7	33.34	4.1239	4.1868	86.62	13.88	-12.2 136.0
1973	4	27	0.0	2441799.5	8	5.298	7	40.07	8	6.552	7	36.00	4.1287	4.1751	85.67	13.91	-12.2 136.1
1973	4	28	0.0	2441800.5	8	5.364	7	42.66	8	6.618	7	38.59	4.1335	4.1634	84.73	13.93	-12.2 136.1
1973	4	29	0.0	2441801.5	8	5.445	7	45.20	8	6.700	7	41.13	4.1382	4.1517	83.79	13.96	-12.2 136.1
1973	4	30	0.0	2441802.5	8	5.541	7	47.68	8	6.796	7	43.60	4.1429	4.1400	82.86	13.97	-12.3 136.2
1973	5	1	0.0	2441803.5	8	5.653	7	50.09	8	6.909	7	46.01	4.1475	4.1282	81.92	13.99	-12.3 136.2
1973	5	2	0.0	2441804.5	8	5.780	7	52.44	8	7.036	7	48.36	4.1521	4.1164	80.99	13.99	-12.3 136.3
1973	5	3	0.0	2441805.5	8	5.922	7	54.73	8	7.179	7	50.64	4.1566	4.1046	80.07	14.00	-12.3 136.3

1973	5	4	0.0	2441806.5	8	6.079	7	56.95	8	7.336	7	62.86	4.1610	4.0928	79.15	14.00	-12.3	136.3
1973	5	5	0.0	2441807.5	8	6.251	7	59.11	8	7.509	7	55.01	4.1654	4.0810	78.23	14.00	-12.3	136.3
1973	5	6	0.0	2441808.5	8	6.438	8	1.21	8	7.696	7	57.10	4.1697	4.0692	77.32	14.00	-12.3	136.4
1973	5	7	0.0	2441809.5	8	6.640	8	3.24	8	7.898	7	59.13	4.1740	4.0573	76.42	13.99	-12.3	136.4
1973	5	8	0.0	2441810.5	8	6.856	8	5.21	8	8.114	8	1.09	4.1781	4.0454	75.51	13.98	-12.3	136.4
1973	5	9	0.0	2441811.5	8	7.086	8	7.11	8	8.345	8	2.98	4.1822	4.0336	74.61	13.97	-12.3	136.5
1973	5	10	0.0	2441812.5	8	7.331	8	8.94	8	8.590	8	4.81	4.1862	4.0216	73.72	13.95	-12.3	136.5
1973	5	11	0.0	2441813.5	8	7.589	8	10.71	8	8.849	8	6.57	4.1900	4.0097	72.83	13.93	-12.3	136.5
1973	5	12	0.0	2441814.5	8	7.862	8	12.41	8	9.122	8	8.26	4.1938	3.9978	71.94	13.90	-12.3	136.6
1973	5	13	0.0	2441815.5	8	8.149	8	14.05	8	9.409	8	9.89	4.1975	3.9858	71.06	13.87	-12.3	136.6
1973	5	14	0.0	2441816.5	8	8.449	8	15.62	8	9.710	8	11.45	4.2011	3.9738	70.18	13.84	-12.3	136.6
1973	5	15	0.0	2441817.5	8	8.763	8	17.13	8	10.024	8	12.95	4.2045	3.9619	69.31	13.81	-12.3	136.7
1973	5	16	0.0	2441818.5	8	9.090	8	18.57	8	10.351	8	14.38	4.2079	3.9498	68.44	13.77	-12.3	136.7
1973	5	17	0.0	2441819.5	8	9.431	8	19.94	8	10.692	8	15.74	4.2111	3.9378	67.57	13.73	-12.3	136.7
1973	5	18	0.0	2441820.5	8	9.785	8	21.24	8	11.047	8	17.04	4.2142	3.9258	66.71	13.69	-12.3	136.8
1973	5	19	0.0	2441821.5	8	10.152	8	22.48	8	11.414	8	18.26	4.2172	3.9137	65.85	13.64	-12.3	136.8
1973	5	20	0.0	2441822.5	8	10.532	8	23.65	8	11.794	8	19.42	4.2201	3.9016	64.99	13.60	-12.3	136.8
1973	5	21	0.0	2441823.5	8	10.925	8	24.76	8	12.188	8	20.51	4.2229	3.8895	64.14	13.54	-12.3	136.9
1973	5	22	0.0	2441824.5	8	11.331	8	25.79	8	12.594	8	21.54	4.2255	3.8774	63.29	13.49	-12.3	136.9
1973	5	23	0.0	2441825.5	8	11.750	8	26.76	8	13.013	8	22.49	4.2280	3.8653	62.45	13.43	-12.4	136.9
1973	5	24	0.0	2441826.5	8	12.181	8	27.66	8	13.444	8	23.38	4.2303	3.8531	61.61	13.37	-12.4	137.0
1973	5	25	0.0	2441827.5	8	12.625	8	28.49	8	13.888	8	24.20	4.2325	3.8410	60.77	13.31	-12.4	137.0
1973	5	26	0.0	2441828.5	8	13.081	8	29.25	8	14.344	8	24.95	4.2346	3.8288	59.94	13.24	-12.4	137.0
1973	5	27	0.0	2441829.5	8	13.549	8	29.95	8	14.812	8	25.63	4.2365	3.8166	59.10	13.17	-12.4	137.1
1973	5	28	0.0	2441830.5	8	14.029	8	30.57	8	15.293	8	26.24	4.2383	3.8043	58.28	13.10	-12.4	137.1
1973	5	29	0.0	2441831.5	8	14.522	8	31.13	8	15.786	8	26.78	4.2399	3.7921	57.45	13.02	-12.4	137.2
1973	5	30	0.0	2441832.5	8	15.027	8	31.61	8	16.290	8	27.26	4.2413	3.7798	56.63	12.94	-12.4	137.2
1973	5	31	0.0	2441833.5	8	15.543	8	32.03	8	16.807	8	27.65	4.2426	3.7675	55.82	12.86	-12.4	137.2
1973	6	1	0.0	2441834.5	8	16.071	8	32.37	8	17.335	8	27.98	4.2438	3.7552	55.01	12.78	-12.4	137.3
1973	6	2	0.0	2441835.5	8	16.611	8	32.65	8	17.875	8	28.24	4.2447	3.7429	54.20	12.70	-12.4	137.3
1973	6	3	0.0	2441836.5	8	17.162	8	32.86	8	18.426	8	28.43	4.2456	3.7306	53.39	12.61	-12.4	137.3
1973	6	4	0.0	2441837.5	8	17.725	8	32.99	8	18.989	8	28.55	4.2462	3.7182	52.59	12.52	-12.4	137.4
1973	6	5	0.0	2441838.5	8	18.299	8	33.06	8	19.563	8	28.60	4.2467	3.7060	51.79	12.42	-12.4	137.4

1973	6	6	0.0	2441839.5	8	18.884	8	33.05	8	20.148	8	28.58	4.2470	3.6934	50.99	12.33	-12.4	137.5
1973	6	7	0.0	2441840.5	8	19.480	8	32.97	8	20.744	8	28.48	4.2471	3.6810	50.20	12.23	-12.4	137.6
1973	6	8	0.0	2441841.5	8	20.086	8	32.83	8	21.351	8	28.32	4.2470	3.6685	49.41	12.13	-12.4	137.5
1973	6	9	0.0	2441842.5	8	20.704	8	32.61	8	21.968	8	28.09	4.2468	3.6561	48.63	12.03	-12.4	137.6
1973	6	10	0.0	2441843.5	8	21.332	8	32.33	8	22.596	8	27.78	4.2464	3.6436	47.85	11.92	-12.4	137.6
1973	6	11	0.0	2441844.5	8	21.970	8	31.97	8	23.235	8	27.41	4.2458	3.6311	47.07	11.81	-12.4	137.7
1973	6	12	0.0	2441845.5	8	22.619	8	31.54	8	23.884	8	26.96	4.2450	3.6186	46.29	11.71	-12.4	137.7
1973	6	13	0.0	2441846.5	8	23.279	8	31.04	8	24.543	8	26.44	4.2440	3.6060	45.52	11.59	-12.4	137.7
1973	6	14	0.0	2441847.5	8	23.948	8	30.47	8	25.212	8	25.85	4.2428	3.5935	44.76	11.48	-12.5	137.8
1973	6	15	0.0	2441848.5	8	24.628	8	29.84	8	25.891	8	25.20	4.2415	3.5809	43.99	11.36	-12.5	137.8
1973	6	16	0.0	2441849.5	8	25.317	8	29.13	8	26.581	8	24.47	4.2399	3.5683	43.23	11.24	-12.5	137.9
1973	6	17	0.0	2441850.5	8	26.017	8	28.34	8	27.280	8	23.67	4.2382	3.5556	42.47	11.12	-12.5	137.9
1973	6	18	0.0	2441851.5	8	26.726	8	27.49	8	27.990	8	22.79	4.2363	3.5430	41.72	11.00	-12.5	138.0
1973	6	19	0.0	2441852.5	8	27.445	8	26.57	8	28.709	8	21.85	4.2342	3.5303	40.97	10.88	-12.5	138.0
1973	6	20	0.0	2441853.5	8	28.174	8	25.57	8	29.437	8	20.83	4.2318	3.5176	40.22	10.75	-12.5	138.0
1973	6	21	0.0	2441854.5	8	28.912	8	24.50	8	30.175	8	19.74	4.2293	3.5049	39.47	10.62	-12.5	138.1
1973	6	22	0.0	2441855.5	8	29.660	8	23.37	8	30.923	8	18.58	4.2266	3.4921	38.73	10.49	-12.5	138.1
1973	6	23	0.0	2441856.5	8	30.418	8	22.16	8	31.681	8	17.35	4.2237	3.4794	37.99	10.36	-12.5	138.2
1973	6	24	0.0	2441857.5	8	31.184	8	20.87	8	32.447	8	16.05	4.2206	3.4666	37.26	10.23	-12.5	138.2
1973	6	25	0.0	2441858.5	8	31.961	8	19.51	8	33.223	8	14.67	4.2172	3.4538	36.53	10.09	-12.5	138.3
1973	6	26	0.0	2441859.5	8	32.746	8	18.08	8	34.009	8	13.22	4.2137	3.4410	35.80	9.95	-12.5	138.3
1973	6	27	0.0	2441860.5	8	33.541	8	16.58	8	34.803	8	11.69	4.2100	3.4281	35.07	9.81	-12.5	138.3
1973	6	28	0.0	2441861.5	8	34.345	8	15.00	8	35.607	8	10.09	4.2060	3.4152	34.35	9.67	-12.5	138.4
1973	6	29	0.0	2441862.5	8	35.158	8	13.35	8	36.419	8	8.42	4.2019	3.4023	33.64	9.53	-12.5	138.4
1973	6	30	0.0	2441863.5	8	35.979	8	11.63	8	37.241	8	6.68	4.1975	3.3894	32.92	9.38	-12.5	138.5
1973	7	1	0.0	2441864.5	8	36.810	8	9.83	8	38.072	8	4.86	4.1929	3.3765	32.21	9.24	-12.5	138.5
1973	7	2	0.0	2441865.5	8	37.650	8	7.96	8	38.911	8	2.96	4.1881	3.3635	31.51	9.09	-12.6	138.6
1973	7	3	0.0	2441866.5	8	38.498	8	6.02	8	39.759	8	0.99	4.1831	3.3505	30.80	8.94	-12.6	138.6
1973	7	4	0.0	2441867.5	8	39.355	8	4.00	8	40.615	7	58.95	4.1779	3.3375	30.10	8.79	-12.6	138.7
1973	7	5	0.0	2441868.5	8	40.220	8	1.90	8	41.480	7	56.84	4.1725	3.3244	29.41	8.64	-12.6	138.7
1973	7	6	0.0	2441869.5	8	41.094	7	59.74	8	42.354	7	54.64	4.1668	3.3114	28.72	8.48	-12.6	138.8
1973	7	7	0.0	2441870.5	8	41.976	7	57.50	8	43.236	7	52.38	4.1609	3.2983	28.03	8.33	-12.6	138.8
1973	7	8	0.0	2441871.5	8	42.867	7	55.18	8	44.126	7	50.04	4.1548	3.2852	27.35	8.17	-12.6	138.9

1973	7	9	0.0	2441872.5	8	43.765	7	52.79	8	45.024	7	47.63	4.1485	3.2720	26.67	8.02	-12.6	138.9
1973	7	10	0.0	2441873.5	8	44.672	7	50.33	8	45.931	7	45.14	4.1420	3.2589	26.00	7.86	-12.6	139.0
1973	7	11	0.0	2441874.5	8	45.587	7	47.79	8	46.846	7	42.57	4.1353	3.2457	25.33	7.70	-12.6	139.0
1973	7	12	0.0	2441875.5	8	46.510	7	45.17	8	47.768	7	39.94	4.1283	3.2325	24.67	7.54	-12.6	139.1
1973	7	13	0.0	2441876.5	8	47.442	7	42.48	8	48.699	7	37.22	4.1211	3.2192	24.01	7.38	-12.6	139.1
1973	7	14	0.0	2441877.5	8	48.381	7	39.72	8	49.638	7	34.43	4.1137	3.2059	23.36	7.22	-12.6	139.2
1973	7	15	0.0	2441878.5	8	49.328	7	36.88	8	50.585	7	31.57	4.1061	3.1926	22.71	7.06	-12.6	139.2
1973	7	16	0.0	2441879.5	8	50.283	7	33.96	8	51.540	7	28.63	4.0983	3.1793	22.07	6.90	-12.6	139.3
1973	7	17	0.0	2441880.5	8	51.246	7	30.97	8	52.502	7	25.61	4.0902	3.1660	21.43	6.74	-12.6	139.3
1973	7	18	0.0	2441881.5	8	52.217	7	27.90	8	53.473	7	22.51	4.0819	3.1526	20.80	6.57	-12.6	139.4
1973	7	19	0.0	2441882.5	8	53.196	7	24.75	8	54.451	7	19.34	4.0734	3.1392	20.18	6.41	-12.7	139.4
1973	7	20	0.0	2441883.5	8	54.182	7	21.53	8	55.437	7	16.09	4.0647	3.1258	19.56	6.25	-12.7	139.5
1973	7	21	0.0	2441884.5	8	55.177	7	18.22	8	56.431	7	12.76	4.0558	3.1123	18.95	6.09	-12.7	139.5
1973	7	22	0.0	2441885.5	8	56.179	7	14.84	8	57.433	7	9.36	4.0466	3.0988	18.35	5.93	-12.7	139.6
1973	7	23	0.0	2441886.5	8	57.189	7	11.38	8	58.443	7	5.87	4.0372	3.0853	17.76	5.77	-12.7	139.7
1973	7	24	0.0	2441887.5	8	58.207	7	7.85	8	59.460	7	2.31	4.0276	3.0718	17.18	5.61	-12.7	139.7
1973	7	25	0.0	2441888.5	8	59.233	7	4.23	9	0.486	6	58.67	4.0178	3.0582	16.61	5.45	-12.7	139.8
1973	7	26	0.0	2441889.5	9	0.266	7	0.53	9	1.519	6	54.95	4.0077	3.0446	16.05	5.29	-12.7	139.8
1973	7	27	0.0	2441860.5	9	1.307	6	56.76	9	2.559	6	51.14	3.9975	3.0310	15.50	5.14	-12.7	139.9
1973	7	28	0.0	2441891.5	9	2.356	6	52.90	9	3.608	6	47.26	3.9870	3.0173	14.96	4.98	-12.7	139.9
1973	7	29	0.0	2441892.5	9	3.413	6	48.96	9	4.664	6	43.30	3.9763	3.0036	14.43	4.83	-12.7	140.0
1973	7	30	0.0	2441893.5	9	4.477	6	44.94	9	5.728	6	39.25	3.9653	2.9899	13.93	4.69	-12.7	140.1
1973	7	31	0.0	2441894.5	9	5.549	6	40.84	9	6.799	6	35.12	3.9542	2.9762	13.43	4.55	-12.7	140.1
1973	8	1	0.0	2441895.5	9	6.629	6	36.66	9	7.878	6	30.92	3.9428	2.9624	12.96	4.41	-12.7	140.2
1973	8	2	0.0	2441896.5	9	7.716	6	32.39	9	8.964	6	26.63	3.9312	2.9486	12.51	4.27	-12.7	140.2
1973	8	3	0.0	2441897.5	9	8.810	6	28.05	9	10.058	6	22.25	3.9193	2.9348	12.08	4.15	-12.7	140.3
1973	8	4	0.0	2441898.5	9	9.912	6	23.62	9	11.160	6	17.80	3.9073	2.9209	11.67	4.03	-12.8	140.4
1973	8	5	0.0	2441899.5	9	11.022	6	19.11	9	12.269	6	13.26	3.8950	2.9070	11.29	3.92	-12.8	140.4
1973	8	6	0.0	2441900.5	9	12.139	6	14.52	9	13.386	6	8.64	3.8825	2.8931	10.93	3.81	-12.8	140.5
1973	8	7	0.0	2441901.5	9	13.264	6	9.84	9	14.510	6	3.94	3.8698	2.8791	10.61	3.72	-12.8	140.6
1973	8	8	0.0	2441902.5	9	14.396	6	5.08	9	15.641	5	59.15	3.8569	2.8651	10.32	3.64	-12.8	140.6
1973	8	9	0.0	2441903.5	9	15.536	6	0.23	9	16.781	5	54.28	3.8437	2.8511	10.07	3.56	-12.8	140.7
1973	8	10	0.0	2441904.5	9	16.683	5	55.30	9	17.928	5	49.32	3.8304	2.8370	9.85	3.51	-12.8	140.8

1973	8	11	0.0	2441905.5	9	17.838	5	50.28	9	19.082	5	44.27	3.8168	2.8229	9.68	3.46	-12.8	140.8
1973	8	12	0.0	2441906.5	9	19.001	5	45.18	9	20.244	5	39.14	3.8030	2.8088	9.65	3.43	-12.8	140.9
1973	8	13	0.0	2441907.5	9	20.171	5	39.99	9	21.414	5	33.93	3.7890	2.7946	9.46	3.42	-12.8	141.0
1973	8	14	0.0	2441908.5	9	21.350	5	34.71	9	22.592	5	28.62	3.7748	2.7804	9.41	3.42	-12.8	141.0
1973	8	15	0.0	2441909.5	9	22.536	5	29.34	9	23.777	5	23.23	3.7604	2.7662	9.42	3.43	-12.8	141.1
1973	8	16	0.0	2441910.5	9	23.730	5	23.89	9	24.971	5	17.75	3.7457	2.7519	9.46	3.47	-12.8	141.2
1973	8	17	0.0	2441911.5	9	24.932	5	18.34	9	26.172	5	12.18	3.7309	2.7376	9.55	3.52	-12.9	141.2
1973	8	18	0.0	2441912.5	9	26.141	5	12.71	9	27.381	5	6.52	3.7158	2.7233	9.68	3.58	-12.9	141.3
1973	8	19	0.0	2441913.5	9	27.360	5	6.98	9	28.599	5	0.76	3.7005	2.7089	9.85	3.66	-12.9	141.4
1973	8	20	0.0	2441914.5	9	28.586	5	1.16	9	29.824	4	54.92	3.6850	2.6946	10.05	3.76	-12.9	141.5
1973	8	21	0.0	2441915.5	9	29.820	4	55.25	9	31.058	4	48.98	3.6693	2.6801	10.29	3.87	-12.9	141.5
1973	8	22	0.0	2441916.5	9	31.063	4	49.25	9	32.300	4	42.95	3.6534	2.6656	10.57	3.99	-12.9	141.6
1973	8	23	0.0	2441917.5	9	32.314	4	43.15	9	33.551	4	36.82	3.6373	2.6511	10.87	4.12	-12.9	141.7
1973	8	24	0.0	2441918.5	9	33.573	4	36.95	9	34.809	4	30.60	3.6210	2.6366	11.20	4.27	-12.9	141.8
1973	8	25	0.0	2441919.5	9	34.841	4	30.66	9	36.077	4	24.28	3.6045	2.6220	11.55	4.43	-12.9	141.8
1973	8	26	0.0	2441920.5	9	36.118	4	24.27	9	37.353	4	17.86	3.5878	2.6073	11.92	4.59	-12.9	141.9
1973	8	27	0.0	2441921.5	9	37.403	4	17.78	9	38.637	4	11.35	3.5708	2.5927	12.31	4.77	-12.9	142.0
1973	8	28	0.0	2441922.5	9	38.697	4	11.20	9	39.931	4	4.74	3.5537	2.5780	12.72	4.96	-13.0	142.1
1973	8	29	0.0	2441923.5	9	39.999	4	4.51	9	41.233	3	58.03	3.5363	2.5632	13.14	5.14	-13.0	142.2
1973	8	30	0.0	2441924.5	9	41.311	3	57.73	9	42.543	3	51.22	3.5188	2.5484	13.58	5.34	-13.0	142.2
1973	8	31	0.0	2441925.5	9	42.631	3	50.84	9	43.863	3	44.30	3.5011	2.5336	14.03	5.54	-13.0	142.3
1973	9	1	0.0	2441926.5	9	43.961	3	43.85	9	45.192	3	37.29	3.4831	2.5187	14.49	5.76	-13.0	142.4
1973	9	2	0.0	2441927.5	9	45.300	3	36.76	9	46.530	3	30.17	3.4650	2.5038	14.96	5.97	-13.0	142.5
1973	9	3	0.0	2441928.5	9	46.648	3	29.57	9	47.877	3	22.95	3.4467	2.4889	15.43	6.19	-13.0	142.6
1973	9	4	0.0	2441929.5	9	48.005	3	22.27	9	49.234	3	15.62	3.4281	2.4739	15.92	6.42	-13.0	142.7
1973	9	5	0.0	2441930.5	9	49.372	3	14.86	9	50.600	3	8.19	3.4094	2.4588	16.41	6.65	-13.0	142.8
1973	9	6	0.0	2441931.5	9	50.748	3	7.35	9	51.976	3	0.65	3.3905	2.4437	16.90	6.89	-13.0	142.8
1973	9	7	0.0	2441932.5	9	52.136	2	59.72	9	53.362	2	53.00	3.3714	2.4286	17.40	7.13	-13.0	142.9
1973	9	8	0.0	2441933.5	9	53.531	2	51.99	9	54.758	2	45.24	3.3522	2.4135	17.90	7.37	-13.0	143.0
1973	9	9	0.0	2441934.5	9	54.938	2	44.15	9	56.164	2	37.37	3.3327	2.3982	18.41	7.63	-13.0	143.1
1973	9	10	0.0	2441935.5	9	56.355	2	36.19	9	57.581	2	29.39	3.3131	2.3830	18.91	7.87	-13.1	143.2
1973	9	11	0.0	2441936.5	9	57.783	2	28.12	9	59.008	2	21.29	3.2932	2.3677	19.42	8.13	-13.1	143.3
1973	9	12	0.0	2441937.5	9	59.222	2	19.93	10	0.446	2	13.07	3.2732	2.3523	19.94	8.39	-13.1	143.4

1973	9	13	0.0	2441938.5	10	0.672	2	11.62	10	1.895	2	4.74	3.2630	2.3369	20.45	8.65	-13.1	143.8
1973	9	14	0.0	2441939.5	10	2.133	2	3.19	10	3.356	1	56.29	3.2327	2.3215	20.96	8.92	-13.1	143.6
1973	9	15	0.0	2441940.5	10	3.605	1	54.65	10	4.828	1	47.72	3.2122	2.3060	21.48	9.19	-13.1	143.7
1973	9	16	0.0	2441941.5	10	5.090	1	45.98	10	6.312	1	39.02	3.1915	2.2904	21.99	9.46	-13.1	143.8
1973	9	17	0.0	2441942.5	10	6.586	1	37.18	10	7.808	1	30.20	3.1706	2.2749	22.51	9.74	-13.1	143.9
1973	9	18	0.0	2441943.5	10	8.095	1	28.26	10	9.316	1	21.25	3.1495	2.2592	23.02	10.02	-13.1	144.0
1973	9	19	0.0	2441944.5	10	9.617	1	19.30	10	10.837	1	12.17	3.1283	2.2435	23.53	10.30	-13.1	144.1
1973	9	20	0.0	2441945.5	10	11.151	1	10.02	10	12.371	1	2.96	3.1069	2.2278	24.05	10.58	-13.2	144.2
1973	9	21	0.0	2441946.5	10	12.699	1	0.70	10	13.918	0	53.62	3.0854	2.2120	24.56	10.87	-13.2	144.3
1973	9	22	0.0	2441947.5	10	14.260	0	51.25	10	15.479	0	44.14	3.0637	2.1961	25.07	11.17	-13.2	144.4
1973	9	23	0.0	2441948.5	10	15.835	0	41.66	10	17.053	0	34.53	3.0418	2.1802	25.58	11.46	-13.2	144.6
1973	9	24	0.0	2441949.5	10	17.424	0	31.93	10	18.642	0	24.77	3.0198	2.1643	26.09	11.76	-13.2	144.7
1973	9	25	0.0	2441950.5	10	19.028	0	22.06	10	20.245	0	14.88	2.9976	2.1483	26.59	12.06	-13.2	144.8
1973	9	26	0.0	2441951.5	10	20.646	0	12.04	10	21.863	0	4.84	2.9753	2.1322	27.09	12.37	-13.2	144.9
1973	9	27	0.0	2441952.5	10	22.280	0	1.88	10	23.496	- 0	5.35	2.9528	2.1161	27.59	12.67	-13.2	145.0
1973	9	28	0.0	2441953.5	10	23.929	- 0	8.43	10	25.145	- 0	15.68	2.9302	2.0999	28.09	12.98	-13.2	145.1
1973	9	29	0.0	2441954.5	10	25.594	- 0	18.89	10	26.809	- 0	26.17	2.9074	2.0837	28.59	13.30	-13.3	145.3
1973	9	30	0.0	2441955.5	10	27.276	- 0	29.51	10	28.490	- 0	36.81	2.8845	2.0674	29.08	13.62	-13.3	145.4
1973	10	1	0.0	2441956.5	10	28.974	- 0	40.28	10	30.188	- 0	47.60	2.8614	2.0510	29.57	13.94	-13.3	145.5
1973	10	2	0.0	2441957.5	10	30.690	- 0	51.21	10	31.904	- 0	58.56	2.8382	2.0346	30.05	14.26	-13.3	145.7
1973	10	3	0.0	2441958.5	10	32.424	- 1	2.31	10	33.637	- 1	9.68	2.8149	2.0181	30.53	14.59	-13.3	145.8
1973	10	4	0.0	2441959.5	10	34.176	- 1	13.57	10	35.388	- 1	20.97	2.7914	2.0016	31.01	14.92	-13.3	145.9
1973	10	5	0.0	2441960.5	10	35.947	- 1	25.00	10	37.159	- 1	32.42	2.7678	1.9850	31.48	15.25	-13.3	146.1
1973	10	6	0.0	2441961.5	10	37.737	- 1	36.61	10	38.949	- 1	44.05	2.7441	1.9683	31.95	15.59	-13.3	146.2
1973	10	7	0.0	2441962.5	10	39.548	- 1	48.39	10	40.759	- 1	55.85	2.7202	1.9516	32.42	15.93	-13.4	146.3
1973	10	8	0.0	2441963.5	10	41.379	- 2	0.35	10	42.591	- 2	7.83	2.6962	1.9348	32.88	16.28	-13.4	146.5
1973	10	9	0.0	2441964.5	10	43.233	- 2	12.50	10	44.443	- 2	20.00	2.6721	1.9179	33.33	16.63	-13.4	146.6
1973	10	10	0.0	2441965.5	10	45.108	- 2	24.83	10	46.318	- 2	32.36	2.6479	1.9009	33.79	16.98	-13.4	146.8
1973	10	11	0.0	2441966.5	10	47.006	- 2	37.36	10	48.217	- 2	44.91	2.6236	1.8839	34.23	17.34	-13.4	146.9
1973	10	12	0.0	2441967.5	10	48.929	- 2	50.08	10	50.139	- 2	57.65	2.5992	1.8669	34.67	17.70	-13.4	147.1
1973	10	13	0.0	2441968.5	10	50.876	- 3	3.01	10	52.085	- 3	10.60	2.5747	1.8497	35.10	18.07	-13.4	147.2
1973	10	14	0.0	2441969.5	10	52.848	- 3	16.14	10	54.058	- 3	23.75	2.5501	1.8325	35.53	18.44	-13.4	147.
1973	10	15	0.0	2441970.5	10	54.847	- 3	29.48	10	56.057	- 3	37.12	2.5254	1.8152	35.95	18.81	-13.5	147.

1973	10	16	0.0	2441971.5	10	56.874	- 3	43.05	10	58.083	- 3	50.70	2.5006	1.7978	36.37	19.19	-13.5	147
1973	10	17	0.0	2441972.5	10	58.529	- 3	56.83	11	0.138	- 4	4.50	2.4767	1.7804	36.77	19.68	-13.5	147.
1973	10	18	0.0	2441973.5	11	1.014	- 4	10.84	11	2.223	- 4	18.53	2.4507	1.7628	37.18	19.97	-13.5	148.1
1973	10	19	0.0	2441974.5	11	3.129	- 4	25.08	11	4.338	- 4	32.79	2.4266	1.7462	37.57	20.36	-13.6	148.2
1973	10	20	0.0	2441975.5	11	5.276	- 4	39.56	11	6.485	- 4	47.29	2.4005	1.7275	37.95	20.76	-13.5	148.4
1973	10	21	0.0	2441976.5	11	7.457	- 4	54.28	11	8.665	- 5	2.03	2.3763	1.7098	38.33	21.17	-13.5	148.6
1973	10	22	0.0	2441977.5	11	9.671	- 5	9.26	11	10.880	- 5	17.02	2.3500	1.6919	38.70	21.58	-13.6	148.8
1973	10	23	0.0	2441978.5	11	11.921	- 5	24.49	11	13.130	- 5	32.27	2.3246	1.6740	39.06	22.00	-13.6	149.0
1973	10	24	0.0	2441979.5	11	14.208	- 5	39.98	11	15.417	- 5	47.78	2.2992	1.6560	39.41	22.42	-13.6	149.2
1973	10	25	0.0	2441980.5	11	16.533	- 5	55.74	11	17.743	- 6	3.55	2.2738	1.6378	39.76	22.85	-13.6	149.4
1973	10	26	0.0	2441981.5	11	18.899	- 6	11.77	11	20.108	- 6	19.60	2.2483	1.6196	40.09	23.28	-13.6	149.6
1973	10	27	0.0	2441982.5	11	21.306	- 6	28.09	11	22.516	- 6	35.93	2.2227	1.6013	40.41	23.72	-13.6	149.8
1973	10	28	0.0	2441983.5	11	23.756	- 6	44.69	11	24.967	- 6	52.55	2.1971	1.5829	40.72	24.17	-13.6	150.0
1973	10	29	0.0	2441984.5	11	26.252	- 7	1.59	11	27.463	- 7	9.46	2.1715	1.5644	41.02	24.63	-13.7	150.2
1973	10	30	0.0	2441985.5	11	28.795	- 7	18.79	11	30.006	- 7	26.68	2.1458	1.5458	41.31	25.09	-13.7	150.4
1973	10	31	0.0	2441986.5	11	31.387	- 7	36.30	11	32.599	- 7	44.20	2.1202	1.5271	41.59	25.56	-13.7	150.7
1973	11	1	0.0	2441987.5	11	34.030	- 7	54.13	11	35.243	- 8	2.04	2.0945	1.5083	41.85	26.04	-13.7	150.9
1973	11	2	0.0	2441988.5	11	36.728	- 8	12.29	11	37.941	- 8	20.21	2.0688	1.4894	42.10	26.53	-13.7	151.1
1973	11	3	0.0	2441989.5	11	39.481	- 8	30.78	11	40.696	- 8	38.71	2.0431	1.4704	42.34	27.02	-13.7	151.4
1973	11	4	0.0	2441990.5	11	42.294	- 8	49.61	11	43.509	- 8	57.55	2.0175	1.4513	42.56	27.53	-13.8	151.6
1973	11	5	0.0	2441991.5	11	45.168	- 9	8.79	11	46.384	- 9	16.74	1.9918	1.4321	42.77	28.04	-13.8	151.9
1973	11	6	0.0	2441992.5	11	48.106	- 9	28.33	11	49.323	- 9	36.28	1.9662	1.4127	42.96	28.56	-13.8	152.2
1973	11	7	0.0	2441993.5	11	51.112	- 9	48.23	11	52.331	- 9	56.19	1.9406	1.3932	43.13	29.09	-13.8	152.4
1973	11	8	0.0	2441994.5	11	54.189	-10	8.51	11	55.400	-10	16.48	1.9151	1.3737	43.29	29.64	-13.8	152.7
1973	11	9	0.0	2441995.5	11	57.340	-10	29.17	11	58.561	-10	37.14	1.8896	1.3539	43.43	30.19	-13.9	153.0
1973	11	10	0.0	2441996.5	12	0.569	-10	50.22	12	1.792	-10	58.19	1.8642	1.3341	43.55	30.75	-13.9	153.3
1973	11	11	0.0	2441997.5	12	3.881	-11	11.67	12	5.105	-11	19.64	1.8389	1.3141	43.68	31.33	-13.9	153.6
1973	11	12	0.0	2441998.5	12	7.278	-11	33.63	12	8.504	-11	41.49	1.8136	1.2940	43.73	31.92	-13.9	153.9
1973	11	13	0.0	2441999.5	12	10.765	-11	55.79	12	11.993	-12	3.76	1.7885	1.2738	43.78	32.52	-13.9	154.3
1973	11	14	0.0	2442000.5	12	14.348	-12	18.48	12	15.578	-12	26.43	1.7635	1.2534	43.82	33.13	-13.9	154.6
1973	11	15	0.0	2442001.5	12	18.030	-12	41.58	12	19.263	-12	49.53	1.7385	1.2329	43.83	33.75	-14.0	154.9
1973	11	16	0.0	2442002.5	12	21.818	-13	5.11	12	23.053	-13	13.06	1.7138	1.2122	43.82	34.39	-14.0	155.3
1973	11	17	0.0	2442003.5	12	25.716	-13	29.07	12	26.954	-13	37.00	1.6892	1.1913	43.78	35.04	-14.0	155.7

1973	11	18	0.0	2442004.5	12	29.730	-13	53.46	12	30.971	-14	1.37	1.6647	1.1704	43.72	35.71	-14.0	156.1
1973	11	19	0.0	2442005.5	12	33.867	-14	18.28	12	35.110	-14	26.17	1.6405	1.1492	43.62	36.39	-14.0	156.5
1973	11	20	0.0	2442006.5	12	38.132	-14	43.62	12	39.379	-14	51.39	1.6164	1.1279	43.50	37.09	-14.1	156.9
1973	11	21	0.0	2442007.5	12	42.533	-15	9.19	12	43.783	-15	17.02	1.5926	1.1064	43.35	37.80	-14.1	157.3
1973	11	22	0.0	2442008.5	12	47.076	-15	35.26	12	48.331	-15	43.07	1.5690	1.0847	43.16	38.53	-14.1	157.8
1973	11	23	0.0	2442009.5	12	51.770	-16	1.74	12	53.029	-16	9.51	1.5456	1.0628	42.94	39.27	-14.1	158.2
1973	11	24	0.0	2442010.5	12	56.622	-16	28.69	12	57.885	-16	36.33	1.5226	1.0408	42.69	40.03	-14.1	158.7
1973	11	25	0.0	2442011.5	13	1.641	-16	55.82	13	2.909	-17	3.51	1.4998	1.0185	42.40	40.81	-14.2	159.2
1973	11	26	0.0	2442012.5	13	6.835	-17	23.38	13	8.108	-17	31.02	1.4774	0.9960	42.07	41.60	-14.2	159.8
1973	11	27	0.0	2442013.5	13	12.214	-17	51.25	13	13.492	-17	58.84	1.4554	0.9734	41.70	42.41	-14.2	160.3
1973	11	28	0.0	2442014.5	13	17.787	-18	19.39	13	19.071	-18	26.92	1.4338	0.9505	41.29	43.23	-14.2	160.9
1973	11	29	0.0	2442015.5	13	23.564	-18	47.76	13	24.855	-18	55.22	1.4125	0.9274	40.84	44.07	-14.2	161.5
1973	11	30	0.0	2442016.5	13	29.557	-19	16.30	13	30.853	-19	23.68	1.3918	0.9040	40.34	44.93	-14.2	162.2
1973	12	1	0.0	2442017.5	13	35.774	-19	44.96	13	37.078	-19	52.25	1.3715	0.8804	39.79	45.79	-14.3	162.9
1973	12	2	0.0	2442018.5	13	42.228	-20	13.64	13	43.539	-20	20.84	1.3517	0.8565	39.20	46.67	-14.3	163.6
1973	12	3	0.0	2442019.5	13	48.930	-20	42.28	13	50.249	-20	49.38	1.3325	0.8324	38.55	47.57	-14.3	164.4
1973	12	4	0.0	2442020.5	13	55.892	-21	10.78	13	57.218	-21	17.76	1.3139	0.8080	37.85	48.47	-14.3	165.2
1973	12	5	0.0	2442021.5	14	3.124	-21	39.01	14	4.458	-21	45.87	1.2960	0.7832	37.10	49.37	-14.3	166.0
1973	12	6	0.0	2442022.5	14	10.638	-22	6.86	14	11.981	-22	13.58	1.2787	0.7582	36.29	50.28	-14.3	166.9
1973	12	7	0.0	2442023.5	14	18.446	-22	34.18	14	19.798	-22	40.75	1.2622	0.7329	35.42	51.18	-14.3	167.9
1973	12	8	0.0	2442024.5	14	26.558	-23	0.81	14	27.920	-23	7.21	1.2464	0.7072	34.50	52.08	-14.3	169.0
1973	12	9	0.0	2442025.5	14	34.986	-23	26.57	14	36.358	-23	32.80	1.2315	0.6812	33.51	52.96	-14.3	170.1
1973	12	10	0.0	2442026.5	14	43.739	-23	51.27	14	45.121	-23	57.29	1.2175	0.6548	32.46	53.81	-14.3	171.3
1973	12	11	0.0	2442027.5	14	52.828	-24	14.68	14	54.219	-24	20.49	1.2044	0.6280	31.34	54.64	-14.3	172.6
1973	12	12	0.0	2442028.5	15	2.259	-24	36.57	15	3.661	-24	42.15	1.1923	0.6008	30.16	55.41	-14.2	174.1
1973	12	13	0.0	2442029.5	15	12.041	-24	56.69	15	13.453	-25	2.02	1.1813	0.5731	28.91	56.12	-14.2	175.6
1973	12	14	0.0	2442030.5	15	22.180	-25	14.75	15	23.602	-25	19.82	1.1713	0.5451	27.58	56.74	-14.1	177.4
1973	12	15	0.0	2442031.5	15	32.682	-25	30.47	15	34.114	-25	35.25	1.1625	0.5165	26.19	57.25	-14.0	179.3
1973	12	16	0.0	2442032.5	15	43.552	-25	43.54	15	44.993	-25	48.01	1.1549	0.4874	24.73	57.62	-13.9	181.4
1973	12	17	0.0	2442033.5	15	54.796	-25	53.63	15	56.246	-25	57.76	1.1486	0.4579	23.18	57.79	-13.8	183.9
1973	12	18	0.0	2442034.5	16	6.420	-26	0.39	16	7.877	-26	4.17	1.1436	0.4277	21.56	57.72	-13.6	186.6
1973	12	19	0.0	2442035.5	16	18.431	-26	3.45	16	19.895	-26	6.86	1.1398	0.3971	19.86	57.32	-13.3	189.8
1973	12	20	0.0	2442036.5	16	30.843	-26	2.44	16	32.312	-26	5.46	1.1374	0.3659	18.06	56.48	-12.9	193.5

1973	12	21	0.0	2442037.5	16	43.675	-25	56.93	16	45.149	-25	59.53	1.1362	0.3343	16.17	55.07	-12.4	197.9
1973	12	22	0.0	2442038.5	16	56.959	-25	46.45	16	58.436	-25	48.60	1.1362	0.3028	14.18	52.86	-11.7	203.1
1973	12	23	0.0	2442039.5	17	10.741	-25	30.48	17	12.218	-25	32.16	1.1371	0.2700	12.05	49.54	-10.8	209.6
1973	12	24	0.0	2442040.5	17	25.489	-25	8.38	17	26.565	-25	9.67	1.1386	0.2380	9.79	44.63	-9.3	217.8
1973	12	25	0.0	2442041.5	17	40.092	-24	39.45	17	41.565	-24	40.12	1.1400	0.2072	7.35	37.42	-7.1	228.4
1973	12	26	0.0	2442042.5	17	55.043	-24	2.97	17	57.310	-24	3.09	1.1390	0.1790	4.72	26.91	-3.9	242.3
1973	12	27	0.0	2442043.5	18	12.357	-23	18.62	18	13.816	-23	18.16	1.1358	0.1564	1.92	12.17	0.7	260.7
1973	12	28	0.0	2442044.5	18	29.306	-22	27.40	18	30.834	-22	26.35	1.1252	0.1438	1.30	8.92	6.4	283.8
1973	12	29	0.0	2442045.5	18	46.268	-21	32.61	18	47.703	-21	30.98	1.1061	0.1448	4.22	30.00	11.3	309.3
1973	12	30	0.0	2442046.5	19	2.260	-20	36.40	19	3.682	-20	36.22	1.0799	0.1691	7.03	49.20	13.8	332.9
1973	12	31	0.0	2442047.5	19	17.082	-19	46.91	19	18.492	-19	44.24	1.0502	0.1826	9.59	63.80	14.3	351.7
1974	1	1	0.0	2442048.5	19	30.889	-18	58.03	19	32.287	-18	54.91	1.0200	0.2113	11.93	74.09	13.6	6.8
1974	1	2	0.0	2442049.5	19	43.958	-18	10.79	19	45.345	-18	7.25	0.9909	0.2424	14.10	81.16	12.6	16.3
1974	1	3	0.0	2442050.5	19	56.532	-17	24.21	19	57.908	-17	20.28	0.9637	0.2745	16.17	85.96	11.6	24.3
1974	1	4	0.0	2442051.5	20	8.787	-16	37.50	20	10.151	-16	33.21	0.9386	0.3067	18.17	89.17	10.6	30.6
1974	1	5	0.0	2442052.5	20	20.841	-15	50.11	20	22.194	-15	45.47	0.9158	0.3387	20.14	91.23	9.7	35.8
1974	1	6	0.0	2442053.5	20	32.773	-15	1.64	20	34.115	-14	56.66	0.8953	0.3703	22.10	92.44	8.9	39.8
1974	1	7	0.0	2442054.5	20	44.631	-14	11.84	20	46.962	-14	6.55	0.8770	0.4014	24.06	93.99	8.2	43.3
1974	1	8	0.0	2442055.5	20	56.441	-13	20.58	20	57.762	-13	14.98	0.8609	0.4319	26.02	93.02	7.6	46.3
1974	1	9	0.0	2442056.5	21	8.214	-12	27.82	21	9.525	-12	21.93	0.8469	0.4620	27.99	92.66	7.0	48.9
1974	1	10	0.0	2442057.5	21	19.950	-11	33.60	21	21.250	-11	27.44	0.8351	0.4915	29.97	91.96	6.5	51.2
1974	1	11	0.0	2442058.5	21	31.636	-10	38.03	21	32.927	-10	31.61	0.8254	0.5205	31.95	91.00	6.1	53.3
1974	1	12	0.0	2442059.5	21	43.258	- 9	41.28	21	44.540	- 9	34.63	0.8177	0.5490	33.93	89.82	5.6	55.0
1974	1	13	0.0	2442060.5	21	54.794	- 8	43.58	21	56.067	- 8	36.71	0.8120	0.5770	35.91	88.47	5.3	56.6
1974	1	14	0.0	2442061.5	22	6.220	- 7	45.18	22	7.486	- 7	38.11	0.8083	0.6046	37.87	86.98	4.9	58.1
1974	1	15	0.0	2442062.5	22	17.511	- 6	46.38	22	18.769	- 6	39.13	0.8064	0.6317	39.80	85.39	4.6	59.4
1974	1	16	0.0	2442063.5	22	28.641	- 5	47.47	22	29.893	- 5	40.06	0.8065	0.6585	41.71	83.71	4.3	60.7
1974	1	17	0.0	2442064.5	22	39.585	- 4	48.77	22	40.832	- 4	41.22	0.8083	0.6848	43.67	81.98	4.0	61.8
1974	1	18	0.0	2442065.5	22	50.321	- 3	50.57	22	51.564	- 3	42.90	0.8118	0.7108	45.39	80.21	3.8	62.9
1974	1	19	0.0	2442066.5	23	0.828	- 2	53.14	23	2.065	- 2	45.37	0.8170	0.7364	47.16	78.42	3.6	63.8
1974	1	20	0.0	2442067.5	23	11.087	- 1	56.76	23	12.323	- 1	48.90	0.8237	0.7617	48.86	76.62	3.3	64.7
1974	1	21	0.0	2442068.5	23	21.084	- 1	1.64	23	22.317	- 0	53.71	0.8320	0.7867	50.49	74.83	3.1	65.6
1974	1	22	0.0	2442069.5	23	30.806	- 0	7.98	23	32.039	- 0	0.00	0.8417	0.8114	52.05	73.05	2.9	66.4

1974	1	23	0.0	2442070.5	23	40.246	0	44.07	23	41.478	0	52.08	0.8627	0.8367	53.64	71.31	2.7	67.2
1974	1	24	0.0	2442071.5	23	49.397	1	34.37	23	50.629	1	42.40	0.8650	0.8598	54.95	69.60	2.5	67.9
1974	1	25	0.0	2442072.5	23	58.256	2	22.85	23	59.489	2	30.89	0.8785	0.8837	56.28	67.93	2.3	68.6
1974	1	26	0.0	2442073.5	0	6.823	3	9.44	0	8.057	3	17.47	0.8932	0.9072	57.54	66.30	2.2	69.2
1974	1	27	0.0	2442074.5	0	15.101	3	54.10	0	16.336	4	2.13	0.9089	0.9306	58.71	64.72	2.0	69.8
1974	1	28	0.0	2442075.5	0	23.092	4	36.85	0	24.329	4	44.85	0.9255	0.9537	59.80	63.19	1.9	70.4
1974	1	29	0.0	2442076.5	0	30.801	5	17.68	0	32.041	5	25.65	0.9431	0.9765	60.81	61.71	1.7	70.9
1974	1	30	0.0	2442077.5	0	38.237	5	56.64	0	39.480	6	4.56	0.9616	0.9992	61.75	60.28	1.6	71.4
1974	1	31	0.0	2442078.5	0	45.406	6	33.76	0	46.651	6	41.64	0.9808	1.0216	62.62	58.90	1.5	71.9
1974	2	1	0.0	2442079.5	0	52.315	7	9.10	0	53.565	7	16.94	1.0007	1.0438	63.41	57.58	1.4	72.4
1974	2	2	0.0	2442080.5	0	58.976	7	42.74	1	0.229	7	50.61	1.0214	1.0659	64.13	56.30	1.2	72.9
1974	2	3	0.0	2442081.5	1	5.397	8	14.73	1	6.654	8	22.44	1.0426	1.0877	64.79	55.07	1.1	73.3
1974	2	4	0.0	2442082.5	1	11.588	8	45.14	1	12.848	8	52.80	1.0645	1.1094	65.38	53.88	1.0	73.7
1974	2	5	0.0	2442083.5	1	17.559	9	14.07	1	18.823	9	21.65	1.0869	1.1308	65.92	52.74	0.9	74.1
1974	2	6	0.0	2442084.5	1	23.319	9	41.67	1	24.587	9	49.08	1.1098	1.1521	66.39	51.65	0.8	74.5
1974	2	7	0.0	2442085.5	1	28.878	10	7.73	1	30.150	10	15.17	1.1331	1.1733	66.81	50.59	0.7	74.9
1974	2	8	0.0	2442086.5	1	34.246	10	32.61	1	35.521	10	39.98	1.1569	1.1943	67.18	49.58	0.6	75.3
1974	2	9	0.0	2442087.5	1	39.431	10	56.29	1	40.710	11	3.59	1.1811	1.2151	67.50	48.60	0.5	75.6
1974	2	10	0.0	2442088.5	1	44.442	11	18.84	1	45.725	11	26.06	1.2057	1.2357	67.77	47.66	0.5	76.0
1974	2	11	0.0	2442089.5	1	49.289	11	40.32	1	50.576	11	47.47	1.2306	1.2562	67.99	46.75	0.4	76.3
1974	2	12	0.0	2442090.5	1	53.980	12	0.80	1	55.270	12	7.87	1.2558	1.2766	68.17	45.87	0.3	76.6
1974	2	13	0.0	2442091.5	1	58.521	12	20.33	1	59.816	12	27.32	1.2813	1.2968	68.32	45.03	0.2	76.9
1974	2	14	0.0	2442092.5	2	2.922	12	38.97	2	4.220	12	45.88	1.3071	1.3169	68.42	44.21	0.1	77.2
1974	2	15	0.0	2442093.5	2	7.189	12	56.77	2	8.491	13	3.61	1.3331	1.3369	68.49	43.42	0.1	77.5
1974	2	16	0.0	2442094.5	2	11.329	13	13.79	2	12.634	13	20.55	1.3594	1.3567	68.53	42.66	-0.0	77.8
1974	2	17	0.0	2442095.5	2	15.348	13	30.07	2	16.657	13	36.75	1.3859	1.3764	68.53	41.92	-0.1	78.1
1974	2	18	0.0	2442096.5	2	19.253	13	45.64	2	20.565	13	52.25	1.4126	1.3960	68.50	41.20	-0.1	78.3
1974	2	19	0.0	2442097.5	2	23.050	14	0.57	2	24.365	14	7.09	1.4394	1.4154	68.44	40.51	-0.2	78.6
1974	2	20	0.0	2442098.5	2	26.743	14	14.87	2	28.062	14	21.32	1.4664	1.4347	68.36	39.84	-0.3	78.8
1974	2	21	0.0	2442099.5	2	30.338	14	28.59	2	31.660	14	34.96	1.4935	1.4540	68.25	39.18	-0.3	79.1
1974	2	22	0.0	2442100.5	2	33.841	14	41.76	2	35.166	14	48.05	1.5208	1.4731	68.12	38.55	-0.4	79.3
1974	2	23	0.0	2442101.5	2	37.255	14	54.41	2	38.583	15	0.63	1.5482	1.4921	67.96	37.93	-0.5	79.5
1974	2	24	0.0	2442102.5	2	40.585	15	6.57	2	41.916	15	12.72	1.5758	1.5110	67.78	37.33	-0.5	79.8

1974	2 25	0.0	2442103.5	2 43.835	15 18.27	2 45.169	15 24.34	1.6034	1.5297	67.58	36.74	-0.6	80.0
1974	2 26	0.0	2442104.5	2 47.008	15 29.52	2 48.346	15 35.53	1.6312	1.5484	67.36	36.17	-0.6	80.2
1974	2 27	0.0	2442105.5	2 50.110	15 40.37	2 51.450	15 46.30	1.6590	1.5670	67.12	35.61	-0.7	80.4
1974	2 28	0.0	2442106.5	2 53.142	15 50.82	2 54.485	15 56.68	1.6869	1.5856	66.87	35.07	-0.7	80.6
1974	3 1	0.0	2442107.5	2 56.108	16 0.90	2 57.454	16 6.68	1.7148	1.6039	66.59	34.54	-0.8	80.8
1974	3 2	0.0	2442108.5	2 59.012	16 10.62	3 0.360	16 16.33	1.7428	1.6223	66.30	34.02	-0.8	81.0
1974	3 3	0.0	2442109.5	3 1.856	16 20.01	3 3.207	16 25.65	1.7709	1.6403	66.00	33.51	-0.9	81.2
1974	3 4	0.0	2442110.5	3 4.642	16 29.07	3 5.996	16 34.65	1.7990	1.6585	65.68	33.01	-0.9	81.4
1974	3 5	0.0	2442111.5	3 7.374	16 37.84	3 8.730	16 43.34	1.8272	1.6765	65.35	32.53	-1.0	81.6
1974	3 6	0.0	2442112.5	3 10.054	16 46.31	3 11.412	16 51.75	1.8863	1.6944	66.01	32.06	-1.0	81.8
1974	3 7	0.0	2442113.5	3 12.683	16 54.51	3 14.045	16 59.88	1.8835	1.7122	64.65	31.58	-1.1	81.9
1974	3 8	0.0	2442114.5	3 15.265	17 2.44	3 16.629	17 7.74	1.9117	1.7300	64.28	31.12	-1.1	82.1
1974	3 9	0.0	2442115.5	3 17.802	17 10.13	3 19.168	17 15.36	1.9400	1.7477	63.90	30.67	-1.1	82.3
1974	3 10	0.0	2442116.5	3 20.295	17 17.67	3 21.663	17 22.74	1.9682	1.7653	63.51	30.23	-1.2	82.4
1974	3 11	0.0	2442117.5	3 22.746	17 24.78	3 24.116	17 29.88	1.9965	1.7828	63.10	29.80	-1.2	82.6
1974	3 12	0.0	2442118.5	3 25.157	17 31.78	3 26.530	17 36.81	2.0247	1.8002	62.69	29.37	-1.3	82.8
1974	3 13	0.0	2442119.5	3 27.530	17 38.57	3 28.905	17 43.54	2.0529	1.8176	62.27	28.95	-1.3	82.9
1974	3 14	0.0	2442120.5	3 29.867	17 46.15	3 31.244	17 50.06	2.0812	1.8349	61.84	28.53	-1.3	83.1
1974	3 15	0.0	2442121.5	3 32.168	17 51.54	3 33.547	17 56.38	2.1094	1.8521	61.40	28.13	-1.4	83.2
1974	3 16	0.0	2442122.5	3 34.436	17 57.76	3 35.817	18 2.53	2.1376	1.8692	60.96	27.72	-1.4	83.4
1974	3 17	0.0	2442123.5	3 36.671	18 3.78	3 38.054	18 8.49	2.1657	1.8863	60.50	27.33	-1.5	83.5
1974	3 18	0.0	2442124.5	3 38.876	18 9.64	3 40.261	18 14.29	2.1938	1.9033	60.04	26.94	-1.5	83.7
1974	3 19	0.0	2442125.5	3 41.050	18 15.33	3 42.437	18 19.92	2.2219	1.9202	59.57	26.55	-1.5	83.8
1974	3 20	0.0	2442126.5	3 43.196	18 20.86	3 44.585	18 25.39	2.2500	1.9371	59.09	26.17	-1.6	83.9
1974	3 21	0.0	2442127.5	3 45.315	18 26.24	3 46.705	18 30.70	2.2780	1.9539	58.61	25.80	-1.6	84.1
1974	3 22	0.0	2442128.5	3 47.407	18 31.47	3 48.799	18 35.87	2.3060	1.9706	58.12	25.43	-1.6	84.2
1974	3 23	0.0	2442129.5	3 49.473	18 36.56	3 50.868	18 40.90	2.3339	1.9873	57.62	25.06	-1.7	84.3
1974	3 24	0.0	2442130.5	3 51.515	18 41.51	3 52.911	18 45.79	2.3617	2.0039	57.12	24.70	-1.7	84.5
1974	3 25	0.0	2442131.5	3 53.533	18 46.32	3 54.931	18 50.54	2.3896	2.0204	56.62	24.34	-1.7	84.6
1974	3 26	0.0	2442132.5	3 55.529	18 51.01	3 56.928	18 55.17	2.4173	2.0369	56.10	23.99	-1.8	84.7
1974	3 27	0.0	2442133.5	3 57.502	18 55.57	3 58.903	18 59.67	2.4450	2.0533	55.59	23.63	-1.8	84.8
1974	3 28	0.0	2442134.5	3 59.453	19 0.00	4 0.856	19 4.04	2.4726	2.0696	55.06	23.29	-1.8	84.9
1974	3 29	0.0	2442135.5	4 1.384	19 4.32	4 2.789	19 8.30	2.5001	2.0859	54.54	22.94	-1.9	85.1

1974	3	30	0.0	2442136.5	4	3.295	19	8.62	4	4.701	19	12.44	2.5276	2.1021	54.01	22.60	-1.9	85.2
1974	3	31	0.0	2442137.5	4	5.187	19	12.61	4	6.594	19	16.48	2.5549	2.1183	53.47	22.27	-1.9	85.3
1974	4	1	0.0	2442138.5	4	7.069	19	16.69	4	8.468	19	20.40	2.5822	2.1344	52.93	21.93	-1.9	85.4
1974	4	2	0.0	2442139.5	4	8.913	19	20.46	4	10.324	19	24.21	2.6095	2.1505	52.39	21.60	-2.0	85.5
1974	4	3	0.0	2442140.5	4	10.750	19	24.23	4	12.162	19	27.92	2.6366	2.1665	51.84	21.28	-2.0	85.6
1974	4	4	0.0	2442141.5	4	12.569	19	27.89	4	13.982	19	31.53	2.6636	2.1824	51.29	20.95	-2.0	85.7
1974	4	5	0.0	2442142.5	4	14.372	19	31.46	4	15.786	19	35.04	2.6906	2.1983	50.73	20.63	-2.1	85.8
1974	4	6	0.0	2442143.5	4	16.158	19	34.94	4	17.574	19	38.46	2.7174	2.2142	50.17	20.31	-2.1	85.9
1974	4	7	0.0	2442144.5	4	17.929	19	38.31	4	19.346	19	41.78	2.7442	2.2300	49.61	19.99	-2.1	86.0
1974	4	8	0.0	2442145.5	4	19.684	19	41.60	4	21.103	19	45.01	2.7708	2.2457	49.05	19.68	-2.1	86.2
1974	4	9	0.0	2442146.5	4	21.424	19	44.80	4	22.844	19	48.15	2.7974	2.2614	48.48	19.36	-2.2	86.3
1974	4	10	0.0	2442147.5	4	23.151	19	47.91	4	24.572	19	51.21	2.8238	2.2770	47.91	19.05	-2.2	86.4
1974	4	11	0.0	2442148.5	4	24.863	19	50.93	4	26.285	19	54.18	2.8501	2.2926	47.33	18.75	-2.2	86.4
1974	4	12	0.0	2442149.5	4	26.561	19	53.87	4	27.985	19	57.06	2.8764	2.3081	46.75	18.44	-2.2	86.5
1974	4	13	0.0	2442150.5	4	28.247	19	56.73	4	29.672	19	59.86	2.9025	2.3236	46.17	18.14	-2.3	86.6
1974	4	14	0.0	2442151.5	4	29.920	19	59.50	4	31.346	20	2.59	2.9285	2.3391	45.59	17.84	-2.3	86.7
1974	4	15	0.0	2442152.5	4	31.580	20	2.20	4	33.007	20	5.23	2.9544	2.3545	45.00	17.54	-2.3	86.8
1974	4	16	0.0	2442153.5	4	33.228	20	4.82	4	34.656	20	7.79	2.9801	2.3698	44.42	17.24	-2.3	86.9
1974	4	17	0.0	2442154.5	4	34.864	20	7.36	4	36.294	20	10.28	3.0058	2.3851	43.82	16.94	-2.3	87.0
1974	4	18	0.0	2442155.5	4	36.489	20	9.83	4	37.919	20	12.73	3.0313	2.4004	43.23	16.65	-2.4	87.1
1974	4	19	0.0	2442156.5	4	38.102	20	12.23	4	39.530	20	15.04	3.0567	2.4156	42.64	16.36	-2.4	87.2
1974	4	20	0.0	2442157.5	4	39.704	20	14.55	4	41.137	20	17.31	3.0819	2.4307	42.04	16.07	-2.4	87.3
1974	4	21	0.0	2442158.5	4	41.296	20	16.80	4	42.729	20	19.51	3.1071	2.4458	41.44	15.78	-2.4	87.4
1974	4	22	0.0	2442159.5	4	42.876	20	18.98	4	44.311	20	21.64	3.1320	2.4609	40.83	15.49	-2.5	87.4
1974	4	23	0.0	2442160.5	4	44.447	20	21.10	4	45.882	20	23.70	3.1569	2.4759	40.23	15.21	-2.5	87.5
1974	4	24	0.0	2442161.5	4	46.007	20	23.14	4	47.444	20	25.69	3.1816	2.4909	39.62	14.92	-2.5	87.6
1974	4	25	0.0	2442162.5	4	47.557	20	25.12	4	48.995	20	27.62	3.2062	2.5059	39.02	14.64	-2.5	87.7
1974	4	26	0.0	2442163.5	4	49.098	20	27.03	4	50.536	20	29.48	3.2306	2.5208	38.41	14.36	-2.5	87.8
1974	4	27	0.0	2442164.5	4	50.629	20	28.88	4	52.068	20	31.28	3.2549	2.5356	37.79	14.08	-2.6	87.9
1974	4	28	0.0	2442165.5	4	52.150	20	30.66	4	53.590	20	33.01	3.2790	2.5505	37.18	13.80	-2.6	87.9
1974	4	29	0.0	2442166.5	4	53.661	20	32.38	4	55.102	20	34.68	3.3029	2.5653	36.56	13.52	-2.6	88.0
1974	4	30	0.0	2442167.5	4	55.164	20	34.04	4	56.606	20	36.28	3.3268	2.5800	35.95	13.25	-2.6	88.1
1974	5	1	0.0	2442168.5	4	56.657	20	35.64	4	58.100	20	37.83	3.3504	2.5947	35.33	12.98	-2.6	88.2

1974	5	2	0.0	2442169.5	4	58.141	20	37.18	4	59.585	20	39.32	3.3739	2.8094	34.71	12.70	-2.7	88.2
1974	5	3	0.0	2442170.5	4	59.617	20	38.65	5	1.061	20	40.74	3.3973	2.8240	34.09	12.43	-2.7	88.3
1974	5	4	0.0	2442171.5	5	1.084	20	40.07	5	2.528	20	42.11	3.4205	2.8386	33.46	12.16	-2.7	88.4
1974	5	5	0.0	2442172.5	5	2.542	20	41.43	5	3.987	20	43.42	3.4435	2.8531	32.84	11.90	-2.7	88.5
1974	5	6	0.0	2442173.5	5	3.992	20	42.74	5	5.438	20	44.68	3.4664	2.8676	32.21	11.63	-2.7	88.5
1974	5	7	0.0	2442174.5	5	5.433	20	43.98	5	6.888	20	45.88	3.4891	2.8821	31.60	11.36	-2.7	88.6
1974	5	8	0.0	2442175.5	5	6.866	20	45.17	5	8.314	20	47.02	3.5116	2.8965	30.96	11.10	-2.8	88.7
1974	5	9	0.0	2442176.5	5	8.291	20	46.31	5	9.739	20	48.11	3.5340	2.9109	30.32	10.84	-2.8	88.7
1974	5	10	0.0	2442177.5	5	9.709	20	47.39	5	11.157	20	49.14	3.5562	2.7253	29.69	10.57	-2.8	88.8
1974	5	11	0.0	2442178.5	5	11.118	20	48.42	5	12.567	20	50.12	3.5782	2.9396	29.06	10.31	-2.8	88.9
1974	5	12	0.0	2442179.5	5	12.520	20	49.40	5	13.970	20	51.05	3.6000	2.7539	28.42	10.06	-2.8	89.0
1974	5	13	0.0	2442180.5	5	13.914	20	50.32	5	15.364	20	51.92	3.6217	2.9682	27.79	9.80	-2.8	89.0
1974	5	14	0.0	2442181.5	5	15.300	20	51.19	5	16.751	20	52.74	3.6432	2.7824	27.15	9.54	-2.9	89.1
1974	5	15	0.0	2442182.5	5	16.679	20	52.01	5	18.131	20	53.52	3.6646	2.7966	26.61	9.28	-2.9	89.1
1974	5	16	0.0	2442183.5	5	18.051	20	52.78	5	19.503	20	54.24	3.6857	2.8108	25.87	9.03	-2.9	89.2
1974	5	17	0.0	2442184.5	5	19.416	20	53.50	5	20.868	20	54.91	3.7066	2.8249	25.23	8.78	-2.9	89.3
1974	5	18	0.0	2442185.5	5	20.773	20	54.17	5	22.226	20	55.53	3.7274	2.8390	24.59	8.52	-2.9	89.3
1974	5	19	0.0	2442186.5	5	22.123	20	54.79	5	23.577	20	56.11	3.7480	2.8530	23.94	8.27	-3.0	89.4
1974	5	20	0.0	2442187.5	5	23.466	20	55.37	5	24.920	20	56.63	3.7684	2.8670	23.30	8.02	-3.0	89.5
1974	5	21	0.0	2442188.5	5	24.802	20	55.89	5	26.256	20	57.11	3.7886	2.8810	22.65	7.78	-3.0	89.5
1974	5	22	0.0	2442189.5	5	26.131	20	56.37	5	27.586	20	57.54	3.8086	2.8950	22.00	7.53	-3.0	89.6
1974	5	23	0.0	2442190.5	5	27.453	20	56.80	5	28.908	20	57.92	3.8284	2.9089	21.36	7.28	-3.0	89.7
1974	5	24	0.0	2442191.5	5	28.767	20	57.18	5	30.223	20	58.26	3.8481	2.9228	20.71	7.04	-3.0	89.7
1974	5	25	0.0	2442192.5	5	30.075	20	57.52	5	31.531	20	58.55	3.8675	2.9367	20.06	6.79	-3.0	89.8
1974	5	26	0.0	2442193.5	5	31.376	20	57.81	5	32.833	20	58.80	3.8868	2.9505	19.40	6.55	-3.1	89.8
1974	5	27	0.0	2442194.5	5	32.670	20	58.06	5	34.127	20	59.00	3.9058	2.9643	18.75	6.31	-3.1	89.9
1974	5	28	0.0	2442195.5	5	33.957	20	58.26	5	35.414	20	59.16	3.9246	2.9781	18.10	6.07	-3.1	89.9
1974	5	29	0.0	2442196.5	5	35.237	20	58.42	5	36.694	20	59.28	3.9433	2.9918	17.45	5.83	-3.1	90.0
1974	5	30	0.0	2442197.5	5	36.510	20	58.54	5	37.968	20	59.35	3.9617	3.0055	16.79	5.59	-3.1	90.1
1974	5	31	0.0	2442198.5	5	37.776	20	58.61	5	39.234	20	59.38	3.9799	3.0192	16.14	5.36	-3.1	90.1
1974	6	1	0.0	2442199.5	5	39.035	20	58.64	5	40.494	20	59.36	3.9980	3.0329	15.48	5.12	-3.1	90.2
1974	6	2	0.0	2442200.5	5	40.288	20	58.63	5	41.746	20	59.31	4.0158	3.0465	14.83	4.89	-3.1	90.2
1974	6	3	0.0	2442201.5	5	41.533	20	58.58	5	42.992	20	59.21	4.0334	3.0601	14.17	4.65	-3.2	90.3

1974	6	4	0.0	2442202.5	5	42.772	20	58.49	5	44.231	20	59.08	4.0508	3.0737	13.53	4.42	-3.2	90.3
1974	6	5	0.0	2442203.5	5	44.004	20	58.36	5	45.463	20	58.90	4.0681	3.0872	12.86	4.19	-3.2	90.4
1974	6	6	0.0	2442204.5	5	45.230	20	58.19	5	46.689	20	58.69	4.0851	3.1007	12.20	3.97	-3.2	90.4
1974	6	7	0.0	2442205.5	5	46.448	20	57.97	5	47.908	20	58.43	4.1018	3.1142	11.55	3.74	-3.2	90.5
1974	6	8	0.0	2442206.5	5	47.660	20	57.72	5	49.120	20	58.14	4.1184	3.1276	10.89	3.52	-3.2	90.6
1974	6	9	0.0	2442207.5	5	48.866	20	57.43	5	50.326	20	57.80	4.1348	3.1411	10.24	3.29	-3.2	90.6
1974	6	10	0.0	2442208.5	5	50.064	20	57.11	5	51.525	20	57.43	4.1510	3.1545	9.59	3.07	-3.3	90.7
1974	6	11	0.0	2442209.5	5	51.257	20	56.74	5	52.717	20	57.03	4.1669	3.1678	8.94	2.85	-3.3	90.7
1974	6	12	0.0	2442210.5	5	52.443	20	56.34	5	53.902	20	56.58	4.1826	3.1812	8.29	2.64	-3.3	90.8
1974	6	13	0.0	2442211.5	5	53.621	20	55.90	5	55.081	20	56.10	4.1982	3.1945	7.65	2.43	-3.3	90.8
1974	6	14	0.0	2442212.5	5	54.793	20	55.42	5	56.254	20	55.58	4.2135	3.2078	7.01	2.22	-3.3	90.9
1974	6	15	0.0	2442213.5	5	55.959	20	54.91	5	57.420	20	55.03	4.2286	3.2211	6.39	2.01	-3.3	90.9
1974	6	16	0.0	2442214.5	5	57.118	20	54.36	5	58.579	20	54.44	4.2434	3.2343	5.77	1.81	-3.3	91.0
1974	6	17	0.0	2442215.5	5	58.270	20	53.78	5	59.731	20	53.82	4.2581	3.2475	5.17	1.61	-3.3	91.0
1974	6	18	0.0	2442216.5	5	59.416	20	53.16	6	0.877	20	53.16	4.2725	3.2607	4.59	1.43	-3.4	91.1
1974	6	19	0.0	2442217.5	6	0.555	20	52.51	6	2.016	20	52.47	4.2867	3.2739	4.04	1.25	-3.4	91.1
1974	6	20	0.0	2442218.5	6	1.687	20	51.83	6	3.148	20	51.74	4.3007	3.2870	3.54	1.09	-3.4	91.1
1974	6	21	0.0	2442219.5	6	2.813	20	51.11	6	4.274	20	50.98	4.3144	3.3001	3.12	0.96	-3.4	91.2
1974	6	22	0.0	2442220.5	6	3.932	20	50.36	6	5.392	20	50.19	4.3279	3.3132	2.80	0.86	-3.4	91.2
1974	6	23	0.0	2442221.5	6	5.043	20	49.57	6	6.504	20	49.37	4.3413	3.3263	2.63	0.80	-3.4	91.3
1974	6	24	0.0	2442222.5	6	6.148	20	48.76	6	7.609	20	48.51	4.3543	3.3393	2.64	0.80	-3.4	91.3
1974	6	25	0.0	2442223.5	6	7.246	20	47.91	6	8.707	20	47.62	4.3672	3.3523	2.83	0.86	-3.4	91.4
1974	6	26	0.0	2442224.5	6	8.337	20	47.03	6	9.798	20	46.71	4.3798	3.3653	3.16	0.96	-3.4	91.4
1974	6	27	0.0	2442225.5	6	9.421	20	46.12	6	10.882	20	45.76	4.3922	3.3783	3.60	1.08	-3.5	91.5
1974	6	28	0.0	2442226.5	6	10.498	20	45.18	6	11.959	20	44.78	4.4044	3.3912	4.12	1.23	-3.5	91.5
1974	6	29	0.0	2442227.5	6	11.568	20	44.22	6	13.029	20	43.78	4.4163	3.4041	4.68	1.40	-3.5	91.6
1974	6	30	0.0	2442228.5	6	12.631	20	43.22	6	14.092	20	42.74	4.4281	3.4170	6.28	1.67	-3.5	91.6
1974	7	1	0.0	2442229.5	6	13.687	20	42.19	6	15.147	20	41.68	4.4396	3.4299	5.90	1.75	-3.5	91.6
1974	7	2	0.0	2442230.5	6	14.736	20	41.14	6	16.196	20	40.59	4.4508	3.4427	6.55	1.93	-3.5	91.7
1974	7	3	0.0	2442231.5	6	15.777	20	40.06	6	17.237	20	39.47	4.4619	3.4556	7.20	2.11	-3.5	91.7
1974	7	4	0.0	2442232.5	6	16.811	20	38.95	6	18.271	20	38.32	4.4727	3.4684	7.87	2.30	-3.5	91.8
1974	7	5	0.0	2442233.5	6	17.838	20	37.81	6	19.298	20	37.15	4.4833	3.4812	8.54	2.49	-3.5	91.8
1974	7	6	0.0	2442234.5	6	18.858	20	36.65	6	20.318	20	35.95	4.4937	3.4939	9.22	2.67	-3.6	91.9

1974	7	7	0.0	2442235.5	6	19.871	20	35.46	6	21.331	20	34.73	4.5038	3.5067	9.91	2.86	-3.6	91.9
1974	7	8	0.0	2442236.5	6	20.877	20	34.25	6	22.336	20	33.48	4.5137	3.5194	10.60	3.06	-3.6	91.9
1974	7	9	0.0	2442237.5	6	21.875	20	33.01	6	23.334	20	32.20	4.5234	3.5321	11.30	3.23	-3.6	92.0
1974	7	10	0.0	2442238.5	6	22.866	20	31.76	6	24.325	20	30.90	4.5328	3.5447	12.00	3.42	-3.6	92.0
1974	7	11	0.0	2442239.5	6	23.849	20	30.46	6	25.309	20	29.58	4.5421	3.5574	12.71	3.60	-3.6	92.1
1974	7	12	0.0	2442240.5	6	24.826	20	29.16	6	26.285	20	28.23	4.5510	3.5700	13.42	3.79	-3.6	92.1
1974	7	13	0.0	2442241.5	6	25.794	20	27.81	6	27.253	20	26.86	4.5598	3.5826	14.13	3.97	-3.6	92.1
1974	7	14	0.0	2442242.5	6	26.756	20	26.48	6	28.214	20	25.47	4.5683	3.5952	14.85	4.16	-3.6	92.2
1974	7	15	0.0	2442243.5	6	27.710	20	25.07	6	29.168	20	24.06	4.5767	3.6078	15.56	4.34	-3.6	92.2
1974	7	16	0.0	2442244.5	6	28.656	20	23.67	6	30.114	20	22.62	4.5847	3.6203	16.28	4.52	-3.7	92.3
1974	7	17	0.0	2442245.5	6	29.594	20	22.25	6	31.052	20	21.16	4.5926	3.6328	17.01	4.69	-3.7	92.3
1974	7	18	0.0	2442246.5	6	30.525	20	20.80	6	31.983	20	19.69	4.6002	3.6453	17.73	4.87	-3.7	92.3
1974	7	19	0.0	2442247.5	6	31.448	20	19.34	6	32.906	20	18.19	4.6076	3.6578	18.46	5.05	-3.7	92.4
1974	7	20	0.0	2442248.5	6	32.363	20	17.85	6	33.820	20	16.67	4.6147	3.6703	19.20	5.22	-3.7	92.4
1974	7	21	0.0	2442249.5	6	33.270	20	16.35	6	34.727	20	15.13	4.6217	3.6827	19.93	5.40	-3.7	92.5
1974	7	22	0.0	2442250.5	6	34.169	20	14.82	6	35.626	20	13.58	4.6284	3.6951	20.67	5.57	-3.7	92.5
1974	7	23	0.0	2442251.5	6	35.060	20	13.28	6	36.517	20	12.00	4.6348	3.7075	21.40	5.74	-3.7	92.5
1974	7	24	0.0	2442252.5	6	35.943	20	11.72	6	37.399	20	10.41	4.6411	3.7199	22.14	5.91	-3.7	92.6
1974	7	25	0.0	2442253.5	6	36.817	20	10.14	6	38.273	20	8.81	4.6471	3.7323	22.89	6.08	-3.7	92.6
1974	7	26	0.0	2442254.5	6	37.683	20	8.55	6	39.139	20	7.18	4.6529	3.7446	23.63	6.24	-3.7	92.6
1974	7	27	0.0	2442255.5	6	38.541	20	6.94	6	39.996	20	5.54	4.6585	3.7569	24.38	6.41	-3.8	92.7
1974	7	28	0.0	2442256.5	6	39.390	20	5.32	6	40.845	20	3.89	4.6638	3.7692	25.13	6.57	-3.8	92.7
1974	7	29	0.0	2442257.5	6	40.231	20	3.68	6	41.686	20	2.22	4.6689	3.7815	25.88	6.73	-3.8	92.8
1974	7	30	0.0	2442258.5	6	41.063	20	2.02	6	42.518	20	0.53	4.6738	3.7938	26.64	6.89	-3.8	92.8
1974	7	31	0.0	2442259.5	6	41.886	20	0.35	6	43.341	19	58.83	4.6785	3.8060	27.39	7.05	-3.8	92.8

☆ U. S. GOVERNMENT PRINTING OFFICE : 1975 O - 570-186

"The aeronautical and space activities of the United States shall be conducted so as to contribute . . . to the expansion of human knowledge of phenomena in the atmosphere and space. The Administration shall provide for the widest practicable and appropriate dissemination of information concerning its activities and the results thereof."

—NATIONAL AERONAUTICS AND SPACE ACT OF 1958

NASA SCIENTIFIC AND TECHNICAL PUBLICATIONS

TECHNICAL REPORTS: Scientific and technical information considered important, complete, and a lasting contribution to existing knowledge.

TECHNICAL NOTES: Information less broad in scope but nevertheless of importance as a contribution to existing knowledge.

TECHNICAL MEMORANDUMS: Information receiving limited distribution because of preliminary data, security classification, or other reasons. Also includes conference proceedings with either limited or unlimited distribution.

CONTRACTOR REPORTS: Scientific and technical information generated under a NASA contract or grant and considered an important contribution to existing knowledge.

TECHNICAL TRANSLATIONS: Information published in a foreign language considered to merit NASA distribution in English.

SPECIAL PUBLICATIONS: Information derived from or of value to NASA activities. Publications include final reports of major projects, monographs, data compilations, handbooks, sourcebooks, and special bibliographies.

TECHNOLOGY UTILIZATION PUBLICATIONS: Information on technology used by NASA that may be of particular interest in commercial and other non-aerospace applications. Publications include Tech Briefs, Technology Utilization Reports and Technology Surveys.

Details on the availability of these publications may be obtained from:

SCIENTIFIC AND TECHNICAL INFORMATION OFFICE

NATIONAL AERONAUTICS AND SPACE ADMINISTRATION

Washington, D.C. 20546